Development of novel applications for the electron beam texturing and Surfi-Sculpt® processes

EngD Innovation Report

Thomas Matthew Pinto

CEng, MIMechE, MWeldI, MEng

A thesis submitted in partial fulfilment of the requirements for the degree of Doctor of Engineering (EngD)

WMG
THE UNIVERSITY OF WARWICK

TWI

October 2020

This page is intentionally left blank

Abstract

The electron beam texturing (EBT) and Surfi-Sculpt® processes are transformative surface modification technologies used to create customised complex geometrical surfaces rapidly and at low-cost to improve the performance of a surface. These processes are neither additive nor subtractive but rely on the interaction between a workpiece and a power beam, with its subsequent deflection, to locally melt and move the parent material on the surface in the opposite direction to the deflection to create protrusions and corresponding intrusions. The complex novel surface textures and features produced, in many cases, cannot viably be manufactured by other techniques. However, market barriers have restricted the industrial adoption of these processes due to a limited amount of performance data demonstrating the benefits in specific application areas. Furthermore, a lack of fundamental understanding of how features are formed during the processes as well as limited knowledge management had added technical barriers.

In seeking to address these issues, a series of studies and literature reviews were conducted to support improved control of the EBT and Surfi-Sculpt processes and to increase understanding of the physics. Data analysis resulted in the creation of formulas for the prediction of feature heights in three materials. A bespoke technique was developed to record high-speed video of the EB Surfi-Sculpt process from within the vacuum chamber where five distinct phases of feature formation were identified: initial melt track; expansion of feature base and height; increase of height; bridging; and over melting with potential decrease of height. Fundamental analysis of the images was conducted before a model was proposed enabling the prediction of the flow of molten material based upon Marangoni effects, i.e. resulting from differences in surface tension across an interface during the initial beam-material interaction and subsequent beam translation.

Two case studies investigated specific novel applications of the processes for use on liquid cold plates (LCPs) and uncemented acetabular cups for orthopaedic implants. Prototype components were manufactured through the development and optimisation of parameters and resultant surfaces; these were assessed against existing technologies. The prototype LCP demonstrated a reduction in manufacturing time of approximately 40 % per component, increased heat transfer allowing more power in the electronic components being cooled and increased efficiency by 100 % without size or weight penalties. This indicated the ability to use a 50 % smaller LCP for the same cooling power. With the uncemented acetabular cup, an increased coefficient of friction of over 50 % compared with an existing technology was evidenced which created a self-rasping and bone graft generating surface and demonstrated application of a surface to a prototype component with 18.2 seconds beam on time.

A directory and selection tool (Surfi-Sculpt catalogue) was developed which captured all required parameters for the manufacture of specific surfaces including geometrical characterisation, an image of the resultant surface and a search capability to enhance rapid identification and manufacture of surfaces. This improved knowledge management and underpinned the advancement of these technologies.

A mathematical model was proposed to enhance the creation and optimisation of deflection pattern files with associated deflection frequencies for the EBT and Surfi-Sculpt processes. The effect of different materials on the penetration depth of the beam and subsequent feature height variation was explored. The benefit of this work will be a reduction in empirical development and the future creation of a framework for improved automation of the processes which could embed this knowledge into pre-processing software.

In conclusion, this work has directly advanced the EBT and Surfi-Sculpt processes by overcoming many of the market, technical and knowledge management barriers.

Acknowledgements

"The greatest glory in living is not in falling, but in rising every time we fall." Nelson Mandela

The support of my supervisors (Prof. Stuart Barnes, Prof. Kevin Neailey and Dr Anita Ward) has been invaluable; their excellent ability to challenge and develop the work I produce has constantly encouraged me to write my reports with clarity and coherence. I would also like to thank my manager, Mike Nunn, who first supported my idea to commence this Engineering Doctorate.

My colleagues in the Electron Beam Processes Section at TWI have been a great source of advice and guidance – thank you all.

My wife, Holly, has steadfastly provided wisdom, support, encouragement and proof reading throughout my EngD.

'*Those who hope in the Lord will renew their strength. They will soar on wings like eagles; they will run and not grow weary, they will walk and not be faint.*' Isaiah 40:31

Declaration

All of the work reported in this document is the work of the author except where acknowledged or referenced. The author was the designated project leader within TWI for all of the work described here. As such, the author was solely responsible for setting the objectives for the work in agreement with the partners involved, planning and progressing the experimental work, analysing and providing interpretation of the results and reporting.

Funding for this work has come from the following sources: TWI's Core Research Programme for the benefit of TWI Industrial Members, leading to parts of this work being reported to TWI Industrial Members; the UK's innovation agency, Innovate UK, under grant no. 132496 and; the European Union's Seventh Framework Programme for research, technological development and demonstration, under grant agreement no. 606172.

Contents

List of Figures

List of Tables

List of Equations

Abbreviations and Glossary of Terms

ALARP	As low as reasonably practicable
AM	Additive manufacturing
CFD	Computational fluid dynamics
COF	Coefficient of friction
EB	Electron beam
EBM®	Electron beam melting – trademark: Arcam EBM
EBT	Electron beam texturing
EBSD	Electron backscatter diffraction
EBW	Electron beam welding
Freezing front	'*A zone where the cooled material is transferred from the molten state into the solid state*' (Schiller et al., 1982, p.292)
FF	Folded fin
GTA	Gas tungsten arc
HA	Hydroxyapatite
HAZ	Heat affected zone
IGBT	Insulated-gate bipolar transistor
IP	Intellectual property
LCP	Liquid cold plate
LED	Light emitting diode
LEHCEBs	Low-energy high current electron beams
LMT	Laser melting technology
Marangoni effects	The cause of movement of molten material (liquid) as a result of differences in surface tension across an interface (Mills et al., 1998; Lee et al., 1998)
Melting front	A zone where heated material is transferred from the solid state into the molten state (adapted from Schiller et al., 1982)
MIG	Metal inert gas
MRL	Manufacturing readiness level
Osseointegration	'*The formation of a direct interface between an implant and bone*' (Pakos and Xenakis, 2014, p.68)
pcf	pounds per cubic foot
SEM	Scanning electron microscope
S-SPS	Surfi-Sculpt procedure specification - the parameters and recipe required to reproduce a previously created surface
TCST	Temperature coefficient of surface tension
THR	Total hip replacement
TIG	Tungsten inert gas
TRL	Technology readiness level
USP	Unique selling point
uTHR	uncemented total hip replacement
'Valley of Death'	'*A research gap, and an information and trust gap between technical research and the business model'* (Saxberg, 2005, p.244)
W-EBAM	Wire-feed electron beam additive manufacturing

Glossary of nomenclature associated with the electron beam texturing and Surfi-Sculpt processes; adapted from Earl and Hilton (2012).

Term	Description
Amplitude gain	The peak-to peak value of the arbitrary wave forms used in the deflection patterns for the array and motif.
Array	The deflection pattern co-ordinates required to manipulate the beam to position the locations of each feature. An array can consist of single legged or multi legged motifs.
Feature	The result of the movement of material to create a protrusion with a corresponding intrusion.
Intrusion	Volume from which material has been 'harvested' or relocated (usually from below the surface of the parent material).
Jump	Movement of the beam position rapidly between the end of one swipe to the start of the next.
Leg	A swipe that produces a protrusion and contributes towards a feature. This can be a single swipe, in the case of a simple feature, or multiple swipes in different positions for a more complex feature, e.g. a star motif.
Motif	The deflection pattern co-ordinates required to manipulate the beam to produce a feature. Multiple features can form a motif and are usually produced in a rectangular field, e.g. 2 x 2 or n x m.
Parent material	Base material from which features are created using the electron beam texturing and Surfi-Sculpt processes.
Pattern	A data file detailing the beam path through a series of Cartesian co-ordinates.
Protrusion	Volume of 'feature' to which material has been moved (usually above the original surface of the parent material).
Repeat	The number of times the power beam travels along the same swipe.
Record	The complete information stored in the Surfi-Sculpt catalogue which details the Surfi-Sculpt procedure specification as well as additional information such as the project details and an image of the resultant surface.
Sample	Physical specimen demonstrating a specific surface modification resulting from the Surfi-Sculpt process.
S-SPS	Surfi-Sculpt procedure specification. The parameters and recipe required to reproduce a previously created surface. The S-SPS includes information for the operator at what current and voltage (for example) to set the electron beam to reproduce the surface; adapted from Moore and Booth (2015).
Single (legged) feature	A feature built from repeated swipes over one (linear) melt track.
Star feature	A feature built from many legs (usually 8 or more).
Swipe	Movement of the power beam to interact with the material and create a melt track.
Swipe delay	A time unit between each successive swipe in the same location. This can allow the material to cool between successive swipes.
Tile / tiling	Repeating arrays in a systematic manner, i.e. one tile will be completed before commencing another tile.

1 Introduction

1.1 Overview

The manipulation of surface topography can enhance chemical, biological or physical characteristics of a parent material (Fuentes, 2010). However, it is critical to ensure sufficient ability to control the topography for technical applications due to its influential role in the performance of a material or component (Bodschwinna and Seewig, 2013). Where high functional demands are imposed upon the material or component, surface modification technologies providing high precision and control of the resultant topography of a material are likely to have a competitive advantage over other such technologies (Bodschwinna and Seewig, 2013).

Surface modification can be categorised into three main themes: physical–chemical functional improvements, mechanical–structural functional improvements and surface coating (Fuentes, 2010). This Innovation Report focuses on two related novel technologies which use a power beam, either a laser beam or an electron beam (EB), to elicit a physical–chemical and/or mechanical–structural response on a surface.

The first use of an EB as a heat source for welding was by Dr Stohr in 1957 (Bakish and White, 1964). Meyer et al. (1965) noted that, during welding, a keyhole or capillary is formed by pressure due to the impact of the beam of electrons on the molten metal. Removal of this material is caused by evaporation and the internal pressure generated by the metal vapour in the capillary.

Meleka (1971) was the first to observe a 'bulge' or protrusion, shown in Figure 1.1, formed from re-solidified material at the top of the capillary caused by the impingement of an EB. This peculiarity altered the surface topography of the material.

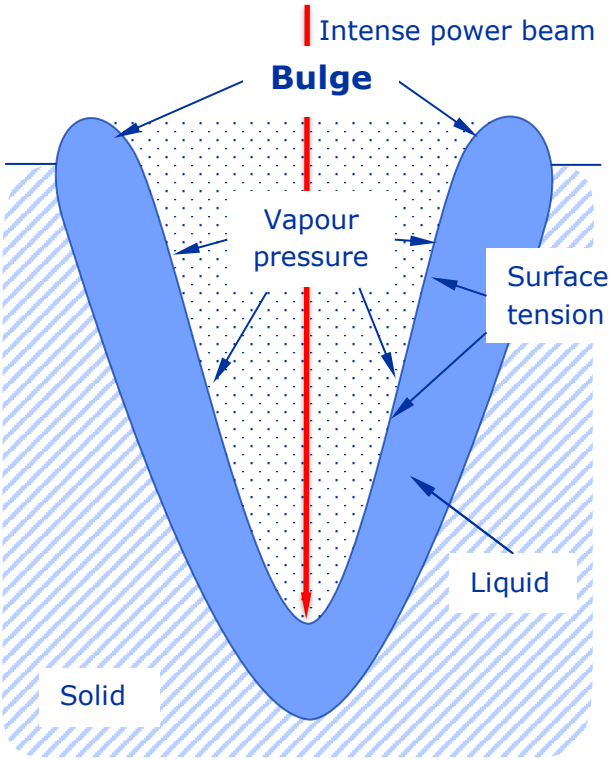

Figure 1.1 'Bulge' or protrusion caused by the formation of a capillary during impingement of an electron beam, adapted from Meleka (1971) © Courtesy of TWI Ltd.

Exploiting this phenomenon, TWI Ltd, an independent research and technology organisation established in 1946, developed and patented two surface modification technologies: the electron beam texturing (EBT) process (Dance, 2002) and the Surfi-Sculpt® process (Dance and Kellar, 2003). Being neither additive nor subtractive, these transformative processes rely on the interaction between an EB and a workpiece to locally melt and move the parent material on the surface. They are material processing technologies able to produce complex surface textures and features which, in many cases, cannot viably be manufactured by other techniques. Figure 1.2 shows the mechanism of the EBT and Surfi-Sculpt processes and they are explored in more detail in Chapters 2 and 3.

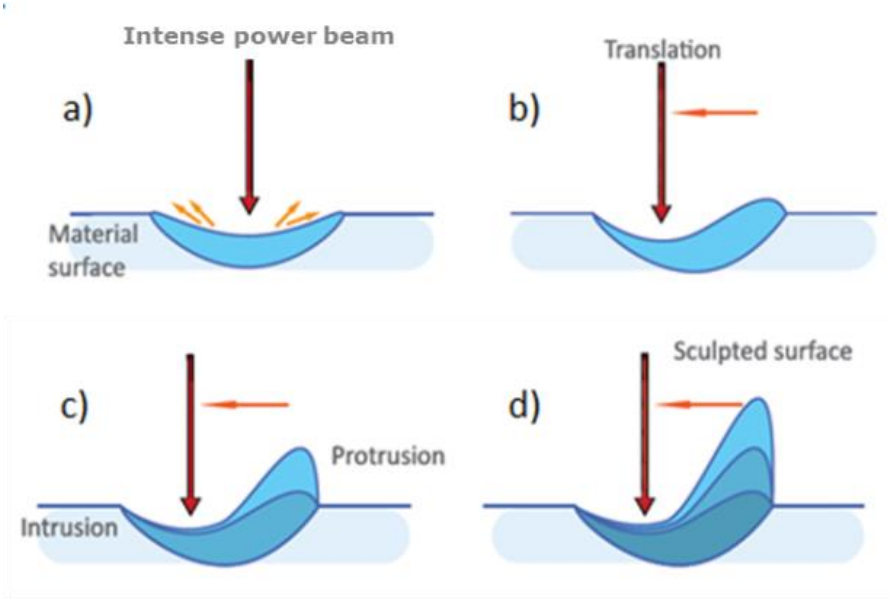

Figure 1.2 Feature formation of the EBT and Surfi-Sculpt processes, taken from Pinto (2013):
a) Initial beam material interaction – common to both processes;
b) Initial beam translation (swipe) – common to both processes;
c) Second beam translation (swipe) – unique to the Surfi-Sculpt process;
d) Third beam translation (swipe) – unique to the Surfi-Sculpt process.

Figure 1.3 shows a scanning electron microscope (SEM) image of a feature created from a series of uni-directional beam swipes as described in Figure 1.2. A feature with a height of 1.2 mm can be made from as few as four uni-directional swipes of the beam as shown in Chapter 3.

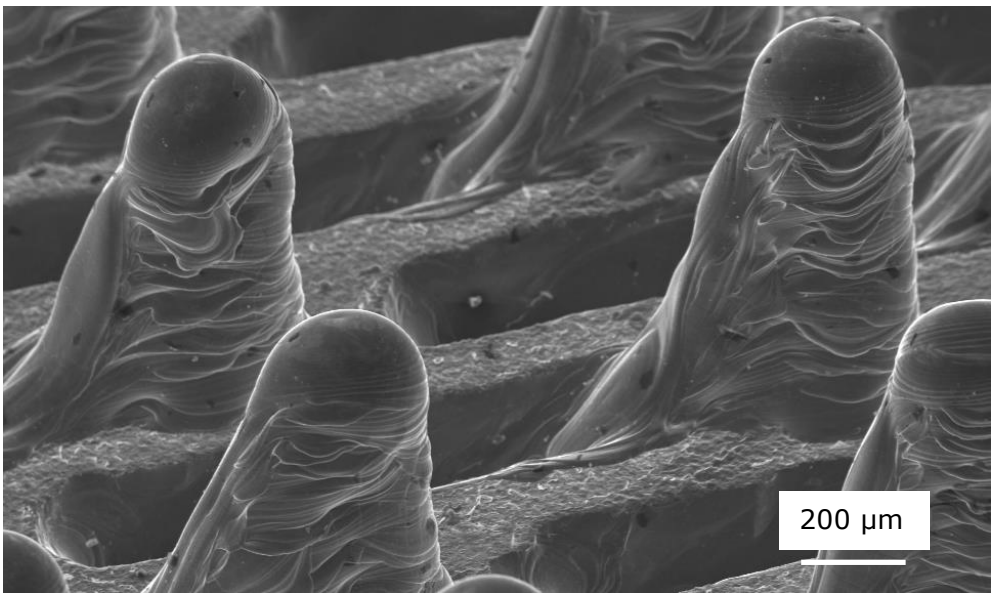

Figure 1.3 SEM image of an example feature formation using the Surfi-Sculpt process.

Figure 1.4 shows a SEM image of a group of features created from a series of uni-directional beam swipes across a surface.

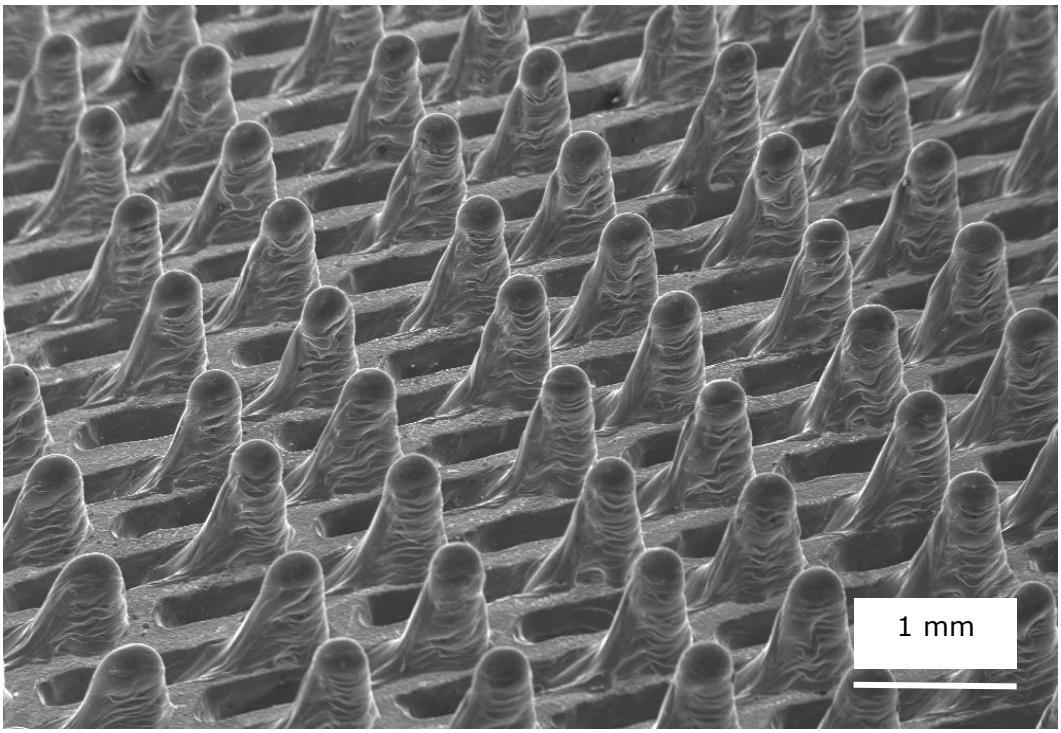

Figure 1.4 SEM image of an example group of features formed using the Surfi-Sculpt process.

In order for the EBT and Surfi-Sculpt processes to work, customisable deflection of the beam is necessary beyond standard pre-set deflections provided by EB equipment manufacturers for EB welding (EBW) systems, shown in Figure 1.5, such as a sine wave, a circle, an ellipse and a 'figure of eight' pattern.

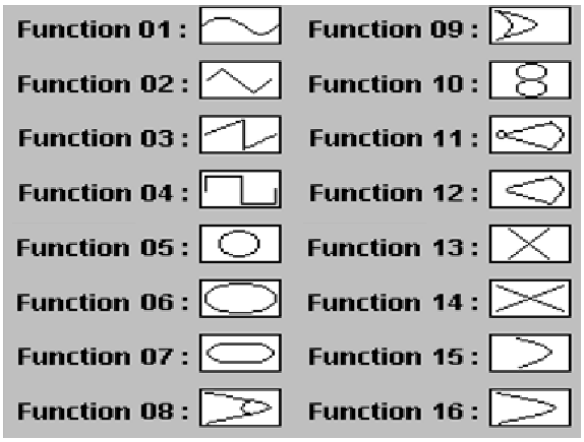

Figure 1.5 Typical standard pre-set deflection patterns from an EB manufacturer, adapted from Steigerwald Strahltechnik GmbH (2013).

Figure 1.6 shows a diagram of the equipment and setup required for arbitrary deflection of an EB which is essential for the EBT and EB Surfi-Sculpt processes.

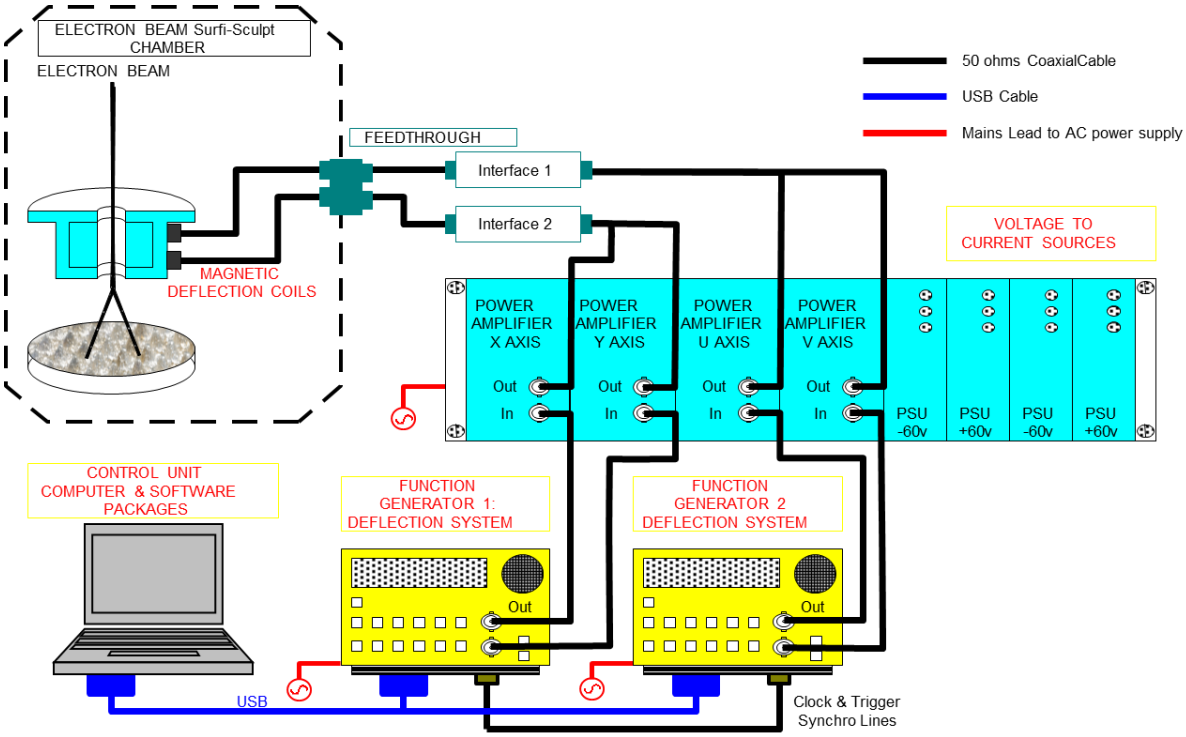

Figure 1.6 Programmable beam deflection showing the mechanism of using a series of function generators and amplifiers to achieve deflection of an electron beam.

An electro-magnetic field is formed perpendicular to the flow of the EB by the deflection coils to cause beam translation. In order to control the required beam manipulation, two pairs of deflection coils are utilised which are separated into a high inductance and high impedance set (*X,Y*) and a low inductance and low impedance set (*U,V*). The creation of a pattern of features can use both a motif (*U,V* beam deflection) to define the geometry of the features produced and an array (*X,Y* beam deflection) to define the position of the features. These are described using a Cartesian coordinate system which generates a beam path and the coordinates are transferred to two arbitrary waveform function generators which supply voltage signal outputs for both the motif and array. The voltage signal outputs are subsequently converted to current signals by power amplifiers enabling the deflection coils to deflect the beam and ultimately control the beam position. The existing software package to control the EBT and

Surfi-Sculpt processes developed by TWI is entitled 'Electron Beam Deflection Control System Mark III'.

1.2 Research question, aims and objectives

The main research question guiding the author's work was:

"How to develop further the EBT and Surfi-Sculpt processes to meet industrial needs, achieve wider adoption and implementation and to get return on investment for TWI?"

The innovations required to address this research question included development of greater understanding of the fundamental mechanisms of the processes, optimisation of the data management surrounding them, generation of novel surfaces and application of the processes to specific industrial areas demonstrated through case studies.

To achieve this, the author focused on the following aims:

- Identify the state-of-the-art and gaps in knowledge of the EBT and Surfi-Sculpt processes in order to establish research questions and future development plans [Submissions 1 and 2].
- Demonstrate benefit to a segment of the heat exchange industry with improved performance compared to an existing technology [Submission 3].
- Demonstrate that the EBT and Surfi-Sculpt processes can produce surfaces which have a high coefficient of friction (COF) against a bone substitute to enhance mechanical interlocking requirements of an uncemented acetabular cup for next generation orthopaedic implants and manufacture prototype uncemented acetabular cups using the EBT and Surfi-Sculpt processes [Submission 6].

- Develop a directory and selection tool (Surfi-Sculpt catalogue) for improved knowledge management of the EBT and Surfi-Sculpt processes [Submission 4].
- Develop and define a model explaining the EBT and Surfi-Sculpt processes and the formation of a feature [Submission 5].

This Engineering Doctorate (EngD) aimed to take a substantial step towards industrial usage of the EBT and Surfi-Sculpt processes by overcoming the existing market barriers and helping the technologies to cross the 'Valley of Death' (Saxberg, 2005); this is explored further in Section 1.3.3.

There were three primary objectives of this EngD designed to overcome the market barriers:

- Establish a broader understanding of these material processing technologies. This is explored in Chapter 3.
- Overcome the lack of industrially relevant performance data thus reducing the technical risk associated with adopting these technologies which is currently the largest 'barrier to entry' for industrial uptake. This development was focused on two primary markets/sectors:
  - Heat exchangers – increasing surface area and directing the flow in liquid cold plates (LCPs) with phase change by manufacturing prototype LCP components (over an area of approximately 95 x 31 mm) using the Surfi-Sculpt process. This is explored in Chapter 4.
  - Orthopaedic implants – improved initial fixation by increasing the COF of acetabular cups in uncemented total hip replacements (uTHRs) leading to greater load transfer and bone ingrowth thus preventing bone resorption and stress shielding. This is explored in Chapter 5.
- Develop improved knowledge management supporting the EBT and Surfi-Sculpt processes. This is explored in Chapter 6.

The case studies in Chapters 4 and 5 were selected as a result of both the industrial pull of the EBT and Surfi-Sculpt processes based upon sales and technical work conducted by the author and through visits to companies to promote the technologies.

1.3 Outline of EngD portfolio

1.3.1 Overview of the portfolio

The EngD portfolio comprises of six Submissions seeking to address the research question stated in Section 1.2. This overview provides a summary of the content of each Submission.

Submission 1 was a literature review which critically assessed the background of the EBT and Surfi-Sculpt processes and discussed future development plans. The review concluded that additional investigation was required to support the development of the manufacturing processes for wider adoption and implementation. This required extended understanding of the mechanism of the processes, development of a directory and selection tool (Surfi-Sculpt catalogue) detailing surfaces available and the creation of application specific case studies. Since Submission 1, three new English language articles have been published based upon work using the EBT and Surfi-Sculpt processes (Li et al., 2018; Painter et al., 2017; Ramskogler et al., 2017); these are discussed in Chapter 2. A further paper was published in 2017, based upon initial work in 2015, regarding a competing technology closely related to the EBT process, 'WaveShape', which uses a laser beam to melt and restructure metals (Temmler et al., 2015; Temmler et al., 2017). This process demonstrates the same redistribution of the molten material which is utilised by the EBT and Surfi-Sculpt processes therefore rivalling the EBT process. Further competing technologies are discussed in Section 2.2.

Submission 2 identified the objectives and potential solutions for the production of surfaces for orthopaedic implants using the EBT and Surfi-Sculpt processes. The review of the literature concluded that the problem of bone resorption, seen in uncemented implants, could be addressed by use of the EBT and Surfi-Sculpt processes.

Submission 3 was a specific case study on LCPs which investigated the creation of surfaces to promote heat transfer, assessed the surfaces using data received from computational fluid dynamics (CFD), manufactured and tested LCP prototypes and assessed the prototypes against existing technologies. It resulted in relevant data demonstrating improved performance of the prototypes LCPs with innovative surfaces applied using the Surfi-Sculpt process and discussed the progression of the technology. The benefits over the state-of-the art are reviewed in Chapter 4.

Submission 4 included the development of a directory and selection tool (Surfi-Sculpt catalogue), creation of formal documentation surrounding the 'Electron Beam Deflection Control System Mark III' software, improved electronic deflection pattern file storage in a structured manner and the creation and collation of display samples demonstrating example features created using the EBT and Surfi-Sculpt processes. These activities supported the knowledge management to underpin the advancement of these technologies.

Submission 5 proposed models to predict the flow of molten material by Marangoni effects (Lee et al., 1998; Mills et al., 1998) during the initial beam-material interaction and subsequent beam translation through fundamental analysis using high-speed videoing of the EB Surfi-Sculpt process.

Submission 6 was a specific case study exploring the use of the EBT and Surfi-Sculpt processes to manufacture bone interface surfaces for acetabular cups in uTHRs. Prototype components were manufactured, tested and assessed against existing technologies; an increase in the COF was evidenced thereby increasing the load transfer with the aim of minimising bone resorption.

The individual Submissions that constitute the portfolio are represented in Table 1.1 where the main aims and research methods are summarised and outcomes, achievements and innovations are identified.

Table 1.1 Overview of Submissions to the EngD portfolio.

Submission	Aims	Main Research Methods	Outcomes/ Achievements/ Innovations
1. Background of the Surfi-Sculpt process and future development plans	To determine mechanisms producing feature geometries using the EBT and Surfi-Sculpt processes	Literature review and critical analysis	Identification of state-of-the-art and gaps in knowledge and creation of future development plans
2. Fundamentals of orthopaedic implants, their challenges and the potential use of the Surfi-Sculpt process	To identify objectives and potential solutions for producing surfaces for orthopaedic implants	Literature review and critical analysis	Targets defined for the Surfi-Sculpt process to ensure successful implementation in an industrial environment
3. Liquid Cold Plate Case Study	To evidence the benefits of the Surfi-Sculpt process for manufacturing novel LCPs and assess the performance of a prototype	Processing trials, metallurgical and property assessment, manufacture of prototypes, analysis and assessment of performance	Demonstration that the Surfi-Sculpt process could produce features which performed better than an existing technology
4. Improved knowledge management of the EBT and Surfi-Sculpt processes	To address the challenge of knowledge management related to the EBT and Surfi-Sculpt processes	Processing trials and framework for storing of data relating to the processes	Development of a catalogue for the EBT and Surfi-Sculpt processes
5. Exploring the fundamental principles (mechanics) of the Surfi-Sculpt process	To explore and describe the principles of the process	Processing trials and high-speed video filming and analysis	Development of a model explaining the Surfi-Sculpt process and five phases of the formation of a feature
6. Orthopaedic Implant Case Study	To evidence the benefits of using the EBT and Surfi-Sculpt processes for manufacturing novel uncemented acetabular cup bone interface surfaces	Processing trials, metallurgical assessment, manufacture of prototypes, understanding and collation of industrial requirements and cost analysis	Demonstration that the EBT and Surfi-Sculpt processes could perform to the requirements of uTHRs

1.3.2 Application of innovation

The work towards the EngD portfolio has incorporated demonstrable application of innovation and this Innovation Report draws together the separate

innovations from the individual Submissions. It covers, in a publically reportable context, the development of the EBT and Surfi-Sculpt processes and explores how the work has progressed the technologies through the technology readiness levels (TRLs) and manufacturing readiness levels (MRLs) to develop processes which are mature for adoption in manufacturing environments. Collaborators from the case studies summarised in this Innovation Report along with the author are progressing the implementation of the EBT and Surfi-Sculpt processes in their manufacturing facilities.

Figure 1.7 shows a map of the EngD portfolio structure (highlighted within the blue box encompassing the six Submissions) alongside TRLs and MRLs and therefore directs the reader as to the most coherent order to read the portfolio Submissions.

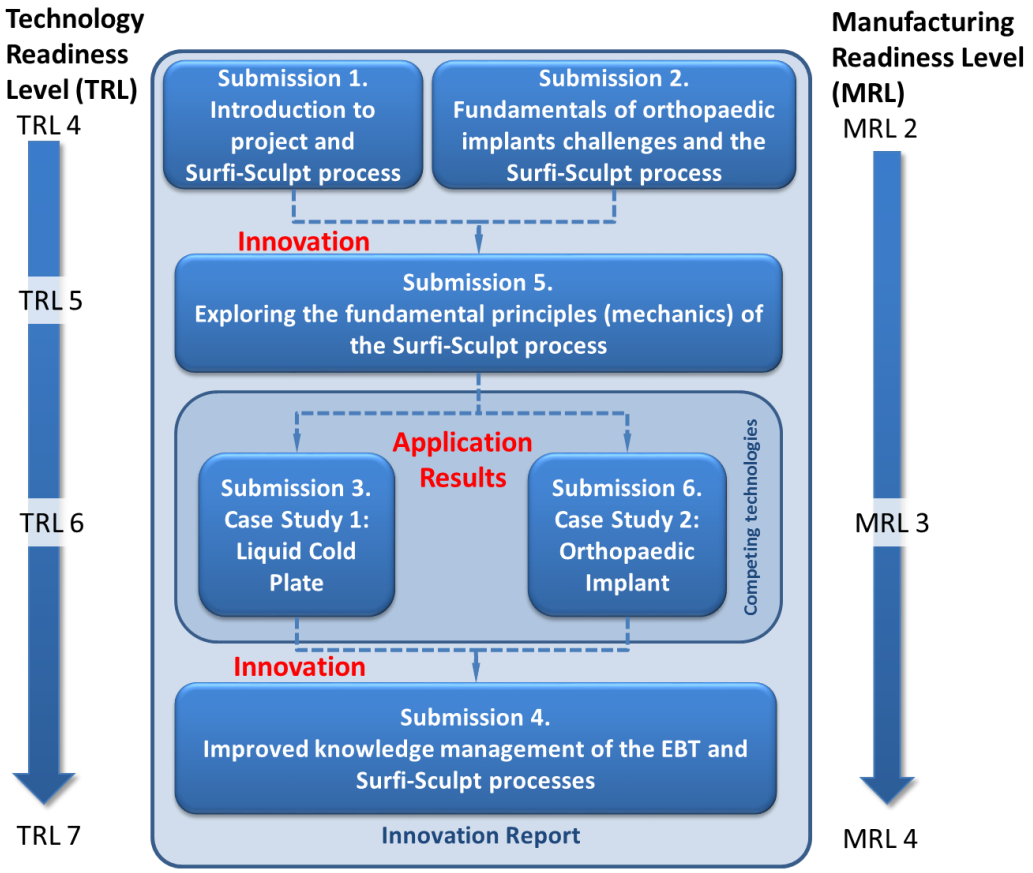

Figure 1.7 Map of the EngD portfolio structure.

Each TRL is defined by the European Commission in Annex G of the General Annexes to the Horizon 2020 Work Programme 2016/17 (European Commission, 2016, p.29) as follows:

- '*TRL 3 – experimental proof of concept.*
- *TRL 4 – Technology validated in laboratory.*
- *TRL 5 – Technology validated in a relevant environment (industrially relevant environment in the case of key enabling technologies).*
- *TRL 6 – Technology demonstrated in a relevant environment (industrially relevant environment in the case of key enabling technologies).*
- *TRL 7 – System prototype demonstration in operational environment'*.

The MRLs are defined by the US Department of Defense Manufacturing Technology (OSD Manufacturing Technology Program in collaboration with The Joint Service/Industry MRL Working Group, 2017, p.11) as follows:

- '*MRL 2: Manufacturing concepts identified.*
- *MRL 3: Manufacturing proof of concept developed.*
- *MRL 4: Capability to produce the technology in a laboratory environment.'*

The OSD Manufacturing Technology Program in collaboration with The Joint Service/Industry MRL Working Group (2017) concluded that together TRLs and MRLs can be used to support risk management and to assess both the underlying process technology and manufacturing system.

Therefore, this framework is used in the subsequent chapters of this Innovation Report, following the structure laid out in Figure 1.8, to aid the adoption and implementation of the EBT and Surfi-Sculpt processes.

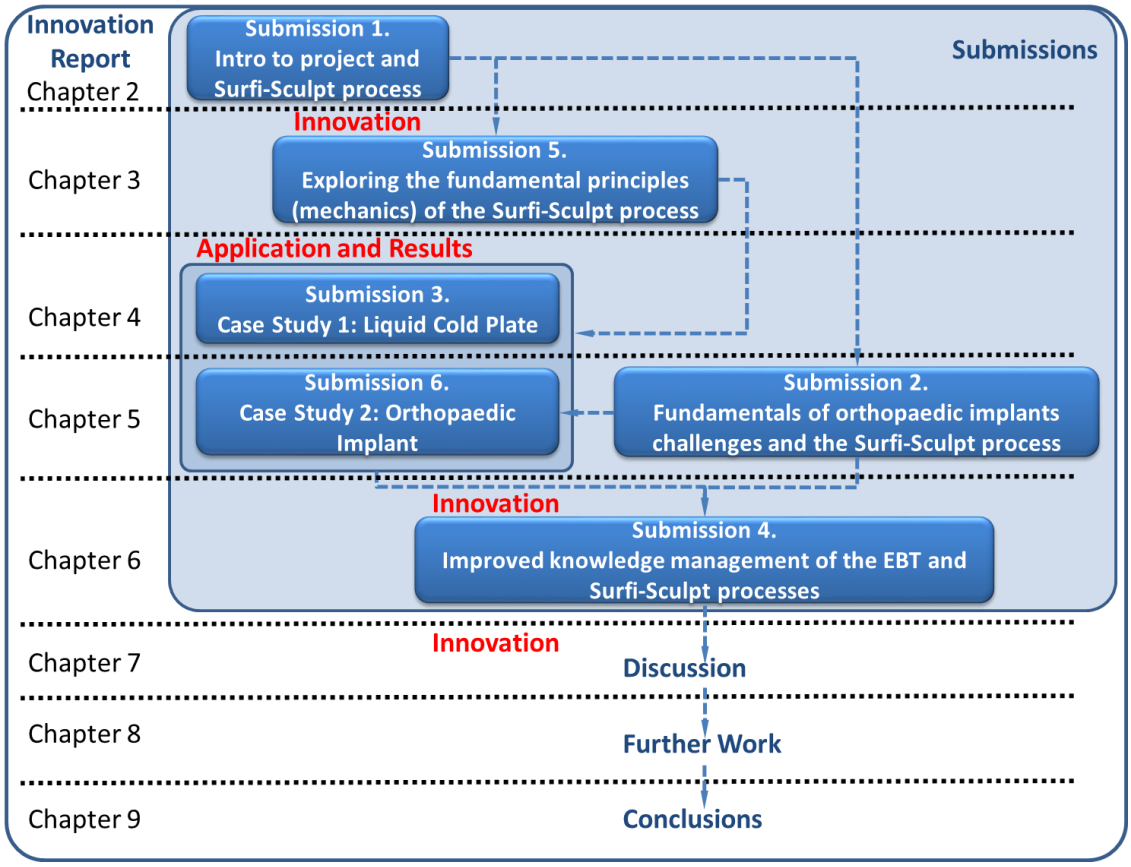

Figure 1.8 Outline of the structure of this Innovation Report.

1.3.3 Bridging the 'Valley of Death'

> *'Innovation is the application of new knowledge to the production of goods and services; it means improved product quality and enhanced process effectiveness. Innovation generates wide improvements in productivity.'*
>
> *(Department for Business, Innovation and Skills, 2011, p.7).*

Within this Innovation Report, the case studies summarised in Chapters 4 and 5 demonstrate the application of the EBT and Surfi-Sculpt processes. Chapters 3, 6 and 7 provide an overview of the innovation generated through the EngD namely the expanded understanding of the processes and creation of a directory and selection tool. This applied research has helped to advance the processes. Often innovations, such as the EBT and Surfi-Sculpt processes, can fail to

progress due to the 'Valley of Death' defined by Saxberg (2005, p.244) as '*a research gap, and an information and trust gap between technical research and the business model'*. This term refers to the high risk of failure of innovations until sufficient data has been validated and demonstrated in relevant industrial environments. This gap is widely agreed to be between TRL 4 and TRL 7 (Beard et al., 2009; Saxberg, 2005; Hug, 2009). Ehlers (1998) and Auerswald and Branscomb (2003) explain that innovations require additional financial support, often from Government funding, to demonstrate application and meet industrial needs thus achieving adoption and implementation.

Prior to the author's work, the EBT and Surfi-Sculpt processes were struggling to cross the 'Valley of Death' and had stalled in their progression as innovative transformative surface modification processes due to the market barriers discussed in Section 1.2. Beard et al. (2009) argue that the 'Valley of Death' is usually created at the basic research stage but is revealed at the applied research stage as demonstrated in Figure 1.9. Fresh impetus was required to drive these processes forward by demonstrating application of these innovations. Figure 1.9 shows the EBT and Surfi-Sculpt processes currently at TRL 7 having crossed the 'Valley of Death' as a direct result of the work of the author, predominately through this EngD. This culminated in a system prototype demonstration in an operational environment in the liquid cold plate case study.

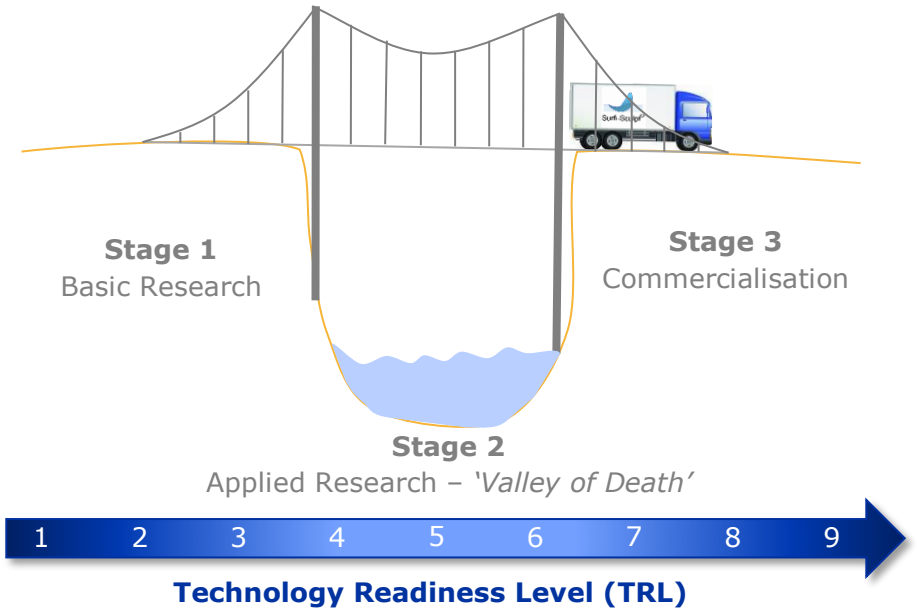

Figure 1.9 Bridging the 'Valley of Death', adapted from Beard et al. (2009).

The author considers the work of this EngD, summarised in this Innovation Report, to be the substructure of the suspension bridge that has provided the framework for these processes to safely progress to TRL 7. The superstructure has been the associated revenue generated by the author for TWI from project work and income. This Innovation Report demonstrates the progression of the technology from TRL 4 up to TRL 7 and from MRL 2 up to MRL 4.

2 Electron Beam Texturing and Surfi-Sculpt Processes

2.1 Background to electron beam texturing and Surfi-Sculpt processes

Basic research investigating the EBT and Surfi-Sculpt processes was conducted until 2010 up to and including the completion of TRL 3 with limited uptake of the technologies in manufacturing environments. The uptake was not increased as a result of the processes being progressed to validation in a laboratory (TRL 4), where the author's work commenced, thus the processes required further validation and demonstration of application.

There are four published books (Bakish and White, 1964; Meleka, 1971; Schiller et al., 1982; Schultz, 1993) forming the basis of current knowledge surrounding EB processing and understanding of the fundamental principles, which have not changed since Dr Stohr's demonstration of EB welding (EBW) in 1954 (Bakish and White, 1964; Meleka, 1971). Dr Stohr's demonstration was the precursor for modern commercial EBW systems used by industrial manufacturers, particularly aircraft and aerospace (American Welding Society, 2007). These industrial systems have been modernised since the 1950s with the addition of computer numerical control (CNC) and electrical software control replacing the mechanical dial controls; however, the basic principles of the equipment have not changed. With minor adaptations, such as the incorporation of the customisable deflection of the beam, any EBW system is capable of the EBT and Surfi-Sculpt processes. Equally, modified SEMs in the region of 30 kV could realise the EBT and Surfi-Sculpt processes (Otten et al., 2012) if equipped with programmable arbitrary waveform function generators controlling the deflection coils and a beam current potential (60 mA) providing a power of 2 kW.

2.2 Literature review

2.2.1 Initial literature search

A systematic literature search was conducted using the Scopus database to ensure that new literature generated since Submission 1 was identified. Since the

EBT and Surfi-Sculpt processes are patented by TWI, much of the know-how resides within the organisation and the aim of the systematic search was to highlight any previously unknown articles; the results are shown in Table 2.1.

Table 2.1 Results from a systematic literature search using the Scopus database.

	Search term (key words)	Results
1	'Electron beam'	740,358
2	TITLE-ABS-KEY (electron AND beam)	236,404
3	TITLE-ABS-KEY ('Electron beam' AND processing)	129,198
4	'Electron beam' and 'processing' and 'surface modification'	20,159
5	'Electron beam' and 'electron beam texturing'	406
6	'Electron beam' and 'electron beam texturing' or 'Surfi-Sculpt'	428
7	'Surfi-Sculpt'	57
8	'Surfi-Sculpt' and 'laser'	31
9	'Surfi-Sculpt' and 'electron beam'	39
10	'Electron beam' and 'processing' and 'surface modification' and 'Surfi-Sculpt'	19

Of the 19 key articles identified through the Scopus database search, twelve were relevant to the author's work (Blackburn and Hilton, 2011; Earl et al., 2012; Earl et al., 2016; Hilton and Nguyen, 2008; Li et al., 2018; Painter et al., 2017; Ramskogler et al., 2017; Taendl and Enzinger, 2014; Temmler et al., 2015; Temmler et al., 2017; Wang et al., 2015; Weglowski et al., 2016). However, Temmler et al. (2017) reported that the 'WaveShape' technology is currently only capable of producing features of up to 300 µm in height. This means that it cannot currently compete with the Surfi-Sculpt process in terms of feature heights created but is a direct competitor to the EBT process.

The remaining seven publications were excluded since two articles were TWI authored review papers incorporating the Surfi-Sculpt process with one including 'Comeld™' which is the application of the Surfi-Sculpt process to a joint between composite materials and metals (Smith, 2004). Comeld was outside the scope of this Innovation Report therefore a further four results were excluded including a book regarding engineering design rationales for hybrid ship hulls. One article was written in Chinese and therefore was not included as it was not possible to

translate. Li et al. (2018) published an English paper which considered the fluid drag reduction of titanium alloys with surfaces textured to heights of 60 μm with an EB. This work demonstrated a fluid-drag reduction efficiency of over 15 %; however, no processing parameters were provided and the study did not consider the mechanism of feature formation beyond that previously reported (Buxton and Dance, 2005; Dance and Buxton, 2007; Buxton and Dance, 2010; Blackburn and Hilton, 2010; Blackburn and Hilton, 2011; Pinto et al., 2014). None of these studies detailed a model of the predicted flow of molten material within the melt pool, which identified a gap in the knowledge. This prompted literature searches on solidification kinetics in weld pools and effects driving these kinetics such as the Marangoni effects. This effect is reviewed in Section 2.2.4 and expanded upon to create a model specific to the EBT and Surfi-Sculpt processes in Section 3.5.

The study by Painter et al. (2017) included the assessment of features produced by the author using the Surfi-Sculpt process through impaction using a 50 mm bore single stage gas gun fired at a velocity of 500 ms^{-1}. The study found that the ramp waves of the pressure and temperature generated by the impact could be reduced by the use of features created by the Surfi-Sculpt process. Ramskogler et al. (2017) investigated the application of the Surfi-Sculpt process to cell growth and this is therefore discussed within the context of the orthopaedic implant case study in Chapter 5.

Figure 2.1 shows a timeline of key activities and development of the EBT and Surfi-Sculpt processes between 1986 and the present day (2020). The light blue boxes summarise the key TWI work prior to the author commencing involvement, including two granted patents (shown in the red boxes): Surface Modification (termed EBT) in 2001, WO 2002/094497 (Dance, 2002), and Workpiece Structure Modification Method (termed Surfi-Sculpt) in 2003, WO 2004/028731

(Dance and Kellar, 2003). The green boxes are work external to TWI including patents such as Popiolkowski et al. (2003) and West et al. (2009). The dark blue boxes summarise the application of innovation by the author based upon work within the EngD and wider activities. These have ensured progression of the processes into further applications. A list of the author's published papers can be found in Appendix A.

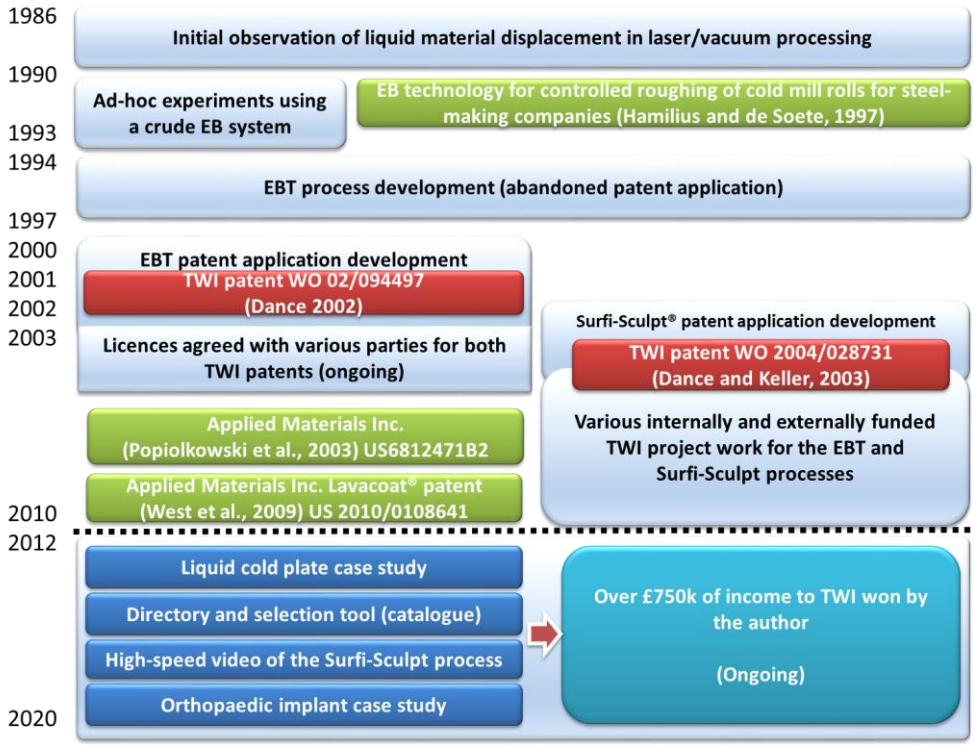

Figure 2.1 Timeline of key events in the development of the electron beam texturing and Surfi-Sculpt processes between 1986 and present day (2020).

A literature review of competing surface modification processes would support comparison and identification of whether the EBT and Surfi-Sculpt processes could be considered unique.

Specific literature reviews were therefore conducted in the following areas:

- Surface modification.
- Solidification kinetics in weld pools.
- Marangoni effects.

The latter two literature reviews support the development of a model (explored in Section 3.5) which discusses the formation of features using the EBT and Surfi-Sculpt processes.

2.2.2 Surface modification

2.2.2.1 Literature review of surface modification

The EBT and Surfi-Sculpt processes are surface modification techniques, therefore a literature review was conducted into the surface modification of titanium, the titanium alloy Ti-6Al-4V, aluminium 6000 series and stainless steel alloys including 316L; since these were all materials investigated using the EBT and Surfi-Sculpt processes during the scope of this EngD. Articles by Cross and Spycher (2008) and Breme et al. (2008) were used to support the creation of a framework for the literature search on surface modification.

Cross and Spycher (2008) highlighted the following two categories of current research for surface modification:

- Development of new surface materials.
- Modification of existing surfaces to promote better bonding.

The development of new surface materials is excluded from this literature review as this encompasses surface treatments, films, coatings, chemical additions or the physical removal or addition of material mechanically. Additive manufacturing (AM) was excluded since it uses powder or deposited wire to create a modified surface therefore it is not considered to use the existing parent material unlike the EBT and Surfi-Sculpt processes. The scope and focus of this literature review is on modification of existing surfaces through the creation of geometric features.

Breme et al. (2008) explained there are two broad categories to alter existing surfaces:

- Structural surface modification altering the surface topography; the EBT and Surfi-Sculpt processes fall within this category.
- Chemical surface modification using thermal, coating or etching techniques.

The search terms used in the surface modification literature search in Weldasearch and Scopus on 18 March 2019 are listed in Table 2.2.

Table 2.2 Weldasearch and Scopus surface modification literature search terms.

	Search terms	Search group metals	Results
1	TITLE-ABS-KEY ((surface W/2 modification) AND melt* AND ("Ti 6Al 4V" or Ti6Al4V) AND NOT TITLE-ABS-KEY (surface W/3 treatment) OR coating* OR film* OR alumina OR Al2O3 OR "Al2 O3" OR "Al 2 O 3" OR CLAD*)	**Titanium alloy (Ti-6Al-4V) results**	30
2	TITLE-ABS-KEY ((surface W/2 modification) AND melt* AND (titanium OR Ti) AND NOT TITLE-ABS-KEY (surface W/3 treatment) OR coating* OR film* OR alumina OR Al2O3 OR "Al2 O3" OR "Al 2 O 3" OR CLAD*) AND NOT ("Ti 6Al 4V" or Ti6Al4V) AND NOT TITLE-ABS-KEY (surface W/3 treatment) OR coating* OR film* OR CLAD*)	**Titanium results** *(with duplicates from search 1 removed)*	125
3	TITLE-ABS-KEY ((surface W/2 modification) AND melt* AND (aluminium OR aluminium OR al OR aa) AND KEY (Al Si Mg alloy) AND NOT TITLE-ABS-KEY (surface W/3 treatment) OR coating* OR film* OR alumina OR Al2O3 OR "Al2 O3" OR "Al 2 O 3" OR CLAD*)	**Aluminium 6000 series (Al Mg Si alloys) results**	41
4	TITLE-ABS-KEY ((surface W/2 modification) AND melt* AND (*316l or "316 L") AND NOT TITLE-ABS-KEY (surface W/3 treatment) OR coating* OR film* OR CLAD*)	**Stainless steel (316L) results**	17
5	TITLE-ABS-KEY ((surface W/2 modification) AND melt* AND (austenitic) AND NOT TITLE-ABS-KEY (surface W/3 treatment) OR coating* OR film* OR CLAD*) AND NOT TITLE-ABS-KEY ((surface W/2 modification) AND melt* AND (*316l or "316 L") AND NOT TITLE-ABS-KEY (surface W/3 treatment) OR coating* OR film* OR CLAD*)	**Austenitic stainless steels results** *(with duplicates from search 4 removed)*	44

Figure 2.2 shows the breakdown of the wider search criteria to explore 22 relevant papers of which 10 papers were identified as being of interest and relevant to the literature review on structural surface modification and had not previously been reviewed. Other reasons for relevant papers to be discounted

included being duplications of the same work and not being able to be obtained. The 10 relevant papers identified and explored were Balla et al., 2014; Blake, 1998; Breme et al., 2008; Chikarakara et al., 2012; Man et al., 2003; Panin et al., 2018; Rotshtein and Shulov, 2011; Uno et al., 2018; Yang et al., 2006; Zou et al., 2008.

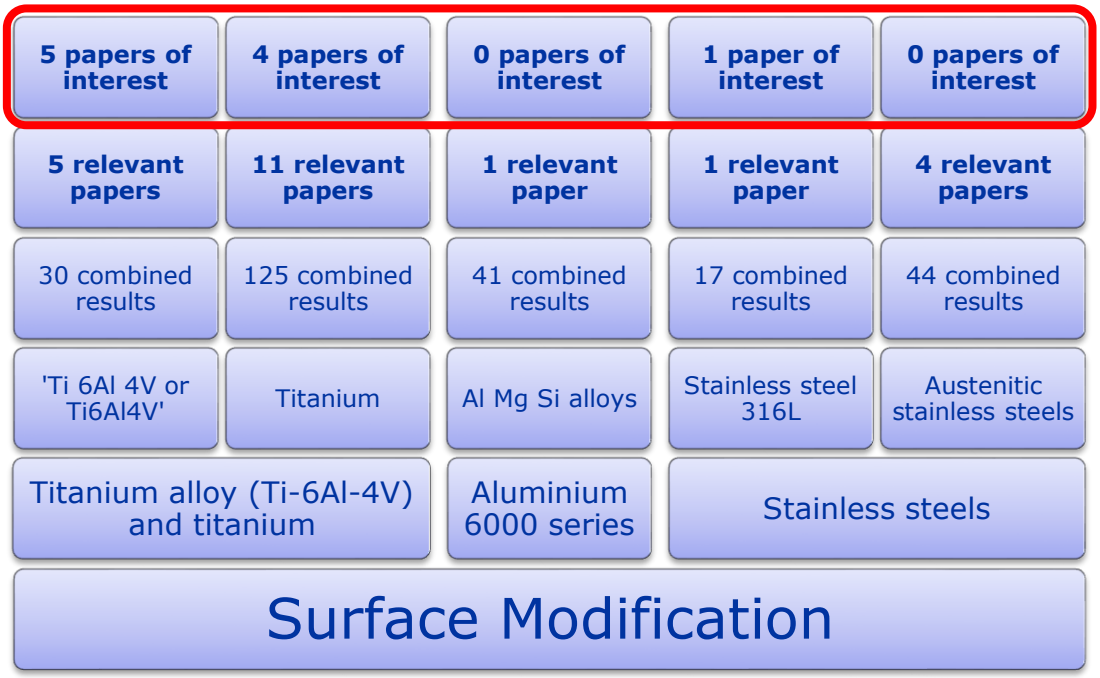

Figure 2.2 Breakdown of combined Weldasearch and Scopus results on surface modification literature search.

Two of the papers identified (Man et al., 2003; Blake, 1998) incorporated a gas during processing to achieve surface modification via chemical changes. Man et al. (2003) used nitrogen gas to nitride the surface of Ti-6Al-4V whilst Blake (1998) developed a surface modification process to produce metal surfaces as part of the flexible laser automated intelligent research (FLAIR) programme using a 50 W CO_2 laser. These both fall within chemical surface modification and not structural surface modification therefore they are unlike the EBT and EB Surfi-Sculpt processes, which do not use any gas or additional material to alter the surface, and were excluded from the literature review.

Yang et al. (2006) explained that the ultimate success of an orthopaedic implant is reliant upon the optimisation of the local surface structure due to the fact that the resultant topology has the ability to transfer load and encourage bone ingrowth, although other factors such as quality bone formation can also impact on the success. Yang et al. (2006, p. 75) concluded that '*the performance of implant devices can be improved with better understanding of osseointegration and its enhancement with surface-modified titanium implants'*.

A Japanese company, Daicel, developed a competing mechanism to the EBT and Surfi-Sculpt processes using a continuous wave Ytterbium fibre laser at 1070 nm wavelength called DLAMP™. Figure 2.3 shows that the process creates anchor features which are achieved by creating molten material which permeates through the undercuts and tunnel-like structures (Uno et al., 2018).

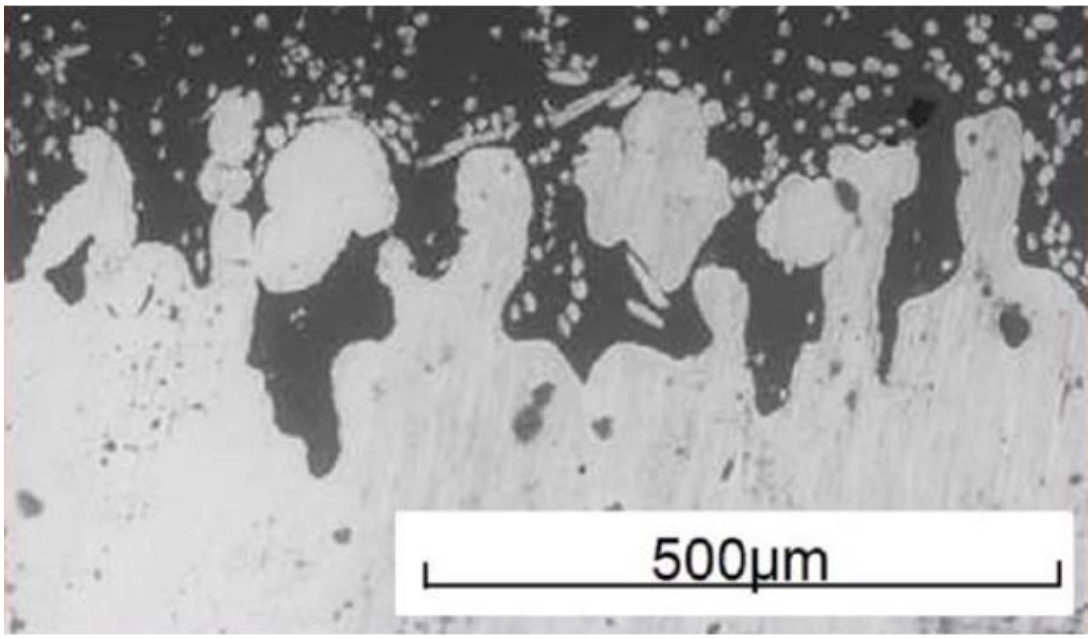

Figure 2.3 Cross-section of jointed area of metal/plastics joining part using DLAMP™ (TWI Ltd, 2019).

Uno et al. (2018) presented work on aluminium alloy 5052, austenitic stainless steel 304 and brass 2801. These wide range of materials were investigated for application in the automotive industry. A galvo scanner was used to manipulate

the beam (also used for the laser Surfi-Sculpt process) and the scanning speed was 10 m/s. The scanning speed detailed was higher than those observed in the EBT and Surfi-Sculpt processes (see Section 7.4). The surfaces were revisited by the beam which is similar to the Surfi-Sculpt process; however, valleys and trenches were created instead of protrusions because the high scanning speed prevented molten material forming into features. The surfaces appear to be irregular after the first pass and the maximum depth achieved using the DLAMP™ process was approximately 700 μm after 60 repetitions. Whilst the methodology of manipulating molten material using a power beam is common with both the EBT and Surfi-Sculpt processes, the resultant surfaces using the DLAMP™ process appear to be more closely aligned to the EBT process than the Surfi-Sculpt process. The high scanning speed (10 m/s) may explain why the depth of the valleys and trenches were similar to those observed using the EBT process since the beam is travelling faster than is required for allowing remelted material to form features.

Rotshtein and Shulov (2011) explored the use of low-energy high current electron beams (LEHCEBs) with an accelerating voltage of up to 40 kV and a beam current of up to 50 kA at microsecond durations; the electrons were reported to have penetrated ~1 μm into the surface. However, the author does not agree with this calculated penetration depth; instead calculating the depth to be 7 μm for Ti-6Al-4V using the formula to calculate the penetration depth of electron beams, Equation 4, which is discussed in Section 2.4. At energy densities of 2-5 J/cm^2, it was observed that only a thin surface layer of the material absorbed the electron energy. In the case of Ti-6Al-4V a layer of ~5 μm was affected by the process resulting in globular alpha (α) grains. Analysis of the surfaces was performed by SEM, X-ray diffraction, layer-by-layer transmission electron microscopy and Auger electron spectroscopy. The energy input was less than the 100s of J/m observed in the EBT and Surfi-Sculpt process (see

Section 7.4). Furthermore, the fact that no beam deflection was used, but rather beam pulsing (forty times) at 0.1 Hz, explained why no protrusions and intrusions were formed. Rotshtein and Shulov (2011) presented results for both the aluminium alloy, Al6061, and the titanium alloy, Ti-6Al-4V, demonstrating enhancement of the properties of the surface through improved corrosion resistance which was the result of distributing the impurities uniformly through the processed material. This is closer to the EBT process rather than the Surfi-Sculpt process as distinct geometric features on a millimetre scale were not formed from the parent material. The paper noted that the surface roughness was decreased by up to 0.1 μm (with a reported maximum R_a of ~0.2 μm when followed by vacuum annealing); this peculiarity led the author to consider that the original surface roughness must have been higher than machined surfaces that are typically used for the EBT and Surfi-Sculpt processes in order for it to decrease as a result of processing. Similar work, using LEHCEBs, was also reported by Zou et al. (2008, p. 4) using up to 10 pulses of the beam which concluded that '*as a result of the quasi-static thermal stresses and shock waves produced by the* [EB] *treatment, a deformation induced martensitic transformation is triggered in the sub-surface of the material'*..

Panin et al. (2018) and Chikarakara et al. (2012) achieved similar thicknesses of the modified molten layer below the surface (~70 μm) using either an EB or a laser as a power beam source with powers ranging between 1.5 and 1.8 kW with an energy density of 450 – 2,096 J/cm^2 either continuously or, in the case of the laser, pulsed at 3 kHz. Furthermore, Balla et al. (2014) achieved a melted depth of 1.2 mm using a higher maximum energy density laser of 0.68 J/cm^2 through a single pass of the beam over the surface. None of these papers reported the use of beam deflection to enhance the formation of features and none of these processes demonstrated the creation of features as a result which is a

fundamental aspect of the modification of surfaces using the EBT and Surfi-Sculpt processes.

2.2.2.2 Surface modification summary

In conclusion, the Surfi-Sculpt process appears to be unique as literature searches have not revealed any other processes which transform existing material (with no addition to or subtraction from it) to create structural surface modification with geometric features on a millimetre scale.

Conversely, the literature searches have revealed competing processes to the EBT process; two such examples are 'WaveShape' reported by Temmler et al., (2017) and DLAMP™ reported by Uno et al. (2018). These processes can create structural features using only the parent material and no additional material or subtractive processes on a sub millimetre scale.

2.2.3 Solidification kinetics in weld pools

2.2.3.1 Literature review on solidification kinetics in weld pools

The scope and focus of this literature review is on modification of existing surfaces through the creation of geometric features. To achieve these features microstructural changes occur i.e. the EB applies a heat treatment on the existing material since it is a power beam process. The heat treatment is not the main aim of the EBT and Surfi-Sculpt processes; instead it is a by-product of the processes. However, a literature search and review was conducted to support the development of a model of predicted flow of molten material within the melt pool in the EBT and Surfi-Sculpt processes as this was identified as a gap in the knowledge in Section 2.2 and increased knowledge in this area would support the development of predictive modelling of the EBT and Surfi-Sculpt processes.

The search terms used in the solidification kinetics in weld pools literature search in Weldasearch and Scopus on 18 March 2019 are listed in Table 2.3.

Table 2.3 Solidification kinetics in weld pools literature search terms.

	Search terms	Search group title	Results
1	TITLE-ABS-KEY ((solidification) AND melt* AND KEY (molten pool) AND KEY (eb welding) AND KEY (titanium)	**Titanium results**	5
2	TITLE-ABS-KEY ((solidification) AND melt* AND KEY (molten pool) AND KEY (eb welding) AND KEY (titanium)	**Aluminium results**	12
3	TITLE-ABS-KEY ((solidification) AND melt* AND KEY (molten pool) AND KEY (weld*) AND NOT TITLE-ABS-KEY ((solidification) AND melt* AND KEY (molten pool) AND KEY (eb welding) AND KEY (titanium) AND NOT TITLE-ABS-KEY ((solidification) AND melt* AND KEY (molten pool) AND KEY (eb welding) AND KEY (titanium)	**General welding results**	6

Figure 2.4 shows the breakdown of search criteria to explore 23 papers of which nine papers were identified as relevant to the solidification kinetics in weld pools literature review having not been reviewed in previous Submissions. Reasons for papers from the search results to be excluded were not being directly relevant or multiple editions of the same book being available. The nine relevant papers identified and explored were Arata et al., 1976; Babu et al., 2001; Brooks and Mahin, 1990; Cooper, 2005; Cooper and Lambrakos, 2005; David and Vitek, 1989; Kou, 2002; Short, 2009; Terentyev et al., 2015.

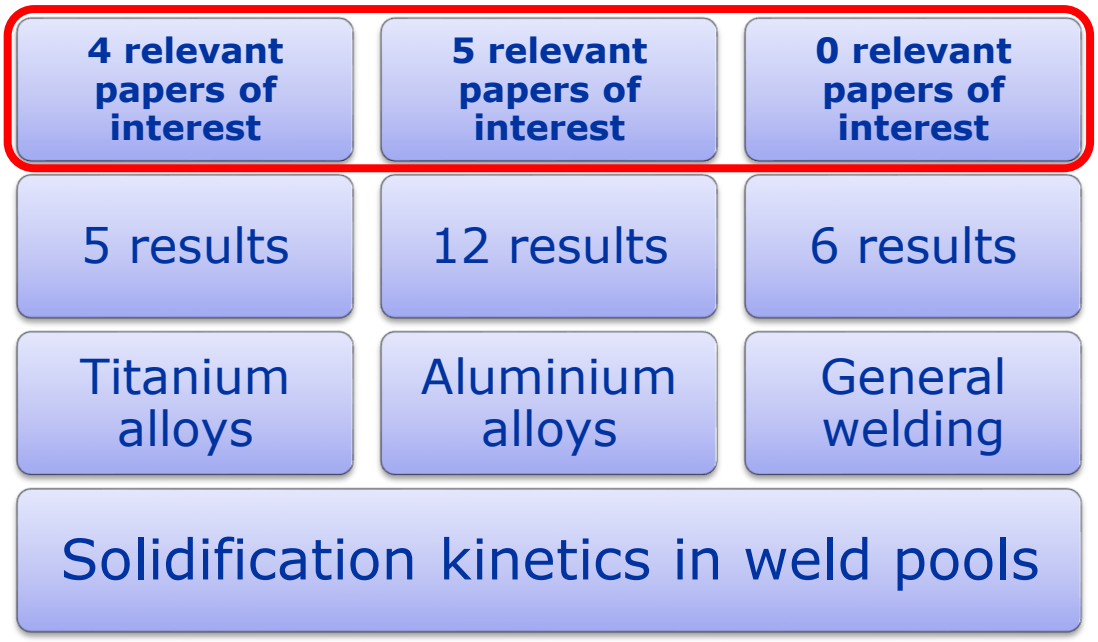

Figure 2.4 Breakdown of combined Weldasearch and Scopus results on solidification kinetics in weld pools literature search.

Terentyev et al. (2015) concluded that, in the 1G processing position (beam interacting vertically down on the workpiece), conditions were optimal for solidification of the molten material since at the weld root liquid melt is prohibited from being discharged at higher welding speeds. The liquid metal at the front wall of the beam workpiece interaction was displaced downwards during free formation; this was corroborated by a review paper written by Weglowski et al. (2016). Terentyev et al. (2015) determined that, assuming a constant solidification rate, the discharge of liquid metal is reduced by an increase in the processing speed. The assumption that the solidification rate is constant could be argued as appropriate for single pass EBW (although the material will heat up and thus over time this will be incorrect), however, the multiple swipes of the EBT and Surfi-Sculpt processes mean that the solidification rate decreases as the temperature of the parent material increases. The liquid metal being displaced downwards during formation supports the development of the model of the predicted flow of molten material within the melt pool in Section 3.5.

There are four solidification modes (David and Vitek, 1989; Kou, 2002):

- Cellular.
- Planar.
- Columnar dendritic.
- Equiaxed dendritic.

Fine columnar solidification substructure is often observed in high precision EB processing which is finer than other fusion processes such as metal inert gas (MIG) or tungsten inert gas (TIG) welding (Babu et al., 2001). This is due to the comparatively low heat input and thermal impact on the material. Arata et al. (1976) stated that the thermal efficiency of the EB process was 0.8 which is higher than 0.6 for TIG therefore more of the energy is transferred into the workpiece using EB than for TIG. This means that the EB process can be considered more efficient at transferring energy and as such is well suited to the EBT and Surfi-Sculpt processes.

Cooper (2005) considered the use of wire-feed electron beam additive manufacturing (W-EBAM) where a series of overlapped weld pools were observed in each layer and the melt pool. The paper did not report any beam manipulation to affect the melt pool geometry nor the melt pool being revisited rapidly after initial solidification suggesting that the microstructure observed in Figure 2.5 had more similarities to that in multi-pass welding and not the EBT and Surfi-Sculpt processes. Figure 2.5 shows a TWI setup (not the same as Cooper, 2005) and cross section of a build using W-EBAM which is a direct energy deposition (DED) AM process using EB to create structures layer by layer through the introduction of a wire under the electron gun and into the melt pool.

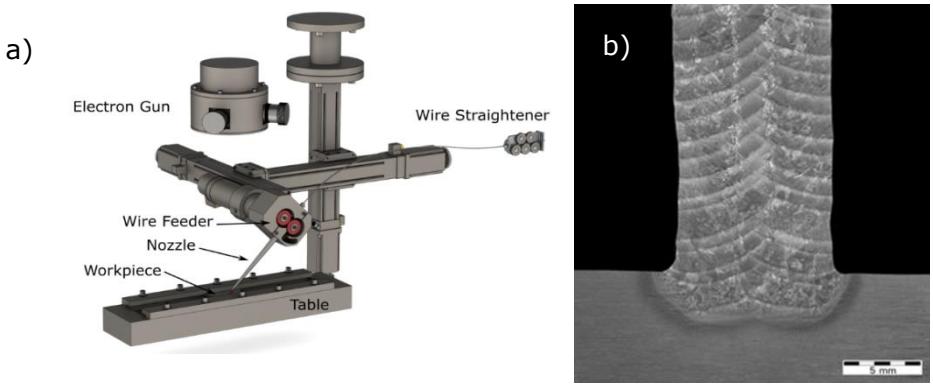

Figure 2.5 Wire-feed electron beam additive manufacturing (W-EBAM):
a) Setup of introduction of a wire under the electron gun and into the melt pool;
b) Transverse microstructure of W-EBAM build created using two beads per layer.
© Courtesy of TWI Ltd

2.2.3.2 Ti-6Al-4V metallurgy

Ti-6Al4V is an alpha and beta (α and β) titanium alloy; therefore, at room temperature, the microstructure is a mixture of hexagonally close packed α phase and body centred cubic β phase. During solidification and cooling to room temperature, liquid Ti-6Al-4V solidifies as β phase and then transforms to a mixture of α and β via a solid state phase transformation once the temperature falls below the β transus temperature which is approximately 995 °C for Ti-6Al-4V (Lütjering and Williams, 2007). The α and β phase fractions and morphologies in the room temperature microstructure are dependent upon the thermomechanical processing history of the material.

The columnar solidification substructure (David and Vitek, 1989; Kou, 2002) can be observed in a geometric feature created using the Surfi-Sculpt process in Ti-6Al-4V which is shown in Figure 2.6 and 2.7 (from Submission 6, the orthopaedic implant case study). It is possible to observe the equiaxed α with intergranular β microstructure of the parent material in its conventional wrought condition (mill annealed Ti-6Al-4V). The parent material used in Figure 2.6 had a microstructure that consisted of recrystallised α/β grains; this was also witnessed by Oluleke (2014).

Figure 2.6 Macrostructure of Ti-6Al-4V feature created using the Surfi-Sculpt process (blue square denotes location of Figure 2.7) etched in 0.4 % nitric acid and 0.7 % hydrofluoric acid.

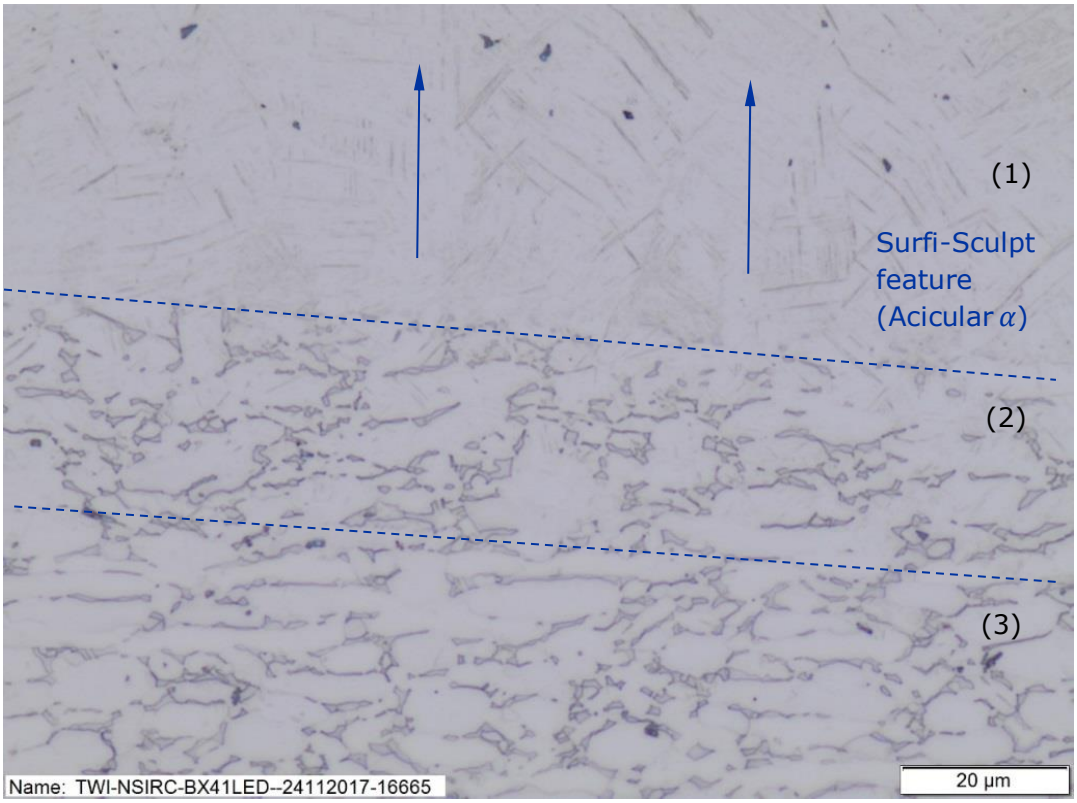

Figure 2.7 Change in microstructure observed between the parent material (3), heat affected zone (2) and the feature (1) in the protrusion created using the Surfi-Sculpt process.

There is evidently a change in microstructure caused by the EBT and Surfi-Sculpt processes. The observed microstructure had acicular α in the geometric feature produced and a mixture of intergranular β grains and a fine lamellar α transformation microstructure in the narrow (15 μm) heat affected zone (HAZ) which was also observed by Ramskogler et al. (2017) and Oluleke (2014) for the Surfi-Sculpt process. The latter study observed grains formed in the direction of heat flow which can also be seen in Figure 2.7 as highlighted by the vertical arrows. However, due to the multiple thermal cycles of the Surfi-Sculpt process, it is not possible to ascertain the solidification morphology (whether it is dendritic or not) since the thermal cycle caused by each subsequent swipe of the beam remelts the material and, as such, creates a new (modified) morphology each swipe.

Figure 2.8 (Oluleke, 2014) shows electron backscatter diffraction (EBSD) mapping of a similar feature to that of Figure 2.6; the prior β grains ranged in size from 32 μm and 67 μm at a height of 100 μm and 500 μm above the HAZ, respectively. Oluleke (2014, p.322) concluded that the microstructure of the *β* grains after the creation of the features demonstrated *'coarse columnar β grains that developed by epitaxial re-growth from the base plate'* rising vertically then diverging in the direction of heat flow. This was specific to the orientation and sequencing of the swipes used in a pattern.

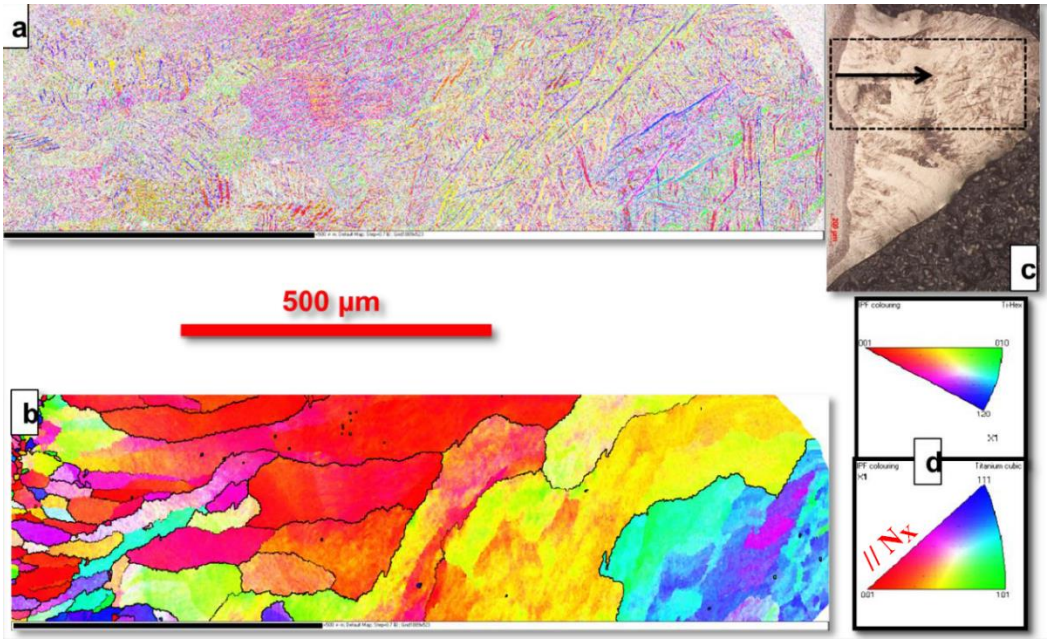

Figure 2.8 EBSD mapping of a similar feature to that in Figure 2.6
(Taken from Oluleke, 2014, Figure 5.60, used with permission)
a) Raw data of the room temperature alpha;
b) A reconstructed high temperature EBSD Map of the prior beta grains;
c) Optical image of the sample with an insert of the EBSD area;
d) IPF colour legend for both the alpha phase and high temperature beta phase.

This substructure is as a result of the thermal cycle of the material at a given location which determines the phase transformation (Short, 2009). Continuous cooling transformation (CCT) diagrams are beneficial to understanding the effect of the cooling rate on the transformation, however their application to the EBT and Surfi-Sculpt processes is limited since CCT diagrams are for single heat cycles and not multiple heat cycles, ie if subsequent heat treatments induce melting then the CCT describes what happens upon resultant cooling. A swipe can be processed in 1.35×10^{-4} seconds if the frequency is 10.55 Hz and there are 70 swipes in a motif. This means that traditional metallurgy models from arc welding or power beam welding cannot be directly applied as the depth that each swipe affects the thermal history of the material and preceding swipe is not currently known. The estimated cooling rate ranges for traditional EB surface modification process are 10^5 to 10^7 K/s (Elmer et al., 1989). With high precision EBW, traditionally the cooling rate is considered to be higher (~550 K/s) than other fusion processes, as stated by Brooks and Mahin (1990) and Short (2009),

which leads to modified microstructures. However, for the Surfi-Sculpt process, the EB revisits the same location multiple times unlike traditional EB surface modification processes and thus an age hardening effect can be observed as a result of the decreased cooling rate. Each swipe of the beam causes a heat treatment on the material moved in the previous swipe and will alter the microstructure of both the remelted material and the material beneath it in the HAZ. Furthermore, the revisiting of the EB can also reduce the cracking noted by Brooks and Mahin (1990) associated with high speed EB processing therefore minimising the degree of cracking observed in features created using the Surfi-Sculpt process.

Cooper and Lambrakos (2005) reported that the liquid-solid interface alloy liquidus temperature for Ti-6Al-4V was ~ 1530 °C and that the melt temperature below a heat source such as an EB was ~ 2500 °C. Therefore, each swipe of the beam causes the material beneath to rise above the liquidus temperature and the approximate 995 °C β transus temperature for Ti-6Al-4V (Lütjering and Williams, 2007). This is the temperature above which only β transformed microstructures are formed; below this, both α and β transformed microstructures are formed. Coarse β grains form during the rapid cooling of the feature between each swipe of the beam. The peak temperatures and cooling rates experienced by the material influence the microstructures attained in the protrusions. The peak temperatures also influence the grain size with higher peak temperatures resulting in larger grain size typically. As described by CCT diagrams, the cooling rate influences the microstructure that is formed in the protrusion and the associated HAZ. Each protrusion experienced hundreds of thermal cycles (dependent on the duration of processing and frequency of deflection) with the effective preheat increasing for each cycle; thus the effective inter pass temperature rose for each cycle.

To understand the thermal cycling caused by the Surfi-Sculpt process, a type K thermocouple was attached in the middle to the underside of a 10 mm thick 64 mm diameter coupon directly below where four solid cone features were created, as shown in Figure 2.9. In order to calculate the number of heat cycles, the *UV* frequency which controls the repeats for each feature (in this case 10.55 Hz) was used to determine the time period to return to a single feature (in this case, 0.095 seconds). The total beam on time was 19.5 seconds compared to a total 79.5 seconds processing time. Therefore, the total number of repeat swipes of the beam (and thus heat cycles) for each feature was 206.

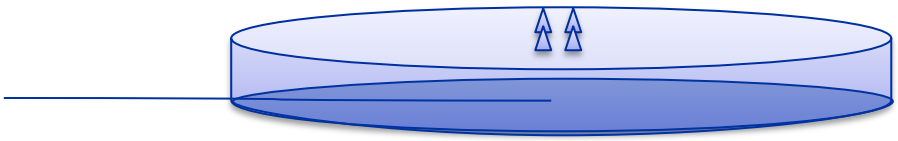

Figure 2.9 Location of thermocouple attached to the underside of the coupon in the middle.

Figure 2.10 shows the temperatures recorded on the base of the coupon and the thermal cycle for the 10 mm coupon demonstrating the relatively slow cooling rate that was achieved through the multiple heats cycles.

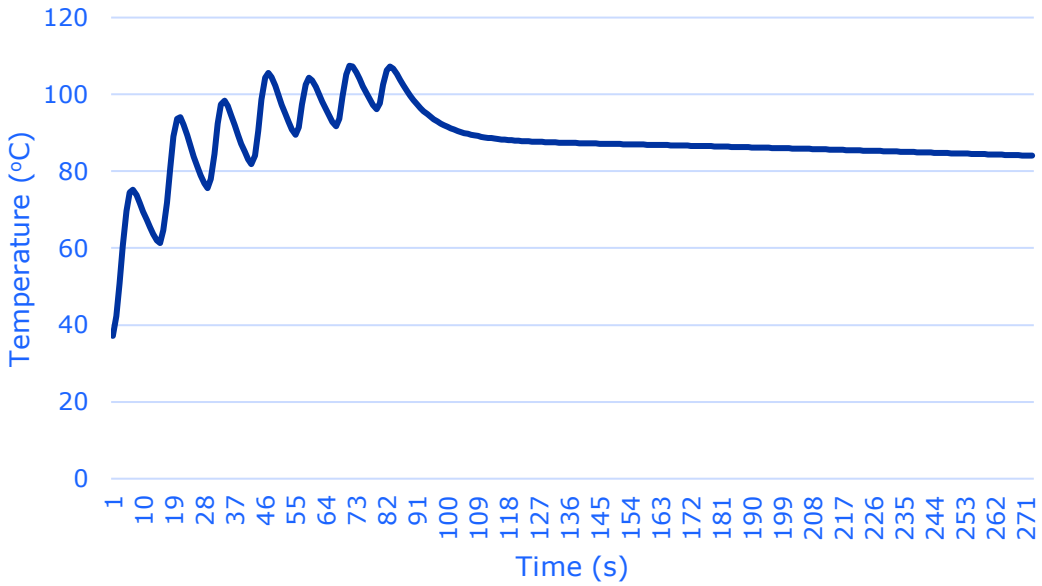

Figure 2.10 Thermocouple data on 10 mm thick coupon for cones created using the Surfi-Sculpt process.

The limitation of this work was that only the temperature of the base of the coupon was recorded and not the features. The final peak temperature of 107 °C was seen approximately 5 seconds after the processing was completed. It is possible to only observe seven peaks of temperature rises over the 206 heat cycles due to the delay of the thermal mass of the coupon.

The melting point and β transus can be influenced by elemental losses. A loss of aluminium concentration was found to be affected by the build height, size, swipe pattern and heat exposure to the EB as a result of the Surfi-Sculpt process (Oluleke, 2014). Oluleke (2014, p.270) reported that '*both the duration of beam contact with the substrate and the movement of the beam had an impact on the resulting material structure, chemistry and properties'*. Therefore, less heterogeneity in composition and microstructure was achieved when beam swipes from multiple locations around the feature were utilised since Oluleke (2014) stated that uni-directional swipes resulted in more evaporation of aluminium.

Figure 2.11 and 2.12 show a SEM image of simple uni-directional beam swipe geometric features using secondary electron type 1 detection (SE1); it is possible to see the unprocessed material between the features and the intrusions. Each feature has a rounded tip due to the characteristic surface tension of the solidifying molten material; this was as a result of the volume of material being moved by each swipe of the beam. A more intense (high brightness) EB with a smaller spot size could ensure the formation of features with sharper peaks due to the smaller volume of material being melted, moved and re-cast with each swipe.

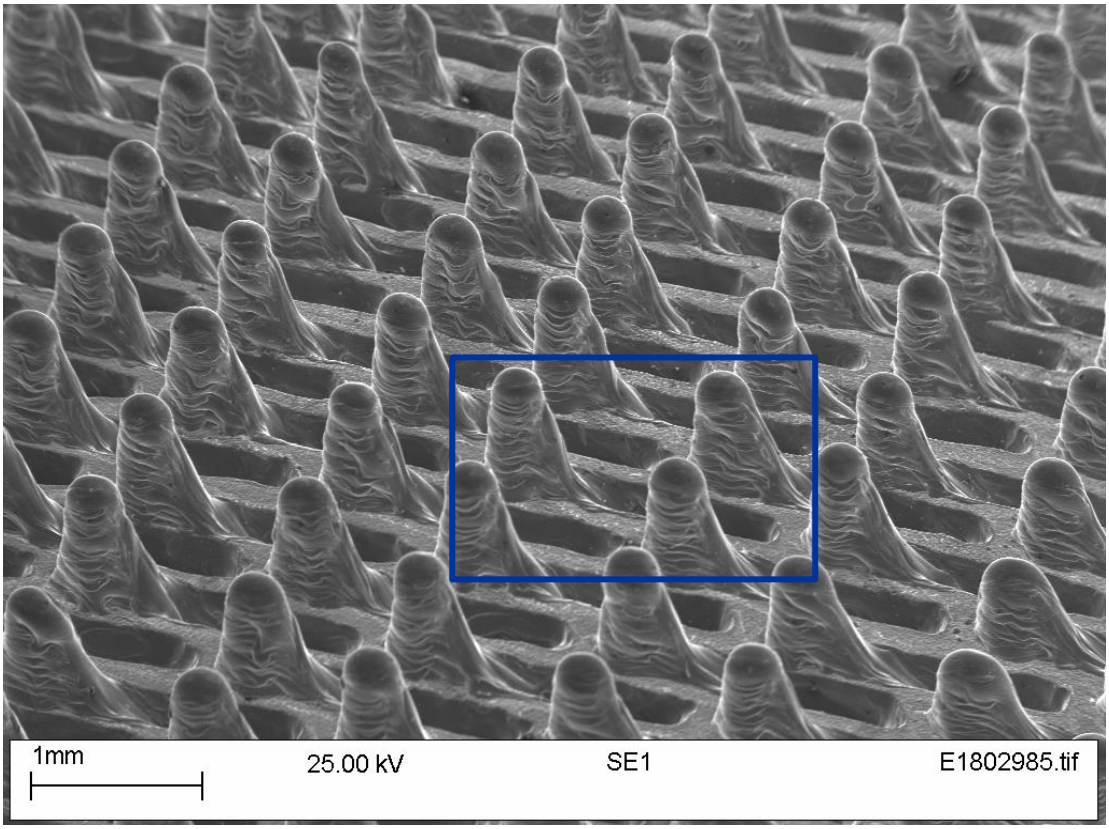

Figure 2.11 Scanning electron microscope image of simple uni-directional swipe pattern protrusions (blue square denotes location of Figure 2.12).

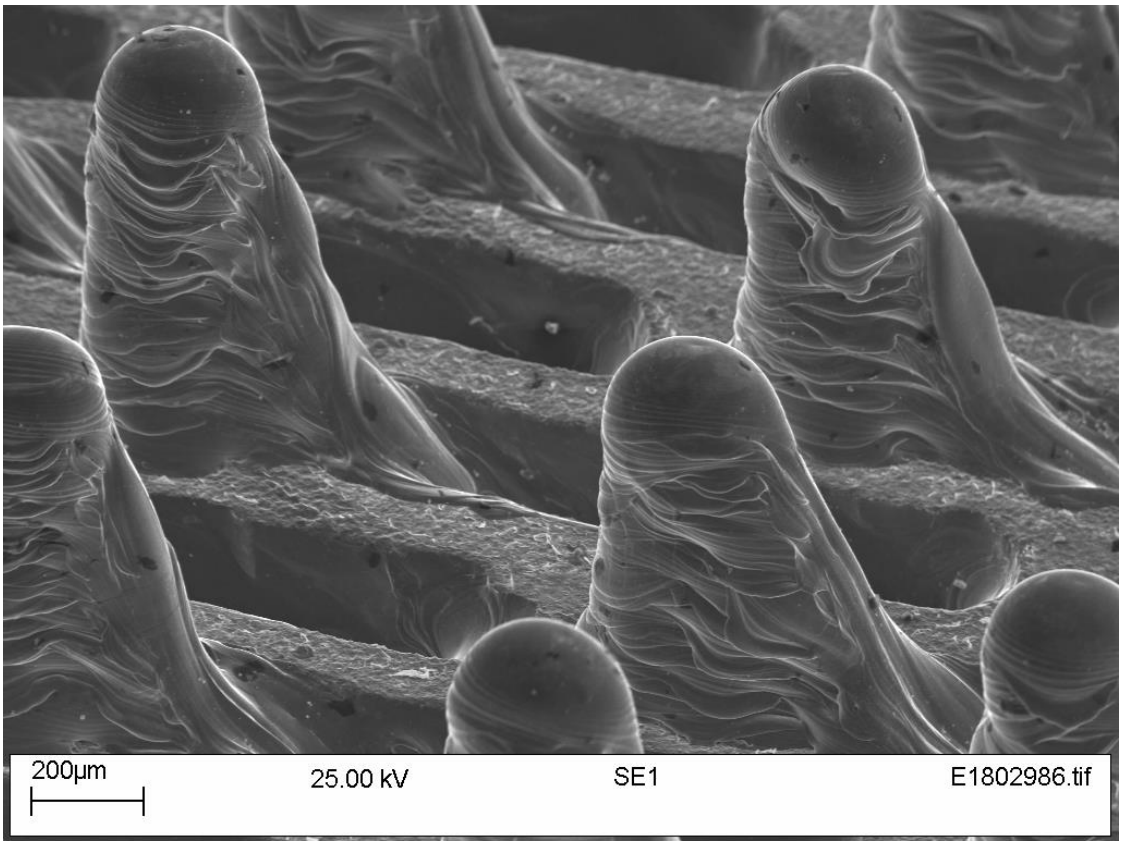

Figure 2.12 Scanning electron microscope image of focussing on a single uni-directional swipe pattern protrusion and associated intrusion.

2.2.3.3 Solidification kinetics in weld pools summary

Previous work on solidification kinetics in EB weld pools has considered single pass processing or slow cycle multi-pass welding such as MIG and TIG. The example Ti-6Al-4V feature created using the Surfi-Sculpt process displayed acicular α whereas, in the narrow (15 µm) HAZ, a mixture of intergranular β grains and a fine lamellar α transformation microstructure was observed. However, due to age hardening of the Surfi-Sculpt process caused by the multiple rapid thermal cycles, it was not possible to establish whether the solidification morphology was dendritic or not. This was because each subsequent swipe of the beam remelts the material forming a new (modified) morphology after each swipe. The morphology of the feature will be governed by the duration of processing and frequency of deflection with the effective preheat increasing for each swipe and thus the effective inter pass temperature rising for each cycle.

2.2.4 Marangoni effects

In order to model the predicted flow of molten material within the melt pool using the EBT and Surfi-Sculpt processes, a literature search and review of the Marangoni effects in relation to welding was performed since this was highlighted as a gap in the knowledge in Section 2.2. The search terms used in Weldasearch and Scopus on 18 March 2019 are listed in Table 2.4.

Table 2.4 Marangoni effects literature search terms.

	Search terms	Search group title	Results
1	TITLE-ABS-KEY ((marangoni W/2 (effect* OR force*) AND "surface tension*" AND (aluminium OR aluminum OR titanium OR Al OR Ti) AND NOT TITLE-ABS-KEY ((marangoni W/2 (effect* OR force*) AND "surface tension*" AND (aluminium OR aluminum OR titanium) AND TITLE-ABS-KEY (eb OR "electron beam*") OR weld*)	**Weldasearch results**	6
2	TITLE-ABS-KEY ((marangoni W/2 (effect* OR force*) AND "surface tension*" AND (aluminium OR aluminum OR titanium OR Al OR Ti) AND NOT TITLE-ABS-KEY ((marangoni W/2 (effect* OR force*) AND "surface tension*" AND (aluminium OR aluminum OR titanium) AND TITLE-ABS-KEY (eb OR "electron beam*") OR weld*)	**Scopus results**	20

Figure 2.13 shows the breakdown of the wider search criteria to explore 26 papers of which seven papers were identified as being of interest and relevant to the literature review on the Marangoni effects. Reasons for papers to be excluded were that they considered the use of drilling or AM techniques, such as using the addition of wire or coatings, or where there were multiple editions of the same book or article including those published in multiple languages such as English and Japanese. The seven relevant papers identified and explored were Abbott, 2017; Bruyere et al., 2013; Khorasani et al., 2018; Ohmura et al., 2000; Pang et al., 2009; Prűss et al., 2016; Tseng and Li, 2019.

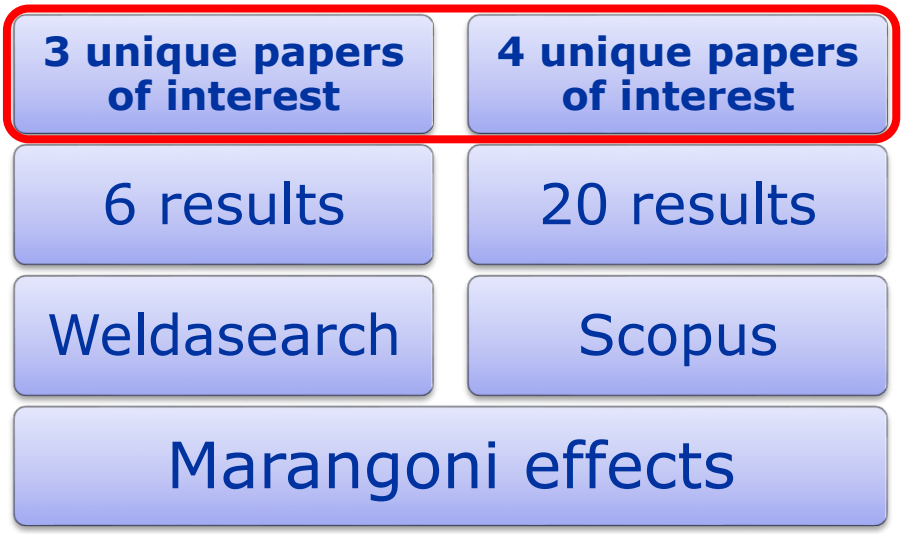

Figure 2.13 Breakdown of combined Weldasearch and Scopus results on Marangoni effects literature search.

Bruyere et al. (2013) studied the thermohydraulic evolution of laser welding on Ti-6Al-4V and considered the Marangoni effects in their numerical model. Their model predicted the temperature at t = 1 and 5 ms and showed that the edge of the melt pool, away from the beam, had the highest velocity vectors since the liquid accumulated at the melt pool periphery as it was ejected. This ejection of material is not observed in either the EBT or the EB Surfi-Sculpt processes; it has however been observed in laser Surfi-Sculpt, as discussed further in Section 2.4. At t = 10 ms a keyhole was being formed in which Bruyere et al. (2013) predicted large velocity vectors adjacent to the vapour column; however, this can no longer be considered representative of the EBT and Surfi-Sculpt processes since there is no vapour column present during these processes.

Prűss et al. (2016) reported that the Marangoni effects which result from the temperature dependence of the surface tension have not been previously considered in thermodynamic models. The paper concluded that a continuous or 'global existence solution' model was created which could calculate the Marangoni force even to the extremities of the model. The mathematical assumptions used in the paper are complex and cannot be verified or robustly argued by the author; thus the model cannot be directly applied to the real world processing of the EBT and Surfi-Sculpt processes and, as such, it was not incorporated into this EngD.

The surface tension coefficient of liquid metal in a vacuum (of ~$6x10^{-3}$ mbar), present in the EBT and Surfi-Sculpt processes, is unknown but this can be considered to be lower than that of air (or argon, if a gas shield is used) which is present for lasers. In the case of EB processing occurring in a vacuum, a decreased surface tension results from the greater attraction of liquid molecules to each other than the attraction to a vacuum. As the temperature increases the surface tension decreases and therefore the propensity of the molten material to flow increases. This however is in opposition to the viscosity of the liquid metal

which is greater in air than in a vacuum. Work completed in Submission 3 concluded that an increase in the viscosity of the molten material (for example, via a change in chemical composition of the parent material such as a decrease in Si content of 0.30 - 0.60 % compared to 0.70 - 1.30 %) improves the material's stability during the Surfi-Sculpt process and higher features can be produced. In this example, feature heights of up to 6.1 mm were successfully created in the lower Si content material compared to 3.3 mm height achieved with a higher Si content.

The Marangoni number is the ratio between the thermocapillary effect and the viscous forces (Comsol, 2017). Abbott (2017, p. 245) calculated the Marangoni number (Ma) using the following formula in Equation 1 for '*a liquid layer of thickness L, viscosity η, and thermal diffusivity ∝, with a surface tension γ which changes with temperature at a rate ∂γ/∂T'*:

$$Ma = -\frac{\delta\gamma}{\delta T} \times \frac{L\Delta T}{\eta \cdot \propto} \qquad \textbf{Equation 1}$$

Pang et al. (2009) simulated the creation of a keyhole in laser welding. Section 2.3.1 discusses the mode by which the EBT and Surfi-Sculpt processes occur, which is not the keyhole mode, and thus the conclusion by Pang et al. (2009, p.75150T-9) that '*the surface tension forces play negligible effects after the keyhole starts to form*' cannot be applied. Instead it may be possible to infer from the conclusion that surface tension forces have a significant role prior to the keyhole forming when there is a melt pool; however, this is not explicitly stated by Pang et al. (2009).

Tseng and Li (2019) considered the melt pool dynamics for the AM process, selective laser melting. This AM process consolidates powder through use of a

laser beam as a power beam heat source. Despite the differences (and therefore limitations in applicability) to the EBT and EB Surfi-Sculpt processes, namely application of the beam to powder rather than parent material and the fact that a laser was used (whereby the ejection of material was observed by Bruyere et al., 2013), several key points can be considered applicable to the EBT and EB Surfi-Sculpt processes. A key point from the modelling work by Tseng and Li (2019) were that two stages were reported in the melt pool dynamics on Ti-6Al-4V at beam scanning speeds of 1.25 m/s in the first ~60 μs of beam-material interaction. The first was dominated by the Marangoni effects which supported the melt pool suppression causing movement of the boundary of the melt pool upwards and subsequent capillary force of the melt flow of 4 – 8 m/s. The author considers this a primary driver as to why the bulge is observed in the EBT and Surfi-Sculpt processes and supports the formation of the protrusion from the upwards movement of the boundary of the melt pool and intrusion from the melt pool suppression respectively.

The second stage (between ~60 μs and 320 μs of beam-material interaction) reported by Tseng and Li (2019) detailed that the Marangoni effects weakened and the surface tension of the molten material had the greater influence on the melt pool morphology causing circulation within the melt pool. The author reflects that the interaction time between the beam and the material for the EBT and Surfi-Sculpt processes cannot currently be reported but use of higher speed filming than that discussed in Chapter 3 should allow for this interaction time to be calculated more precisely.

Furthermore, Tseng and Li (2019) considered the melt pool dynamics in relation to uniformly packed powder particles not the parent material as well as processing in an argon environment and not a vacuum which additionally

differentiates the work that was completed from its application to the EBT and Surfi-Sculpt processes.

Khorasani et al. (2018) reported 'excessive' Marangoni effects in the AM process, electron beam melting (EBM®) which was supported by Rai et al. (2009). However, this 'excess' is not quantified and is considered an issue for the EBM process leading to surface quality issues and unstable melting pool. Conversely, it is an unstable melt pool which drives the formation of features in the EBT and Surfi-Sculpt processes. The same limitations described for the work by Tseng and Li (2019) can be considered since Khorasani et al. (2018) also discussed the melt pool dynamics for the AM process, selective laser melting. Khorasani et al. (2018) observed 'irregularities' (~10 μm in height) on the surface similar in geometry but not in scale to protrusions created by the Surfi-Sculpt process. These irregularities were caused by a higher motion of melting pool as a result of the higher temperatures observed (up to 1050 °C). Khorasani et al. (2018) concluded that energy density influences temperature distribution as, when a higher energy density was applied, the material was locally heated to create a melt pool and surface tension was reduced. '*The gradient of surface tension induced at the interface from the hotter to the cooler area then propagates toward the* [parent material below the] *melting pool*' (Khorasani et al., 2018, p.3764). This identification of 'irregularities', which demonstrate a similar geometry to features created using the EBT and Surfi-Sculpt processes albeit with a significantly smaller feature height, supports the assertion of the author that it is the Marangoni effects that are the driving force in the EBT and Surfi-Sculpt processes. The fact that the beam was being specifically deflected to fuse the powder but not in a repetitive manner with the correct parameters to enhance the 'irregularities' is the significant reason for the difference in feature height.

Ohmura et al. (2000) discussed the formation of bumps on the surface of aluminium using laser texturing and reported reaching maximum temperature (boiling of the material) in 10 ns The bump could not be observed during processing but a feature height of less than 50 nm was formed after 55.35 ns. Ohmura et al. (2000, p.246) concluded, '*Marangoni force* [effect] *is most effective to the surface rise when the solidification starts outside of the bump*'. However, the scale of features produced by Ohmura et al. (2000) are considerably smaller than even the EBT process. Furthermore, there was no discussion as to the impact of high speed deflection of the beam over the surface of the material which is fundamental to both the EBT and Surfi-Sculpt processes.

2.2.4.1 Marangoni effects summary

The impact of Marangoni effects has been proven to be a significant driver in the melt pool dynamics for power beam processes, in particular EB processing. Application of the Marangoni effects and surface tension to the EBT and Surfi-Sculpt processes are further explored in Section 3.5 where the author develops and proposes a model predicting the flow of liquid metal as a result of the Marangoni effects and surface tension.

2.3 The effects of parameters on features

Certain machine specific parameters are known to affect features created using the EBT and Surfi-Sculpt processes. The American Welding Society (2007) and Swift and Booker (2003) state that EB processes are controlled by four key variables, namely beam accelerating voltage (kV), beam current (mA), focal beam spot size (μm) and speed of workpiece manipulation (mm/min). In addition to these variables, the following parameters affect the processes: focus current (A); working distance (mm); vacuum pressure (mbar); beam deflection parameters i.e. pattern, amplitude gain and frequency (Hz); gun design; and filament life (hours). For the EBT and Surfi-Sculpt processes, the

cumulative length of beam swipes in the pattern and the associated frequency of this deflection would determine the beam swipe speed (mm/s). The relationship between key process parameters is explored further in Section 3.6.

2.3.1 Beam accelerating voltage and beam current

The beam power is the single most significant parameter to affect EB processes (Meleka, 1971; Schiller et al., 1982) and is a product of the beam accelerating voltage and beam current. Atkinson and Chapman (2007) reported that the optimal power densities for the EBT and Surfi-Sculpt processes were approximately 250 – 500 W/cm^2. During experimental work, the author demonstrated power ranges between 50 W and 1.5 kW. The EBT and Surfi-Sculpt processes use a moderate amount of power (~10^2 – 10^3 W) and a relatively low power density (~10^4 – 10^5 W/cm^2) compared with primary melting techniques, EBW and EB thermal processing. This is because only a localised region of the material is melted and redistributed as a result of the interaction with the EB and therefore this does not require the same power and power density as the other processes. Short (2009) stated that there are various modes of operation during EB processing depending upon the power density; these are the keyhole mode (between 10^6 W/cm^2 and 10^9 W/cm^2) whereby there is a mixture of vaporisation and conduction and the conduction mode (below 10^6 W/cm^2) where the process is conduction dominated with negligible vapourisation. This establishes that the EBT and Surfi-Sculpt processes do not operate in the keyhole mode but rather the conduction mode and therefore the author argues that a previous assertion by Dance (2007) of the significant role of vapour pressure is incorrect. Figure 2.14 shows the approximate values for the power and power per unit area.

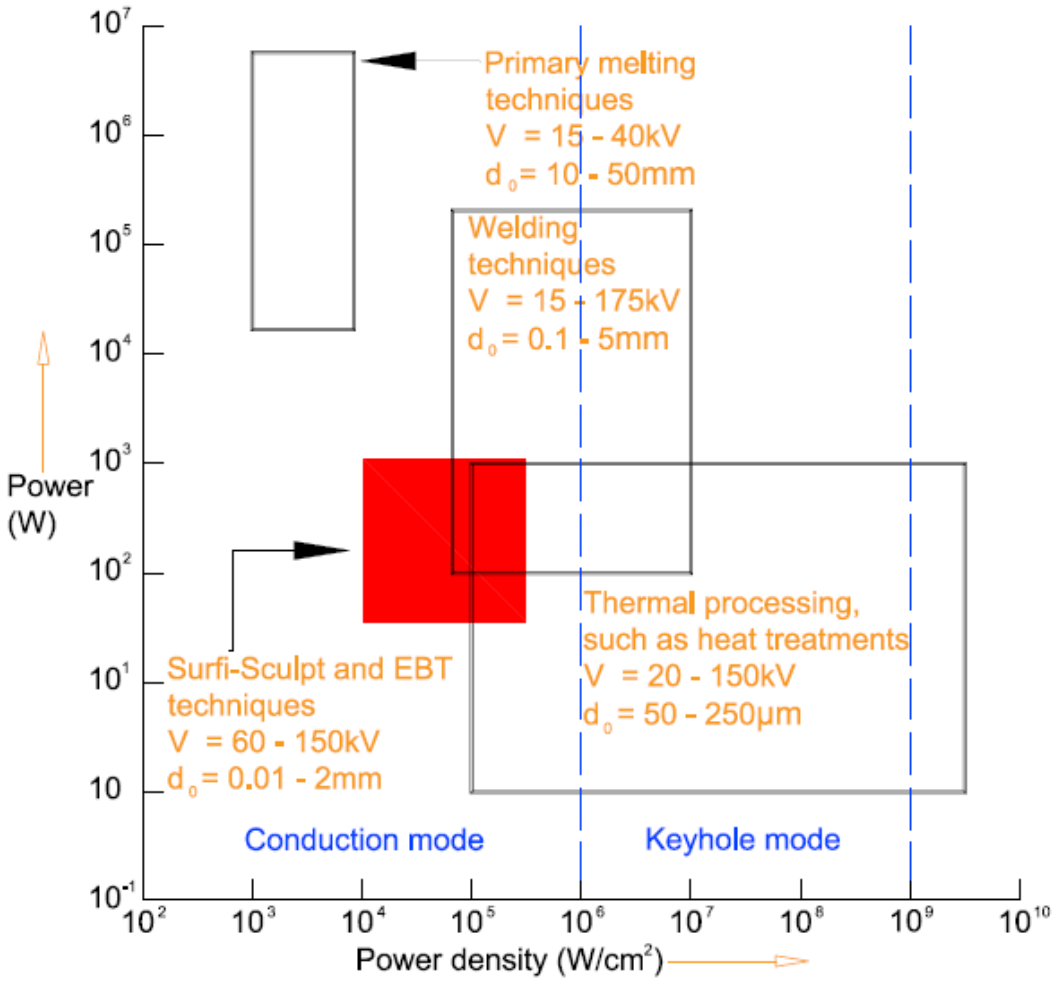

Figure 2.14 Power and power density for various EB processes with specific accelerating voltages (V) and beam diameters (d_o), adapted from Schiller et al. (1982) and Short (2009).

Wang et al. (2015) found that, at a constant accelerating voltage of 150 kV and a deflection frequency of 1,500 Hz, an increase in the beam current from 1.5 to 3.5 and 5 mA resulted in the average feature height increasing from 0.2 to 1.6 and 2.0 mm respectively when using the Surfi-Sculpt process for 20 seconds beam on time processing Ti–6Al–4V. This meant that each feature was created from 30,000 beam swipes which was greater than the amount used by the author at significantly lower frequencies in the creation of similar height features. Wang et al. (2015) did not provide information regarding the swipe length used and therefore it cannot be determined whether a different approach to feature creation was utilised from that used by the author to optimise the swipe speed, discussed in Section 2.3.5. However, it is possible to conclude that less material

was being moved with each beam swipe compared with the author's work. This is similar to the laser Surfi-Sculpt process reviewed in Section 2.4.

2.3.1.1 Heat input

The heat input for processing can be calculated using Equation 2 (Arata et al., 1976, p. 48) whereby Q is the heat input, Ω is the thermal efficiency of the process to the metal (in the case of EB, Arata et al. (1976) stated this as 0.8), U_B is the accelerating voltage and I is the beam current in amperes.

$$Q = 0.24 \times \Omega \times U_B \times I \qquad \textbf{Equation 2}$$

2.3.2 Focus current

To ensure maximum intensity of the beam during the EBT and Surfi-Sculpt processes, the beam should be at sharp focus on the surface of the workpiece (Atkinson and Chapman, 2007). This results in a small melt pool and ensures that the beam energy is targeted to a specific area. If the beam is either over or under focused by as little as <±1 %, whereby the focal point is positioned above or below the surface of the workpiece respectively, the intensity of the beam is reduced and smaller features will be formed by the EBT and Surfi-Sculpt processes; this is supported by the data generated within this EngD in Appendix D (Al6xxx Dataset 2 and 3). This is also due to the increased beam diameter leading to a reduction in the power density (American Welding Society, 2007).

Figure 2.15 shows an example resultant plot of the of beam shape in X and Y axes calculated in Submission 6 using TWI's BeamAssure system. It can be seen that, at lower beam currents, the shape of the beam changes from being circular to an ellipse in the Y axis. In addition, the beam width, or spot size, is proportional to the beam current. This change in beam profile can affect the quality of EB welds (Kaur, 2016). As a result, these changes lead to a variation in the features

being produced using the EBT and Surfi-Sculpt processes. The larger the beam width, the larger the melt pool created during the process.

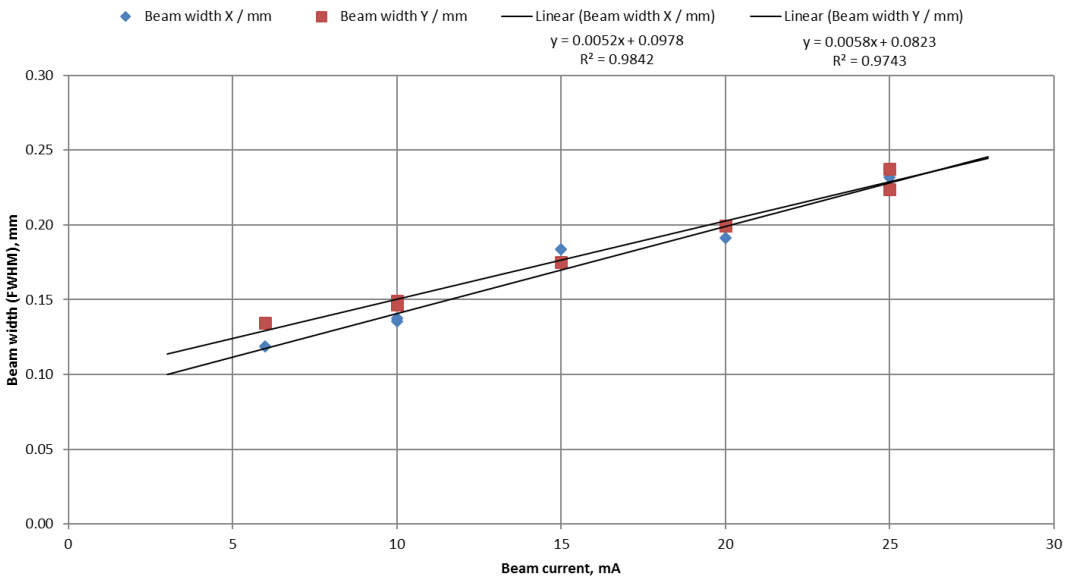

Figure 2.15 Plot of beam shape in *X* and *Y* axes calculated from TWI's BeamAssure system.

As demonstrated in Figure 2.15, operation of the EB machine at beam currents in excess of 10 mA will ensure that the beam profile is sufficient for the EBT and Surfi-Sculpt processes whilst maintaining the smallest spot size possible (approximately 140 µm).

2.3.3 Working distance

Meleka (1971) detailed that working distance, i.e. the distance from the filament to the workpiece, had a significant impact on EB processing. For ease of measurement, the distance between the top of the chamber and the workpiece is measured and reported since the distance between the filament and top of the chamber is constant and would be difficult to measure due to the components within the electron gun column. The study by Meleka (1971) reported that the penetration of an EB weld increased as the working distance decreased. This was due to a reduction in the beam spread caused by the decrease in beam path

within the chamber leading to fewer collisions of the electrons with molecules in the vacuum and increased intensity of the beam.

2.3.4 Vacuum pressure

Whilst there is no reported data on the effect of vacuum pressure on the EBT and Surfi-Sculpt processes, Schiller et al. (1982) and Meleka (1971) investigated the impact of vacuum pressure on penetration depths during EBW. Schiller et al. (1982) processed an austenitic stainless steel (X12CrNi18) at 125 kV using a beam current of 8 mA. Meleka (1971) performed the study using a steel alloy (AISI 4340) at 100 kV using a beam current of 9 mA. The results, shown in Figure 2.16, demonstrated that there would be minimal reduction in the penetration depth of an EB weld until a vacuum pressure of greater than $6x10^{-3}$ mbar was reached. Above this pressure, both Schiller et al. (1982) and Meleka (1971) observed that the penetration of the EB weld was significantly reduced as a result of the additional collisions of the electrons with molecules scattering the beam. Since different parameters and materials were used in these studies, there was a discrepancy in the values reported; however, the black dashed line in Figure 2.16 shows the trend for these datasets which is the key aspect highlighting the drop off of penetration at $6x10^{-3}$ mbar. Therefore, all EBT and Surfi-Sculpt processing should be conducted at vacuum pressures of less than $6x10^{-3}$ mbar to ensure the penetration depth of the beam is not affected and thus the volume of material moved with each swipe is not minimised.

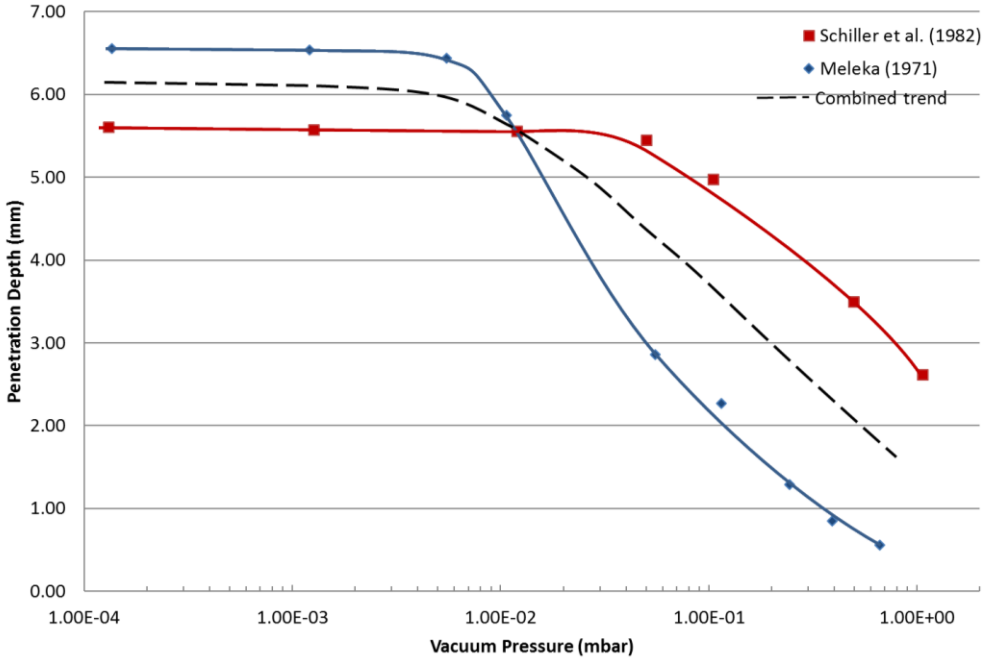

Figure 2.16 Relationship between vacuum pressure and penetration depth, adapted from Meleka (1971) and Schiller et al. (1982).

2.3.5 Beam deflection parameters: pattern, amplitude and frequency

As described in Section 1.1, TWI utilises two sets of deflection coils which are oriented in an orthogonal plane to the beam. These deflection coils are offset by 45 degrees to one another to minimise their interference. An arbitrary waveform drives each set of coils through a series of positions describing the beam path, known as the 'pattern' in the EBT and Surfi-Sculpt processes. The *U,V* pattern defines the overall geometry of the features whilst the *X,Y* pattern defines the overall positions or locations of the features.

For a set working distance and pattern, the size of each feature is dictated by the amplitude gain of the *U,V* pattern. Similarly, the positions of the features are governed by the amplitude gain of the *X,Y* pattern when the working distance and pattern remain constant.

If the working distance is increased, the *U,V* and *X,Y* amplitude gains will need to be increased to maintain the same swipe length in the feature or spacing of features respectively with the converse occurring for a decrease in working

distance. The amplitude gain is defined as the peak-to peak value of the arbitrary wave forms used in the deflection patterns.

The beam swipe speed, ϑ (mm/s), is key to the success of the EBT and Surfi-Sculpt processes, particularly for the creation of each feature (i.e. the *U,V* motif in most cases) since this dictates whether the processes work through the melting and moving of material. The beam swipe speed is calculated, Equation 3, as the product of the swipe length, l (mm), total number of legs (swipes) processed per feature, T_l, and the pattern frequency, λ (Hz). Example beam swipe speeds for 6000 series Al and Ti-6Al-4V are given in Section 7.4. Aluminium alloys, for example, generally require higher beam swipe speeds than Ti-6Al-4V as a result of their lower melting point, density and greater penetration depth of the EB into the material to achieve similar geometric features using the EBT and Surfi-Sculpt processes. This is discussed further in Section 7.3.

$$\vartheta = l \times T_l \times \lambda \qquad \textbf{Equation 3}$$

When setting the amplitude gain, the wider the angle of deflection the greater the working distance of the beam, shown in Figure 2.17 and indicated by the arc described by the dotted blue line. This highlights that the beam is not at sharp focus thus its intensity is reduced leading to the formation of small or no features. The restriction to this deflection is approximately 3 degrees either side of the free fall beam position. For a working distance of 405 mm, this equates to a beam translation distance of 21.55 mm on a stationary workpiece. With 95 % confidence limits, it was confirmed that a significant difference in feature height was created beyond this deflection of the beam (Pinto, 2013). This study is detailed further in Section 2.3.8.

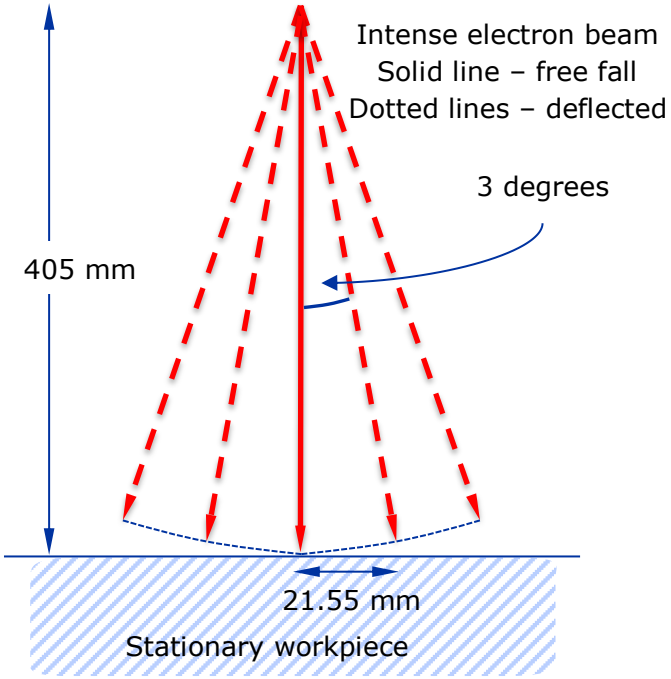

Figure 2.17 Deflection angle of EB affecting working distance and focus.

This limits the area of the surface that can be processed whilst the workpiece is stationary. Therefore, to overcome this issue, there are two strategies which can be utilised: either to 'tile' the array by completing it in one location on the surface before moving to another location and repeating the processing; or to continually move the workpiece at the same time as deflecting the beam within the constraints of the area that can be processed. The advantages of 'tiling' are that the parameters are not affected by the stationary workpiece and are therefore easier to optimise; however, ensuring the correct positioning of the tiles and patching them together can be time consuming, difficult and 'joints' may still be visible upon completion. The advantages of moving the workpiece are that there are no 'joints' in the creation of the surfaces and the processing time can be shortened; however, the optimisation of the parameters are affected by the speed of the workpiece movement. This means that the deflection of the beam must ensure that each repeated swipe used to create a feature is in the same position as the previous one by offsetting it to account for the workpiece motion.

2.3.6 Gun design

The design of the electron gun dictates the profile of the field of electrons which are accelerated towards the anode and hence determines the shape (or geometry) of the beam. There are several designs of gun including diode (two-electrode) and triode (three-electrode) guns. A diode gun consists of a cathode and an anode whilst a triode gun has an additional electrode of a bias grid cup. Examples of different commercially used gun designs include Pierce, Steigerwald and Rogowski. Triode guns are typically used since they create a focusing action on the beam (Schiller et al., 1982) and the Rogowski gun allows control of the beam current without affecting the focus setting (Schiller et al., 1982). TWI utilises a modified Rogowski gun which increases the intensity (or brightness) of the beam, as described in Submission 1. It also decreases the convergence angle of the beam as a result of the design.

2.3.7 Filament life

The filament in the cathode does not directly impact the features produced using the EBT and Surfi-Sculpt processes; however, Schultz (1993) noted that it is the only consumable in EB processing. Over time, through thermionic emission, the filament material evaporates and, when the diameter of the material is reduced by 5 %, failure occurs in the filament stopping the generation of electrons (Schiller et al., 1982; Meleka, 1971). As a high emission current density (approximately 5 – 10 Acm^{-2}) is required for the EBT and Surfi-Sculpt processes, a tungsten filament is used which typically lasts tens of hours.

2.3.8 Beam deflection offset study

2.3.8.1 Introduction to beam deflection offset study

One of the key characteristics of the EBT and Surfi-Sculpt processes is that they are anecdotally considered to have 'machine tool' reproducibility and accuracy. It is well-known that this key characteristic is currently limited by how far the beam can be deflected before the features no longer demonstrate this accuracy and

reproducibility without the need to manipulate the workpiece which adds further complexity to the process. However, this limit has never been calculated statistically as, when TWI used the Surfi-Sculpt process, the area over which the pattern was considered accurately reproducible was estimated. Koleva and Mladenov (2011) applied statistical analysis to the change in focus and power required for EBW and the effect on the weld depth and widths achieved when varying working distances.

Figure 2.18 shows a schematic diagram of how the EBT and Surfi-Sculpt processes are achieved through the deflection of an EB. The deflection is created using deflection coils to induce an electro-magnetic field in the EB. Fast focus coils allow for the beam to be in focus on the workpiece once the beam has been deflected.

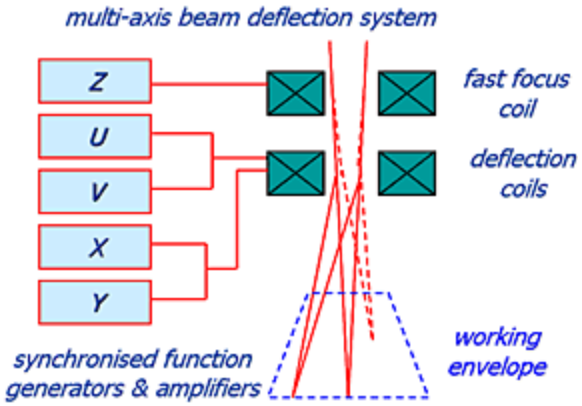

Figure 2.18 Schematic showing the mechanism of using a series of function generators and amplifiers (shown by letters *U, V, X, Y* and *Z*) to achieve a deflection of an electron beam.

A beam offset study was designed, developed and conducted including statistical analysis of the results in to order to support discussion of the following investigation since no suitable data was available to support the analysis of this statement: 'To state (with confidence limits) whether offsetting an electron beam causes a statistically significant difference in the height of features created using the Surfi-Sculpt process.'

2.3.8.2 Beam deflection offset study experiment

Surface modification features were created using a deflection pattern (beam offset study) on seven 15 mm thick plates of a titanium alloy, Ti-6Al-4V, using a 150 kV, 6 kW electron beam machine (3EB). The normalised parameters that were used to create the features are listed in Appendix D. The patterns covering 1,600 mm^2 were created using the Surfi-Sculpt process on the centre of samples that were 4,900 mm^2. The reason for the relatively large thickness and size of the samples, compared to the pattern size and feature height, was to ensure that the effects of distortion and poor heat transfer were minimised as these are factors which are known problems with the Surfi-Sculpt process (Dance, 2007).

The beam was deflected in the *X* and *Y* axis respectively and then both the *X* and *Y* axis combined. Table 2.5 below details the relationship between the beam offset value and the distance the beam was deflected in the *X* and *Y* axis. Each of the seven samples were numbered as follows:

Table 2.5 Beam 'offset' values used for each sample.

Sample number	Beam 'offset' value in *Y* axis (physical distance, mm)	Beam 'offset' value in *X* axis (physical distance, mm)
0	0.00	0.00
1	21.55	0.00
2	43.10	0.00
3	0.00	22.00
4	0.00	44.00
5	21.55	22.00
6	43.10	44.00

A calibrated Mitutoyo FJ300 projector shadowgraph was used to measure the following parameters (in millimetres to 3 decimal places) to examine the impact of using an offset to determine any changes in the height characteristic of the Surfi-Sculpt features created.

Figure 2.19 shows a schematic layout of the experiment to investigate the beam deflection offset study.

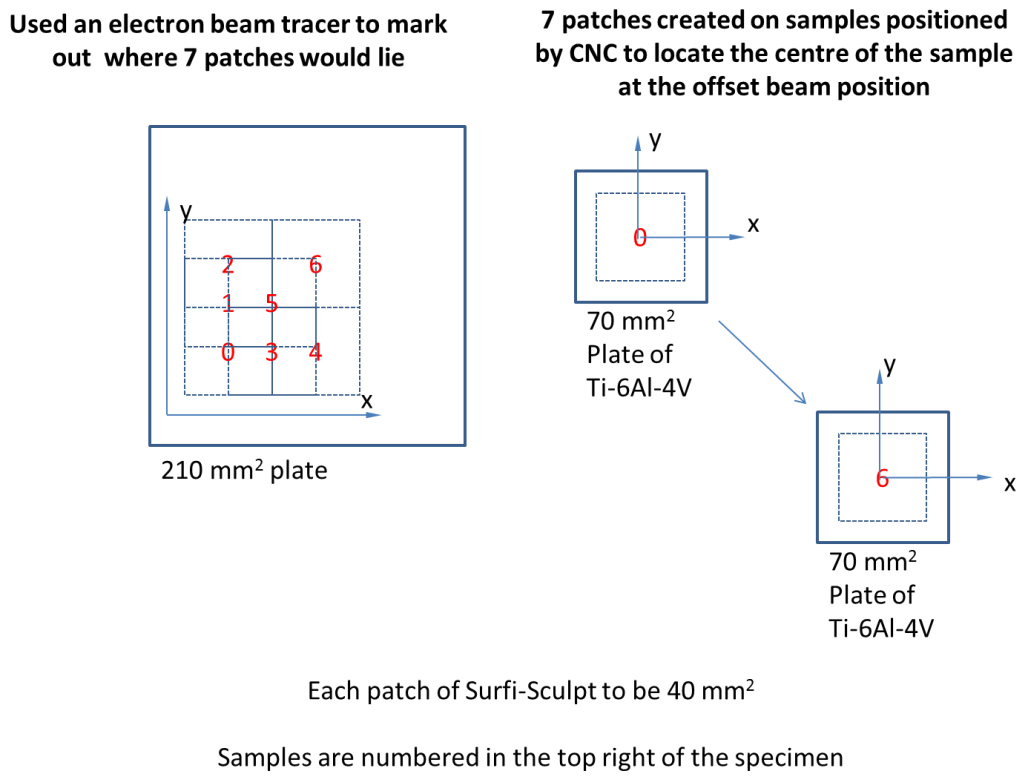

Figure 2.19 Schematic diagram representing experiment details.

In order to make the experiment easier to conduct, the samples were laid out as per Figure 2.20 and a CNC table was used to locate the centre of the sample at the offset beam position.

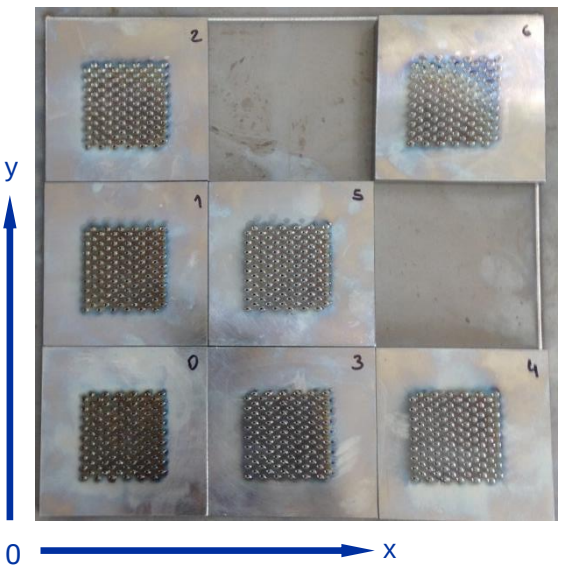

Figure 2.20 Layout of seven samples (0 – 6) on a larger 210 mm² plate.

Each feature can be described by an *X* axis coordinate, labelled by letters a – l, and a *Y* axis coordinate, labelled by numbers 1 – 9 (see Figure 2.21). The pattern was produced a column at a time starting from column 'a' and then working across the *X* axis. The electron beam was controlled by a programme which turned on the beam for 4 seconds to produce the pattern. Given that the frequency of the pattern was 7 Hz, each column would be expected to be processed 28 times. However, they did not receive an equal amount of power since the beam ramped up to 14 mA over 0.5 seconds and the pattern was processed 3.5 times in this duration; therefore not all columns were processed at full power 28 times.

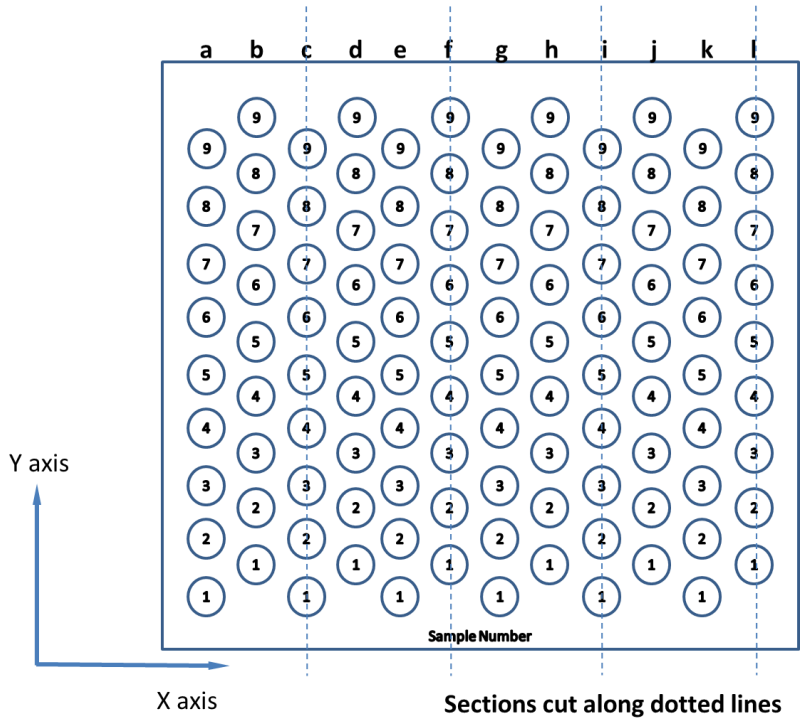

Figure 2.21 Schematic diagram of features created by beam offset study pattern showing how samples were sectioned.

The features were nominally spread 4 mm apart in the pattern; this was to aid the cutting process for sectioning the samples. However, it was not possible to isolate each column of features (*X* axis) and therefore every third column of features (columns c, f, i and l) were cut through to provide specimens with two columns of features for analysis. The height of the feature from the original base

plate surface to the tip of the feature was measured using a calibrated Mitutoyo FJ300 projector shadowgraph. A source of error could come from assuming that the surface of the samples had been machined flat since the machining tolerance of the surface of samples was unknown.

Because of the positioning of the features, it was possible to accurately measure their height when a specimen had only two columns of features. The main limitation of this approach was the loss of data due to four columns of features having to be cut through; hence the population data could not be recorded but instead sampling was introduced, which was not random but followed a set pattern, as shown in Figure 2.21. The sectioning process may have also led to some features being disturbed or broken and this could be a factor in the variation of feature heights.

2.3.8.3 Beam deflection offset study results

Figure 2.22 shows the mean feature height of the seven samples and the error bars show the measured standard deviation. Sample 1 was processed with no offset and created the highest feature height as well as the largest variation. This was due to the large features created at the centre of the pattern compared with the edges, since the beam was most intense near free fall and less intense once deflected off axis. Samples 1, 3 and 5 all had a beam offset of approximately 22 mm in either the *X* or *Y* or both axes. The mean heights were statistically similar and had a lower standard deviation as the beam was less intense thus forming smaller features. The same explanation is true for the further reduction in mean heights and standard deviation was true for Samples 2, 4 and 6, which all had a beam offset of approximately 44 mm in either the *X* or *Y* or both axes. A summary of the data generated in the beam offset study is listed in Appendix C.

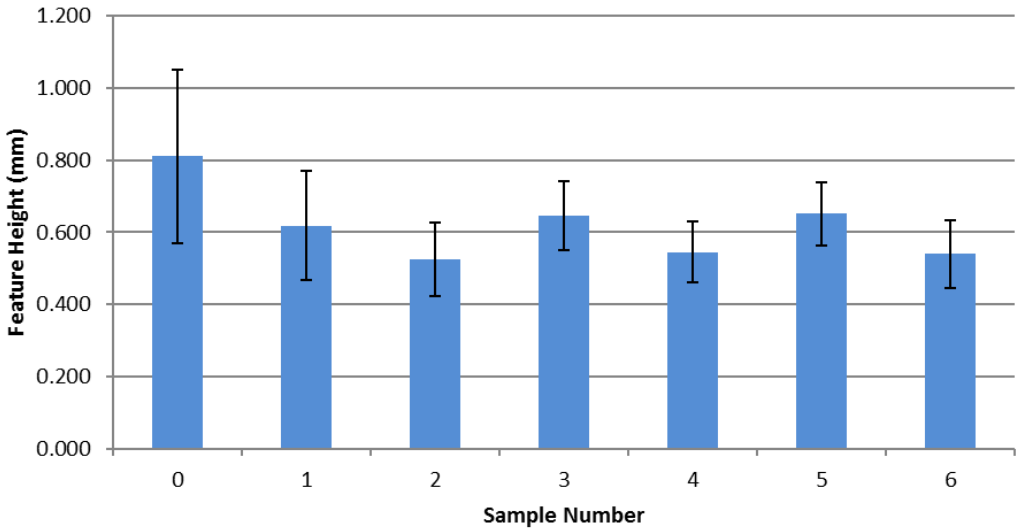

Figure 2.22 Mean feature height created using the Surfi-Sculpt process.

2.3.8.4 Beam deflection offset study review of results and plots

Figures 2.23 to 2.29 plot the results of the data for the seven samples using a surface plot. This was the best method of representing the data in a graphic form that was easy to understand. The scale on the feature height axis remains constant so that these figures can easily be compared against one another.

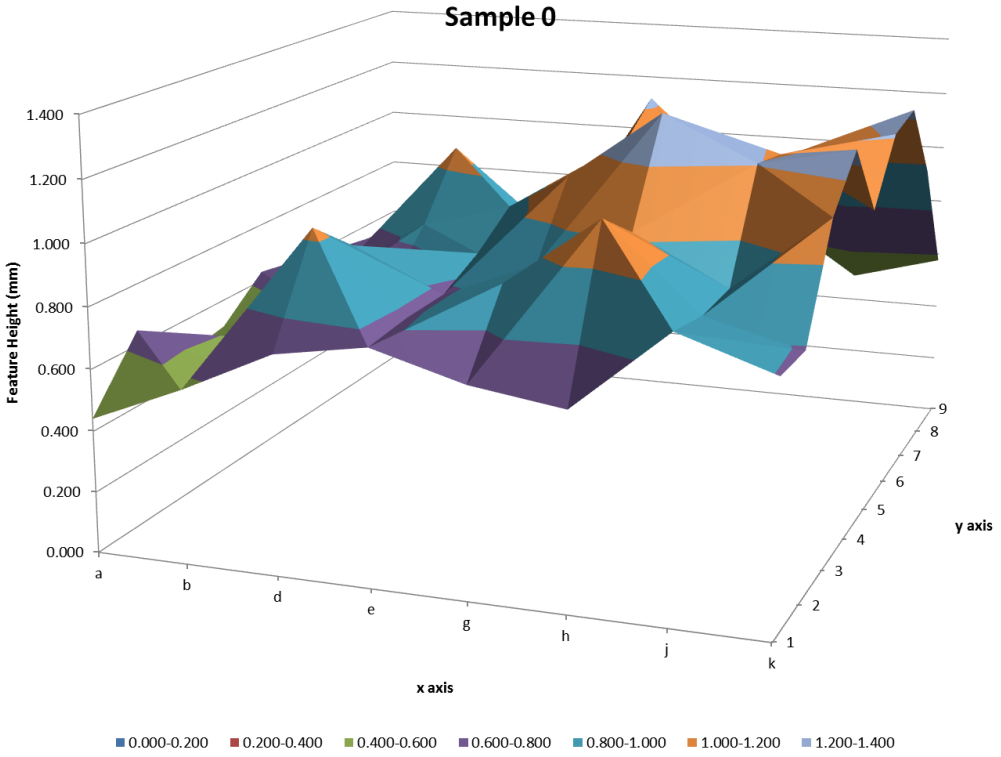

Figure 2.23 Sample 0 feature height plot.

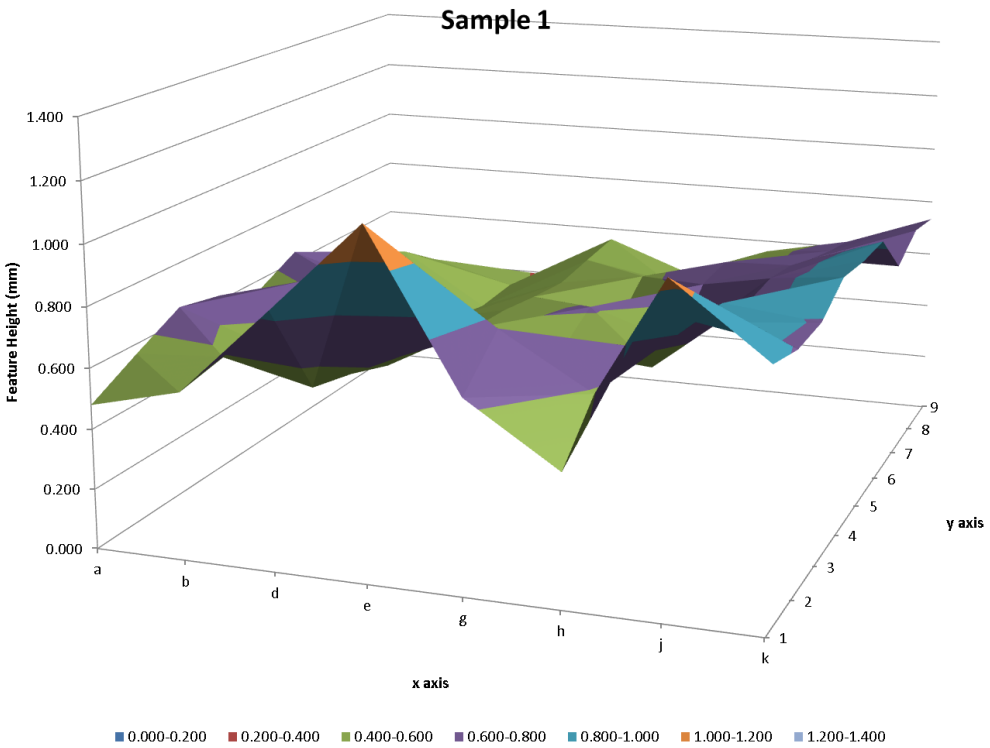

Figure 2.24 Sample 1 feature height plot.

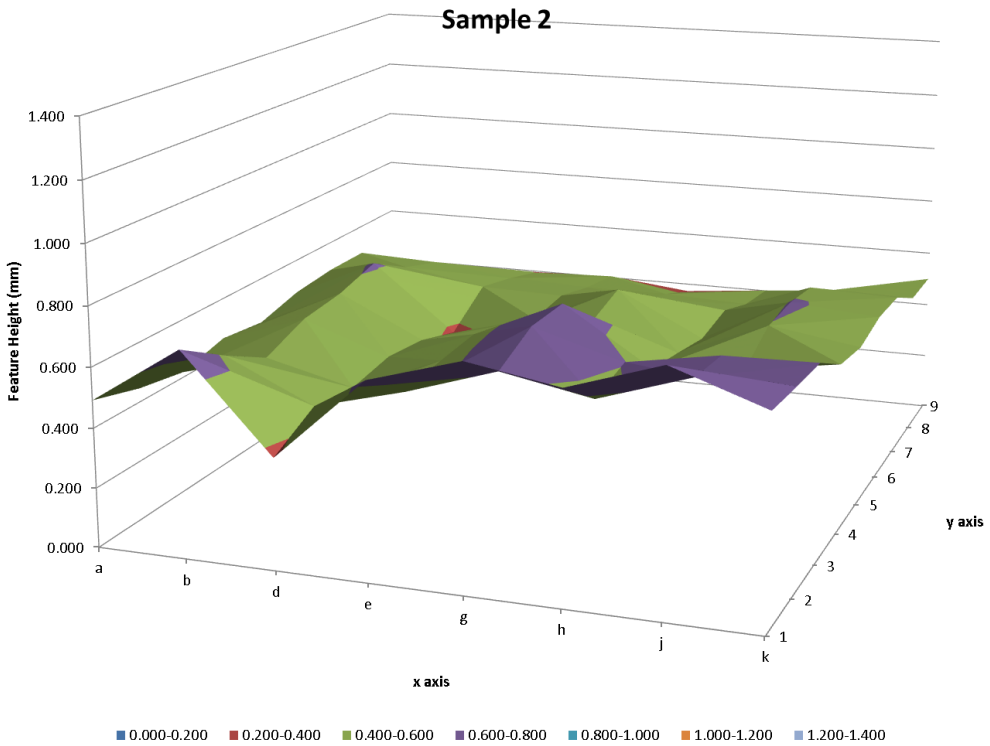

Figure 2.25 Sample 2 feature height plot.

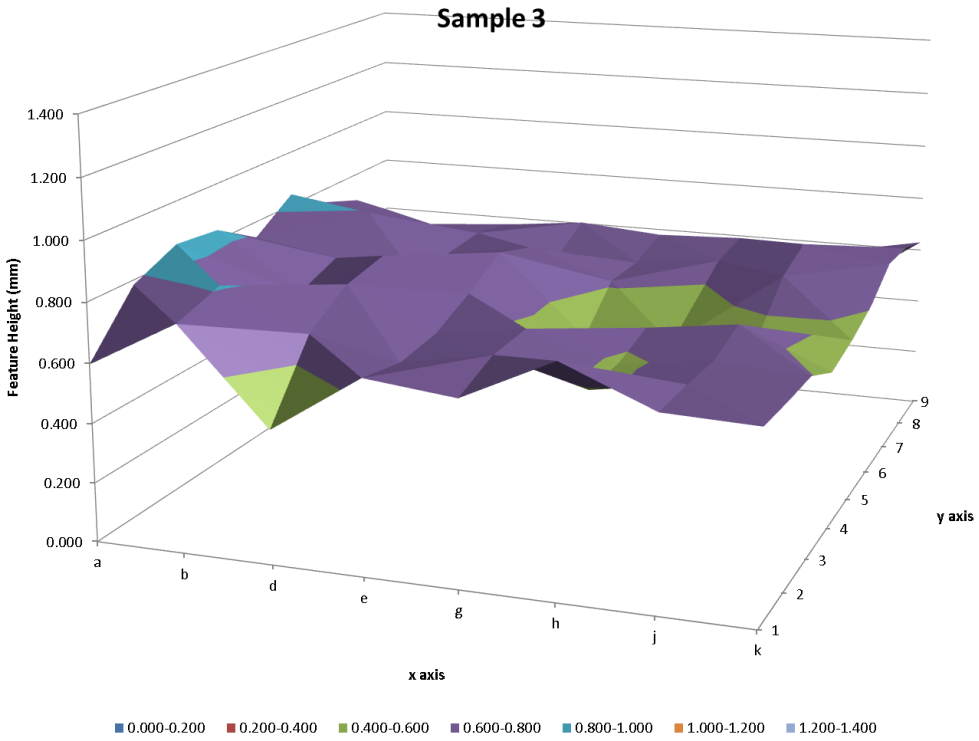

Figure 2.26 Sample 3 feature height plot.

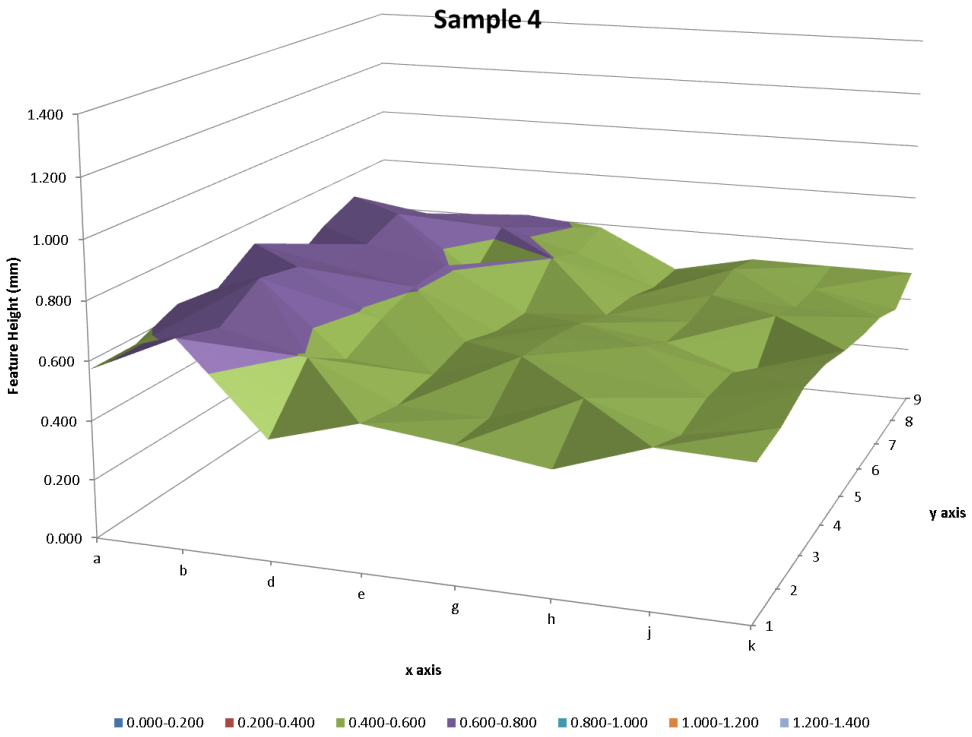

Figure 2.27 Sample 4 feature height plot.

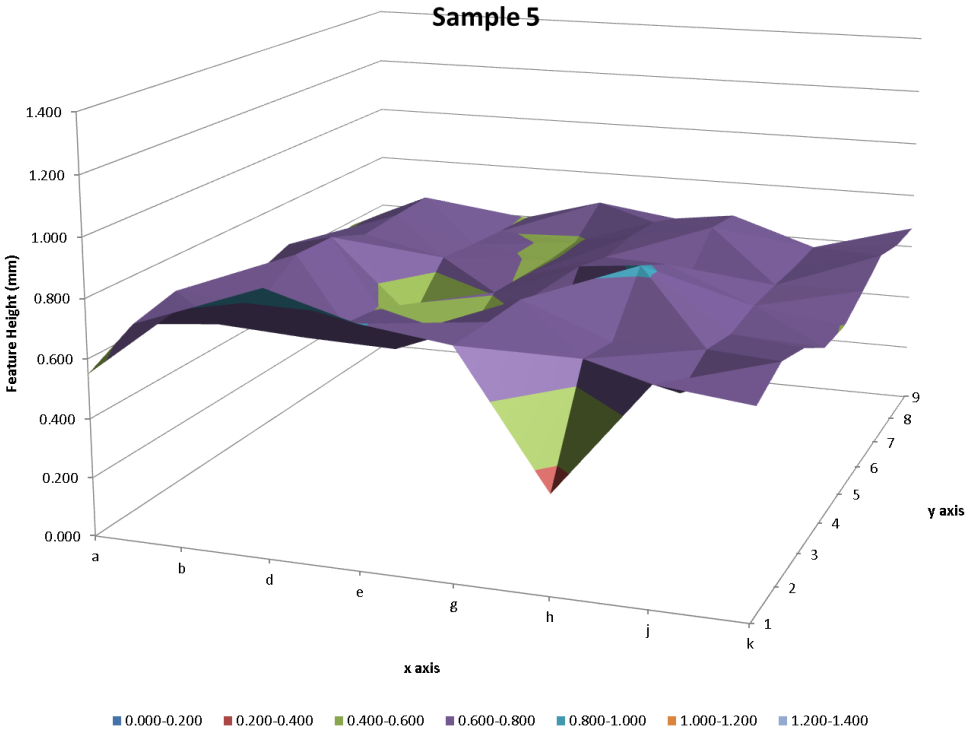

Figure 2.28 Sample 5 feature height plot.

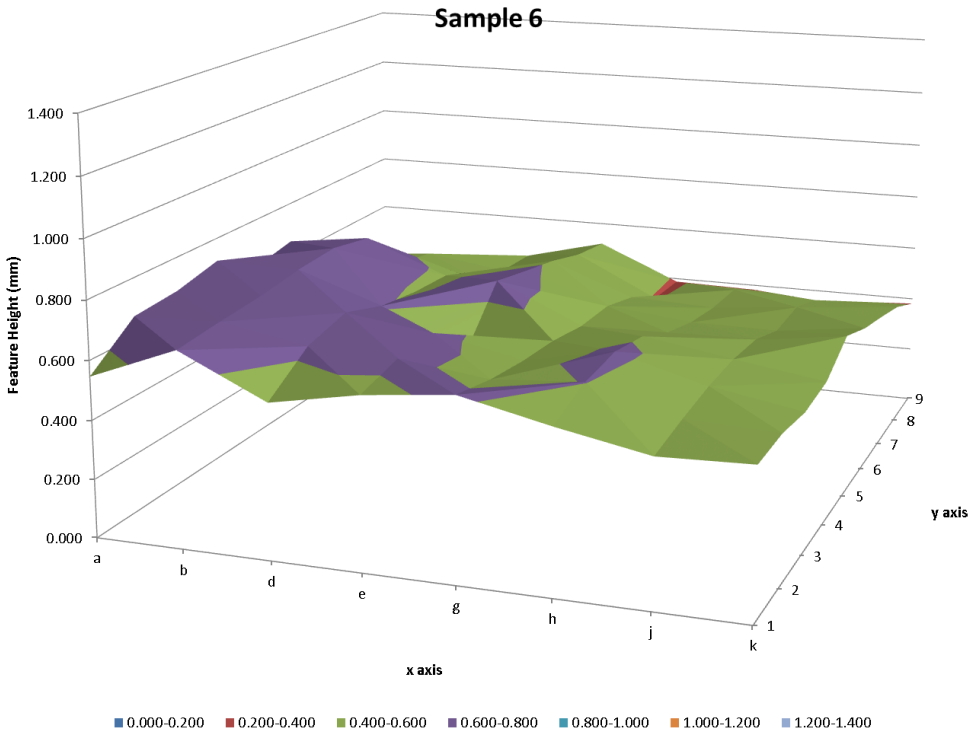

Figure 2.29 Sample 6 feature height plot.

2.3.8.5 Beam deflection offset study statistical analysis

The aim of this study was to understand if the offset of the EB exerted an influence on the feature height; therefore a tool was needed which performed a comparison of the spread of distributions within groups against the spread of means. Since there were a total of seven samples of continuous data, a single factor analysis of variance (ANOVA) was used.

To begin with, a null hypothesis (H_0) was set up:

$H_0: {\sigma_c}^2 = 0$, which states mathematically that there is equal variance in the feature heights between samples 0 – 6 (no change).

Then an alternative hypothesis (H_1) was devised:

$H_1: {\sigma_c}^2 > 0$, which states mathematically that there is unequal variance in the feature heights between samples 0 – 6.

Below is Table 2.6 which shows the single factor ANOVA.

Table 2.6 Single factor ANOVA

Source (of variation)	Sum of Squares	Degrees of Freedom	Mean Square (M.S.)	Quantity Estimated by M.S.
Between samples (S)	0.470269	6	0.078378	${\sigma_0}^2 + 6{\sigma_c}^2$
Within each sample (Residual)	0.392819	49	0.008017	${\sigma_0}^2 + 49{\sigma_c}^2$
Total	0.863089	55	-	-

The single factor ANOVA calculated between samples is shown below and represented in Figure 2.30:

$F_{calc} = \frac{0.078378}{0.008017} = 9.78$ (3 s.f.) F_{crit} = 2.29 (3 s.f.)

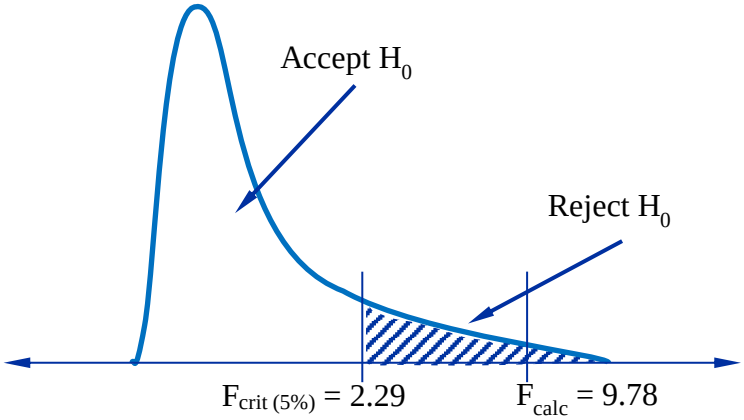

Figure 2.30 ANOVA F-test result for beam offset study.

Since F_{calc} was greater than F_{crit}, H_0 (the null hypothesis) was rejected for the variation in feature heights and H_1 (the alternative hypothesis) was accepted for the variation in feature heights; therefore there is statistically significant variation in feature heights between samples.

2.3.8.6 Beam deflection offset study discussion and sources of potential error

Measurement is a process and therefore will introduce variation much like the Surfi-Sculpt process which is also introducing variation. A challenge of using a shadowgraph to measure the feature heights was ensuring that the surface of the specimen was presented parallel with the *X* axis so that the true perpendicular height of the features created using the Surfi-Sculpt process were measured. Any errors in the flatness of the sample would have also introduced errors into the data collected. The data collection method assumed that the features 'grew' vertically and that therefore using the profile of the feature would give an accurate measurement of the feature height. There is also the possibility that the features could have been damaged by sectioning the samples which would have led to a source of error. This could potentially be addressed by performing a non-destructive test to measure the feature heights such as using ultrasonics.

The calibration sheet (Appendix B) detailed that there was an error in the *X* axis micrometer of 0.004 mm (which was beyond the allowed error of ±0.003 mm)

when a value of above 12.6 mm was measured. Therefore, to counteract this error, the samples were orientated such that traversing along the specimens used the *Y* axis micrometer on the shadowgraph whilst the feature heights were measured using the transverse of the *X* axis micrometer. This ensured that values of 12.6 mm were not exceeded.

2.3.8.7 Beam deflection offset study conclusion

The main aim of the study was to see if there was a significant difference in the heights of the features by only varying the offset values used.

The statistical analysis shows that there was a significant difference in the means between the samples as H_0 was rejected. Relating this back to the original investigation means that with 95 % confidence limits it is possible to state that offsetting the beam by approximately 22 mm when using a working distance of 405 mm creates a statically significant difference in feature height. Therefore it is recommended to not deflect the beam more than 3 ° from the free fall position. However, if feature height can be sacrificed for a lower value then offsetting the beam will reduce the variation of heights achieved.

To manufacture large areas processed by the EBT or Surfi-Sculpt processes, the use of 'tiling' is required or the creation of a travelling pattern whereby the workpiece is moved simultaneously under the beam. The latter approach is more complex since it is important to ensure that the timing of workpiece movement and beam deflection is synchronised so that the swipes are revisited at the exact same location to create defined features.

2.4 Comparison between a laser beam and an electron beam

Several studies (Hilton and Nguyen, 2008; Blackburn and Hilton, 2011; Earl et al., 2012; Earl et al., 2016) have investigated the use of a laser beam as

a power source for the Surfi-Sculpt process. The main differences between a laser beam and an EB used for the Surfi-Sculpt process, other than the power source, are the deflection control used and the processing environment. A galvanometer driven beam scanner is used for deflection of the laser beam, in comparison with magnetic coils used to deflect the EB, and no vacuum is required for the laser beam. However, shielding gas is often required to prevent oxidation of the surface during processing of materials such as Ti-6Al-4V.

In comparison to an EB, the energy from the laser beam only interacts with the surface of the material initially. This was discussed in Submission 5 where the author proposed that this difference led to the ejection of molten material observed using a laser compared to no such observation with the EB Surfi-Sculpt process. Unlike the observations of the laser Surfi-Sculpt process by Earl et al. (2016), the material during the EB Surfi-Sculpt process does not suffer from the expelling of molten material and there is little evidence of the initial molten material being ejected. The energy of a laser beam is absorbed at the surface of the material. This explains why Earl et al. (2016, p. 214) observed '*a protruding liquid filament (jet) is produced in response to the laser power and translation speed* [between 0.3330 m/s and 0.1999 m/s] *which in turn solidifies producing a material feature*'; this is shown in Figure 2.31. Earl et al. (2016) defined this laser phenomenon as the capillary action.

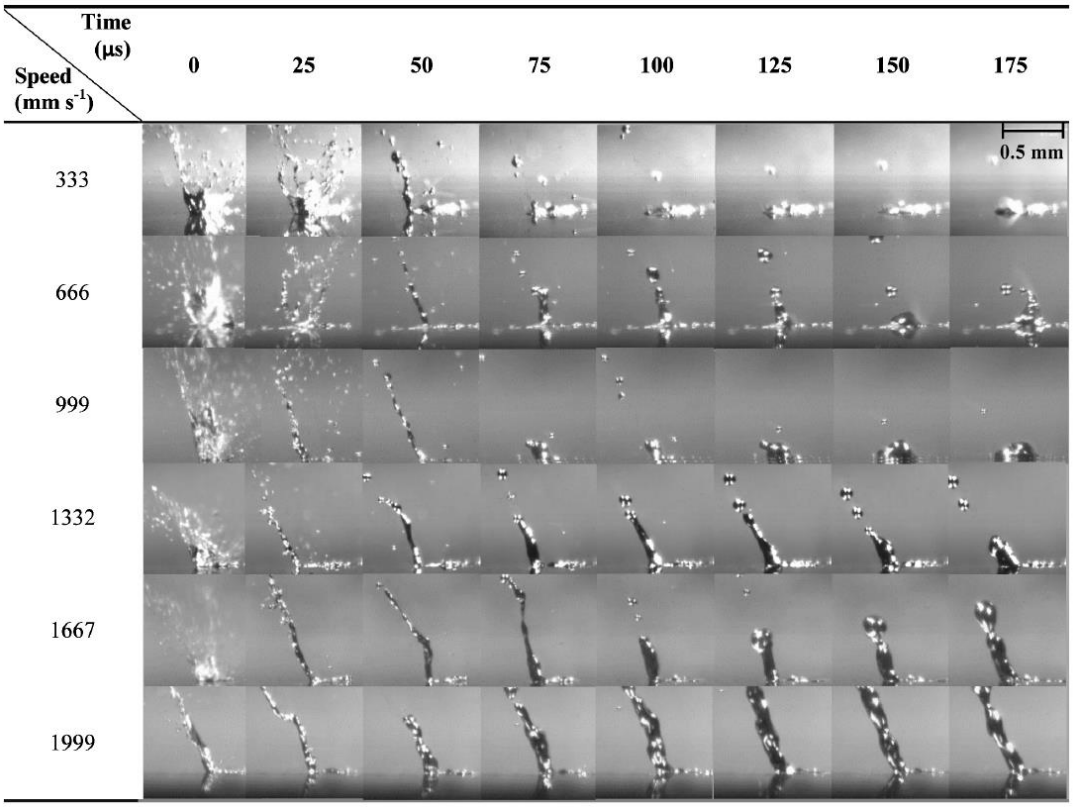

Figure 2.31 Protruding liquid filaments (jets) observed in laser Surfi-Sculpt. The beam is travelling left to right in each figure, taken from Earl et al. (2016, p.217).

This phenomenon was not witnessed during slow motion analysis of the EB Surfi-Sculpt process with the beam travelling an order of magnitude faster despite the fact that the process occurs in vacuum. The author considers this laser phenomenon to be as a result of excess vapour pressure being generated as a result of the beam interacting with a small area of material on the surface initially. However, as described in Equation 4, within the EB Surfi-Sculpt process the EB energy is absorbed by a volume of material which is determined by the electron range, S, below the surface of the material rather than at the surface alone. As described in Submission 1, an EB causes volumetric heating as the kinetic energy from the electrons in the beam is converted into heat and excitation energy within a certain depth of the material (Schiller et al., 1982). Equation 4, defined by Stohr in 1957 (cited in Schiller et al., 1982, p. 39), shows the variables affecting the depth of interaction of the EB for the accelerating

voltages used by the EBT and Surfi-Sculpt processes. Penetration depths for materials used in this EngD are calculated in Section 7.3.

$$S \approx 6.67 \times 10^{-11} U_B^{5/3} \rho^{-1} \qquad \textbf{Equation 4}$$

Where S (cm) is the electron range, U_B (V) is the accelerating voltage (in the range of 10 – 1000 kV), and ρ (gcm^{-3}) is the material density.

Therefore, a greater volume of material (than with a laser) becomes molten as the electrons convert their kinetic energy into heat or atomic or molecular excitation energy (Adam et al., 2011; Schultz, 1993). The author argues that the EB Surfi-Sculpt process will not result in material being ejected as a jet since the vapour pressure is moving a larger volume of material with an EB compared to a laser beam. The ratio between the surface of the molten material and its volume during the Surfi-Sculpt process is smaller in EB (compared with lasers) and therefore the surface tension exerts a smaller force on the mass of molten metal which does not result in the jet of material.

There are distinct advantages as well as potential limitations for using either an EB or a laser beam for the Surfi-Sculpt process. These have been summarised in Table 2.7.

Table 2.7 Comparison of the advantages and limitations of using an EB or a laser beam for the Surfi-Sculpt process.

	Electron beam	Laser beam
Advantages	Rapid beam movement due to the use of magnetic deflection coils (Meleka, 1971; Dance and Kellar, 2003) More developed and mature process; exemplar application case studies available (Dance, 2007) High intensity EB has the potential to generate fine scale features (e.g. 10 μm) (Ribton and Atkinson, 2007) Little oxidation retaining chemical purity of material due to the use of a vacuum (Meleka, 1971) More suited to the creation of larger features due to larger melt pool as a result of the interaction between the EB and the workpiece	Power and wavelength of laser source can be selected according to the material being processed (Blackburn and Hilton, 2011) Low powers can be used; particularly suitable for processing polymers and for reducing capital equipment costs (Blackburn and Hilton, 2011) No vacuum is required hence faster throughput may be possible More suited to the creation of smaller features due to larger melt pool as a result of the interaction between the laser and the workpiece
Limitations	Vacuum is required so cost and throughput issues are possible (Meleka, 1971; Calder, 2006) X-ray source therefore lead shielding is required (Meleka, 1971) as discussed in Section 2.5 High capital equipment costs (Meleka, 1971) Power of the beam is likely to degrade polymers	Mechanisms for deflecting the beam with respect to the material, or vice versa, require development Shielding gas may be required to prevent oxidation of surfaces (Schultz, 1993) Slower processing times

The power beam utilised for the Surfi-Sculpt process should be considered on a case-by-case basis and result from either the requirement of a specific key advantage or negation of a particular limitation. For example, if processing with a vacuum chamber is unacceptable then a laser beam should be used whilst if oxidation is an issue and a high speed of processing is required then an EB should be selected.

2.5 X-rays and regulations

X-rays are generated when electrons impinge upon a metal (Weglowski et al., 2016; Schiller et al., 1982). This is due to Bremsstrahlung or 'braking radiation' (Haug and Nakel, 2004) caused by the deceleration of the primary electrons in the beam. In addition to Bremsstrahlung, characteristic radiation results from the expulsion of secondary electrons caused by the primary electrons from the beam colliding with atoms and emitting photons in the X-ray spectrum. This is specific to the material being processed and is dependent on its atomic number. For example, tungsten has a higher atomic number (74) than titanium (22) and aluminium (13), the alloys of which were investigated within this EngD in Submissions 3 and 6. Therefore, the X-rays from tungsten require greater attenuation than those from aluminium or titanium which affects the amount of shielding required. This risk of X-ray radiation is adequately managed outside the gun column and vacuum chamber using shielding (normally lead or thick steel panels) and should not pose a danger to the machine operator if these vital precautions are taken (Bakish and White, 1964).

The Ionising Radiations Regulations (1999) impacted on the use of an EB, as discussed in Submission 1; subsequently, the Health and Safety Executive has published updated regulations which came into force on 1 January 2018 (The Ionising Radiations Regulations, 2017). However, this has not affected the legal requirements for any electrical equipment emitting ionising radiation (including EB machines) beyond the regulations set out in 1999. An effective dose greater than 1 mSv results in the designation of a 'supervised area' which is within the EB machine operator's location. The regulations recommend a principle of 'as low as reasonably practicable' (ALARP); this has not affected TWI local house rules which stipulate that the maximum radiation level observed during an X-ray assessment should be 1.0 μSv/hr. This is calculated from a worst case

scenario of 1 mSv spread across 5 hours beam on time per day for 200 days a year.

To support the calculation of adequate biological shielding for an electron gun system, a British Standard was issued which details the thicknesses of a range of materials in attenuating X-rays (The British Standards Institution, 1971). Typically martensitic stainless steel or mild steel, used to manufacture the gun column and vacuum chamber respectively, or lead, which has a high attenuation rate resulting in a small thickness of a few mm, are used as biological shielding.

2.6 Early electron beam texturing work

Hamilius and de Soete (1997) demonstrated the application of the EBT process for texturing cold mill rolls used by steel-making companies and identified that it was developed in Kiel, Germany by the company Linotype-Hell AG for use in the printing industry. This development was undertaken as part of an 18 month European Commission funded project 'Compact bearing housings for rolls on EBT machines' between 1991 and 1992 (EU Publications Office Top, 2002). The setup of the system was very similar to that of a standard EB machine setup as described in Submission 1. The key differences being that Hamilius and de Soete (1997) used a continuously operational defocused EB that was only focused to create textures using simple circular beam deflection available on an EBW machine. In contrast, TWI utilises arbitrary waveform generators to create complex beam deflections (up to 1 million points can be described per pair of axes) during which the beam is switched on and off. This has enabled the manufacture of more complex features and geometries for surface modification using the EBT and Surfi-Sculpt processes.

2.7 Summary of the electron beam texturing and Surfi-Sculpt processes

There are a limited number of published articles on the EBT and Surfi-Sculpt processes which was a contributory factor in the lack of industrial adoption of the processes. This resulted in the author extending the review of principles to pre-existing work with similar EB processing techniques. Given the range of parameters affecting the EBT and Surfi-Sculpt processes, development to date has been empirical.

3 Feature Formation

3.1 Background of feature formation

Two different theories for the formation of a feature using the EBT and Surfi-Sculpt processes have been proposed by Dance (2007) and Earl et al. (2016). Dance (2007) concluded that surface tension and vapour pressure control the processes based upon the principal mechanism of deep welding defined by Meleka (1971). In comparison, Earl et al. (2016) advocated capillary action as the mechanism by which the processes occur. However, these theories are limited since they require the formation of a capillary by the vapour pressure generated and characteristic keyhole welding rather than the melting which occurs during processing. Neither Dance (2007) nor Earl et al. (2016) provide schematics offering a model of the material flow within the formation of a feature. This model is needed to support the fundamental understanding of how the molten material is transported to form a feature from a series of beam swipes and thus be able to computationally predict the geometry of a feature based upon the number and position of beam swipes used.

In order to achieve the objective set out in Section 1.2 regarding the underlying mechanism of the EBT and Surfi-Sculpt processes, high-speed filming was undertaken with the aim of providing evidence either to support the theories advocated by Dance (2007) and Earl et al. (2016) or to provide an alternative hypothesis.

3.2 Challenges to high-speed filming of the EB Surfi-Sculpt process

Various challenges had prevented a high-speed filming technique from being used previously for the EB Surfi-Sculpt process. The X-rays present within the vacuum chamber, discussed in Section 2.5, resulted in a challenging environment in which to record high-speed video due to interference with imaging equipment leading to deterioration of image quality. Furthermore, the risk of damage to the glass

optics required protection of these components in the camera via the addition of lead glass to attenuate the X-rays.

Additional challenges associated with this work were the need to provide adequate illumination to allow image capture of the processing and the subsequent removal of heat generated by the lights and camera. The generation of excess heat prevented the lights from working and caused further deterioration of the image quality in the camera. This limited the operating duration for the lights and camera before the chamber needed to be vented and electrical fans achieved forced air cooling of the high-speed video setup through the length of the vacuum chamber. The operating duration was later found by the author to be approximately 3 minutes before the quality of the image capture deteriorated and the lights switched off as a result of an over temperature protection mode.

3.3 High-speed video method

TWI's Hawker Siddeley Dynamics 150 kV, 6 kW beam power EB machine, designated 3EB, was used for the filming of the EB Surfi-Sculpt process. The high-speed video setup is shown in Figure 3.1. To prevent damage from X-rays to the Os7 camera, it was shielded in a lead-covered box section and lead glass was placed in front of the lens. The initial step was to activate the video record function at 2,000 fps using 1280 x 720 pixel resolution on the Os7 high-speed camera. Light emitting diode (LED) illumination was provided by two 120 W LEDs which were turned on prior to the beam generation and deflection. A 15 mm thickness Ti-6Al-4V grade 5 plate was used as the substrate material to ensure that no distortion or effects of the substrate due to the thickness, such as thermal stresses, would affect the image capture since the position of the feature would alter as the substrate material moved and therefore would not allow suitable image capture for analysis.

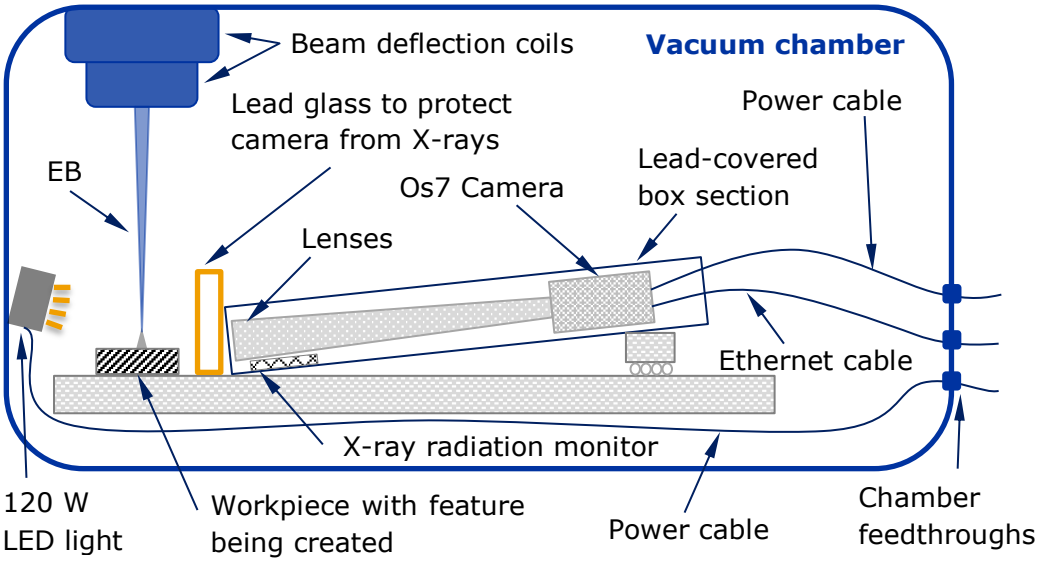

Figure 3.1 The high-speed video setup.

Table 3.1 details the parameters used to create a series of single direction beam swipe features using the EB Surfi-Sculpt process. A series of uni-directional EB swipes (based upon the most simplistic pattern) was used to create features to ensure that the fundamental aspects of the mechanism were observed without considering other factors such as optimisation of the swipes from multiple positions and their impact upon one another. To enable the beam workpiece interaction to be viewed easily, the beam swipes were normal (90 degrees) to the camera.

Table 3.1 Parameters used for the high-speed video of the EB Surfi-Sculpt process.

Parameter		Value
Accelerating voltage		130 kV
Beam current		2.9 mA
Processing time		5 seconds total time
Gun type		R40 RC1
Focus coil current		3.46 mA
Working distance (from base of coils to top of workpiece)		245 mm
Power		377 W
Vacuum chamber pressure		$1x10^{-4}$ mbar
X / *Y* EB deflection (Surfi-Sculpt) pattern file name		22964_HS_Video (a series of uni-directional beam swipe features)
X / *Y*	Amplitude gain	0.7 mA
	Frequency	10 Hz
Total number of swipes in the pattern		22
Material		Ti-6Al-4V grade 5
Thickness of material		15 mm

3.4 Results from the high-speed video

As detailed in Submission 5, this was the first time that the interaction between the EB and the material, a key mechanism of the EBT and Surfi-Sculpt processes, was captured from within the vacuum chamber. Analysis of the high-speed video enabled the representation of the processes to be verified by still image frames. The movement of the molten material did not result in the observation of protruding liquid filaments (jets) which were noted in laser Surfi-Sculpt by Earl et al. (2016). However, due to the restricted frame rate available, 2,000 fps at 0.5 ms frame intervals (calculated from 2,000 fps), it was only possible to observe the translation of the beam across the surface of the Ti-6Al-4V over a distance of 2 mm. Therefore, the constant beam speed was calculated to be approximately 29.3 m/s and the author observed that the molten material appeared on the feature in the opposite direction during the same time period. It was not possible to confirm whether the material was translated at a faster speed than the beam yet the movement of the material must have been at least the same speed as the beam or faster and therefore a minimum speed of 4 m/s can be determined. According to Earl et al. (2016, p.215), '*the melt flow around the keyhole exceeds the laser traverse speed by 2.5 – 10.0 times due to constriction between the cavity sides and the remaining solid material'*. Therefore, if the

findings of Earl et al. (2016) were correct, the molten metal in the EB high-speed video was flowing at a minimum speed of 73 – 293 m/s. However, this provides a wide range of speeds of the molten material and therefore limits the conclusions that can be drawn.

Figure 3.2 shows the production of a simple single direction beam swipe feature using three 'repeat' swipes (horizontal orange arrows) of the beam (vertical black and red arrows). The author was the first to relate and validate the previous schematic of feature formation (Buxton et al., 2012) achieved using the EBT and Surfi-Sculpt processes.

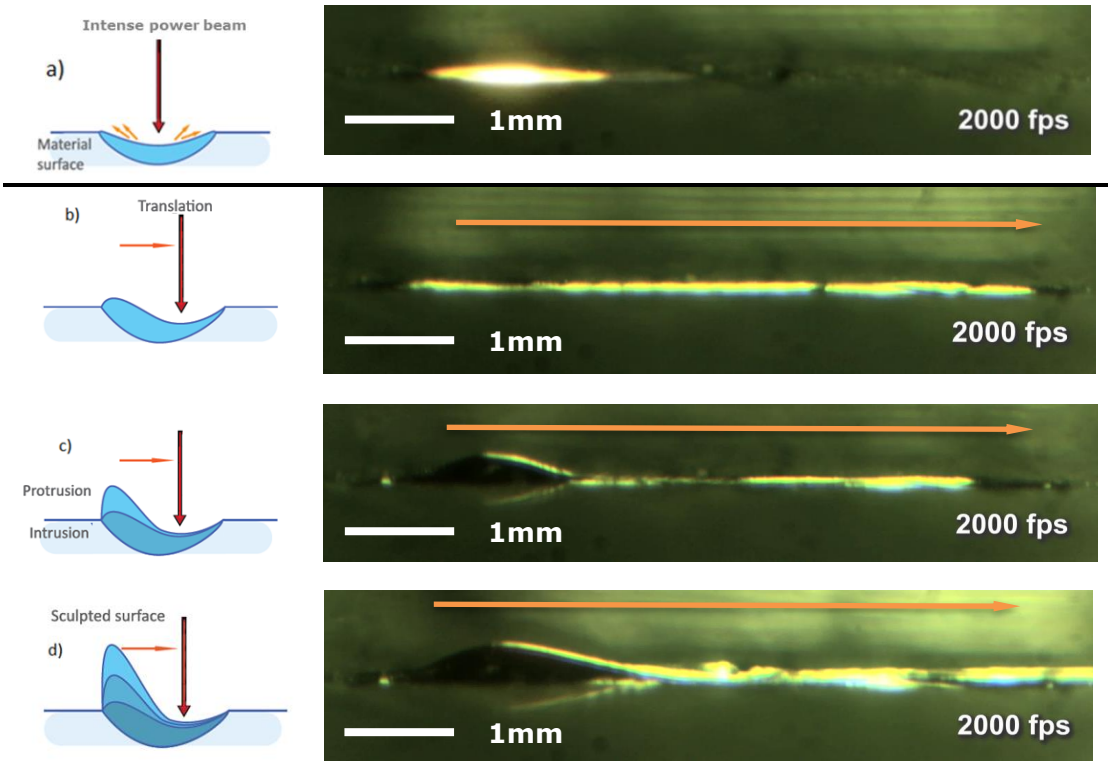

Figure 3.2 Feature formation of the EBT and Surfi-Sculpt processes, adapted from Pinto (2013):
a) Initial beam-material interaction – common to both processes;
b) First beam translation (swipe) – common to both processes;
c) Second beam translation (swipe) – unique to the Surfi-Sculpt process;
d) Third beam translation (swipe) – unique to the Surfi-Sculpt process.

The high-speed video has allowed a greater understanding of the process by enabling identification of five phases of the formation of a uni-directional swipe feature. The distinct phases in the formation of a feature are:

- Phase 1: Melt track.
- Phase 2: Expansion of feature base and height.
- Phase 3: Increase of feature height.
- Phase 4: Bridging occurring during feature formation.
- Repetition of Phase 3: Increase of feature height.
- Phase 5: Over melting and potential decrease of feature height.

3.4.1 Phase 1: Melt track

As shown in Figure 3.3, the video demonstrated that the initial interaction of the beam with the workpiece created a melt track as it translated across the surface. There was minimal height to the feature at this stage.

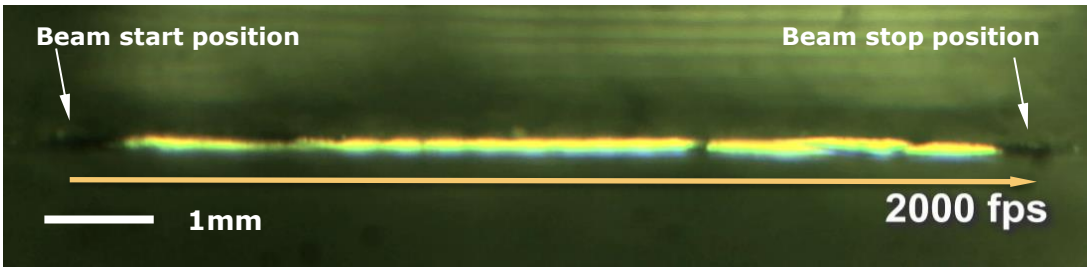

Figure 3.3 First beam translation with melt track (Phase 1).

3.4.2 Phase 2: Expansion of feature base and height

The subsequent two swipes, shown in Figure 3.4, began to expand the length of the base with an increase in the height of the feature.

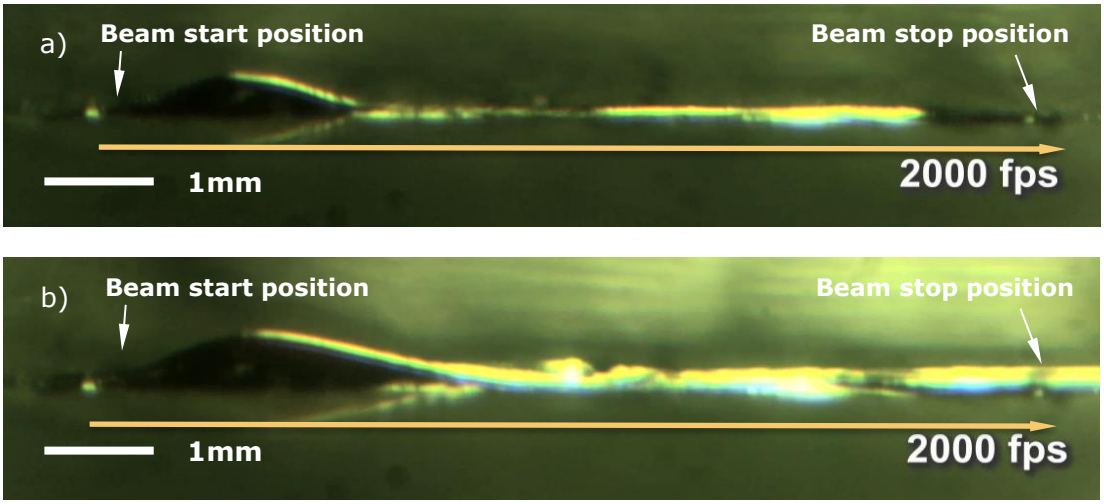

Figure 3.4 Expansion of feature base and height (Phase 2):
a) Second beam translation (swipe);
b) Third beam translation (swipe).

3.4.3 Phase 3: Increase of feature height

With subsequent translations, the height of the feature increased more rapidly without any increase in the length of the feature base, as shown in Figure 3.5. After four beam swipes the feature was approximately 1.2 mm in height.

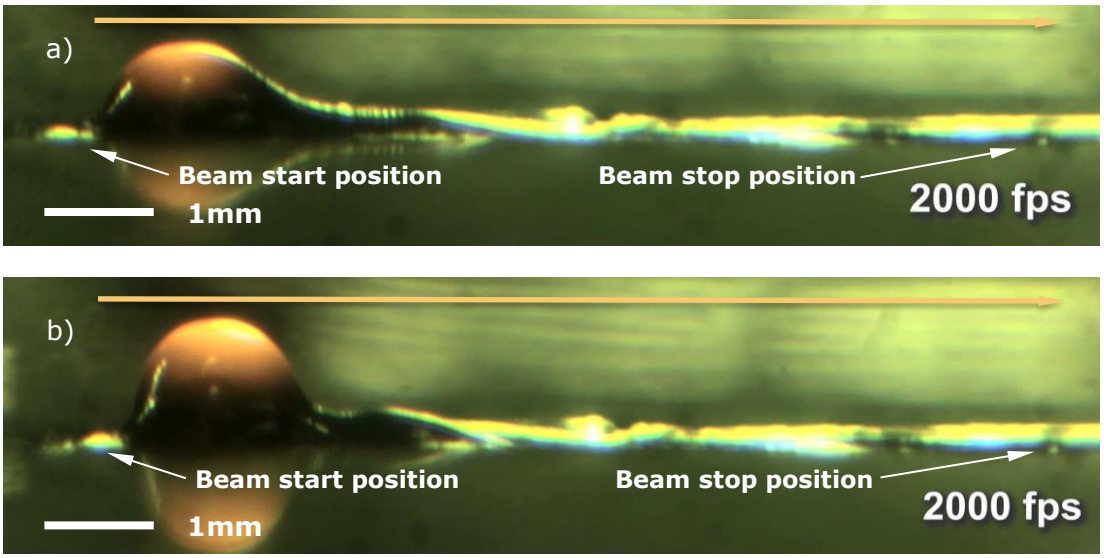

Figure 3.5 Increase of feature height (Phase 3):
a) Fourth beam translation (swipe);
b) Fifth beam translation (swipe).

3.4.4 Phase 4: Bridging occurring during feature formation

Figure 3.6 shows the sixth beam translation (swipe) where bridging of material occurred across the forming feature; this resulted in a distinct phase. The bridging is highlighted by the white dotted line showing the cross section of the feature after the fifth beam translation.

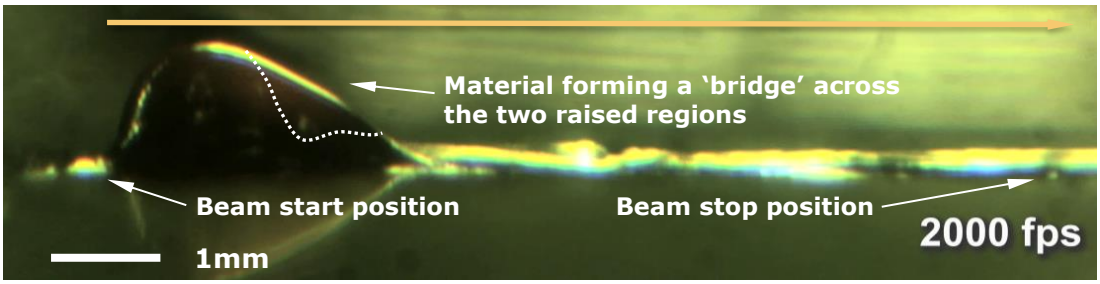

Figure 3.6 Bridging occurring during feature formation (Phase 4) – sixth beam translation (swipe).

3.4.5 Repetition of Phase 3: Increase of feature height

Figure 3.7 shows that additional beam translations from swipe seven onwards resulted in increases in height with the base of the feature remaining constant, as in the Phase 3 mechanism. The shape of the feature altered as a result of the additional molten material moving to the top of the feature and re-solidifying as it cooled.

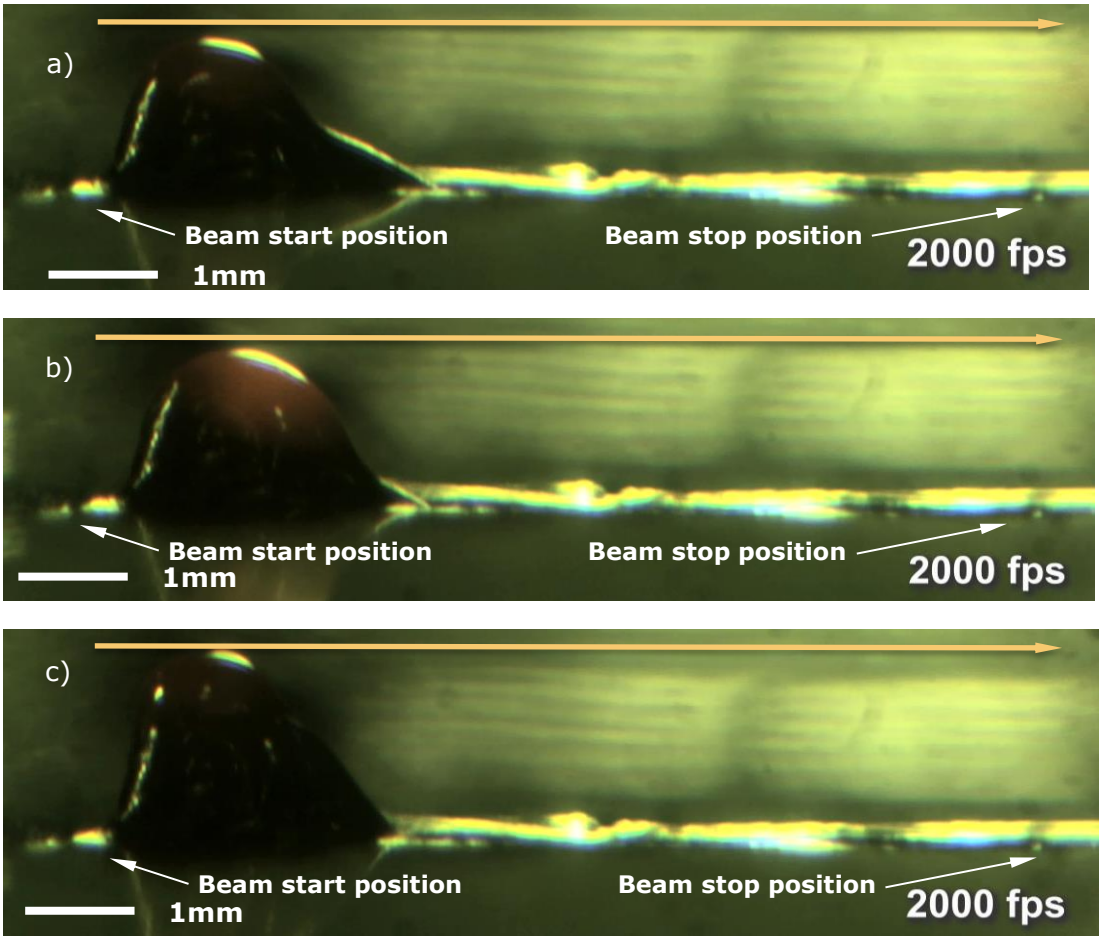

Figure 3.7 Repeated increase of feature height (Phase 3):
a) Seventh beam translation (swipe);
b) Eighth beam translation (swipe);
c) Ninth beam translation (swipe).

This phase, with the increase in feature height, continued up to and included swipe 19.

3.4.6 Phase 5: Over melting and potential decrease of feature height

From swipes 20-23 inclusive there was no longer an increase in feature height associated with each beam swipe; the top of the feature was observed to plateau. Figure 3.8 shows the complete feature formed after 20 beam swipes.

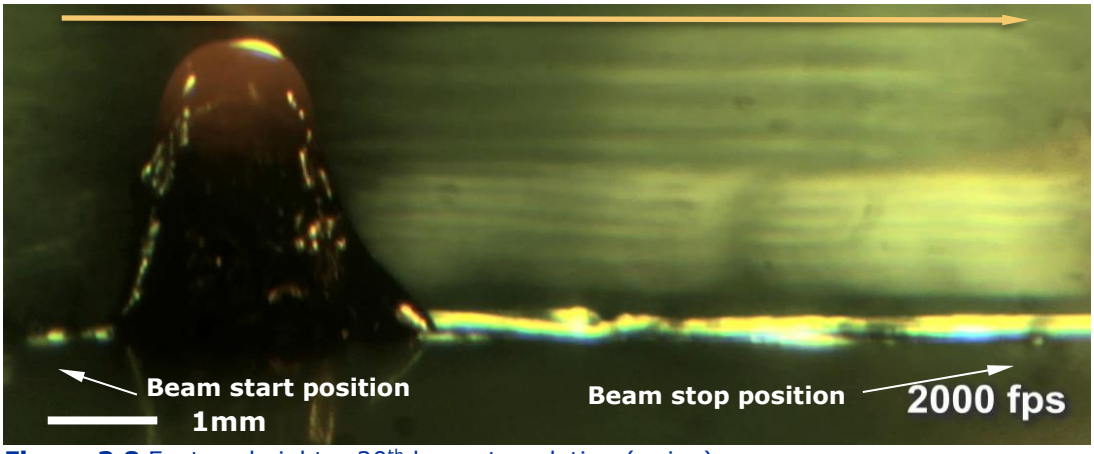

Figure 3.8 Feature height – 20th beam translation (swipe).

3.5 Discussion of feature formation

3.5.1 Movement of molten material via Marangoni effects

Huang (2011) concluded that there was currently no literature on the movement of molten material caused during EB processing. Furthermore, this has not been specified for the deflection of the EB used in the EBT and Surfi-Sculpt process. However, Lee et al. (1998) stated the following four key forces affected the fluid flow during localised EB heating: thermocapillary (Marangoni); buoyancy; aerodynamic drag; and electro-magnetic (Lorentz). The thermocapillary force was considered the dominant force (Heiple and Roper, 1982; Lee et al., 1998) as, in weld pools of less than 10 mm, the buoyancy forces are negligible (Mills et al., 1998). Within the vacuum chamber, the aerodynamic drag would also be minimal and Lee et al. (1998) determine that the Lorentz force was not critical. Therefore, the Marangoni effects on the formation of a feature using the EBT and Surfi-Sculpt processes will be explored further in this section.

Marangoni effects cause the movement of molten material (liquid) as a result of differences in surface tension across an interface (Lee et al., 1998; Mills et al., 1998; Rogers et al., 1993). The molten material flows from areas of low surface tension to those with high surface tension. For Ti-6Al-4V, an increase in the material temperature leads to a decrease in surface tension resulting in an outward flow in the melt pool on the top surface. This is termed a negative

temperature coefficient of surface tension (TCST) (Rai et al., 2009; Huang, 2011). TCST *'is calculated taking into account two contributions: (i) a term resulting from the decrease with temperature of superficial atomic density and calculated from the value of thermal expansion coefficient of liquids, and (ii) an entropic term resulting from the excess entropy of surface atoms with respect to bulk atoms'* (Eustathopoulos et al., 1998, p.274). Simultaneously, an inward counter clockwise flow is formed beneath the surface of the melt pool in the plane perpendicular to the EB and in the opposite direction to the translation of the EB (Dworak, 1992; cited in Weglowski et al. 2016). This cycles the molten material from the edge to the centre point (Jamshidinia et al., 2013). The concentration of surface-active elements present in the alloy, particularly the common group VI elements in the periodic table namely oxygen and sulphur, determine the direction and magnitude of the thermocapillary flow in the molten pool (Lee et al., 1998).

Figure 3.9 shows the author's prediction of the flow of molten material in Ti-6Al-4V by the Marangoni effects (shown by the use of the black arrows) during the initial beam-material interaction and the first beam translation. This prediction is further supported by Mills et al. (1998) who considered the forces applied to molten materials for gas tungsten arc (GTA) / tungsten inert gas (TIG) welding based upon Heiple and Roper (1982). Whilst the GTA/TIG welding process is very different to the EBT and Surfi-Sculpt processes, the principles are transferrable between GTA/TIG and EBW (Heiple et al., 1983).

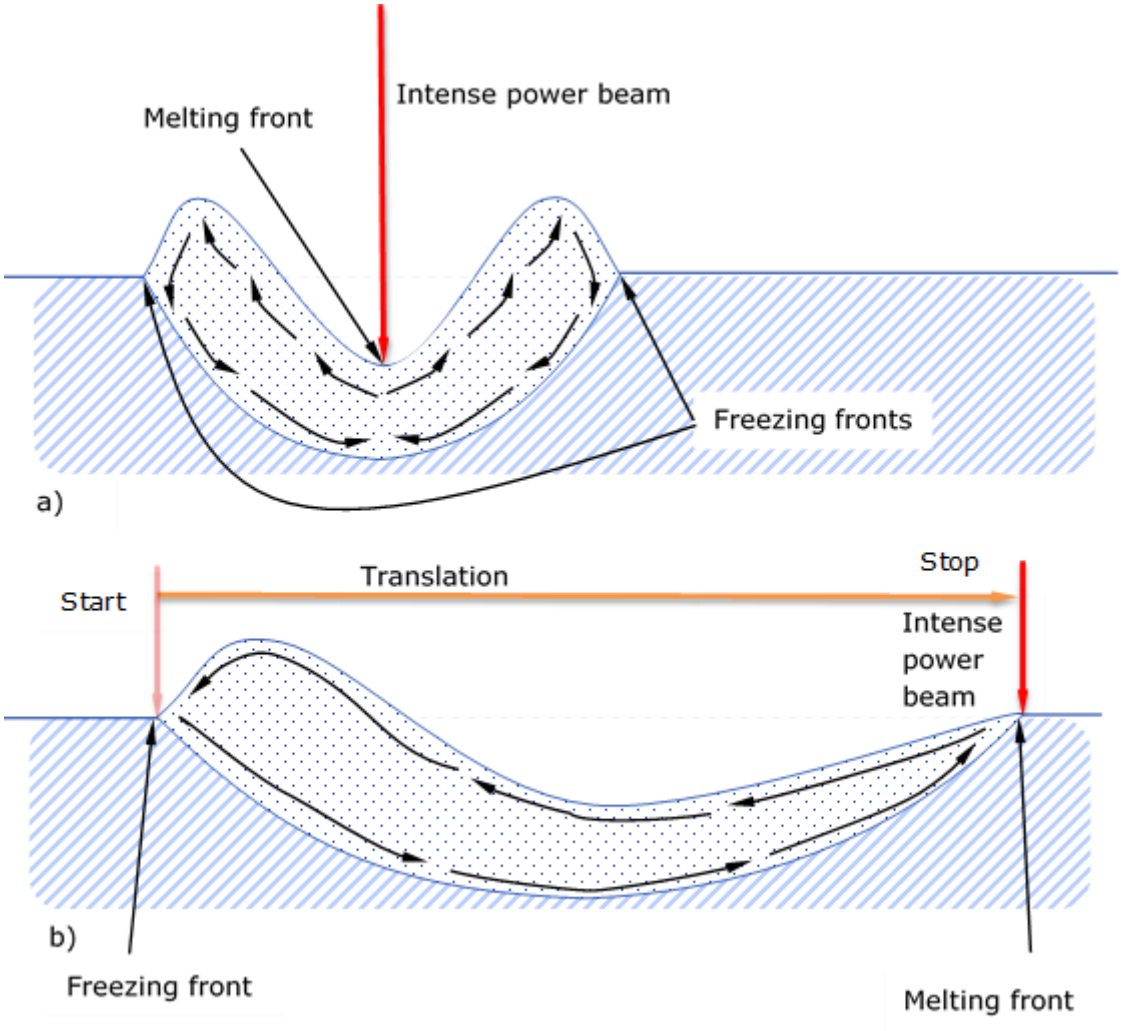

Figure 3.9 Marangoni effects on the fluid flow in a melt pool with a negative temperature coefficient for the EBT and Surfi-Sculpt processes, adapted from Mills et al. (1998):
a) Initial beam-material interaction;
b) First beam translation (swipe) shown by orange arrow.

This model is based upon the melting front, freezing front and material transport in the fused peripheral zone of welding as described by Schiller et al. (1982). The high beam speed of the EBT and Surfi-Sculpt processes leads to '*the melting front increasingly shifting directly below the beam, while the freezing front increasingly lags behind the beam'* (Leskov and Živaga, 1978; cited in Schiller et al., 1982, p.292). This was also observed in EBW when the relative speed of the workpiece and the beam is high. It is this phenomenon which gives rise to the characteristic profile of the feature for a uni-directional beam swipe.

During analysis by the author of the high speed video, 'wobbling' of the material on the tip of the protrusion was observed once the beam had translated over the feature suggesting that the material in this location was the last region to solidify. This is supported by this region being a cherry red colour once the beam had completely translated over it further supporting the author's assertion that this region was the last to solidify and 'freeze'.

3.6 Relationship between processing parameters and other variables affecting the electron beam texturing and Surfi-Sculpt processes

3.6.1 Overview

The geometry, shape and position of features after each swipe are based upon the following variables in Table 3.2. These are compiled from the review in Chapter 2 and based upon the work conducted within this EngD (data can be found in Appendix D).

These variables are split into three groups of parameters: material specific, EB machine, and EBT and Surfi-Sculpt process parameters. The quantity of variables highlights the complexity of the processes. In order to support wider adoption of the processes, these variables should be used as the basis for predictive modelling of the EBT and Surfi-Sculpt processes.

Table 3.2 Parameters affecting the EBT and Surfi-Sculpt processes.

Material parameters	Factor affected by the parameter	EB machine parameters	Factor affected by the parameter	EBT and Surfi-Sculpt processes parameters	Factor affected by the parameter
Density	Mean electron range into substrate	Heat input (accelerating voltage and beam current - power of EB)	EBT and Surfi-Sculpt processes	Direction of beam swipe	EBT and Surfi-Sculpt processes
Melting temperature	Solidification kinetics	Beam diameter – *determines the heat input per cm^2*	EBT and Surfi-Sculpt processes	Beam swipe length	EBT and Surfi-Sculpt processes
Boiling temperature	Solidification kinetics	Beam shape/power density distribution	EBT and Surfi-Sculpt processes	Beam interaction duration at each location	EBT and Surfi-Sculpt processes
Solidification temperature	Solidification kinetics	Beam focus - *needs to be <±1 % of sharp focus, i.e. most intense beam*	EBT and Surfi-Sculpt processes	Deflection pattern frequency (or relative motion of the workpiece and beam)	EBT and Surfi-Sculpt processes
Thermal conductivity	Solidification kinetics	Vacuum pressure in process chamber	EBT and Surfi-Sculpt processes	Number of repeats of the beam swipe over the same location	EBT and Surfi-Sculpt processes
Temperature coefficient of surface tension (TCST)	Marangoni effects	Working distance	EBT and Surfi-Sculpt processes	Processing order of beam swipes *(if multiple swipes in a motif – see Section 7.2)*	EBT and Surfi-Sculpt processes
Thermal diffusivity coefficient	Marangoni effects	Angle of beam to the workpiece	EBT and Surfi-Sculpt processes	Beam interaction position spacing	EBT and Surfi-Sculpt processes
Cooling rate	Solidification kinetics	Beam convergence angle – *this is unique to each gun design and the working distance*	EBT and Surfi-Sculpt processes	Beam speed	EBT and Surfi-Sculpt processes
Viscosity of liquid	Marangoni effects				
Latent heat of fusion	Solidification kinetics				
Freezing range	Solidification kinetics				

The relationships between several of these variables were discussed in Chapter 2. The first two columns of variables in Table 3.2, namely the material parameters and EB machine parameters, have been researched since welding was first conducted via EB in 1957 (Bakish and White, 1964).

However, Koleva and Mladenov (2011) discussed that the relationships between key variables affecting EB techniques (such as the EBT and Surfi-Sculpt processes) are hindered by the unknown values of material characteristics, the limited mathematical models and lack of detailed understanding regarding the EB-material interaction. Koleva and Mladenov (2011, p. 111) assert that '*the physical and mathematical models proposed in the literature are very simplified*' which highlights the complexity of studying and defining any EB-material interaction.

Table 3.3 lists material properties for Al6082, Al6xxx and Ti-6Al-4V for the EBT and Surfi-Sculpt processes at their respective melting points. However, work by Mills (2002, p.17) has concluded that the 'mushy' region (between the solid and liquid phases) is complex and therefore it is difficult to quantify the value accurately with uncertainties of up to ±30 %. An example of this uncertainty is the calculated thermal conductivity as this was determined from a static liquid and not, as is the case for the EBT and Surfi-Sculpt processes, accounting for convective heat flow during solidification.

Table 3.3 Material properties for Al6082, Al6xxx and Ti-6Al-4V, compiled from Mills (2002)[a], Bruyere et al. (2013)[b], Tseng and Li (2019)[c] and datasheets from suppliers[d].

Material properties at melting temperature *(other than where stated*)*	**Al6082**	**Al6xxx**	**Ti-6Al-4V**
Density (g/cm^3)	2.580[d]	2.415[d]	3.920[a]
Melting temperature (°C)	555[d]	665	1650[b]
Boiling temperature* (°C)	2357	2467	3327[b]
Solidification temperature* (°C)	-	600	1604[c]
Thermal conductivity (W/m.K)	180[d]**	218 [d]**	33.4[a]
Temperature coefficient of surface tension (N.m^{-1})	-	-	1.35[b]
Thermal diffusivity coefficient – 10^6 a(m^2.s^{-1})	-	32	9.0[a]
Viscosity of liquid (mPa.s)	1.11[a]	1.15[a]	3250[a]
Latent heat of fusion (kJ/kg)	-	-	390[b]

Where – is an unknown value.
** temperature as stated, not melting temperature*
*** value at room temperature*

Mills (2002, p. 17) calculated property values for the 'mushy' region in Equation 5 for aluminium alloys; however, a limitation with this equation is that it does not factor in the variable of different cooling rates which may be achieved. It is known that the cooling rate of the Surfi-Sculpt process is lower than traditional EBW given the repeat visits of the EB over the surface as discussed in Section 2.2.3.

$$P_T = f_{s(T)} \times P_{T_{sol}} + \left(1 - f_{s(T)}\right) \times P_{T_{liq}} \qquad \textbf{Equation 5}$$

Where P is the required property at temperature T, $f_{s(T)}$ is the fraction at solid at T, and $P_{T_{sol}}$ and $P_{T_{liq}}$ are values of the property at the solidus temperature and the liquid at the liquidus temperature, respectively (Mills, 2002, p.17)

Figure 3.10 shows the primary action(s) required to cause a modification to the geometry of features created using the EBT and Surfi-Sculpt process parameters and the consequential actions required.

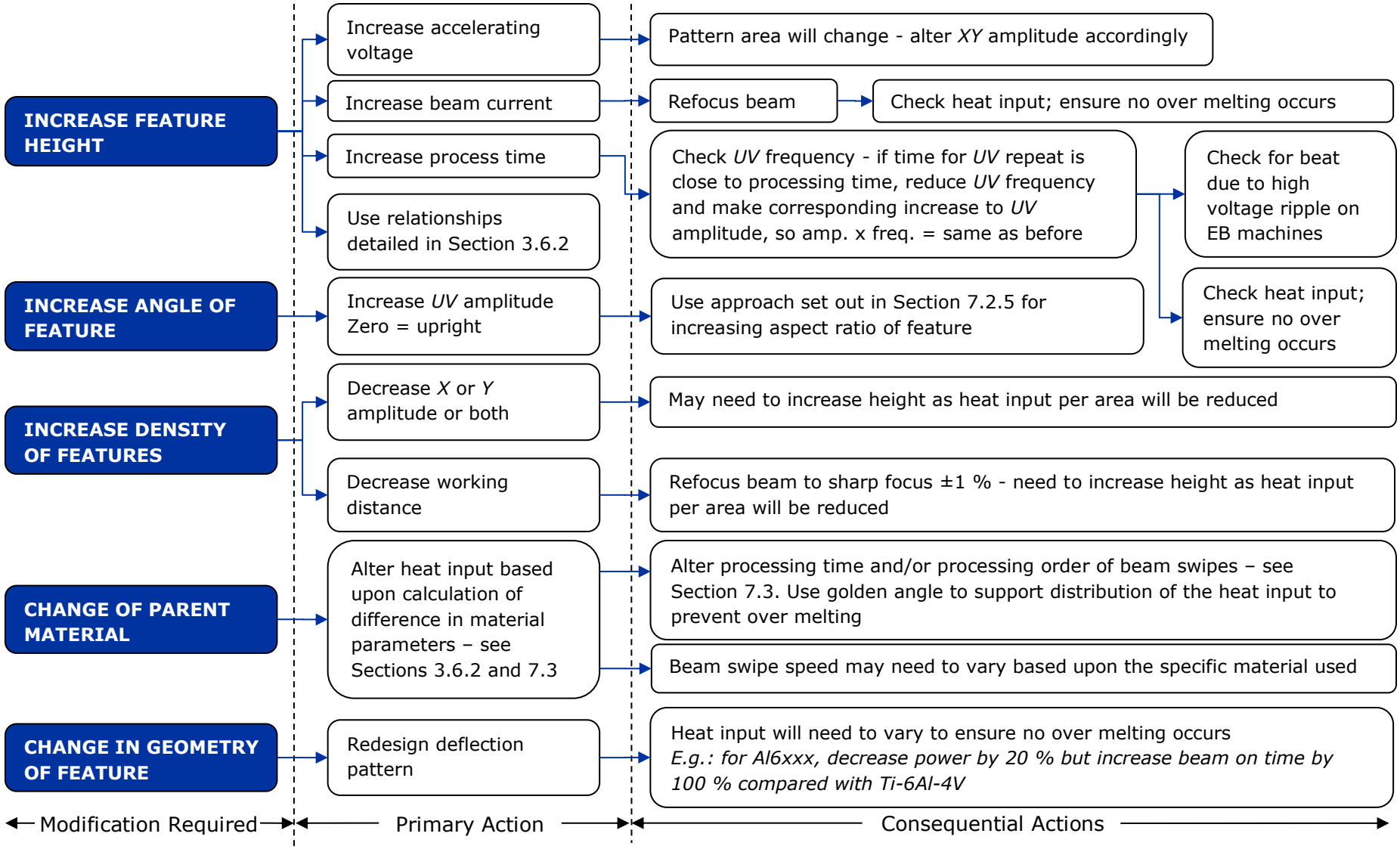

Figure 3.10 EBT and Surfi-Sculpt process parameter optimisation chart.

Within Figure 3.10, the deflection parameters can be described as the following:

XY Amplitude: Scaling parameters for patch area or array

UV Amplitude: Scaling factor for movement of motif
(different scale to that of XY amplitude)

XY Frequency: Number of array repeats per second

UV Frequency: Repetition rate of the *UV* pattern (motif)

For example:

If *UV* Amplitude = 0.5 and *UV* Frequency = 0.1 Hz

Then the pattern moves a distance of 0.5, 0.1 times per second, so in 10 seconds it has moved x 0.5

Furthermore, the ability to computationally predict the geometry and height of the resultant features created would allow further development and integration into manufacturing environments.

3.6.2 Regression analysis and prediction of feature height

Regression analysis was completed to consider the relationship between the feature height (Λ) and the following key variables from Table 3.2 for three materials, Al6082, Al6xxx and Ti-6Al-4V, for the EBT and Surfi-Sculpt processes:

- Number of swipes in the motif – η_s.
- Swipe length (mm) – l.
- Beam swipe speed in the motif (m/s) – ϑ.
- Processing time (s) – P_t *(where appropriate trials were performed)*.
- Beam on time (s) – β.
- Heat input (W) – ω.
- Beam energy input (J/m) – β_E.

The regression analysis (see Table D2 in Appendix D) was conducted using data generated from successfully processed surfaces and therefore is intended solely to be used within the optimised processing parameter window.

Equation 6 calculates the predicted feature height based upon the regression analysis for Al6082. The main parameter affecting the feature height in Al6082 was the swipe length.

$$\Lambda\,(for\ Al6082) = -4.442 \times 0.024\eta_s \times 0.775l \times 0.048\vartheta \times 0.028\beta \times -0.038\omega \times 0.464\beta_E$$

Equation 6

Figure 3.11 shows the residual difference between the predicted and actual feature height for Al6082 based upon Equation 6.

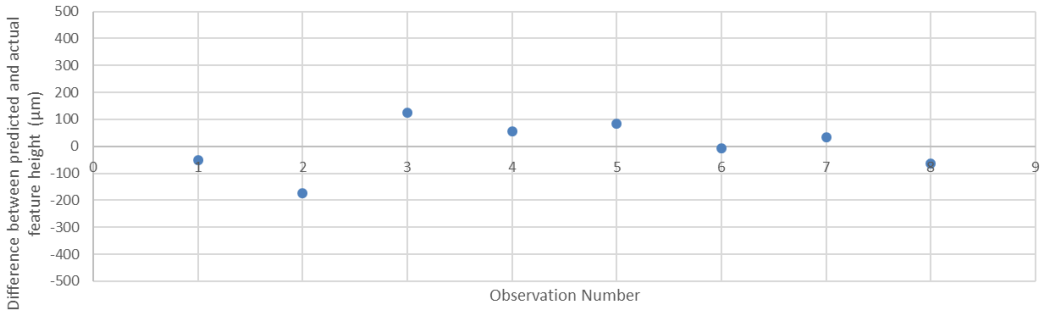

Figure 3.11 Residuals for Al6082.

The R^2 value was 0.928 giving a confidence level of approximately 93 % for the data. This supports the fact that Equation 6 can be used to accurately calculate the feature height for Al6082.

Equation 7 calculates the predicted feature height based upon the regression analysis for Al6xxx.

$$\Lambda\,(for\ Al6xxx) = 5.529 \times -0.075\eta_s \times -0.289l \times 0.022\vartheta \times 0.022P_t \times -0.005\beta \times 0.004\omega \times -0.009\beta_E$$

Equation 7

Figure 3.12 shows the residual difference between the predicted and actual feature height for Al6xxx based upon Equation 7.

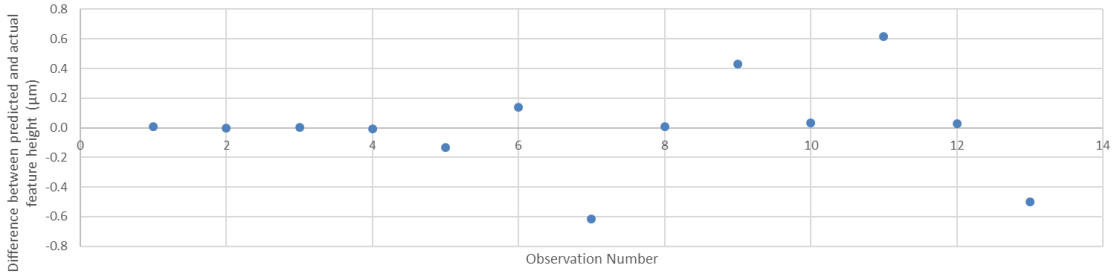

Figure 3.12 Residuals for Al6xxx.

The R^2 value was 0.891 giving a confidence level of close to 90 % for the predicted data. This means that Equation 7 is not statistically accurate within ±10 % for calculating the feature height for Al6xxx.

However, data points 8, 9 and 15 are significantly lower than predicted due two separate factors: i) a change in beam focus setting away from sharp focus by less than 1 % (data points 8 and 9) and ii) over melting occurring with data point 15 as a result of higher power and heat input. The reduction of up to approximately 70 % in the feature height resulted when the beam was not set at sharp focus. The larger spread of higher than predicted feature heights in Al6xxx were as a result of the lower Si content (making the molten material more viscous). This meant that the Marangoni effects had a greater opportunity to support the 'growth' of the features and allow the molten material to solidify and freeze before the gravitational pull and surface tension drew the material down the feature. This explains why there is a variation since the Marangoni effects have greater influence on this material.

Equation 8 calculates the predicted feature height based upon the regression analysis for Ti-6Al-4V.

$$\Lambda\,(for\ Ti-6Al-4V) = -0.358 \times -0.001\eta_s \times 0.878l \times -0.005\vartheta \times 0.017\beta \times 0.008\omega \times -0.001\beta_E$$

Equation 8

Figure 3.13 shows the residual difference between the predicted and actual feature height for Ti-6Al-4V based upon Equation 8.

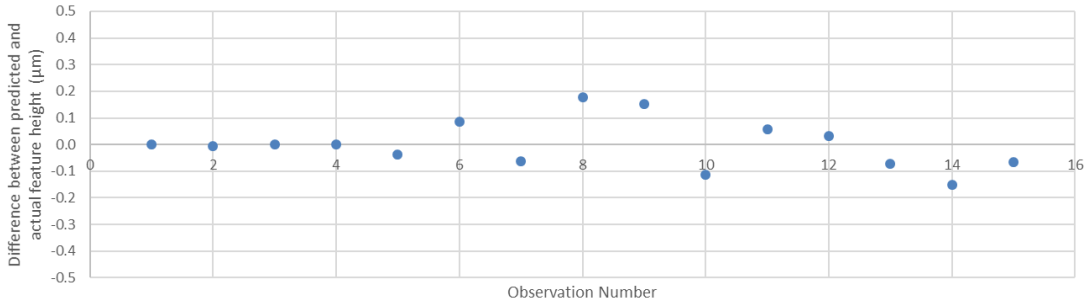

Figure 3.13 Residuals for Ti-6Al-4V.

The R^2 value was 0.985 giving a confidence level of over 98 % for the predicted data. This supports the fact that Equation 8 can be used to accurately calculate the feature height for Ti-6Al-4V.

3.7 Summary of the feature formation

A bespoke technique was developed to record high-speed video of the EB Surfi-Sculpt process from within the vacuum chamber where five distinct phases of feature formation were observed: initial melt track; expansion of feature base and height; increase of height; bridging; and over melting with potential decrease of height.

It was not possible to ascertain the movement of molten material from the high-speed video, only the resultant feature geometry after each beam swipe; therefore the theories of Dance (2007) and Earl et al. (2016) could not be validated. However, the author extended the knowledge through the review of principles to pre-existing work with similar fusion welding processes and proposed a model determining that the most critical force in the flow of molten

material in the EBT and Surfi-Sculpt processes was from the Marangoni effects. This extension of the knowledge concerning the formation of features created by the EBT and Surfi-Sculpt processes has supported the bridging of the 'Valley of Death' and progression towards TRL 5.

It has been demonstrated that it is possible to accurately predict the feature height for two materials, Al6082 and Ti-6Al-4V, based upon key variables for the EBT and Surfi-Sculpt processes. The lack of accuracy on the prediction of the feature height for Al6xxx was due to the beam not being at sharp focus for some processing and over melting occurring as a result of higher power and heat input demonstrating the importance of these variables. However, the complexity of studying and defining any EB-material interaction highlights why there is a lack of predictive modelling and defined relationships between all parameters and variables listed in Table 3.2.

4 Liquid Cold Plate Case Study

4.1 Background to liquid cold plates

This case study investigated the use of the Surfi-Sculpt process to improve thermal performance of liquid cold plates (LCPs) by creating features to enhance the heat transfer coefficient.

When air-cooling does not provide the requisite performance, LCPs use liquid cooling to remove heat from devices such as temperature control systems, laser cooling and medical equipment. A LCP is typically fabricated from a machined plate (body), to form flow paths for the liquid, which is assembled with a cover to capture the flow of liquid. The flow path can be made from holes drilled into the plate, an embedded tube inside the plate or channels machined into the plate. Extended features, shown in Figure 4.1, can be created within the channel of the plate, or folded fins can be used, shown in Section 4.3, to further enhance heat transfer (Wakefield-Vette Inc, 2017). This enables liquid to flow through the channels or tubes in such a way as to maximise heat transfer and to remove the heat from the plate in contact with the device (heat load).

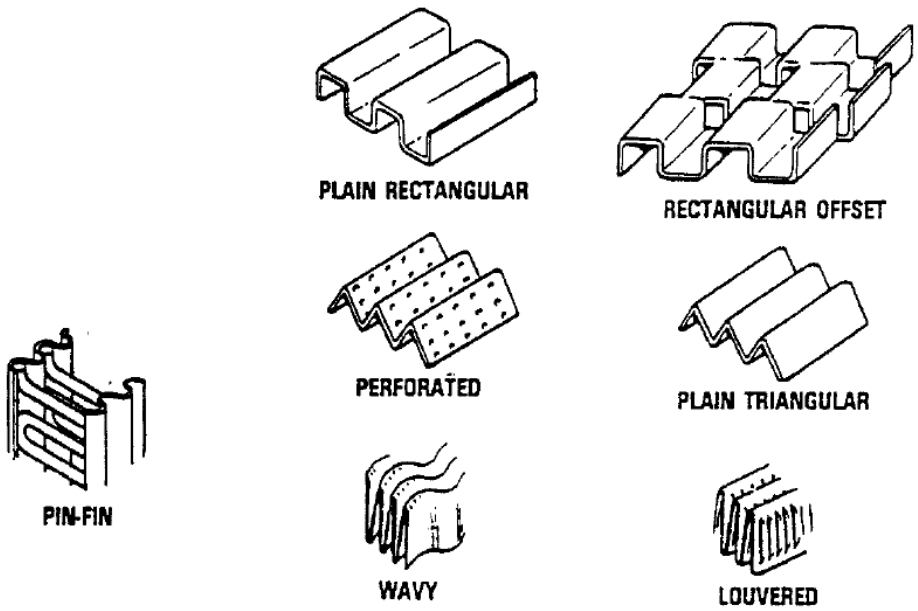

Figure 4.1 Typical plate fin extended surface geometries, used with permission © (Reay, 1991).

The Surfi-Sculpt process has the ability to create complex geometries of features through the manipulation of their shape, height and/or spacing. Existing extended surfaces may be in the form of pin-fins, ellipses, cylinders and squares (Zeren et al., 2017), as well as micro channels, grooves, louvre fins, or ridges (Buxton and Dance, 2010). Ferhati et al. (2015) recognised the potential to apply the Surfi-Sculpt process to heat exchangers, in particular LCPs, as it has the capability to increase the surface area and engineer the flow of liquid.

This case study was based upon a collaborative project, entitled 'Novel Electron Beam Surface Sculpting for Efficient Heat Exchange (HeatSculptor)'. The project received funding from the European Union's Seventh Framework Programme for research, technological development and demonstration under grant agreement No. 606172. The author was the Technical Manager for the overall project and the Project Leader for TWI's contribution. The consortium was led by COOLTECH Srl, a designer and manufacturer of heat exchangers, and included, alongside TWI: Aquasium Technology, an EB equipment manufacturer; Cenaero, a non-profit, private research organisation aimed at providing state-of-the-art simulation tools, such as CFD, to industry; DTK Electronics, an example end user; and WLB, an industrial software design and supply company. COOLTECH provided the designs of the surfaces for the LCPs, as discussed in Submission 3.

The author applied the Surfi-Sculpt process to a LCP with a surface area of 95 x 31 mm (total area of 2,945 mm^2) which was over three times the area of previous studies (Buxton and Dance, 2010; Ferhati et al., 2015). This was a particular challenge because it extended the state-of-the-art beyond the previous work which created small height features (approximately 2 mm in height) on copper over a small area (31 x 35 mm), shown in Figure 4.2. The benefit of this would be the ability to generate a higher heat transfer coefficient and thus cool

larger heat loads with the LCPs providing a wider range of applications. The heat transfer coefficient is calculated using Equation 9 (Ferhati et al., 2015, p. 1170).

$$h_{av} = \frac{\dot{m} c_p (T_e - T_i)}{A_s \Delta T_{LMTD}} \qquad \textbf{Equation 9}$$

Where h_{av} is the average convection heat transfer coefficient, $\dot{m}$ is the mass flow rate of the cooling fluid, c_p is specific heat capacity of the cooling fluid, T_e is the exit temperature of the cooling fluid, T_i is the inlet temperature of the cooling fluid, A_s is the surface area of heat transfer (in this case the area where the features created by the Surfi-Sculpt process are located) and ΔT_{LMTD} is the logarithmic mean temperature difference between the surface temperature and the cooling fluid inlet and exit temperatures respectively.

Alternatively, a reduction in the size of the LCP could be achieved, a reduction in temperature difference between the inlet temperature in the LCP and the heat load could be realised or the capacity of an LCP could be increased (Bergles, 1999; Reay et al., 2013). These applications would address the need of increasing cooling capacity for high power density applications that use liquid cooled solutions. This need stems from the trend of decreasing die sizes and thicknesses with an associated increase in power density and power output in power electronics such as insulated-gate bipolar transistors (IGBTs).

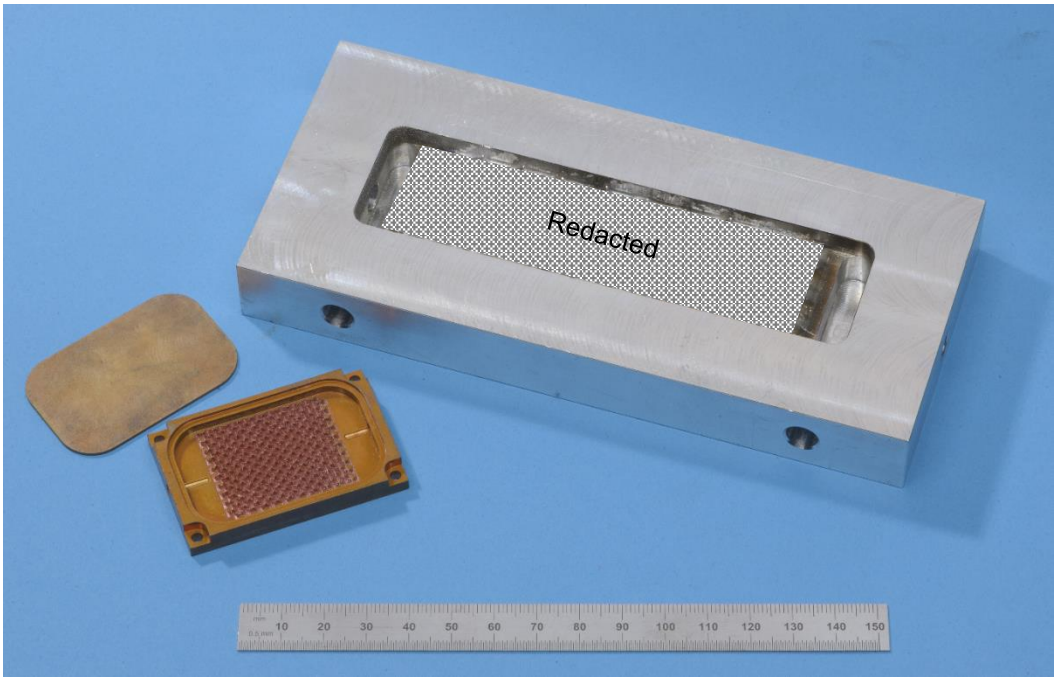

Figure 4.2 Previous LCP (left) manufactured using the Surfi-Sculpt process in copper by Ferhati et al. (2015) and the LCP produced as part of HeatSculptor (right) in aluminium.

The component was manufactured in 6000 series aluminium, detailed in Submission 3, and the Surfi-Sculpt process was carried out over the complete area in approximately 120 seconds beam on time. The author demonstrated that the lower silicon (Si) content of this alloy compared to Al6082 increased the viscosity in the molten material and, as a consequence, improved the material's stability during the Surfi-Sculpt process. As a result, it was possible to produce higher feature heights, in excess of 6 mm, compared to the 3.3 mm height achieved with Al6082. The external dimensions of the assembled LCP were 76 x 170 x 20 mm. The dimension of the features and the internal channel size of the test LCPs were chosen to be similar to typical situations for the most common electronic devices used in power electronics markets, e.g. IGBTs, resistors and inductors. Due to commercial confidentiality, the images of the internal structures and specific grade of material are shown in Submission 3 only.

4.2 Heat exchanger competing technologies

A wide range of other surface texturing techniques are available for heat exchangers; Table 4.1 shows a comparison of the most common state-of-the-art surface modification techniques. The comparison explores the size of features that can be produced, either described as macro or micro, along with the ease of manufacture of each process, the respective speed, associated cost and, finally, an overview of the main limitations.

Enhanced heat transfer surfaces for the majority of heat exchangers are generated through etching, machining or extrusion. As indicated in Table 4.1, currently all manufacturing practices have limitations and some require time-consuming and expensive processes; in the case of chemical etching, may have environmental impacts. Many processes are limited in the geometry of features and surfaces which can be produced as shown with typical tube fin geometries in Figure 4.3. The attribution of a high, medium and low grading for each category in Table 4.1, used to assess the various technologies, was subjective but relative to the benchmark of the EBT and Surfi-Sculpt processes; each grading was allocated with support from the HeatSculptor project partners. A limitation was that data was not readily available to allow exhaustive quantification of all the categories.

Table 4.1 Heat exchanger state-of-the-art competing technologies overview.

Surface modification technique	Feature size	Ease of manufacture (H,M,L)	Speed (H,M,L)	Cost (H,M,L)	Limitations
Machining	Macro and micro	M – H	M	L - H	Material wastage Some materials are difficult to machine e.g. titanium Limited geometries
Folded fin (FF)	Macro	H	M	L - M	Limited geometries
Extrusion	Macro	M - H	H	L - M	Limited geometries to constant cross section e.g. ridges (Black, 2015)
Knurling	Macro	L – M	H	L	Limited geometries Physical contact required
Ball sintering	Macro	L	L	H	Slow process
Foam metal coatings	Macro	L	H	M	Limited range of materials possible
3D Printing such as direct metal deposition / powder bed techniques	Macro	M – H	L	H	Use of high power lasers
Grit blasting and shot peening	Micro	L	H	L	Potential distortion Contamination due to embedded grit particles Masks sometimes necessary creating waste
Chemical photo-etching	Micro	L – M	L	M	Environmental and health issues with use of hazardous chemicals Limited geometries
Electro-discharge texturing	Micro	L	L	L	Relatively slow Use of consumables
Micro-machining	Micro	M – H	M	L - H	Speed dependent on complexity Not suitable for mass/batch production (Prakash and Kumar, 2014)
Ink jet printing	Micro	M	H	M	Mask usually required creating waste
Power beam micro-processing	Micro	L – M	H	M - H	Limited to simple indentation features
EBT and Surfi-Sculpt processes	Macro and micro	H	H	L - H	Developmental processes Limited data on the benefits Limited fundamental knowledge Relatively high capital cost for equipment Features >100 µm

Key: L - low, M – medium and H – high with respect to the EBT and Surfi-Sculpt processes

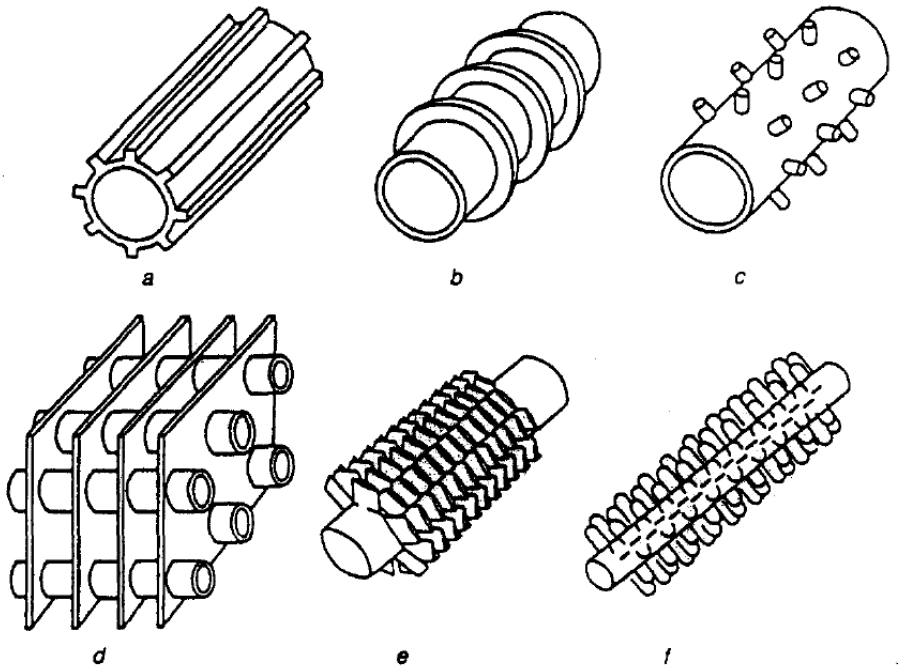

Figure 4.3 Typical examples of tube fins, used with permission © (Reay, 1991):
a) Longitudinal fins;
b) Radial fins;
c) Tube with spines;
d) Continuous fins;
e) Fins with elliptical cross section;
f) Wound-wire fins.

This review of existing micro-manufacturing technologies highlights the unique position of the Surfi-Sculpt process in offering a manufacturing route for complex, bespoke textured surfaces at high production speeds.

To achieve reliability and safety in heat exchange processes, enhancement techniques are continuously being investigated; these may be divided into three groups (Webb and Kim, 2005; Reay et al., 2013; Ferhati et al., 2015):

- Active techniques which require external power.
- Passive techniques which apply surface enhancement or additives.
- Combined techniques which provide better enhancement than a single technique.

Active techniques require either: the use of an agitator such as a turbine, propeller or paddle to stir and mix the fluid; vibration of either the LCP or the

fluid; jet impingement; induced flow instabilities; or rotation of the heat transfer surface (Reay et al., 2013). All of these techniques, whilst providing improved performance, require additional space, power and cost associated with the active element. Since the features created using the Surfi-Sculpt process are passive (Reay et al., 2013), the active techniques are outside the scope of the EngD.

Passive techniques have the advantage of low operation and maintenance costs. These techniques include textured surfaces achieved using fine scale coatings or those created by conventional or chemical processes. Rough surfaces of this type increase convection and condensation by forming artificial nucleation sites and hence provide better heat transfer than non-textured surfaces. Engineered (extended) passive surfaces are introduced into many heat exchangers to further improve performance. Surfaces are designed to encourage greater heat transfer by increasing both the surface area and the convection coefficient. These surfaces are generally manufactured using conventional methods such as wire erosion, machining and chemical processes. However, these methods restrict the complexity of the surface that can be manufactured. For the most efficient heat transfer, the ability to make a range of shape profiles which encourage efficient heat transfer without introducing high drag (high pressure drop) into the working fluid is preferred. An increase in pressure drop requires additional pumping power to overcome this loss in the system.

A number of new technologies have recently emerged for heat exchanger surface structuring. Wong et al. (2009) investigated laser melting technology (LMT) which utilises a high-power laser beam to melt metal powders and create structures. LMT is a slow process and requires raw material in the form of powder. Intensive research has been carried out into microelectronics cooling (Wang et al., 2007; Posew et al., 2009; Honda and Wei, 2004); however, this has yet to result in improved LCP products.

A mechanical displacement process (sometimes known as 'skiving') may also be used to make ribs, pins and fins for cooling purposes. This process works in ductile materials by using sharp tooling to gouge into a surface leaving the displaced material as an upstand. This process can be well-controlled but is limited to the manufacture of a narrow range of features in ductile materials which are typically low strength. In addition, if the process is to be acceptably low cost, it is best utilised to make the same features over an entire surface; therefore, variable cooling requirements over a single surface are not always met using this approach. Workpiece loading during skiving is necessarily high so heat sink designs with delicate base sections are not favoured when using this approach. Smooth fin-type surfaces can be made using skiving; however, these surfaces are known to produce limited heat transfer per unit area under laminar flow conditions and somewhat high fluid pressure drops under turbulent flow conditions when the heat transfer per unit area is high enough for some cooling applications. Pin-fin type structures provide higher heat transfer per unit area but give higher (and variable) pressure drops depending on the pin geometry. Although skiving can produce pin-fin type geometries with high densities, the range of geometries is limited as the features created appear to be exclusively those with sharp edges and corners. Sharp edges on features can give higher fluid pressure drops without a proportional increase in heat transfer which may ultimately limit the efficiency of the cooling system. Skiving technologies have many appealing characteristics but may be limited in this respect to the sharp edges in addition to their inability to process higher strength materials.

Combined techniques are the utilisation of multiple active and/or passive enhancements as described previously in this chapter.

4.3 Aim of the liquid cold plate case study

The aim of the LCP case study, based upon the HeatSculptor project, was to achieve improved cooling at the points of highest temperature with the potential to allow components to be reduced in size for a given thermal performance requirement if enhanced effective heat transfer could be realised. The specification for the LCP features in this case study was that they should have a heat transfer coefficient of at least 800 W/cm^2 and that they should not be easily generated or imitated by a competing technology. The height of the features must be at least 2.0 mm to fit between the body and cover of the LCP. The LCP produced using the Surfi-Sculpt process was benchmarked against COOLTECH's folded fin (FF) series as shown in Figure 4.4.

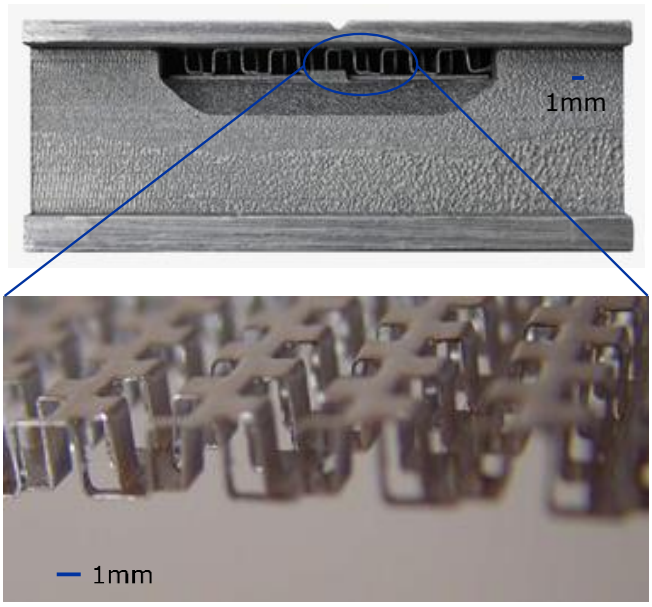

Figure 4.4 COOLTECH's FF (folded fin) series LCP, provided by COOLTECH.

4.3.1 Objectives of the liquid cold plate project

The objectives of the author's work were to:

- Develop surfaces suitable for investigating initial feasibility of increasing thermal performance using the Surfi-Sculpt process.
- Optimise the Surfi-Sculpt process for a representative prototype component over a specified processing area (approximately 95 x 31 mm).
- Manufacture prototype LCP components.

4.4 Manufacture of the liquid cold plate

After the initial development and optimisation work was completed, the prototype LCP was milled to create a blank prior to applying the Surfi-Sculpt process. The blank was loaded into an EB machine capable of the Surfi-Sculpt process and features were produced on the LCP within approximately 120 seconds beam on time using proprietary EB deflection patterns and parameters created by the author. A final machining stage was required for the LCP prior to it being hermetically sealed by vacuum brazing the cover plate. The details of the manufacture were discussed in Submission 3.

4.5 Method of testing the liquid cold plates

The testing was performed by TWI Member Company, COOLTECH, and the test rig is shown in Figure 4.5. The liquid was a 50:50 mixture of demineralised water and ethylene glycol. The flow was regulated to between two and twelve litres per minute through the LCP and was measured using a flowmeter. The power supply generated the load on the system and was measured by the power meter. The power input to the copper heat blocks via the cartridge heaters (load) was between 750 and 1300 W. Each test was repeated three times and mean values were calculated from the three tests. The standard deviation of the results was less than 3 % of the mean values.

The temperature and pressure of the water were measured at the inlet and outlet of the LCP. This data provided the enthalpy rise and pressure drop within the test part.

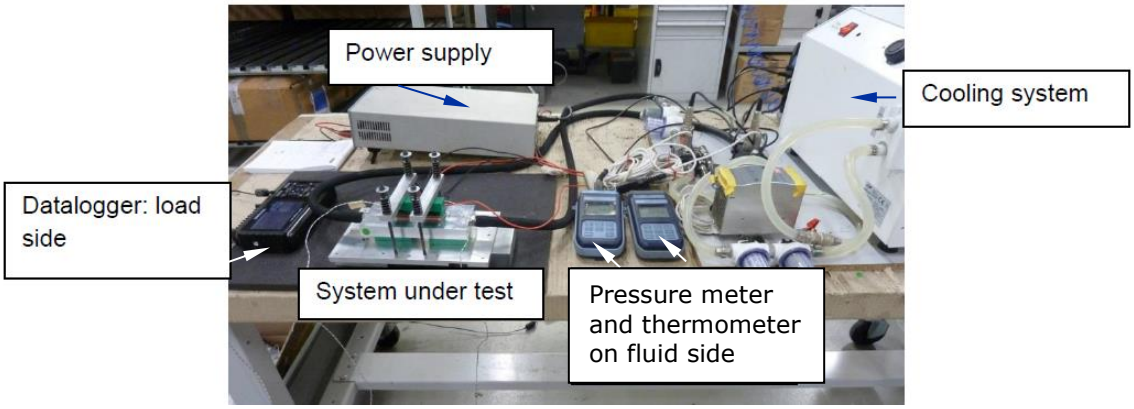

Figure 4.5 Overview of test setup © HeatSculptor, used with kind permission.

The heat load was composed of two LPS800 power resistors manufactured by Vishay, Figure 4.6; these were selected as suitable electronic devices that require cooling using LCPs.

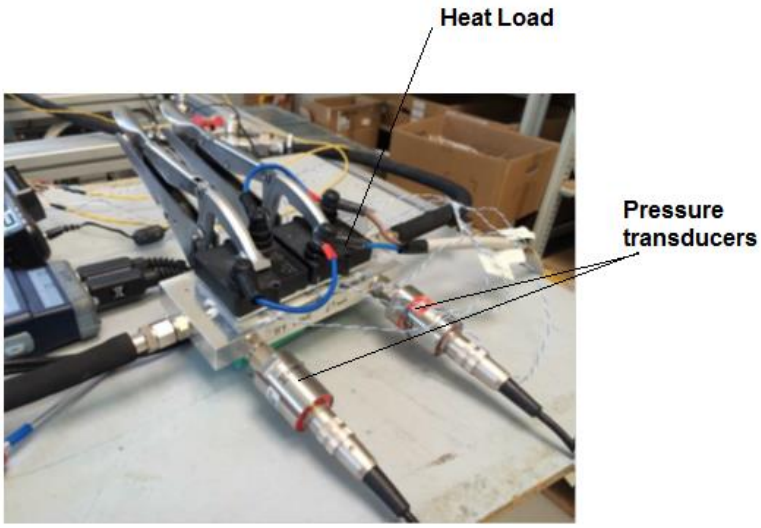

Figure 4.6 Power resistors (heat load) placed upon LCPs © HeatSculptor, used with kind permission.

There are various assembly methods utilised within manufacturing for the body and cover, including welding or brazing, but these depend upon the requirements of the operating environment and performance requirements (Wakefield-Vette Inc, 2017).

An EB machine is appropriate for 'all-in-one manufacturing' of LCPs as the equipment can utilise the Surfi-Sculpt process to both create the features and braze and seal the lid onto the assembly using the EB. A quick response (QR)

code (or similar) can be marked onto the component alongside a logo or any desired mark on the products or parts for easy tracking and traceability. This could allow increased after-market service and support to customers. These manufacturing steps are shown in Figure 4.7.

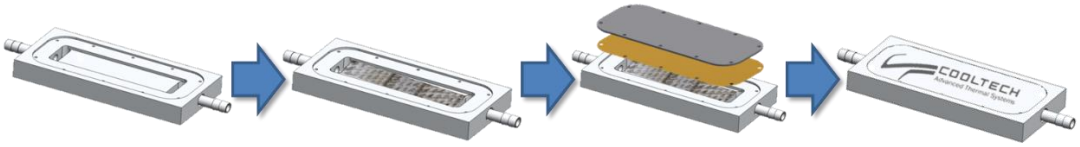

Figure 4.7 Proposed production process of an LCP using the Surfi-Sculpt process with an EB machine.

The current manufacturing time of COOLTECH's Design FF and the expected manufacturing time of an LCP using the 'all-in-one manufacturing' by an EB system are shown in Figure 4.8; this represents a time saving of 40 minutes (approximately 40 %) per component. The cost for each component is dependent on the throughput and volume of production required and how this would be achieved. This is discussed further in Sections 5.8 and 6.8.

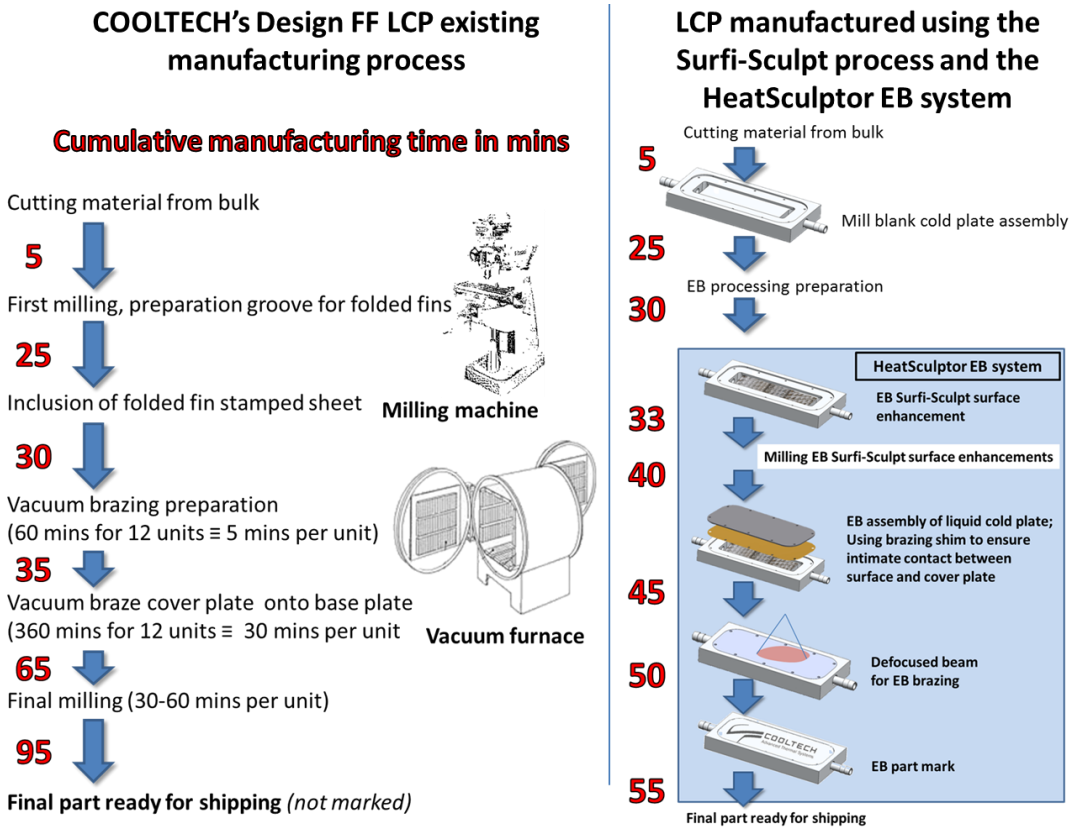

Figure 4.8 Comparison between the manufacturing of an existing machined and vacuum brazed LCP and one manufactured using the Surfi-Sculpt process on an 'all-in-one' EB machine.

4.6 Heat transfer results

Due to commercial confidentiality, the images of the internal structures and specific grade of material are shown in Submission 3 only. The heat transfer results in Figure 4.9 (with each test repeated three times) show an increase in the heat transfer coefficient for a LCP manufactured using the Surfi-Sculpt process compared to COOLTECH's Design FF of approximately 100 % at similar pressure drops for a 1300 W heat load. However, in order to achieve these results, approximately seven times more pumping power was required to overcome the increased pressure drop associated with this performance increase. In applications where this would not be restrictive or prohibitive to usage or cost, the use of the Surfi-Sculpt process to produce features in the heat exchange area would be advantageous compared to the FF technology. For example, this may be where space is restricted and a higher performance LCP is required such as

data projectors where there is a need for increased efficiency, low cost, good performance, high reliability, brighter and bigger bulbs and miniaturisation.

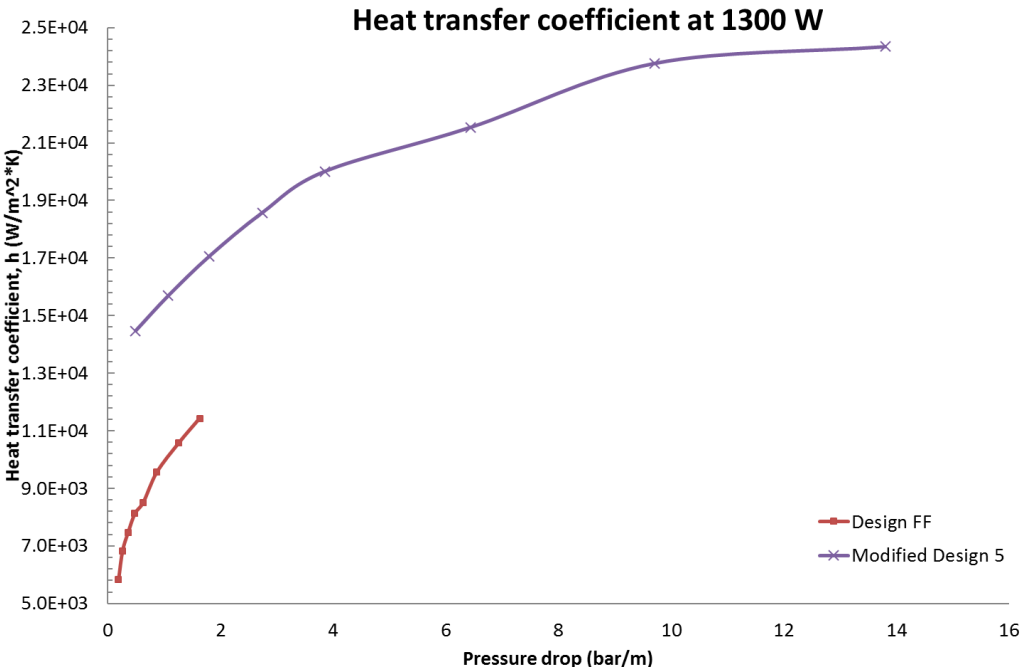

Figure 4.9 Heat transfer coefficient at various pressure drops for Design FF and the LCP with the Surfi-Sculpt process, data provided by COOLTECH.

The performance results in Table 4.2 show temperature measurements during testing for Design FF and a LCP manufactured using the Surfi-Sculpt process.

Table 4.2 Comparison of a LCP manufactured using the Surfi-Sculpt process to Design FF for cooling two LPS800 power resistors, provided by COOLTECH.

Liquid cold plate	Inlet liquid temperature (°C)	Temperature at the base of the power resistor (°C)	Difference
Design FF	30.0	93.1	Reference
LCP produced using the Surfi-Sculpt process	30.0	60.6	32.5 °C cooler

4.7 Discussion of the heat transfer results

The maximum working condition of the power resistor, as listed by the manufacturer Vishay, was 95 °C on the base of the power resistor case. The comparison against Design FF showed that the LCP produced using the Surfi-Sculpt process maintained the two LPS800 power resistors at a temperature

a third cooler than Design FF. This result means that there are two options available for the LCP produced using the Surfi-Sculpt process; either it could be designed smaller to achieve the same performance as Design FF or power resistors with a greater heat load could be cooled. This is advantageous since it would represent the potential for substantial energy saving costs based upon this improved performance (Reay, 1991).

The ability of the EB system to be able to braze and part mark the component highlights its flexibility. However, the consequence of this improved performance is the requirement to increase the pumping power. Furthermore, the capital cost of the EB equipment and the associated operator training and health and safety implications mean that a relatively high volume of production is required to offset the initial cost. To address the cost issue, initial low volume production could be provided by an EB jobbing shop until such a time as production rates have reached a viable position when equipment purchase and the manufacturing could be brought in-house.

4.8 Dissemination activities of the liquid cold plate case study

A project video (HeatSculptor - Novel Electron Beam Surface Sculpting for Efficient Heat Exchange, 2015) was scripted and narrated by the author to aid the dissemination of the project. The video included the test setup, partner interviews conducted by the author and the author's operation of an EB machine (60 kV, 4 kW) showcasing the use of the Surfi-Sculpt process to produce a prototype LCP in an operational environment. The video can be found at: www.youtube.com/watch?v=LoGwhucUO28.

4.9 Conclusions from the liquid cold plate case study

The LCP case study, detailed in Submission 3, proved that a lower thermal resistance could be achieved with the Surfi-Sculpt process compared with an existing product. The HeatSculptor project was able to demonstrate that the heat transfer coefficient could be increased by approximately a factor of two compared with an existing technology (COOLTECH Srl, 2015).

The value proposition and unique selling points (USPs) of the LCP manufactured using the Surfi-Sculpt process are that it:

- Enables more power in the electronic components being cooled.
- Increases efficiency by 100 % without size or weight penalties.
- Enables use of a 50 % smaller LCP for the same cooling power as an existing technology.
- Reduces manufacturing time by over 40 % allowing rapid response to orders at low cost.

The case study and resultant USPs have evidenced the demonstration of the Surfi-Sculpt process in a relevant environment and thus further contributed to crossing the 'Valley of Death' bridge to TRL 6 and MRL 3.

5 Orthopaedic Implant Case Study

5.1 Background to orthopaedic implants

Submission 2 highlighted the problem of bone resorption (Horowitz et al., 1993) whereby implants can cause bone loss and reduced bone mineral density in a total hip replacement (THR). Uncemented implants rely on enhancing the fixation to the bone directly through the process of osseointegration, defined by Pakos and Xenakis (2014, p.68) as '*the formation of a direct interface between an implant and bone'*. This is achieved through surface textures or structures which give the interface its strength by relying on mechanical interlocking into which the bone infiltrates (Karachalios et al., 2014; Jones et al., 2012; Park et al., 2000).

Galvani (1791, translated 1953) first noted that physiological activity resulted from the insertion of metals into frogs. Despite this, the first use of an uncemented implant in a clinical trial was a porous stainless steel coating in 1969 (Pegg et al., 2014). In September 1985, the first commercially available uncemented THR (uTHR) was performed (Furlong and Osborn, 1991; Epinette and Manley, 2013). Since then, there has been a drive to improve the design of the interface between the surface of an implant and the host bone in order to reduce the stress shielding (Kohn, 2011). Matsushita (2010) and Park et al. (2000) defined 'stress shielding' as the prevention of bone being loaded continually which shelters it from the stress required for growth. Submission 2 highlighted that the EBT and Surfi-Sculpt processes were suited to the creation of surfaces on the implant to reduce stress shielding and that these processes would also be cheaper than existing technologies. Currently, the additional cost of existing surface modification processes for uTHRs is why cemented THRs are cheaper.

Morshed et al. (2007) noted that the survivorship for uncemented implants continues to improve; however, Briggs (2015) and Lord Carter of Coles (2016) recommended a reduction in their use in the NHS based upon the associated higher costs. Therefore, any solution for uncemented implants must not result in additional manufacturing costs and must be achieved within the constraints of materials able to realise the mechanical demands and be tolerated biologically. Cross and Spycher (2008) concluded that the interface is the key factor in determining the survivorship of load bearing orthopaedic implants; therefore, Pegg et al. (2014) recognised an opportunity for potentially disruptive technologies which can increase the survivorship.

The author proposed that the EBT and Surfi-Sculpt processes were suitable candidates as lower cost disruptive technologies based upon the fact that the parent material is used and therefore, no additional challenges would result from the introduction of multiple materials. This led directly to the work in Submission 6 based upon a collaborative project, OrthoSculpt, funded by Innovate UK. The author was the Project Leader for the TWI project, in collaboration with the lead partner, JRI Orthopaedics Ltd, a British orthopaedic manufacturer.

5.2 Orthopaedic implant competing technologies

There are a range of commercially available surface modification methods for uTHRs with good survivorship at both ten years (Norwegian Arthroplasty Register, 2016) and 15 years (Hailer et al., 2010). However, these methods are currently limited in their ability to produce new complex designed geometries of structures to load match the mechanical properties of bone (Macheras et al., 2014; Karachalios et al., 2014). An overview of the competing commercial technologies is shown in Table 5.1.

Table 5.1 Comparison of the advantages and limitations of commercially available surface modification methods for uncemented implants.

Implant surface modification method	Benefits compared to EBT and Surfi-Sculpt processes	Limitations compared to EBT and Surfi-Sculpt processes
Fibre mesh created by diffusion bonding.	Good clinical history. Adds porosity. More appropriate size of features for enhanced bone ingrowth.	Not flexible. Slow process – diffusion bonding is slow and requires time consuming pre-processing.
Electron beam melting (EBM®) – an additive manufacturing (AM) process.	10 years clinical history (Lima Corporate, 2017). Adds porosity.	Slow process – requires the whole component to be manufactured using EBM®.
Hydroxyapatite (HA) coating mimics naturally occurring bone mineral.	Good clinical history. Adds porosity. Enhances bone growth across a gap. Longest clinical history for a coating (Daugaard et al., 2014).	Time-consuming to apply. Not suited for in-line or single batch manufacturing.
Metal foam Tantalum (Ta) surface coating is applied by physical vapour deposition (PVD) to polymer skeleton on the implant surface.	Good clinical history. Adds porosity. More appropriate size of features for enhanced bone ingrowth.	Ta is an expensive material (Bencharit et al., 2014). Polymer skeleton, PVD processing and removal is slow, and thus expensive manufacturing method (Bargiotas, 2014). Difficult to tailor the surface porosity at different regions – each region processed separately to give desired porosity.
Porous plasma spray coating Thickness ranges between 625 and 900 µm; average porosity of approximately 35 %. (Biomet Orthopaedics Inc., 2007).	Good clinical history. Adds porosity. A study comparing the scratch-fit stability of acetabular shells concluded that porous plasma sprayed cups were twice as strong in resistance to rim failure as sintered beads or fibre mesh cups (Markel et al., 2002).	Time-consuming. Difficult to achieve consistent results as relies on operator ability.
Sintered beads Small or large spherical balls sintered together directly on the implant surface. The interstices between the balls form an open cell structure.	Good clinical history. Adds porosity. More appropriate size of features for bony response.	Balls can detach from the implant during use possibly causing infection and loosening of the surrounding bone. Slow - can take up to 12 hours.

The EBT and Surfi-Sculpt processes are quicker than those listed in Table 5.1; this means that they offer a cost reduction compared to existing technologies based upon the required manufacturing time duration. A further advantage is the ability to tailor the surface features at different regions during processing.

However, there was no data pertaining to the performance of these features and the processes have no clinical history.

5.3 Aim of the orthopaedic implant case study

The aim of the orthopaedic implant case study was to investigate the application of the EBT and Surfi-Sculpt processes to next generation uncemented acetabular cups for uTHRs based upon the OrthoSculpt project.

5.3.1 Objectives of the orthopaedic implant case study

The objectives of the author's work were to:

- Develop a range of surfaces suitable for investigating initial feasibility using the EBT and Surfi-Sculpt processes.
- Increase the coefficient of friction (COF) when the developed surfaces are pushed in and pulled out of simulated bone.
- Optimise a design using the EBT and Surfi-Sculpt processes on a representative prototype acetabular component.
- Manufacture demonstrator prototype acetabular cups.
- Evaluate the resources and infrastructure required to scale up the surface modification processes for commercialisation.

5.4 Manufacture of the orthopaedic implant features

The author developed and optimised four designs of geometrical features to engage with the simulated bone and increase the COF, namely Maltese cross (Design 1), Sawtooth (Design 2), Honeycomb (Design 3) and Dimpled texture pattern (Design 4); these were based upon the designs provided by JRI and were explored in detail in Submission 6. According to JRI, successful outcome of the OrthoSculpt project should enable them to increase their sales of THRs by 4 % by 2021 (Draper, 2016) with more patients being treated with uTHR.

The concept for the designs was to improve load transfer by increasing the COF thus addressing the problem of stress shielding. This would ensure load-matching to the host bone and the biomaterial and therefore provide a region for the formation of osteoblasts which are responsible for the growth of new bone (Caetano-Lopes et al., 2007).

Due to budgetary and time constraints within the OrthoSculpt project, the following two designs were progressed to mechanical testing: Design 2 (Sawtooth) and Design 4 (Dimpled texture pattern) as both achieved higher feature densities compared to the other designs which was the most significant requirement set out by JRI in their design guidelines. The wide intrusions associated with the large features of Design 1 (Maltese cross) limited the achievable feature density due to the inability to closely pack the features. The features in Design 3 (Honeycomb) had shallow side walls and rounded tips which did not match the requirements from JRI for steep side walls and sharp edges of the features needed to increase the COF and allow enhanced load transfer.

The Design 2 (Sawtooth) rationale was to create a surface which demonstrated directionality to the COF so that the push-in and pull-out characteristics of the surface were different with closely packed features to maximise their density and the initial contact points between the implant and the bone.

The Design 4 (Dimpled texture pattern) concept was to mimic JRI's existing Supravit® Zoned vacuum plasma sprayed hydroxyapatite (HA) coating whilst also aiming to achieve less ordered anisotropic features in the region of 200 μm.

5.5 Analysis of feature hardness

Design 2 (Sawtooth) was tested using a micro Vickers hardness tester applying a 0.1 kg load to assess the hardness of the features created using the EBT and Surfi-Sculpt processes compared to the parent material; the results are shown in Table 5.2. Due to the small size of the features created in Design 4 (Dimpled texture pattern) which could not accommodate the impactor, hardness testing was not conducted on this design.

Table 5.2 Micro Vickers hardness results from OrthoSculpt Design 2 (Sawtooth).

Mean feature hardness (HV0.1)	Mean parent material hardness (HV0.1)	Increase in feature hardness
226 ± 12 HV0.1	172 ± 8 HV0.1	31.0 %

The hardening observed was as a result of the fine martensitic α microstructure formed by the high cooling rates during the EBT and Surfi-Sculpt processing which confirmed the observations of Ramskogler et al. (2017) who also noted hardening of features. However, this hardening of the material did not adversely affect the performance of the features.

5.6 Method of testing for increased coefficient of friction

Damm et al. (2015) described a series of tests which modified standard testing to replicate loading conditions observed during implant insertion utilising push-in motion to simulate the contact between the metal surface and the bone. Measurement of COF in both push-in and pull-out directions show that surfaces which displayed high COF on insertion subsequently demonstrated a greater drop in COF readings in the pull-out direction. This means that the implantation COF calculated during the push-in would be greater than the stability of the implant COF calculated during the pull-out (Bishop et al., 2014). However, this measurement would be for the initial mechanical interlock between the bone-implant interface created prior to any bone growth stimulated after implantation which should enhance the stability.

The friction test procedure observed the protocol described by Bishop et al. (2014) within the constraints of using an adapted universal mechanical tester system, Figure 5.1. F_{Radial} describes the force on an acetabular cup which is hemispherical and hence the force on the actual product would be radial. Departures from this protocol involved the substitution of cellular rigid polyurethane 20 pcf foam 'Sawbone' for bone, produced by Sawbones (Malmö, Sweden), in addition to reduced loads and a different mounting system. The change in material was made so that ethical approval was not required to use bone in the testing; however, as a result of using Sawbone, lower loads were recorded. The setup of the test machine necessitated the modification from horizontal to vertical therefore requiring an altered mounting system.

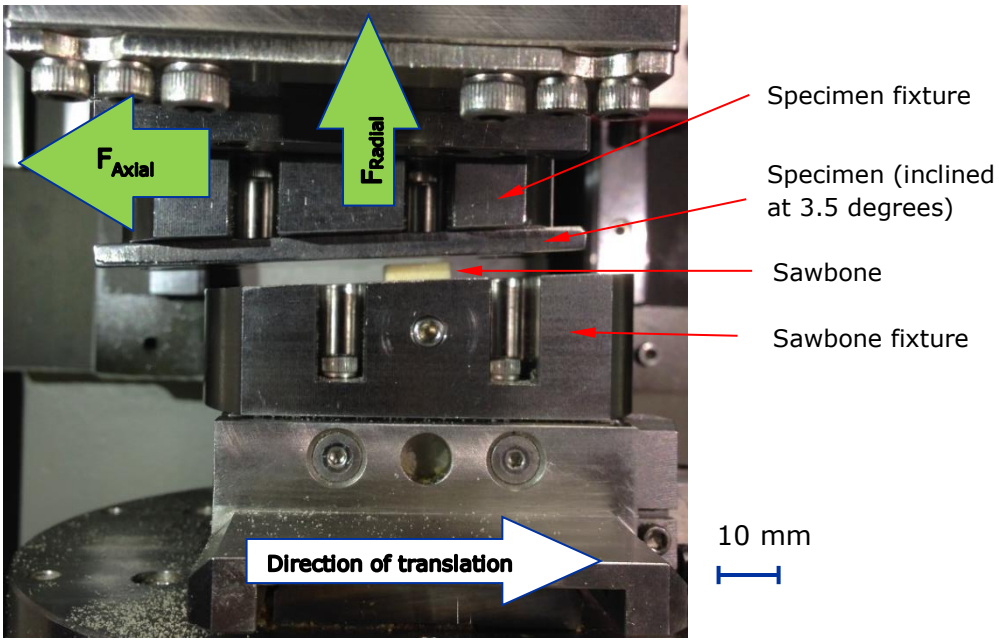

Figure 5.1 Friction testing specimen setup, adapted from JRI.

Figure 5.2 shows the four designs of surfaces investigated in the friction testing:

- Polished (blank control) sample.
- JRI's existing Supravit Zoned HA coating; used as the commercial benchmark.
- Design 4 (Dimpled texture pattern).
- Design 2 (Sawtooth) and Design 2 reverse (Sawtooth.rev).

Design 2 (Sawtooth) and Design 2 reverse (Sawtooth.rev) were identical except for the direction of mounting.

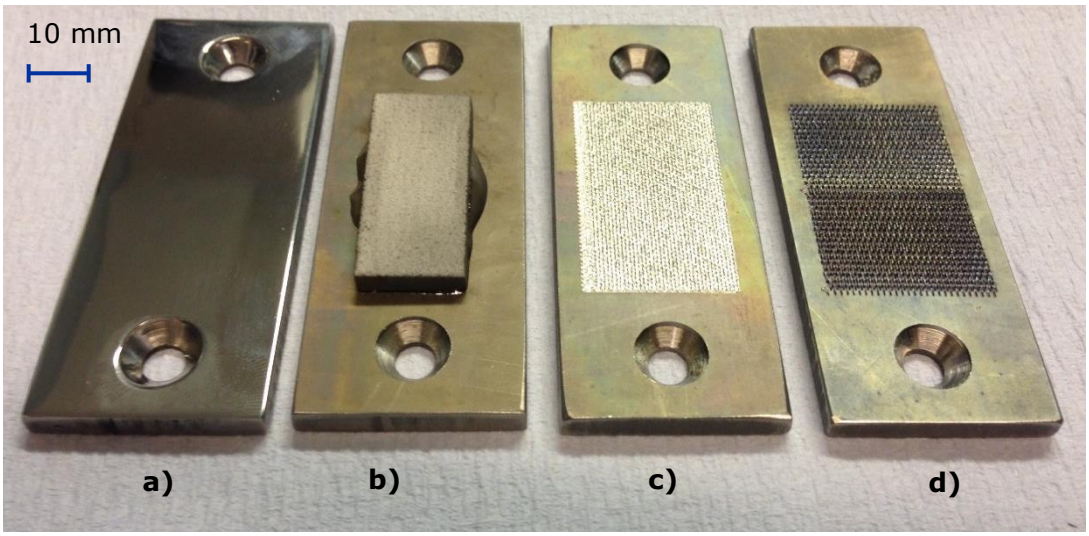

Figure 5.2 Friction test specimens, provided by JRI:
a) Polished (blank control) sample;
b) JRI's Supravit Zoned HA coating;
c) Design 4 (Dimpled texture pattern);
d) Design 2 (Sawtooth pattern) – tested both with normal and reversed (opposite direction) loading.

As discussed in Section 5.4, the size of features between Designs 2 and 4 were significantly different in geometry since they were focused on creating anisotropic COF (and thus generated anisotropic friction) and mimicking JRI's existing Supravit Zoned HA coating respectively. However, Design 4 was limited by the spot size of the EB (140 μm) and hence the features were larger than JRI's existing Supravit Zoned HA coating.

The bespoke fixtures introduced a 3.5 degree angle ($\boldsymbol{\theta}$) between the lateral stage motion and the orientation test pieces which resulted in them being wedged against one another. As a consequence, the pressure increased with the translation distance as proposed by Damm et al. (2015). A 0.5 mm/s translation rate was set in the tests and the system recorded the axial and radial forces. The normal and shear stresses were calculated for the Sawbone foam-metal interface using the 3.5 degree rotated frame of reference. The COF was calculated

using a ratio of shear to normal stresses as shown in Equation 10 (Damm et al. 2015, p. 3518).

$$\boldsymbol{Coeffiecient\ of\ friction\ (COF)} = \frac{F_{shear}}{F_{normal}} = \frac{-F_{Radial}\sin(\theta)+F_{Axial}\cos(\theta)}{+F_{Radial}\cos(\theta)+F_{Axial}\sin(\theta)}$$

Equation 10

Figure 5.3 shows the mean protrusion height and intrusion depth for the 560 data points generated from each of the six Design 2 (Sawtooth) specimens for the shear testing created using the Alicona Infinite Focus SL 3D non-contact profilometer. It was then possible to analyse the data generated to consider the distribution of heights and their subsequent location on the sample.

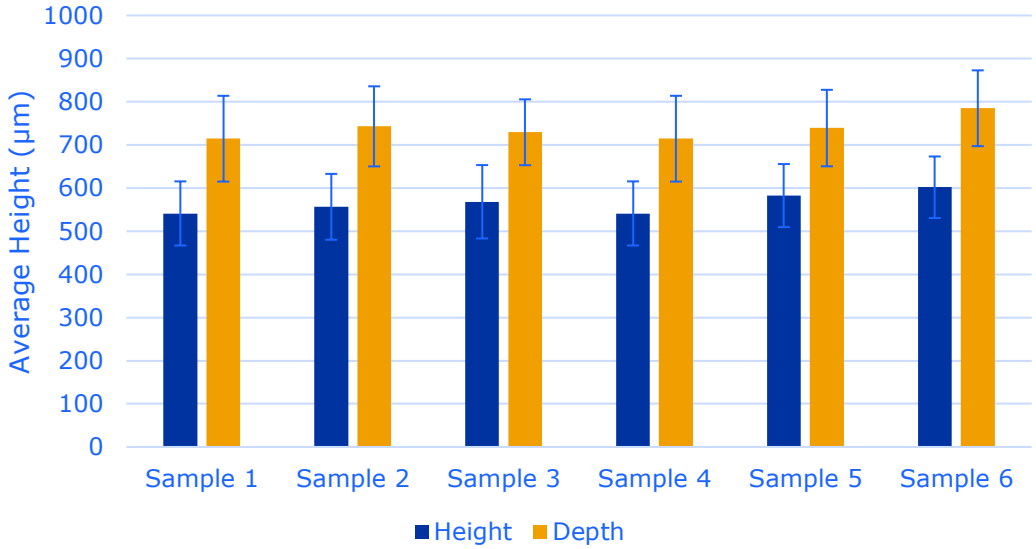

Figure 5.3 Protrusion height and intrusion depth of Design 2 (Sawtooth) for six friction samples.

Figure 5.4 shows that the distribution of feature heights on the six samples appear to conform to a normal distribution. However, the spread of the data ranges, grouped into 25 µm clusters from 350 µm at the lowest up to in excess of 750 µm at the highest, indicated that the Surfi-Sculpt process parameters were causing a large spread of feature heights.

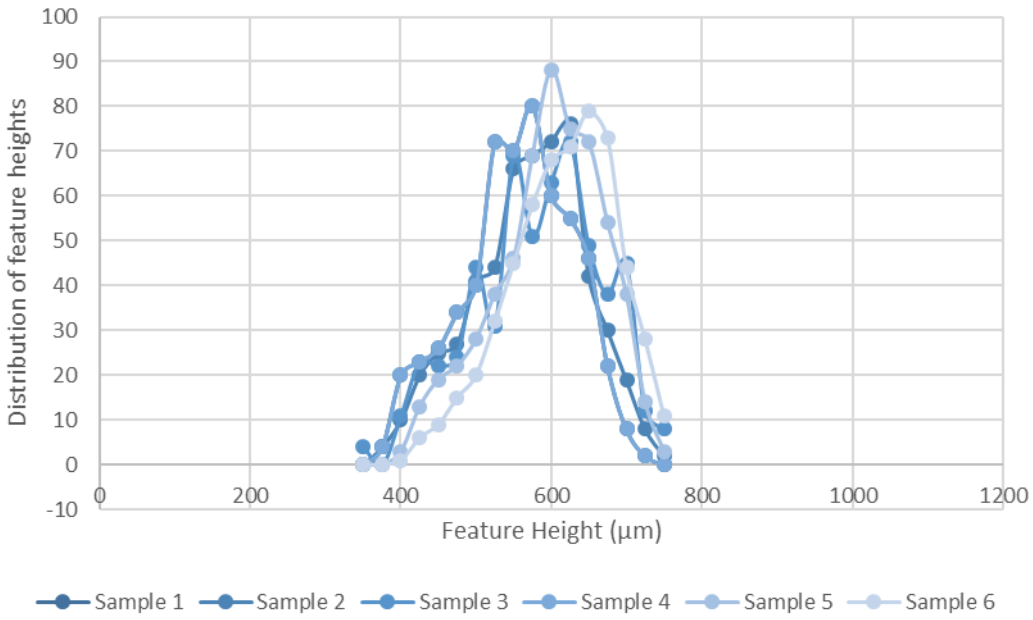

Figure 5.4 OrthoSculpt friction sample Design 2 (Sawtooth) protrusion height distribution.

Figure 5.5 shows that the highest feature height was closest to the centre of the pattern and that, as the features of the pattern extend radially towards the edges, the maximum height decreased. This principle was discussed in Section 2.3.8.

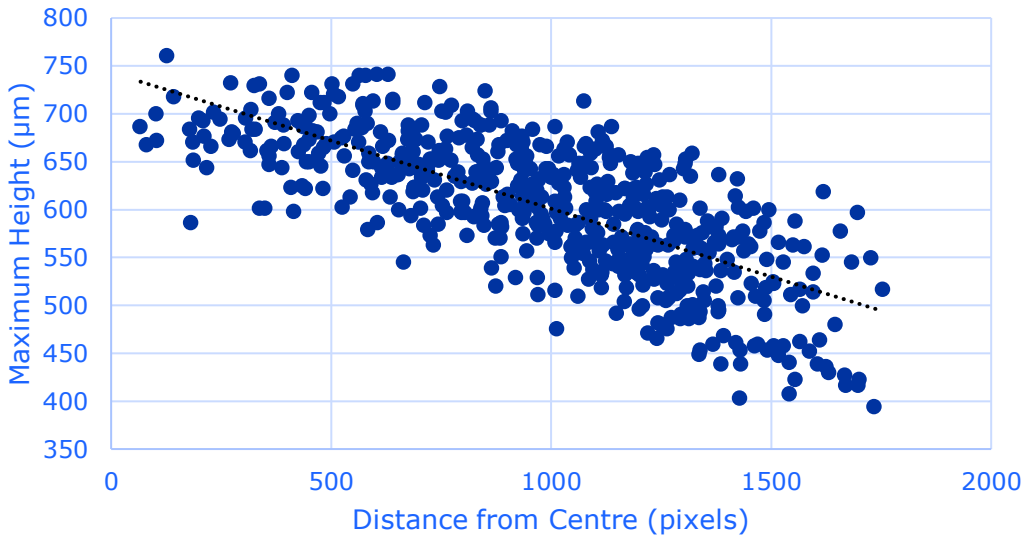

Figure 5.5 OrthoSculpt friction sample Design 2 (Sawtooth) protrusion height and radial distribution from the centre of the pattern.

5.7 Results from the friction testing

The main aim of the friction tests was to calculate COF values for the four specimen types. As the interference increased, the COF values varied throughout

the tests. For Design 2 (Sawtooth) and Design 2 reverse (Sawtooth.rev), this fluctuation was due to deformation and wear caused to the Sawbone foam by the specimens. Figure 5.6 shows the COF plotted against the interference calculated between the Sawbone foam and the specimen demonstrating that Design 4 (Dimpled texture pattern) and the polished (blank control) specimens generated minimal amounts of friction. The test results are shown by the dark red and blue lines calculated by a local regression method for the push-in and pull-out respectively. The lighter red and blue coloured areas shows the data generated for all five test specimens.

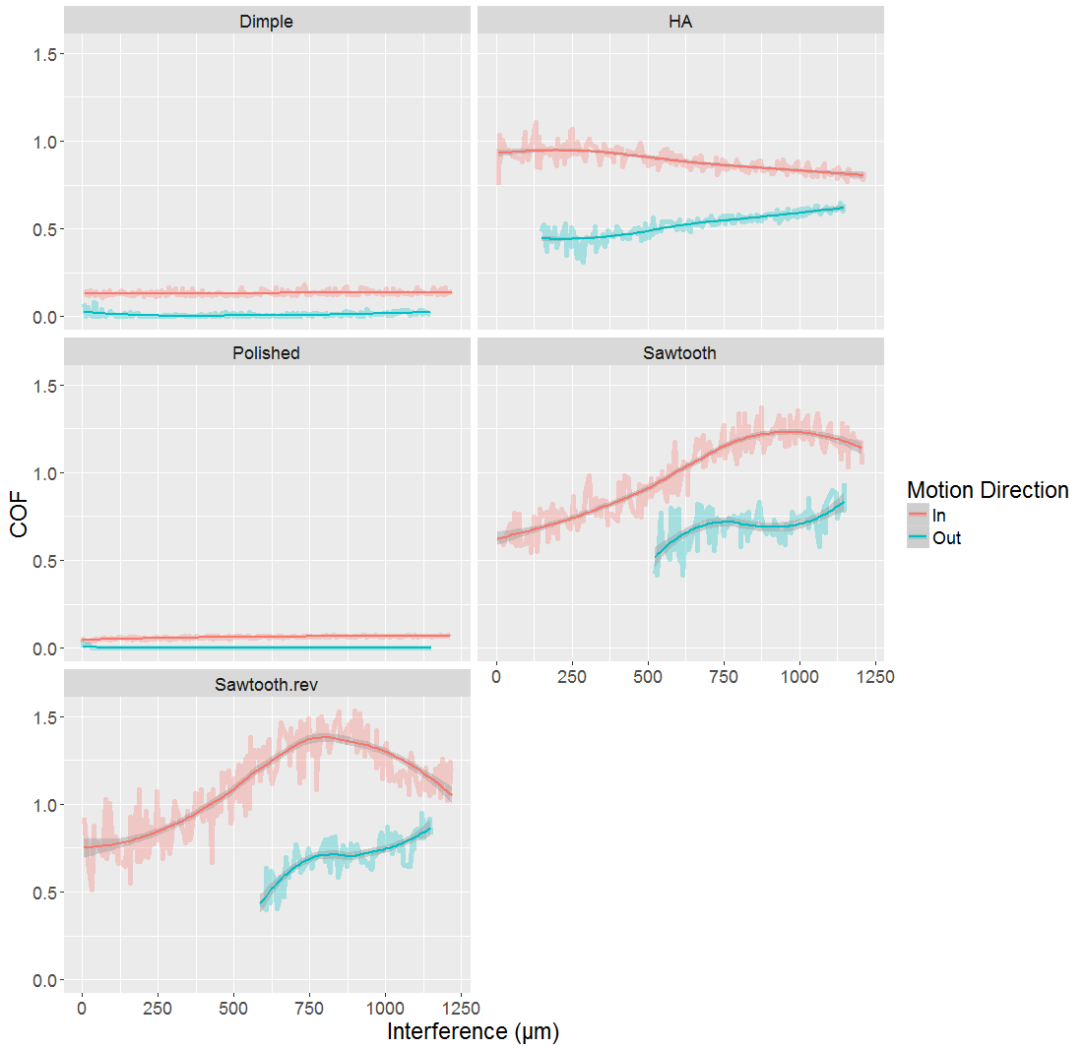

Figure 5.6 COF plotted against interference for all tested specimens, provided by JRI.

Design 2 (Sawtooth) and Design 2 reverse (Sawtooth.rev) generated high COF, of approximately 1.25 and 1.38 respectively, and hence were the best results. Both Design 2 (Sawtooth) and Design 2 reverse (Sawtooth.rev) generated higher friction and a different profile than the HA coating during push-in as well as pull-out. JRI's HA coating generated a maximum COF of approximately 0.95 after 200 μm of interference. This increase in COF compared with JRI's HA coating was anticipated given the geometry of the features which were designed to provide a mechanical interlock into the Sawbone foam.

Approximately 1 mm of radial interference is equivalent to 15 mm axial implantation displacement which is typically used in mechanical testing of implant surface structures (Bishop et al., 2014).

Comparison between Design 2 (Sawtooth) and Design 2 reverse (Sawtooth.rev), showed that the latter generated the highest COF during the mid-point of the test. The orientation of the features in Design 2 reverse (Sawtooth.rev) resulted in the engagement of a larger cross-sectional area of the feature with the Sawbone foam. However, by the end of the test, the COF for both Design 2 (Sawtooth) and Design 2 reverse (Sawtooth.rev) had aligned due to the Sawbone foam debris reaching an equilibrium state.

As the interference reached approximately 250 μm, the COF for the specimens with the HA coating demonstrated a small increase compared to Design 2 (Sawtooth) and Design 2 reverse (Sawtooth.rev). Subsequently, the COF decreased for the remaining duration of the push-in tests. These results were in contrast to those reported by Damm et al. (2015); this difference is due to a film of debris being generated by the abraded particulate debris. This abrasion may be advantageous if the implant was also considered to be part of the surgical tool set for implantation since it cuts into the bone; this is discussed further in Section 5.8.

Figure 5.7 shows the COF plotted against normal pressure and the results demonstrated validation of the above observations. They also highlighted an additional difference in that Design 2 (Sawtooth) and Design 2 reverse (Sawtooth.rev) generated approximately 0.65 MPa of pressure which was close to half of that demonstrated by the other surfaces. Since the specimens were all tested up to 1,200 μm interference, the difference in pressure was as a result of Sawbone foam abrasion. In comparison, the HA coating achieved pressure values of approximately 1.25 MPa; Design 4 (Dimpled texture pattern) and the polished (blank control) specimen exhibited comparative pressure values in excess of 1.25 MPa.

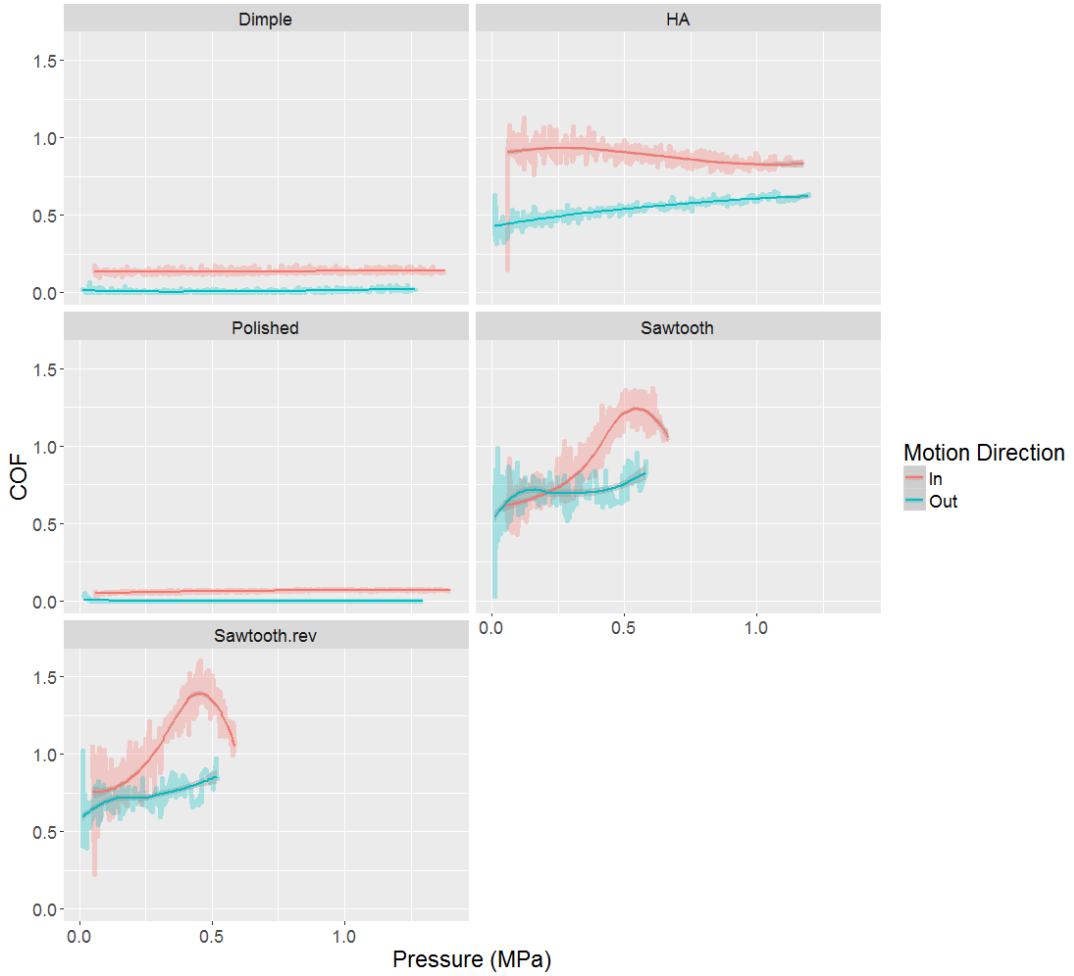

Figure 5.7 COF plotted against pressure for all tested specimens, provided by JRI.

Figure 5.8 shows the absolute values of shear force compared to the interference. The specimens with the HA coating generated approximately 85 N of fixation force which was the highest recorded. A high COF and fixation force was calculated from the dataset for Design 2 (Sawtooth) and Design 2 reverse (Sawtooth.rev) despite a lower contact pressure compared to that of the HA coating. The results show that the kinetic mode of friction (sliding) was occurring during the testing.

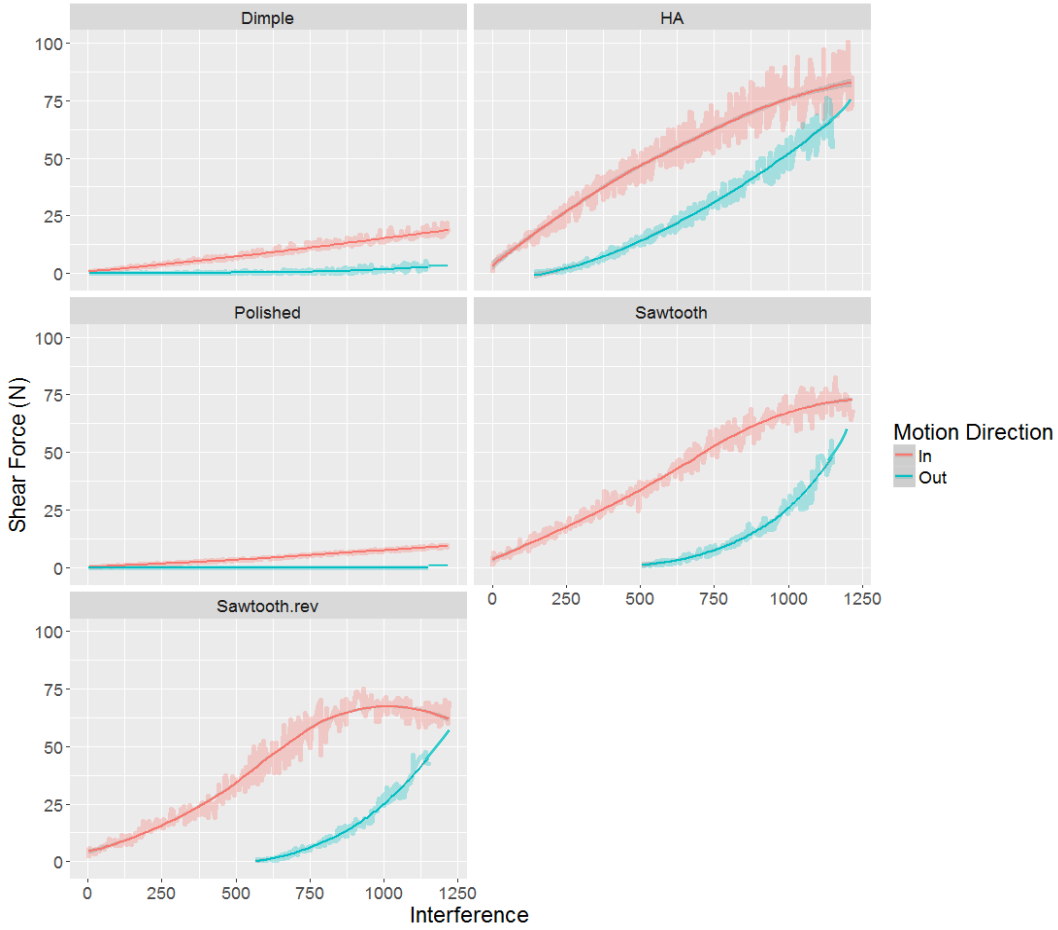

Figure 5.8 Shear force plotted against interference for all tested specimens, provided by JRI.

5.8 Discussion of the orthopaedic implant case study

Similarly to JRI's existing HA coating, Design 2 (Sawtooth) exhibited a high COF; however, it was accompanied by a higher amount of abrasion of the Sawbone foam thus creating debris. Since bone is harder than the Sawbone foam utilised in the testing, the author predicts that less debris would be formed when tested with bone. This small amount of debris would be beneficial when applied to bone since bone tissue has an open-cell structure causing the abraded debris to be pushed deeper between trabeculae therefore acting as an advantageous bone graft by creating fragments through the provision of a scaffold to support the deposition of new bone (Revell 2008; Daugaard et al., 2014). Furthermore, in bone, this debris would be less prone to yield and remain at the bone-implant interface generating a debris layer as observed with the Sawbone foam. As a result, the self-rasping and bone grafting aspects of Design 2 (Sawtooth) could

be beneficial and, correctly harnessed, would reduce the surgical tools required during surgery.

In order to realise smaller features, similar in size to JRI's Supravit Zoned HA coating using the EBT and Surfi-Sculpt processes, a higher brightness EB is required, as discussed in Section 2.2.3. Focus GmbH (2017) manufacture EB machines with a reported beam diameter of less than 50 µm at 1 mA beam current and down to 30 µm for lower currents which may be modified and utilised to create smaller features with the EBT and Surfi-Sculpt processes.

To aid the commercialisation of the outcomes of the OrthoSculpt project, unit processing costs for using the EBT and Surfi-Sculpt parameters, developed on JRI's Furlong® CSF *Plus* cup, were calculated in Table 5.3. This was compiled to detail the associated unit processing cost and to determine if it could be considered commercially viable. The total cost was less than the cost of the HA coating process; the calculations and saving comparison are detailed in Submission 6. This highlighted that the EBT and Surfi-Sculpt processes could address the problem of higher associated costs of uTHRs detailed by Briggs (2015) and Lord Carter of Coles (2016); thus contributing to the £200m saving over 5 years (£40m per annum) proposed by Briggs (2015). However, further clinical trials and work are required to confirm that the processes are suitable for adoption in the orthopaedic industry.

Table 5.3 Unit processing cost of using the EBT and Surfi-Sculpt parameters developed in the OrthoSculpt project on JRI's Furlong® CSF Plus cup.

Category	Value
Manufacturing method	Single piece batch
Loading time (s)	20
Unload time (s)	20
Parts per cycle	1
Pump time (s)	40
Beam on time per unit (s)	18.2
Time per cycle (s)	98
Unit cycle time (s)	98
Units per 37 hr capacity	1,359
Units based upon 85 % utilisation and 85 % availability	982
Annual capacity per shift	49,101
Capital cost (£)	409,000
Operator cost £30 per hr	1
Annual demand^	15,000
Demand / capacity ratio*	5.89
Cost of loan per unit over 5 years 6 % interest (£)	7.09
Labour per unit (£)	0.82
Unit processing cost (£)	**7.91**

^ *Assuming 3 % share of the available European market of approximately 500,000 uTHRs*
* *Exceeds 3 = single shift has capacity; less than 1 = not enough capacity*

5.9 Cell response to features and intrusions

Previous studies have demonstrated that both stem cells (Otten et al., 2012) and pre-osteoblast cells (Ramskogler et al., 2017) can be successfully cultivated on surfaces created using the EBT and Surfi-Sculpt processes.

5.10 Demonstrator acetabular cup

The demonstrator acetabular cup created within OrthoSculpt utilised Design 4 (Dimpled texture pattern). The component was based upon the blank metallic shell used to manufacture JRI's primary acetabular replacement Furlong® CSF *Plus* cup, shown in Figure 5.9, which took 18.2 seconds beam on time to process. The deflection patterns used required modification to allow for the rotation of the hemispherical cup under the beam whilst processing. Prior to this work, the EBT and Surfi-Sculpt processes had only been applied to flat surfaces or cylinders; therefore, the author created an *X,Y* deflection pattern from the equator to the pole of the hemisphere and a *U,V* deflection pattern which accommodated the rotation of the cup.

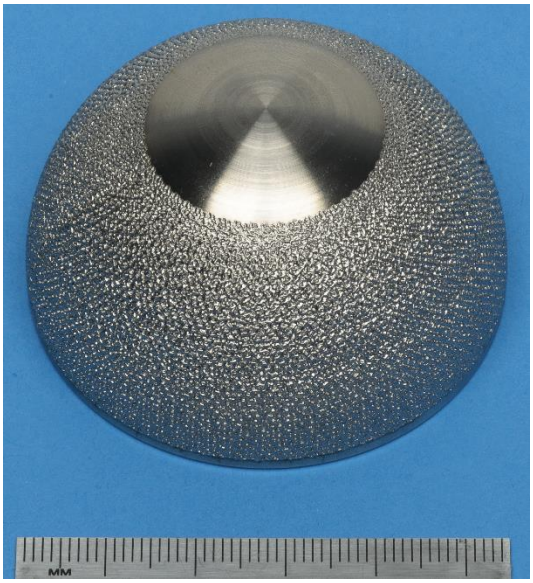

Figure 5.9 Demonstrator acetabular cup produced using the EBT process.

5.11 Conclusions from the orthopaedic implant case study

The work conducted has shown that the EBT and Surfi-Sculpt processes have the capability to create a range of surfaces suitable for demonstrating initial feasibility for increasing the COF for uTHRs. It has been possible to create a self-rasping and bone graft generating surface which provides new design possibilities for uTHRs. Unique to the EBT and Surfi-Sculpt processes are the facts that the protrusion supports an increase in the COF whilst the corresponding intrusion provides a region for bone in-growth and cell growth.

The resources and infrastructure required to scale up the surfacing process for commercialisation were discussed and evaluated and a unit processing cost of £7.91 was calculated for the EBT and Surfi-Sculpt processes. This demonstrated a significant cost and time saving compared with JRI's HA coating.

The USPs in this case study have been the creation of suitable surfaces using the EBT process on a prototype acetabular cup requiring only 18.2 seconds beam on time on a hemispherical component for the first time and the increase in COF using the Surfi-Sculpt process. Similar to the LCP case study, the manufacturing time has been shortened significantly compared to existing technologies at a

lower cost. The ability to process workpieces with more complex geometries will facilitate greater possibilities of applications and potential industrial adoption. These USPs have further evidenced the demonstration of the EBT and Surfi-Sculpt processes in a relevant environment thus crossing the 'Valley of Death' bridge to TRL 6 and MRL 3.

6 Surfi-Sculpt Directory and Selection Tool

6.1 Background and challenges to the directory and selection tool

Successful knowledge management is critical to thriving organisations (Hawley, 2012) and allows the transfer of information and expertise to ensure retention and access by non-expert personnel. It ultimately aims to remove the need for an expert by enabling distribution of the expertise. Effective knowledge management of the EBT and Surfi-Sculpt processes was limited by the comprehensive understanding of the processes being retained by a few key experts, parameter records being stored in paper form without clear links to the resultant surfaces and samples, and unstructured electronic storage of deflection pattern files. Effective knowledge is summarised by Brooking (1999, p.5) as:

'Knowledge = Information in Context + Understanding'.

In addition to the challenges surrounding the knowledge management, a licensee of the EBT and Surfi-Sculpt processes using the technology in an industrial setting reported that in excess of 500 parameters per day could be required to be input manually with their current production levels and setup. This volume of manual input can result in data entry errors potentially leading to the scrapping of high value components. Therefore, systems and tools which can minimise this would be beneficial in supporting the industrial application and uptake of the EBT and Surfi-Sculpt processes.

TWI had previously developed software for controlling the EBT and Surfi-Sculpt processes entitled 'Electron Beam Deflection Control System Mark III'. However, it was not developed to current standards such as TickITplus, which is based upon ISO 9001:2008, ISO/IEC 20000-1, ISO/IEC 27001, ISO/IEC 25030, IEC 61508 and BS 25999. This means that its development was not adequately controlled and recorded and therefore it was unsuitable for industrial use.

6.2 Aims of the Surfi-Sculpt directory and selection tool

The aims of the author's work were to:

- Decrease the development time for creating new records, patterns and parameters for the EBT and Surfi-Sculpt processes.
- Reduce the potential for operator errors when inputting the parameters and patterns.
- Increase the efficiency during implementation of the processes.
- Increase the quality of record keeping of Surfi-Sculpt procedure specifications (S-SPS) which detail the parameters and recipe required to reproduce a previously created surface.

The ultimate aim of this work was to embed into software the required expertise, knowledge and knowhow for the EBT and Surfi-Sculpt processes to enable increased industrial deployment.

6.2.1 Objectives of the Surfi-Sculpt directory and selection tool

The objectives of this work were to:

- Enhance the effectiveness of TWI's knowledge management for the EBT and Surfi-Sculpt processes to improve storage, access and information sharing.
- Develop a directory and selection tool, the 'Surfi-Sculpt catalogue', as a repository for the S-SPS for the EBT and Surfi-Sculpt processes.
- Store existing electronic deflection pattern files associated with parameters in a methodical and controlled manner to enable easy access and to ensure that they are not altered without the correct permissions.
- Store the complete S-SPS required to replicate surfaces created using the EBT and Surfi-Sculpt processes in the Surfi-Sculpt catalogue.
- Provide a framework to explore additional automation of the EBT and Surfi-Sculpt processes enabling application in production environments and allowing transfer of records to licensees.

6.2.2 Business needs for the directory and selection tool

The three main business needs for the Surfi-Sculpt catalogue were to: provide a directory and selection tool accessible for clients, TWI research staff or anyone interested in the EBT and Surfi-Sculpt processes; allow people with the right credentials and permissions to access the technical data to reproduce records of the EBT and Surfi-Sculpt processes; and centralise the technical knowledge from all completed research.

TWI is a knowledge based organisation; therefore, addressing these business needs will benefit the company especially since the EBT and Surfi-Sculpt processes are developing technologies which require evidence to support their industrial adoption along with an initial directory of publically available S-SPS.

6.3 Development of manuals for existing software

No formal documentation previously existed to guide new users in effective use of the software needed to utilise the EBT and Surfi-Sculpt processes. To address this issue, the author created a comprehensive suite of manuals for the Mark III software: a user manual; a technical manual; and a maintenance manual for the deflection control system as a whole. These were included in the appendices in Submission 4.

6.4 Surfi-Sculpt catalogue

Figure 6.1 shows a screenshot of the homepage of the Surfi-Sculpt catalogue that was created by the author based upon the requirements detailed in Submission 4.

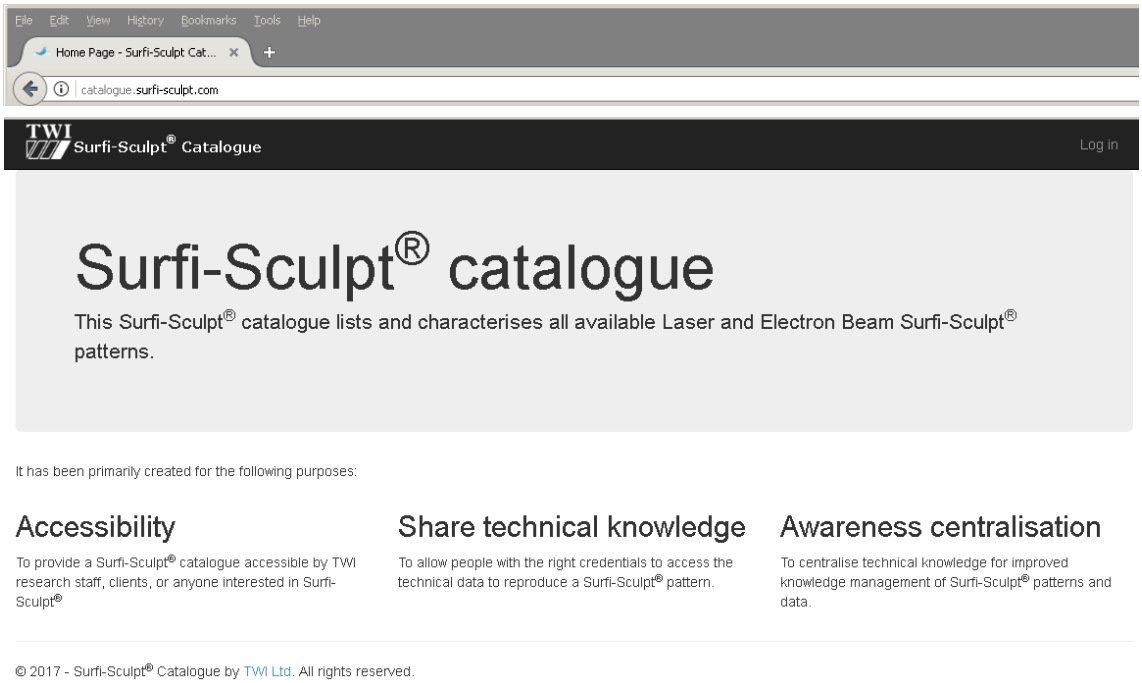

Figure 6.1 Home page of the Surfi-Sculpt catalogue.

To address intellectual property (IP) concerns for the catalogue and to ensure appropriate knowledge management, the catalogue grouped data for each S-SPS into three distinct sections relevant to specific audiences. Figure 6.2 shows the accessible public view of a record in the Surfi-Sculpt catalogue.

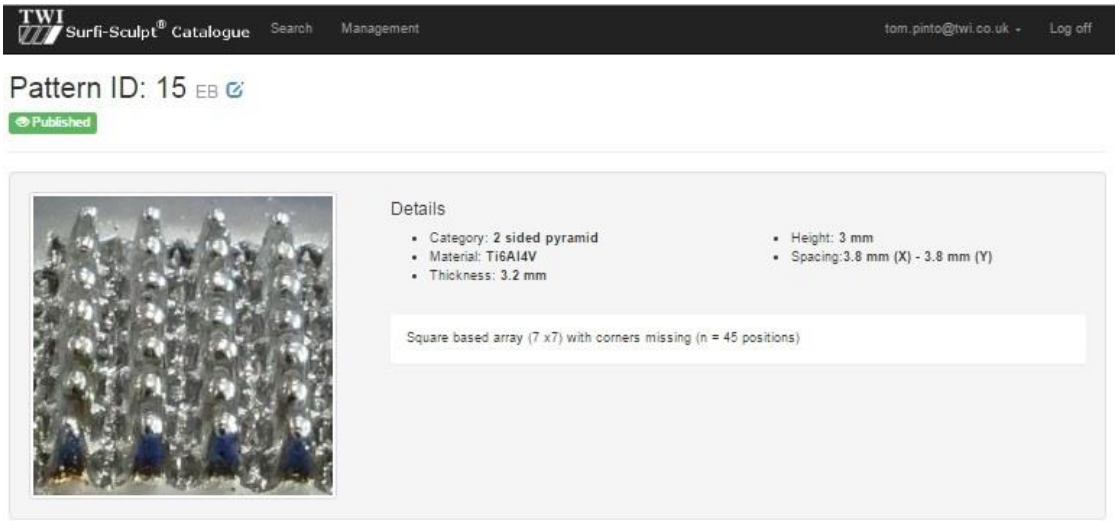

Figure 6.2 'Guest' user Surfi-Sculpt catalogue public view providing the top level summary of the record.

An additional two sections are available to users with the relevant access: one contains all the information and parameters, pattern files and machine setup data

to recreate the surfaces; whilst the last section, for TWI employees only, contains specific information regarding the client it was used for, the associated project number and the date it was last used. This is all confidential information and hence it has not been disclosed in this Innovation Report but is detailed in Submission 4.

The vision and exploitation plan for the Surfi-Sculpt catalogue is discussed in Section 6.6.

6.5 Search function of the Surfi-Sculpt catalogue

A search function was created within the Surfi-Sculpt catalogue to enable specific records to be located quickly or to generate a list of records that met specific requirements. Results of the initial search could be restricted further by applying search filters using fields as shown in Figure 6.3. The orange boxes represent fields that are confidential and therefore only available as search options depending on user privileges i.e. whether they are a TWI or a Guest user.

Figure 6.3 Fields available as search filters in the Surfi-Sculpt catalogue.

Specific records can be found within the Surfi-Sculpt catalogue by inputting the unique record ID into the search function, if known. Broader results can be returned by searching for desired fields within the public record details using the following options:

- Technique: EB, laser beam or both techniques.
- Category: Type of feature created selected from a pre-populated drop down list.
- Material: Selected from a pre-populated drop down list.
- Thickness: From min to max.
- Feature height: From min to max.
- Feature spacing: From min to max in both *X* and *Y* axis.

In the current format of the directory and selection tool, the user needs to know the different category types which are available based upon the geometrical shape of the features, such as cone, pyramid, pin, and honeycomb. It is planned

that a future development could be that users may not need to know the geometry of the features created, instead a search criteria will be performance related for example COF or heat transfer coefficient.

6.6 Exploitation plans for the Surfi-Sculpt catalogue

The exploitation plans for the Surfi-Sculpt catalogue, shown in Figure 6.4, were based around three distinct phases:

- Phase 1 was the population of data within the Surfi-Sculpt catalogue (both that which existed prior to the author's involvement and that created by the author) to establish sufficient records.
- Phase 2 plans to roll out the Surfi-Sculpt catalogue as a sales tool in 2021 to promote the EBT and Surfi-Sculpt processes and showcase example surfaces that can be generated.
- Phase 3 intends to make the catalogue (or part of the records) available as part of licence agreements for the EBT and Surfi-Sculpt processes from 2022 onwards.

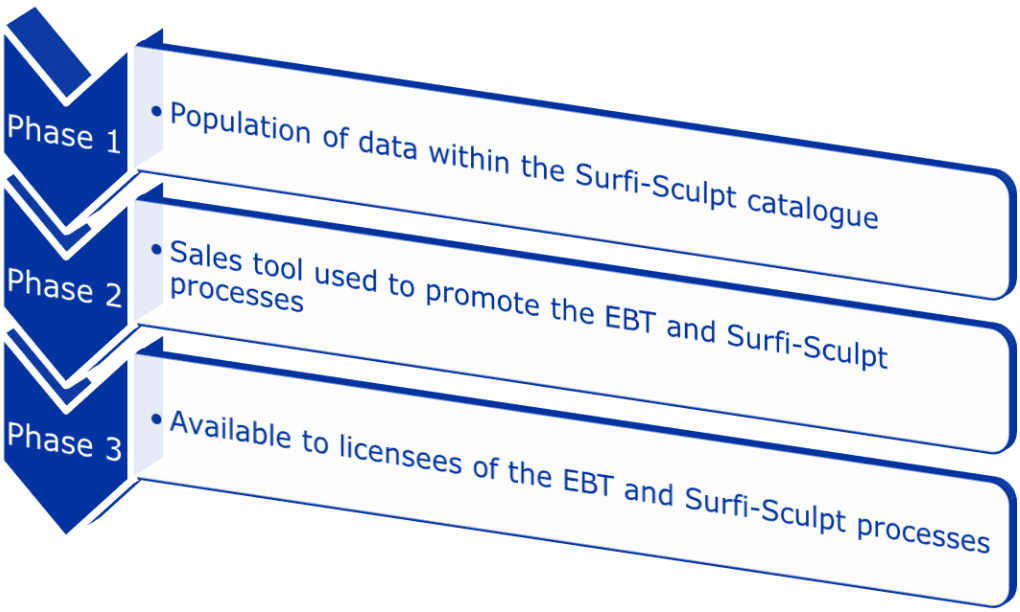

Figure 6.4 Exploitation plan for the Surfi-Sculpt catalogue.

6.7 Benefits of the Surfi-Sculpt catalogue

The Surfi-Sculpt catalogue stores detailed information for each record incorporating the S-SPS, an image of the resultant surface and the electronic deflection pattern file which can be uploaded directly into the deflection control software. Each record can be found easily using a variety of search criteria and therefore samples can be reproduced quickly without having to search through paper-based records. These solutions addressed the challenges discussed in Section 6.1. Additionally, the Surfi-Sculpt catalogue can be used to demonstrate available surfaces without releasing confidential information and IP and enable new patterns to be developed more quickly using information on existing successful patterns as a starting point.

6.8 Servitisation of electron beam texturing and Surfi-Sculpt processes

'The cornerstone for new service adoption is the customer firm's actual need for the service.'

(Vaittinen et al., 2018, p.52).

Matthyssens and Vandenbempt (2008) and Sawhney (2006) reported that, to increase returns and create additional growth opportunities, manufacturers have changed their focus towards customer solutions and away from traditional products, defined as 'servitisation' (Vandermerwe and Rada, 1988). Gebauer et al. (2005) and Lee et al. (2016; cited in Rabetino et al., 2017) concluded that this was not a straightforward process and that a beneficial outcome could not be guaranteed.

Currently, the EBT and Surfi-Sculpt processes are most suited to a traditional jobbing shop business model but further consideration should be given when

implementing the processes to investigate the most appropriate business model for their provision as a service or to provide licences for the servitisation of the processes in order to add value to the technology.

6.9 Conclusions from the directory and selection tool

The effectiveness of the knowledge management for the EBT and Surfi-Sculpt processes has been greatly improved by the author through the creation of a comprehensive Surfi-Sculpt catalogue and development of formal documentation for the Electron Beam Deflection Control System Mark III software. Consequently, promotion of the innovative technologies has developed alongside increased industrial interest in the EBT and Surfi-Sculpt processes. The information no longer resides with individual experts but is accessible to the appropriate audience at a corporate level. This directory and selection tool has contributed to bridging the 'Valley of Death' through improved knowledge management and the ability to control the storage, access and manipulation of data and parameters demonstrating the processes in a relevant environment (TRL 7).

7 Discussion

7.1 Introduction

The work discussed in Chapters 2 to 6 addressed many of the market, technical and knowledge management barriers that existed and thus has supported the progression of the EBT and Surfi-Sculpt processes across the 'Valley of Death' to TRL 7 and MRL 4. However, apart from the model by the author in Section 3.5, the work conducted previously on the EBT and Surfi-Sculpt processes has not provided models, methodologies or discussed approaches to its automation.

Therefore, to address an implementation barrier resulting from the advances in this EngD, the author has proposed models and methodologies to reduce empirical developments. These enhance the creation and optimisation of deflection pattern files and the associated deflection frequencies and predict the variation associated with different materials used for the EBT and Surfi-Sculpt processes which are affected by the penetration depth. The deflection pattern files and frequencies used in Chapters 3, 4 and 5 were calculated empirically with the development work to date utilising this methodology. However, for a manufacturing process to be adopted, there must be predictable machine and process flexibility when making changes (Kristianto et al. 2012). Therefore, since applying the EBT and Surfi-Sculpt processes in industrial applications (Chapters 4 and 5), the author has explored how the parameters for the processes can be calculated mathematically. This would support the creation of pre-processing software discussed in Section 8.1.3 and also prevent the occurrence of over melting of features observed in Section 3.4.6 by ensuring an even distribution of beam energy and thus heat input.

7.2 Optimisation of deflection pattern files and deflection frequencies

7.2.1 Process strategy

The basic process strategy for the Surfi-Sculpt process is to displace material in the liquid phase to build up protrusions from the base material. Both the heat required to melt the material and the displacement actions are generated by the precise EB. The process is only possible by moving the beam at high speed in a complex path of swipes over the workpiece surface; this was achieved via a digital programmable beam deflection system discussed in Section 1.1.

7.2.2 Pattern building using arrays and motifs

Figure 7.1 shows a simple process strategy and would give repeats of a simple 'motif' of n_2 legs (swipes) at various positions defined in an 'array' of n_1 points. For maximum choice in parameters, $n_2 = (N \times n_1) \pm 1$ where N is an integer. Alternatively the converse relationship may apply, $f_2 = (N \times f_1) \pm 1$, where f is the frequency or number of repeats.

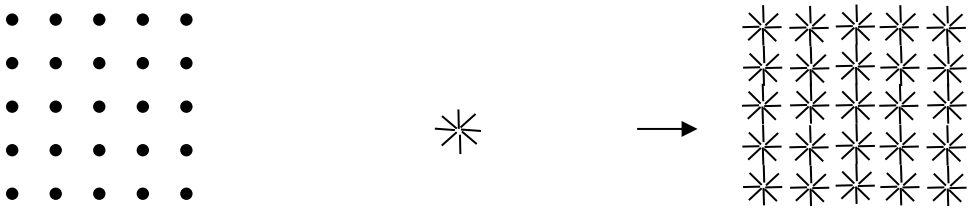

Figure 7.1 Simple array (5 x 5) and eight legged (swipe) motif.

If the processes were as simple as marking the surface with no deflection of the beam, the direction and sequence of the beam movements would not alter the process outcome. However, the exact sequence and path of beam motion has a profound effect on the resultant surface with the Surfi-Sculpt process.

The use of separate *X,Y* and *U,V* deflections allows increased pattern complexity as well as the improved control and optimisation of process strategy. Given that material is displaced in the reverse direction of the beam movement, the same

pattern in reverse will either build protrusions (spikes) or make walls as represented by the arrows in Figure 7.2. The arrow head represents the end of the swipe and the tail the start of the swipe.

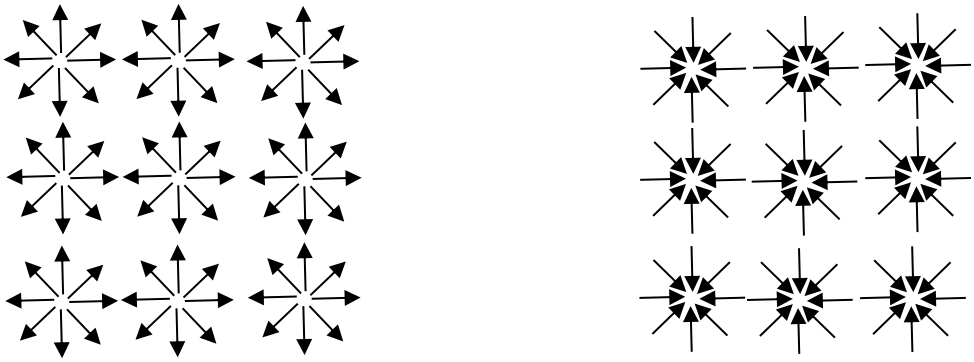

a) Protrusion b) Walls

Figure 7.2 Directionality of swipes alters the geometry of features:
a) Builds protrusions centrally within the swipes;
b) Makes walls radially outside the swipes.

7.2.3 Pattern sequencing

Previous pattern and sequence work on the Surfi-Sculpt process was achieved by experimentation, as reported by Dance (2007). Therefore, consideration was made by the author as to how this could be calculated and mathematical models proposed to support the development of new pattern and sequence work.

The motif describes the shape of the feature created whilst the array describes the locations of the features. Both the motif and array are controlled by their amplitude and frequency which define the size (based upon the working distance) and the time period to complete the beam deflection. There is process variation that comes from the ripple in accelerating voltage and beam current as well as the noise from the function generators which affect the deflection of the beam and hence its position. This affects the features on a microscopic level unless these are significant variations and the EB machine is out of tolerance.

7.2.3.1 Sequential swipes

The most obvious sequence where the swipes are created sequentially in each motif, as shown in Figure 7.3, is often the least likely to work correctly for most patterns since the heat input is too high based upon the next beam swipe being adjacent to the previous. Distribution of the heat input evenly across the features is critical to the success of the EBT and Surfi-Sculpt processes.

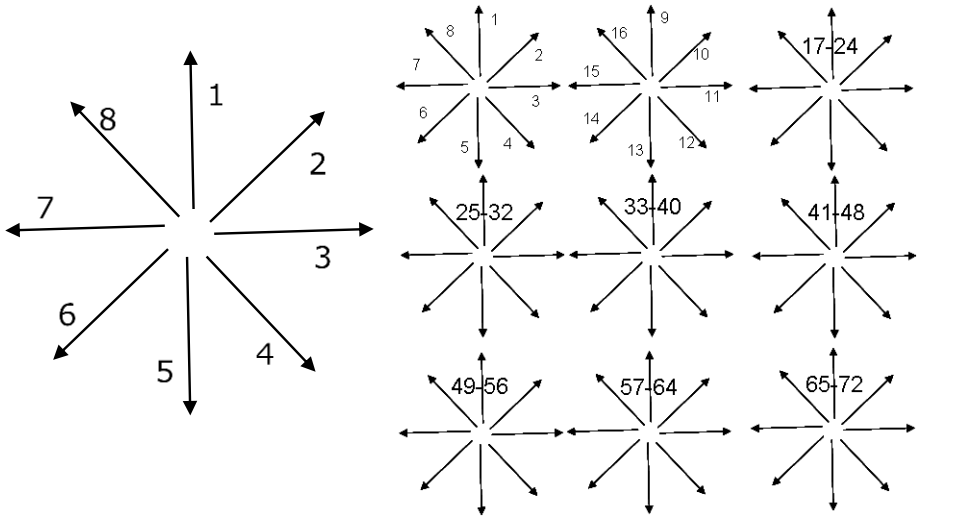

a) Motif sequence b) Pattern (array) sequence for $f_2 = n_1 f_1$

Figure 7.3 Basic motif sequence and pattern (array) sequence:
a) Motif sequence;
b) Pattern (array) sequence.

7.2.3.2 Skipping swipes

The concept of skipping swipes onto the next position in the array and sequence in the motif addresses the heat input challenge as the beam swipes are not adjacent to one another thus reducing the build-up of heat in the features.

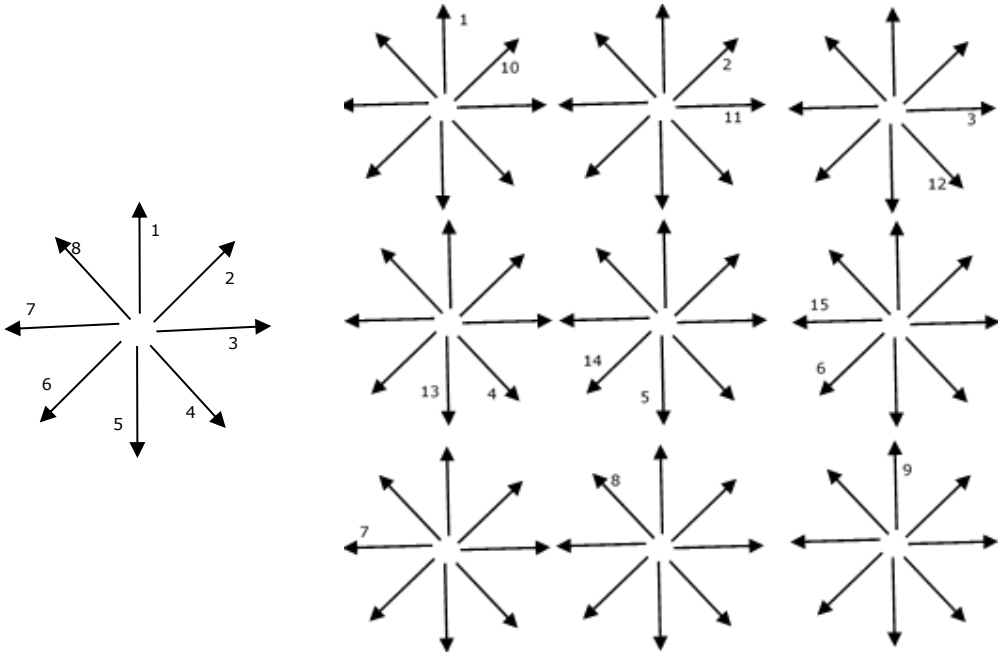

a) Motif sequence b) Skipping pattern sequence for $f_2 = f_1 n_2 / n_1$

Figure 7.4 Skipping motif sequence and pattern (array) sequence:
a) Motif sequence;
b) Skipping pattern (array) to the next swipe in the motif sequence.

7.2.3.3 Grouped skipping swipes

Figure 7.5 shows the application of a sequence where the swipes are 'grouped' and implemented as adjacent pairs. This may be acceptable in a material where there is high thermal conductivity and greater heat input can be absorbed by the material before the features over melt.

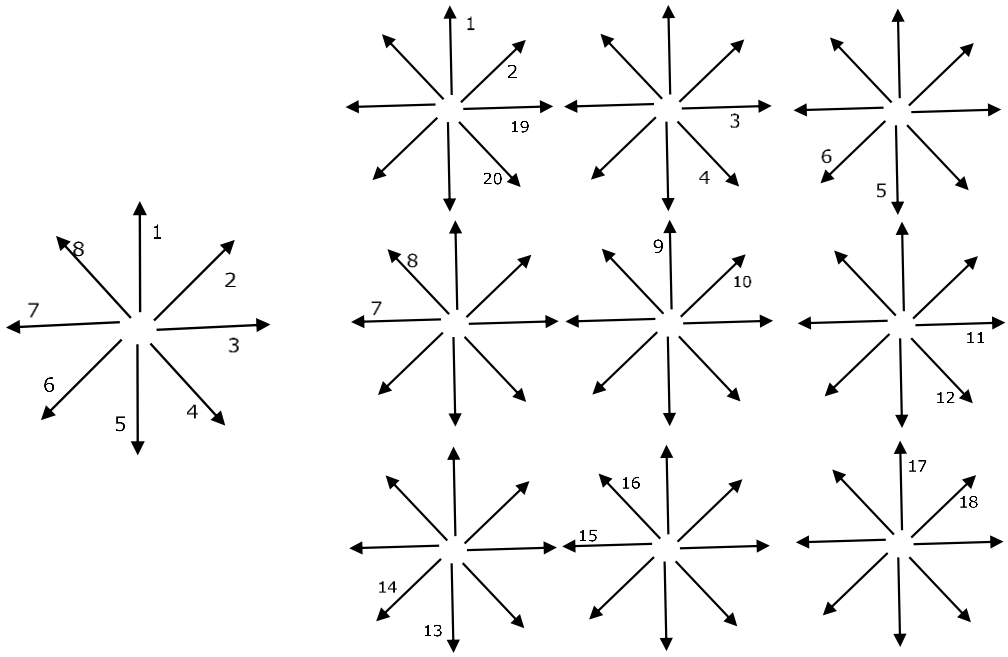

a) Motif sequence b) Group skipping pattern sequence for $f_2 = 2f_1n_2/n_1$

Figure 7.5 Grouped skipping motif sequence and pattern (array) sequence:
a) Motif sequence;
b) Grouped skipping pattern (array) sequence.

7.2.3.4 Non-adjacent skipping swipes using the golden ratio

To calculate the optimum frequencies and sequence of swipes for features created using the Surfi-Sculpt process with multiple degrees of rotational symmetry, such as a cone, pyramid or honeycomb, the golden angle should be applied to support the even distribution of heat input from a series of EB swipes. This is based upon the principle observed in nature where leaves are spread on a stem to capture maximum sunlight and support photosynthesis without overlapping one another (Vogel, 1979) and provides a mathematical model with which to base the spread of a series of EB swipes in a feature.

To find the golden angle, first the golden ratio (φ) needs to be defined; this is shown in Equation 11 (Abbas, 2017, p. 55; Livio, 2003).

$$\varphi = \frac{1+\sqrt{5}}{2} \approx 1.618\ (4\ sig.fig.) \qquad \textbf{Equation 11}$$

Figure 7.6 shows the golden angle subtended by the arc generated between swipes 1 and 2 when a circle is divided using the golden ratio (φ).

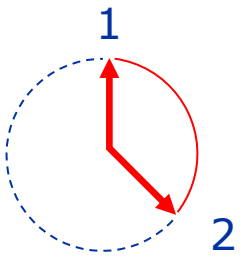

Figure 7.6 Golden angle shown by the red arc subtended between swipes 1 and 2.

Equation 12 (Vogel, 1979) shows that the golden angle between swipes 1 and 2 can be calculated using the golden ratio (φ).

$$\boldsymbol{Golden\ angle = 360° \ x \left(\frac{1}{1+\varphi}\right) \approx 137.5° \ (4\ sig.fig.)} \qquad \textbf{Equation 12}$$

Use of the golden angle to offset the processing of legs in a feature means that the power from the EB can be distributed consistently over the surface of the material. This addresses the problem of over melting of the feature, discussed earlier in Section 7.2.3, as it ensures that the EB evenly processes the parent material taking the longest possible time period to return to the original beam swipe; this is represented in Figure 7.7.

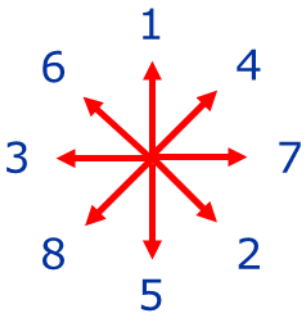

Figure 7.7 Eight legged motif highlighting the order of beam swipes when using an approximation of the golden angle.

Figure 7.8 shows an example of a motif pattern that sequences around each leg.

Figure 7.8 Example of sequencing of swipes in a motif pattern across an array.

Figure 7.9 shows a simple eight swipe *U,V* motif and a nine position *X,Y* array.

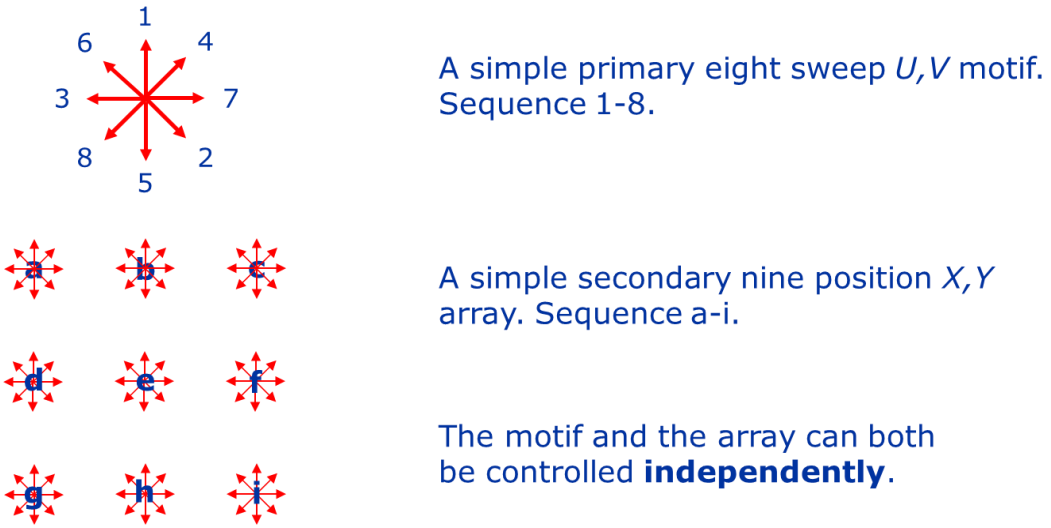

Figure 7.9 Example motif with eight swipes and an array of nine positions, adapted from Pinto (2017).

The sequence of positions in the array is important because, if the 'jump' between them is too large, the beam is required to move a large distance in a short time period which causes an error in its positional accuracy, typically by overshooting. This is observed in moving from position 'i' to 'a' in the example in Figure 7.9 and is known as a 'flyback' error, shown in Figure 7.10, when the movement of the EB occurs at a very high speed potentially causing it to overshoot and not be in the correct location.

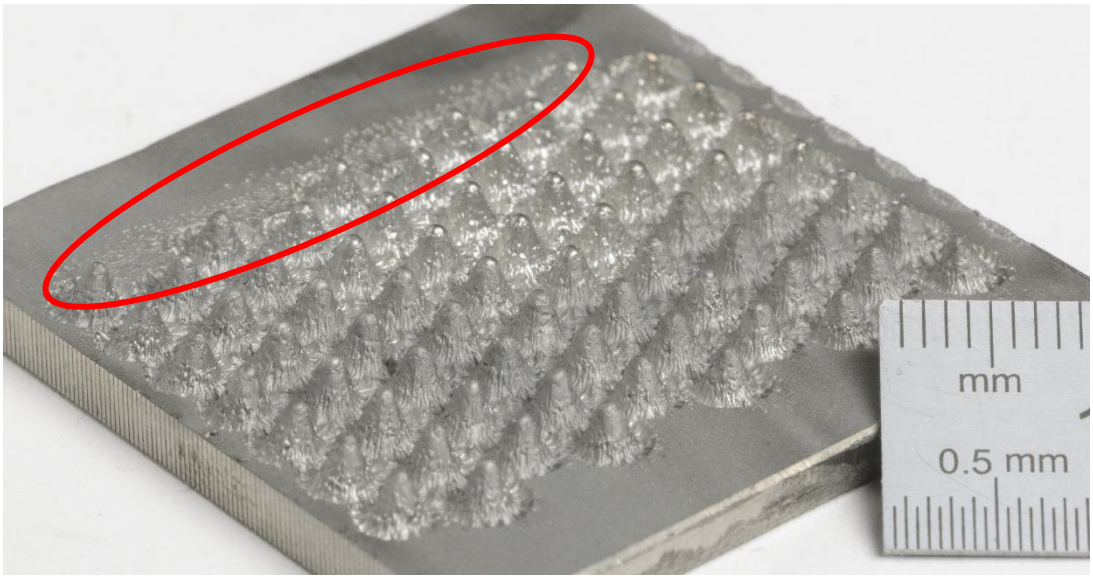

Figure 7.10 'Flyback' issue (highlighted in red) marking the surface of the material caused by the locations set in the array.

Due to the design of the electro-magnetic coils, it is not possible to actively drive the beam to the freefall position in the centre of the coil set. To return to this position, the voltage output from the function generators will be zero which effectively disables the deflection. Therefore, it is best practice to offset all patterns away from the 0,0 Cartesian position.

After the motif frequency (f_m) has been set, Equation 13 determines how much of a feature (F) is processed during one complete cycle of the array based upon the number of positions in the array (p).

$$F = \frac{f_m}{f_m \, x \, p} \qquad \textbf{Equation 13}$$

Using an example of 9 Hz for the *U,V* motif frequency (f_m) and 8 Hz for the *X,Y* array frequency (f_a), it will take 1/8th of a second to complete a cycle of the array compared to 1/9th of a second to complete a single motif. An example of this is shown in Figure 7.11.

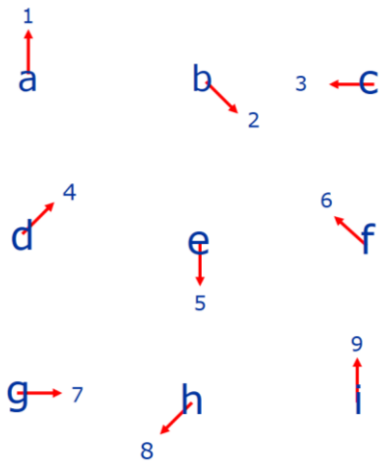

Figure 7.11 Sequence of first nine beam swipes used in the example from Figure 7.9.

Swipes 1 and 2 (of the motif) are sequential when moving between positions *a* and *b* (of the array) because both the motif and array are running in parallel and therefore the swipes translate around the feature as they process through the array.

In this example, it would take eight repeats to complete the motifs in the array in 1 second. Since the motif in this example is made from 8 legs (swipes), one leg will be completed per cycle. The frequency of the motif (f_m) and the amplitude of the motif determine the beam speed of each swipe. Since the beam speed for optimal EBT and Surfi-Sculpt processing is known, f_m must be altered in line with the size of the motif. From this, the frequency of the array (f_a) can be calculated by applying the golden ratio (φ) using an integer (r); this is equivalent to the number of swipes completed in the motif per cycle of the array. Equation 14 shows the relationship between the frequencies of the array and motif.

$$f_a = \frac{f_m}{r+\frac{1}{1+\varphi}} = \frac{f_m}{r+0.38197} \qquad \textbf{Equation 14}$$

Based upon the use of the golden ratio (φ), it can be concluded that a 6.51 Hz frequency should be used for the array if one swipe of the motif is completed in the array cycle when the frequency for the motif is set to 9 Hz.

However, the golden angle rule cannot be applied to features with fewer than eight legs such as Sawtooth, created by a single swipe, or a textured pattern, as the amount of beam swipes would not create an evenly processed feature.

In summary, the methodology for using the golden ratio (φ) to calculate the optimal frequency for f_a is:

1 Calculate the frequency of the motif (f_m) to achieve the optimum swipe speed for the EBT and Surfi-Sculpt processes based upon the swipe length. This ensures that a suitable fraction of a feature per cycle is completed.
2 Determine the equivalent number of swipes completed in the motif per cycle of the array to calculate the frequency of the array (f_a) using the golden ratio (φ) in Equation 11 and determine the *r* + 0.38197. From this, the frequencies should then be altered so that the ratio of $\frac{f_m}{f_a}$ should be close to where *r* is an integer to ensure the golden ratio (φ) is achieved.

The purpose of this methodology is to ensure that a mathematical calculation of the deflection pattern frequencies is used rather than an empirical approach.

Additional processing considerations include the following:

1 To completely cover a surface area (with no unprocessed regions on the surface), motifs must be square, rectangular, triangular, or hexagonal symmetry.
2 On 3D curved surfaces, occasional pentagonal features may be combined with hexagonal features, or triangles with squares, to give surface area coverage.

3 Radial swipes (or swipe groups) in motifs must be the same speed and the same duration to be effective and to synchronise correctly. This leads to increasing compromise in beam swipe speed and duration unless short and long swipes are paired in hexagonal motifs (~18 % difference in swipe length between longest and shortest), square motifs (~41 %), and triangular motifs (~73 %).

7.2.4 Example creation of a pattern

Figure 7.12 shows the outline of a 96 leg square motif (the majority of swipes have been omitted for clarity) which would create a square based pyramid feature. This is effectively a 48 leg motif, as swipes 1 and 2 are designed to be a pair, as are 3 and 4, and so on. By pairing swipes in this way as well as adjusting the lengths, a constant swipe speed can be obtained. Angular swipe spacing can be adjusted to give a uniform effect if required with this pattern type.

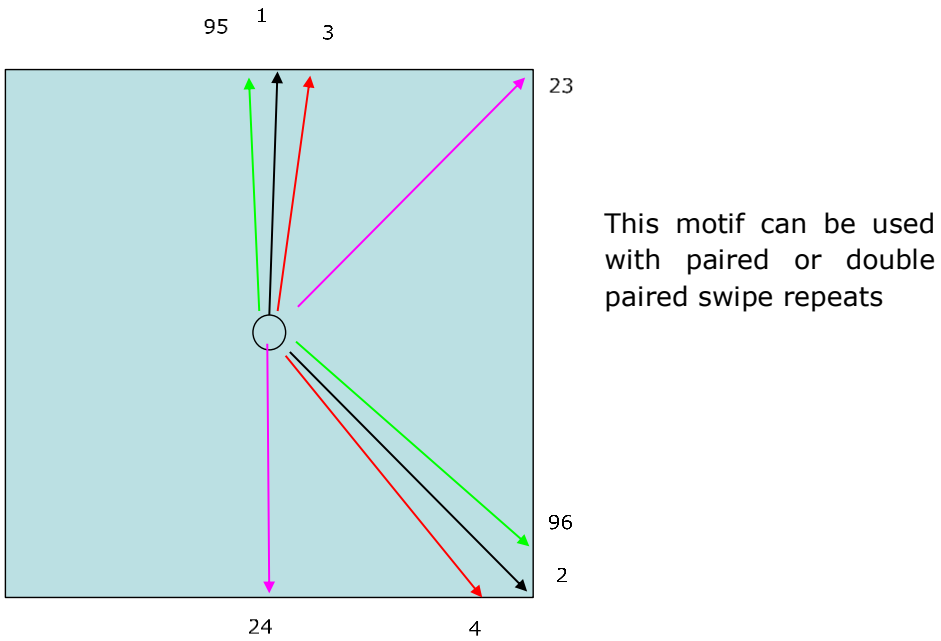

Figure 7.12 Sequence of beam swipes on a 96 leg motif using the golden angle principle.

7.2.5 Progression of feature building

When creating features with high aspect ratio, it is required to reduce the *U,V* amplitude processing parameters to move less material but concentrate it closer to the centre of the feature. Figure 7.13 shows how three stages of processing can be utilised to support the creation of these features using the Surfi-Sculpt process.

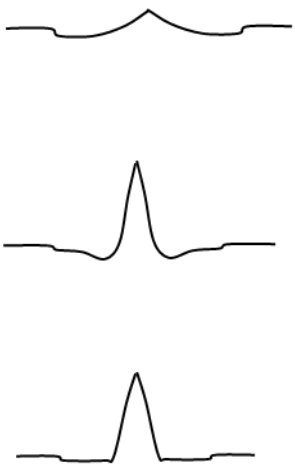

Figure 7.13 Stages of a build to minimise the intrusions whilst achieving a higher feature (protrusion) height.

For more sophisticated patterns, for example the LCP produced using the Surfi-Sculpt process, discussed in Chapter 4, a trigger signal can be generated and used to provide accurate timing points for parameter changes as described in Section 7.2.5.1.

7.2.5.1 Example stages in processing

Table 7.1 shows an example of how Surfi-Sculpt process parameters can be varied to optimise the formation of features and ensure that the geometry is as desired, for example achieving a high aspect ratio.

Table 7.1 Example process stages for feature building.

Increment (#)	Stage	Time (s)	Beam current	Beam focus	Beam deflection
0	0	00.00	0	SF	100 %
1	1	02.38	H	SF	100 %
2	1	04.76	H	SF	100 %
3	1	07.14	H	SF	100 %
4	1	09.52	H	SF	93 %
5	2	11.90	H	SF	86 %
6	2	14.28	H	SF	79 %
7	2	16.66	H	SF	72 %
8	2	19.04	H	SF	65 %
9	2	21.04	H	SF	58 %
10	2	23.80	0	SF	58 %
11	2	26.18	H	SF	58 %
12	3	28.56	0	SF – 5 % SF	100 %
13	3	30.94	0	SF – 5 % SF	100 %
14	3	33.32	H	SF – 5 % SF	100 %
15	3	35.70	H	SF – 5 % SF	100 %
16	3	38.08	>	SF – 5 % SF	100 %
17	3	40.46	0	SF – 5 % SF	100 %

Where SF – Sharp focus, H – processing current, 0 – beam off, > indicates a slope out in beam power over ~1.5 seconds, and beam defection amplitudes vary from full size to 0.58 x full size for the motif.

7.3 Electron beam interaction with materials

Currently a S-SPS is material specific and there are no conversion or look-up tables to support the translation to a different material. Schiller et al. (1982) noted that the maximum power of the EB absorbed by the material is at a third of the total penetration depth. However, this is material specific and consequently, as detailed in Equation 4, the beam energy must be aligned to the density of the material to generate a similar sized melt pool and move a similar volume of material with each beam swipe.

The orthopaedic industry commonly uses the titanium alloy Ti-6Al-4V, which has a density of 4429 kg/m^3, as it is biocompatible and meets the mechanical requirements for use in the body. Therefore, this was the material used in the orthopaedic implant case study (Chapter 5 and Submission 6). In comparison, an aluminium alloy, with a lower density of 2700 kg/m^3, was used in the LCP case study (Chapter 4 and Submission 3) for application on heat exchangers as it has a high thermal conductivity.

Using Equation 4, the penetration depth of an EB using an accelerating voltage of 130 kV for Ti-6Al-4V and Al6xxx (specific grade not stated due to commercial sensitivity; this is listed in Submission 3) would be 50 µm and 82 µm respectively as shown in Figure 7.14. Consequently, Al6xxx has a larger melt pool than Ti-6Al-4V so each swipe of the beam translates a larger volume of material. Therefore, in order to achieve the same penetration depth in Al6xxx as with Ti-6Al-4V, approximately 100 kV (approximately 75 %) would be required since 100 kV achieves a 53 µm penetration depth.

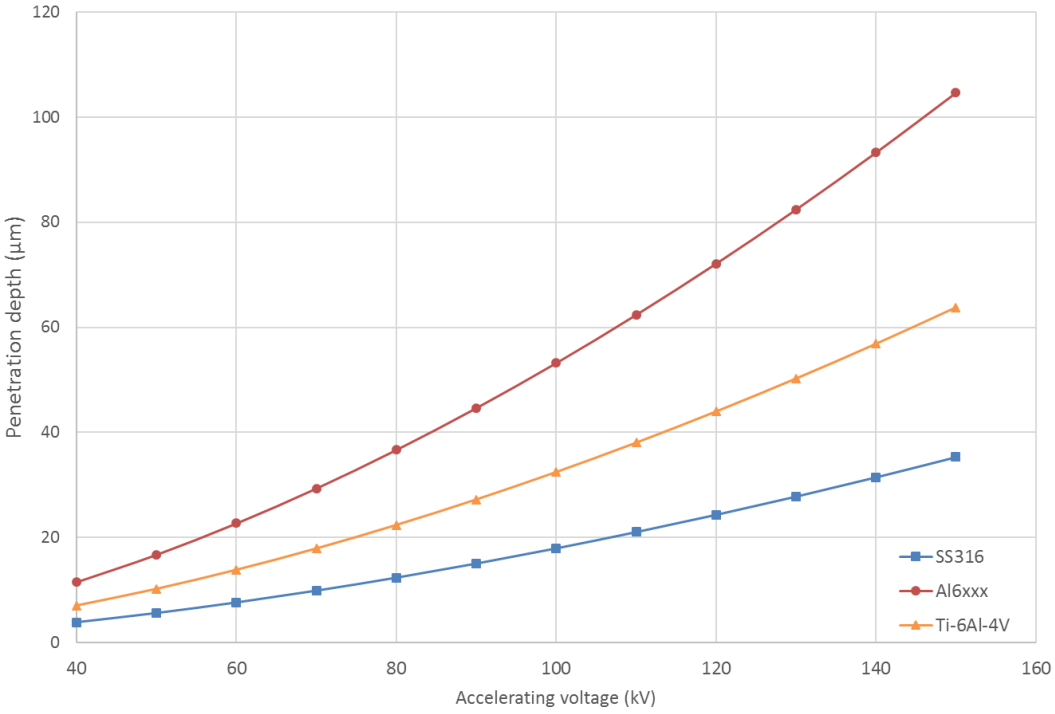

Figure 7.14 Penetration depth plotted against accelerating voltage for SS316, Al6xxx and Ti-6Al-4V using Equation 4.

A comprehensive conversion or look-up table based upon the penetration depth of the material for a range of frequently used materials would be beneficial for the EBT and Surfi-Sculpt processes such as aluminium, copper, titanium and its alloys e.g. Ti-6Al-4V, stainless steel alloys and carbon manganese steels. Additionally, regression analysis and prediction of feature height for a more extensive list of materials would further enhance the understanding of the processes.

7.4 Beam deflection speeds in the motif

Table 7.2 shows a summary of beam deflection requirements expressed as beam swipe speeds and beam energy input from the parameters (some of which are normalised for confidentiality reasons) for 35 of the S-SPS used in this EngD and three records from Ramskogler et al. (2017).

In comparison to the author's work, which utilised beam swipe speeds of predominately greater than 20 ms^{-1} resulting in beam energy input values ranging from 2.5 up to approximately 180 Jm^{-1}, Ramskogler et al. (2017) used beam swipe speeds of approximately 0.34 and 0.68 ms^{-1} and observed melting of the material at the lower beam swipe speed with a beam power of 120 W (355 and 555 Jm^{-1} respectively). The author considered that the slower beam swipe speeds recorded by Ramskogler et al. (2017) were associated with the creation of smaller features at lower beam currents over a longer processing time period; however, it is unknown if the parameters had been optimised. This resulted in similar beam energy input values with the exception of a single value of 555 Jm^{-1} which was described as having solidification lines on the surface that were too strong and distinct (Ramskogler et al., 2017).

Table 7.2 Summary of beam deflection requirements expressed as beam swipe speeds.

Description	Material	Heat input (W)	Swipe length (mm)	Number of swipes in the motif	Pattern frequency (Hz)	Beam motif swipe speed (ms^{-1})	Beam energy input (Jm^{-1})
LCP Design 1	Al6082	170	3.03	70	10.55	67.02	13.2
LCP Design 2	Al6082	275	3.03	96	12.25	177.87	6.4
LCP Design 3	Al6082	275	3.03	96	12.50	181.50	6.3
LCP Design 4	Al6082	150	3.03	24	63.30	137.87	4.5
LCP Design 5	Al6082	212	2.96	70	10.55	65.50	13.5
LCP Design 6	Al6082	187	2.89	70	16.2	98.23	7.9
LCP Design 7	Al6082	175	1.67	96	8.00	64.28	11.3
LCP Design 8	Al6082	125	2.25	22	27.00	40.10	13.0
HeatSculptor Design 6 - Curved Ridges	Al6xxx*	187	3.09	160	10.55	68.54	11.4
HeatSculptor Design 5 - Inclined cones	Al6xxx*	212	1.86	70	16.2	241.59	3.7
HeatSculptor Design 5 - Prototype	Al6xxx*	212	1.75	70	16.2	226.80	3.7
HeatSculptor Design 5 - Final prototype	Al6xxx*	212	3.30	70	16.2	73.11	12.1
EngD Al6xxx* Dataset 1	Al6xxx*	187	3.30	70	10.55	73.11	3.9
EngD Al6xxx* Dataset 2	Al6xxx*	187	3.30	70	10.55	73.11	10.7
EngD Al6xxx* Dataset 3	Al6xxx*	92	1.97	70	10.55	19.81	12.1
EngD Al6xxx* Dataset 4	Al6xxx*	92	1.97	70	10.55	19.81	19.4
EngD Al6xxx* Dataset 5	Al6xxx*	115	1.97	70	10.55	19.81	10.7
EngD Al6xxx* Dataset 6	Al6xxx*	115	1.97	70	10.55	19.81	24.2
EngD Al6xxx* Dataset 7	Al6xxx*	138	1.97	70	10.55	19.81	19.4
EngD Al6xxx* Dataset 8	Al6xxx*	207	1.97	70	10.55	19.81	43.6
EngD Al6xxx* Dataset 9	Al6xxx*	207	1.97	70	10.55	19.81	19.4
Beam Deflection Offset Study	Ti-6Al-4V	72	4.44	22	7.00	29.30	13.9
High-Speed Video	Ti-6Al-4V	377	4.44	22	10.00	29.30	10.3
OrthoSculpt Design 4	Ti-6Al-4V	270	1.57	1	3,000.00	378.00	2.5
OrthoSculpt Friction Test Samples	Ti-6Al-4V	1,200	1.26	560	1.45	1.21	179.1
Ramskogler et al. (2017) Data 1	Ti-6Al-4V	270	1.00^	504	3.54‡	0.34	355

Description	Material	Heat input (W)	Swipe length (mm)	Number of swipes in the motif	Pattern frequency (Hz)	Beam motif swipe speed (ms^{-1})	Beam energy input (Jm^{-1})
Ramskogler et al. (2017) Data 2	Ti-6Al-4V	120	1.00^	96	7.08‡	0.68	555
Ramskogler et al. (2017) Data 3	Ti-6Al-4V	375	1.00^	96	7.08‡	0.68	555
EngD Ti-6Al-4V Dataset 1	Ti-6Al-4V	104	1.92	70	10.55	19.30	22.4
EngD Ti-6Al-4V Dataset 2	Ti-6Al-4V	138	1.92	70	10.55	19.30	29.8
EngD Ti-6Al-4V Dataset 3	Ti-6Al-4V	81	1.92	70	10.55	19.30	17.4
EngD Ti-6Al-4V Dataset 4	Ti-6Al-4V	81	1.92	70	10.55	19.30	17.4
EngD Ti-6Al-4V Dataset 5	Ti-6Al-4V	138	1.92	70	10.55	19.30	29.8
EngD Ti-6Al-4V Dataset 6	Ti-6Al-4V	138	1.92	70	10.55	19.30	29.8
EngD Ti-6Al-4V Dataset 7	Ti-6Al-4V	138	1.92	70	10.55	19.30	29.8
EngD Ti-6Al-4V Dataset 8	Ti-6Al-4V	138	1.92	70	10.55	19.30	29.8

* Specific grade used listed in Submission 3 – commercially sensitive.
^ Assumed by the author based upon polygon figure (motif) diameter being 2.00 mm in Ramskogler et al. (2017).
‡ Calculated by the author based upon information in Ramskogler et al. (2017).

7.5 Summary of the discussion

The principles discussed in Chapter 7 have identified data and knowledge which could support the creation of a 'CAD to Surfi-Sculpt' pre-processing platform tool. The mathematical calculation of the beam path and parameters between different materials would further enhance the adoption and implementation of the EBT and Surfi-Sculpt processes to meet industrial needs. The ability to embed the expertise, knowledge, methodologies and calculations required to use the EBT and Surfi-Sculpt processes in software is critical since these are key aspects which hinder their adoption into manufacturing environments.

8 Further Work

8.1 Developments planned beyond this EngD

8.1.1 Automation of the parameter inputs

Work is planned, led by the author, to commence the automation of parameter input from the Surfi-Sculpt catalogue records and to load them into the Mark III deflection control software in response to the problem statement in Chapter 6 as detailed by a current licensee of the EBT and Surfi-Sculpt processes. The author is currently detailing a specification document to define the framework for the automation element of the software.

8.1.2 High-speed filming

In order to observe the movement of material in the EB Surfi-Sculpt process, a camera with a higher frame rate (e.g. 40,000 fps) would need to be used that could operate within the challenging environment stated in Section 3.2. This could confirm the author's prediction regarding the flow of molten material. Currently, the author is not aware of any suitable camera for this particular application and therefore technical developments in high speed cameras must occur before this work can be realised. The only option available to the author at this time is to use the Os7 high-speed camera but to reduce the vertical resolution to 128 pixels. This would mean that only the initial swipes of the beam could be videoed before the feature became too large to fit in the frame or the image quality would be too pixelated for analysis.

8.1.3 Pre-processing software developments

Pre-processing software was not considered within the scope of this EngD but further work is planned by the author to develop a 'CAD to Surfi-Sculpt' platform. To develop this platform, the beam-material interaction, as discussed in Section 7.3 and studied in Chapter 3, would need to be considered and incorporated into the software. An example of where this could be developed is considering existing computer aided manufacturing (CAM) software used to

provide 'toolpath' strategies for subtractive and additive manufacturing such as Autodesk's PowerMill®. The 'toolpath' for the EBT and Surfi-Sculpt processes is the beam deflection path. This should also include a comprehensive conversion or look-up table for a range of frequently used materials for the EBT and Surfi-Sculpt processes.

8.1.4 Further development of the Surfi-Sculpt catalogue

The author's future plans for the Surfi-Sculpt catalogue in 2021 / 2022 are to generate additional performance data to ensure sufficient volume of knowledge to support categories which are performance-based such as chemical, biological or physical characteristics. This would add more selections of appropriate records for search purposes.

8.1.5 Commercialisation of components from the case studies

The specific commercialisation plans for the acetabular cup were discussed in Submission 6 whereby the clinical investigation and regulatory approval phase of work would run from 2022 - 2026. Prior to this, a follow-on large grant would be prepared, secured and delivered in which the EBT and Surfi-Sculpt processes would be further developed and tested in vivo to the point where they would be ready for a 1st in-human study prior to a product launch in 2026.

8.1.6 Future plans for the processes

All of the further work outlined in this Chapter will continue to develop the EBT and Surfi-Sculpt processes through the TRLs and MRLs and enable them to be ready for adoption in manufacturing environments.

9 Conclusions

9.1 Technical conclusions

As demonstrated through the work of this EngD, the electron beam texturing (EBT) and Surfi-Sculpt processes have progressed up the technology readiness levels (TRLs) and manufacturing readiness levels (MRLs). The author has evidenced the following technical conclusions:

- Creation of a framework to increase fundamental understanding of the influence of parameters controlling the geometry and shape of a feature after each swipe.
  - The feature heights in two materials, Al6082 and Ti-6Al-4V, can now be successfully predicted using the following key parameters for the EBT and Surfi-Sculpt processes: number of swipes in the motif, swipe length, beam swipe speed in the motif, beam on time, heat input and beam energy input.
  - The importance of a specific parameter, beam focus, to the feature height achieved with the processes has been quantified showing the loss of actual feature height, up to approximately 70 %, compared with predicted feature height when there is less than 1 % variation from sharp focus.
- Production of slow motion footage from inside the electron beam (EB) vacuum chamber enabling details of the process to be observed for the first time.
  - This involved the development of a bespoke technique for the setup, analysis and discussion of the resultant footage.
  - The author identified five distinct phases of feature formation: initial melt track; expansion of feature base and height; increase of height; bridging; and over melting with potential decrease of height.
- Application of the golden angle rule to the beam path in the motif (*U,V*) deflection pattern file and associated deflection frequencies for both the array and motif, to features with more than or equal to eight legs, to support the

automation of the EBT and Surfi-Sculpt processes and creation of pre-processing software via mathematical calculation.

- Development and definition of a model of the flow of molten material explaining the Surfi-Sculpt process and the formation of a feature using Marangoni effects.
- Recommendation that a comprehensive conversion or look-up table for a range of frequently used materials is required for the EBT and Surfi-Sculpt processes.

9.2 Business conclusions

The EBT and Surfi-Sculpt processes have clear industrial application in heat exchangers, particularly liquid cold plates (LCPs), and orthopaedic implants, specifically the acetabular cups in uncemented total hip replacements (uTHRs); other applications are still in development. During this EngD, the author has demonstrated the following innovations for industrial application:

- Manufacture of prototype LCP components with a novel surface over an area of approximately 95 x 31 mm using the EB Surfi-Sculpt process.
  - Demonstration of approximately 100 % increase in heat transfer coefficient performance compared with an existing technology.
  - Enabling use of a 50 % smaller LCP for the same cooling power as an existing technology.
  - Reduction of 40 % in the manufacturing time compared with an existing technology.
- Demonstration that the EBT and Surfi-Sculpt processes can produce novel surfaces which enhance the coefficient of friction (COF) and perform to the requirements of an acetabular cup for next generation uTHRs.
  - Manufacture of prototype acetabular cup using the EBT process with a novel surface in 18.2 seconds beam on time.

- Development of a directory and selection tool (Surfi-Sculpt catalogue) for improved knowledge management of the EBT and Surfi-Sculpt processes with 38 entries currently stored.
  - The creation of a search capability to enhance rapid identification and manufacture of surfaces.
  - The controlled storage, access and manipulation of data and parameters within the Surfi-Sculpt catalogue based upon user access levels.

It is recommended that the EBT and Surfi-Sculpt processes should be considered for adoption within the applications identified as they are precise, rapid and flexible manufacturing techniques which demonstrate zero waste as only the parent material is utilised. These developments have supported progression to TRL 7 – 'System prototype demonstration in operational environment'.

9.3 Contribution to TWI business

The work undertaken for this EngD has contributed significantly to TWI; in six years working with the EBT and Surfi-Sculpt processes, the author has generated approximately £780k of external income for his employer. Alongside project work, this has included the recruitment of three new TWI Member companies as a result of the development of the processes.

The contribution (allowing for costs) to TWI's business from the EBT and Surfi-Sculpt processes has been approximately £1m in the duration of the EngD, of which the author is directly responsible for approximately £590k.

10 References

Abbott, S., 2017. 8.8.2 Surfactants to fix other levelling issues. In *Surfactant Science: Principles and Practice.* pp. 244-246. Lancaster, PA, USA: DEStech Publications.

Abbas, S., 2017. Golden ratio. *Resonance: Journal of Science Education,* 22(1), pp. 51-60.

Adam, V., Clauß, U., v. Dobeneck, D., Krüssel, T. & Löwer, T., 2011. *Electron Beam Welding - The fundamentals of a fascinating technology*. 1st edition ed. Planegg, Germany: pro-beam AG & Co. KGaA.

American Welding Society, 2007. WHC3.13 Electron Beam Welding. In: *Welding Handbook. 9th edition, Volume 3. Welding processes - Part 2. - 9th edition.* American Welding Society.

Arata, Y., Terai, K. & Matsuda, S., 1976. Study on Characteristics of Weld Defects and Their Preventions in Electron Beam Welding. Report 4: Relationship Between The Weld Defect And Its Formation Phenomenon. *Transactions of JWRI*, 4(2). pp. 189-196.

Atkinson, T. & Chapman, P., 2007. *TWI internal Report - ASTIA Project Gun Design Report,* Great Abington, Cambridge: TWI Ltd.

Auerswald, P. E. & Branscomb, L. M., 2003. Valleys of death and Darwinian seas: financing the invention to innovation transition in the United States.. *Journal of Technology Transfer,* 28(3-4), pp. 227–239.

Babu, S. S., David, S. A., Vitek, J. M. & Reed, R. W., 2001. Solidification and microstructure modelling of welds in aluminium alloys 5754 and 6111. *Science and Technology of Welding and Joining,* 6(1), pp. 31-40.

Bakish, R. & White, S. S., 1964. *Handbook of Electron Beam Welding.* New York: John Wiley and Sons.

Balla, V. K., Soderlind, J., Bose, S. & Bandyopadhyay, A., 2014. Microstructure, mechanical and wear properties of laser surface melted Ti6Al4V alloy. *Journal of the Mechanical Behavior of Biomedical Materials*, 32, pp. 335-344.

Bargiotas, K. A., 2014. Chapter 9 Trabecular Metal: Bone Interface in Total Joint Arthroplasty. In: T. Karachalios, ed. *Bone-Implant Interface in Orthopedic Surgery.* London: Springer-Verlag, pp. 121-126.

Beard, T. R., Ford, G. S., Koutsky, T. M. & Spiwak, L. J., 2009. A Valley of Death in the innovation sequence: an economic investigation. *Research Evaluation,* 18(5), pp. 343-356.

Bencharit, S., Byrd, W. C, Altarawneh, S., Hosseini, B., Leong, A., Reside, G., Morelli, T. & Offenbacher, S., 2014. Development and Applications of Porous Tantalum Trabecular Metal-Enhanced Titanium Dental Implants. *Clinical Implant Dentistry and Related Research,* 16(6), pp. 817-826.

Bergles, A. E., 1999. Enhanced Heat Transfer: Endless Frontier, or Mature and Routine?. In: M. Lehner & D. Mewes, eds. *Applied Optical Measurements.* Berlin, Germany: Springer, pp. 3-17.

Biomet Orthopaedics Inc., 2007. *Focus On Fixation PPS® Porous Plasma Spray.* Warsaw(Indiana): 46581-0587.

Bishop, N. E., Höhn, J. C., Rothstock, S., Damm, N. B. & Morlock, M. M., 2014. The influence of bone damage on press-fit mechanics. *Journal of Biomechanics,* 47(6), pp. 1472–1478.

Black, B. J., 2015. Primary forming processes. In: B. J. Black, ed. *Workshop Processes, Practices and Materials.* 5th ed. London, UK: Routledge, pp. 251-260.

Blackburn, J. & Hilton, P., 2010. Low Power Laser Surfi-Sculpt. *In: International Conference on Power Beam Processing Technologies (ICPBPT2010).* Beijing, China, 25-29 October 2010. Beijing, China: Beijing Aeronautical Manufacturing Technology Research Institute (BAMTRI).

Blackburn, J. & Hilton, P., 2011. Producing Surface Features with a 200 W Yb-fibre Laser and the Surfi-Sculpt Process. *Physics Procedia,* 12(A), pp. 529-536.

Blake, R., 1998. Laser forming and surface modification. *Surface Engineering,* 14(2), pp. 95-96.

Bodschwinna, H. & Seewig, J., 2013. In: Q. J. Wang & Y. Y. Chung, eds. *Topography of Engineering Surfaces in Encyclopedia of tribology.* New York; London: Springer, pp. 3701-3706.

Breme, J., Kirkpatrick, C. J. & Thull, R., 2008. *Metallic Biomaterial Interfaces.* Weinheim, Germany: Wiley, Weinheim.

Briggs, T., 2015. *A national review of adult elective orthopaedic services in England - Getting It Right First Time,* London, UK: British Orthopaedic Association.

Brooks J. A. & Mahin K. W., 1990. Chapter 2: Solidification and structure of welds. In Book: *Welding Theory and Practice. Materials Processing Theory and Practices,* Vol.8. Ed: Olson, D.L., Dixon, R. & Liby, A.L.,. Publ: 1000 AE Amsterdam, Netherlands; North Holland Elsevier Science Publishers. pp. 35-78.

The British Standards Institution, 1971. *BS 4094-2:1971 Recommendation for Data on shielding from ionizing radiation - Part 2: Shielding from X-radiation,* London, England: The British Standards Institution.

Bruyere, V., Touvrey, C. & Namy, P., 2013. Thermohydraulic modelling of pulsed laser welding. *In: Applications of Lasers and Electro-Optics. Proceedings, 32nd International Congress, ICALEO 2013, Miami, FL, 6-10 Oct.2013.* Publ: Orlando, FL 32826, USA; Laser Institute of America; 2013. Vol.106. Laser Materials Processing Conference. LMP 4: Modelling and Simulation. pp. 60-66.

Brooking, A., 1999. *Corporate Memory: Strategies for Knowledge Management.* London, UK: International Thomson Business Press.

Buxton, A. L. & Dance, B. G. I., 2005. Surfi-Sculpt - Revolutionary surface processing with an electron beam *The Potential of EB Surface Processing within the Aerospace Industry.* St Paul, MN, USA, ASM International, ISEC Congress.

Buxton, A. L. & Dance, B. G. I., 2010. *The Potential of EB Surface Processing within the Aerospace Industry.* Beijing, China, International Conference on Power Beam Processing Technologies.

Buxton, A. L., Oluleke, R. & Prangnell, P., 2012. *Generating and Assessing the Quality and Functionality of EB Structured Surfaces for Dissimilar Material Joints.* Aachen, Germany, Proceedings of the International Electron Beam Welding Conference (IEBW 2012).

Caetano-Lopes, J., Canhão, H. & Fonseca, J. E., 2007. Osteoblasts and bone formation. *Acta Reumatol Port.,* 32(2), pp. 103-110.

Calder, D., 2006. *Industrialisation Study for Surfi-Sculpt (TWI Report: 16582/1/06),* Great Abington, Cambridge, UK: TWI Ltd.

Chikarakara, E., Naher, S. & Brabazon, D., 2012. High speed laser surface modification of Ti-6Al-4V. *Surface and Coatings Technology*, 206 (14), pp. 3223-3229.

Comsol, 2017. *The Marangoni Effect*. [Online]
Available at: https://www.comsol.com/multiphysics/marangoni-effect
[Accessed 30 December 2019].

COOLTECH Srl, 2015. *Innovative Technologies.* [Online]
Available at: http://www.cooltech.it/engineering/innovative-technologies/
[Accessed 15 July 2017].

Cooper, K. P., 2005. Layer-by-layer fabrication of net-shape metallic parts. In: *IIW [International Institute of Welding] International Congress 2005. Frontiers of Welding Science and Technology. Proceedings, Conference, Mumbai, 16-19 Feb.2005.* Chairman: B.Raj. Publ: Calcutta, 700017, India; Indian Institute of Welding; 2005. Session 3A. Paper IWA 041. pp. 1-19.

Cooper, K. P. & Lambrakos, S. G., 2005. Fabrication of net-shape metallic parts by overlapping reinforced weld beads, *ASM Proceedings of the International Conference: Trends in Welding Research 2005*, pp. 647-652.

Cross, M. J. & Spycher, J., 2008. Cementless fixation techniques in joint replacement. In: P. A. Revell, ed. *Joint replacement technology.* Cambridge, England: Woodhead Publishing Ltd, pp. 190-211.

Damm, N. B., Morlock, M. M. & Bishop, N. E., 2015. Friction coefficient and effective interference at the implant-bone interface. *J. Biomech.,* 48(12), pp. 3517-3521.

Dance, B. G. I., 2002. *Surface Modification.* Europe, Patent No. WO 2002/094497.

Dance, B. G. I., 2007. *TWI Internal Report - 2010 IP Course v1,* Great Abington: TWI Ltd.

Dance, B. G. I. & Buxton, A. L., 2007. An Introduction to Surfi-Sculpt Technology - New Opportunities, New Challenges. 7th International Conference on Beam Technology, Halle, Germany.

Dance, B. G. I. & Kellar, E. J. C., 2003. *Workpiece Structure Modification Method.* Europe, Patent No. WO 2004/028731.

Daugaard, H., Bechtold, J. E. & Soballe, K., 2014. Chapter 8 HA-Coated Implant: Bone Interface in Total Joint Arthroplasty. In: T. Karachalios, ed. *Bone-Implant Interface in Orthopedic Surgery.* London: Springer-Verlag, pp. 91-119.

David, S. A. & Vitek, J. M., 1989. Correlation between solidification parameters and weld microstructures. *International Materials Reviews,* 34(1), pp. 213-245.

Department for Business, Innovation and Skills, 2011. *BIS ECONOMICS PAPER NO. 15 - Innovation and Research: Strategy for Growth' DECEMBER 2011 Ref: BIS/Pub/0.0k/12/11.NP. URN 11/1386.* [Online]
Available at: www.bis.gov.uk
[Accessed 16 November 2013].

Draper, E. R. C., 2016. *Personal communication via e-mail on 13 July 2016.* Sheffield: JRI Ltd.

Dworak, J., 1992. Electron beam welding of heat treatment steel with oscillating beam. *Biuletyn Instututu Spawalnictwa,* 36(4), pp. 54-57.

Earl, C., Castrejón-Pita, J. R., Hilton, P. A. & O'Neill, W., 2016. The dynamics of laser surface modification. *Journal of Manufacturing Processes.*(21), pp. 214-223.

Earl, C. & Hilton, P., 2012. *Optimisation and Observation of the Laser Surfi-Sculpt Process. TWI Report 19837.01/2012/1499.2,* Great Abington: TWI Ltd.

Earl, C., Hilton, P. & O'Neill, B., 2012. Parameter influence on Surfi-Sculpt processing efficiency. *Physics Procedia,* Volume 39, pp. 327–335.

Ehlers, V., 1998. *Unlocking Our Future: Toward a New National Science Policy. Committee on Science US House of Representatives.* [Online]
Available at: https://www.gpo.gov/fdsys/pkg/GPO-CPRT-105hprt105-b/pdf/GPO-CPRT-105hprt105-b.pdf
[Accessed 13 March 2018].

Elmer, J. W, Allen, S. M. & Eagar, T. W., 1989. Microstructural development during solidification of stainless steel alloys. *Metallurgical Transactions: A*, 20(10). pp. 2117-2131.

Epinette, J.-A. & Manley, M. T., 2013. Foreword. In: *Fifteen Years of Clinical Experience with Hydroxyapatite Coatings in Joint Arthroplasty.* Springer.

Eustathopoulos, N., Drevet, B. & Ricci, E., 1998. Temperature coefficient of surface tension for pure liquid metals. *Journal of Crystal Growth* 191, pp. 268-274.

EU Publications Office Top, 2002. *Community Research and Development Information System (CORDIS) - Compact bearing housings for rolls on EBT machines.* [Online]
Available at: https://cordis.europa.eu/project/rcn/66414_en.html
[Accessed 10 March 2018].

European Commission, 2016. Horizon 2020 - Work Programme 2016-2017. *G.Technology readiness levels (TRL).* [Online]
Available at:
https://ec.europa.eu/research/participants/data/ref/h2020/other/wp/2016_2017/annexes/h2020-wp1617-annex-g-trl_en.pdf
[Accessed 24 February 2018].

Ferhati, A., Karayiannis, T. G., Lewis, J. S., McGlen, R. J. & Reay, D. A., 2015. Single-Phase Laminar Flow Heat Transfer From Confined Electron Beam Enhanced Surfaces. *Heat Transfer Engineering,* 36(14-15), pp. 1165-1176.

Focus GmbH, 2017. *MEBW-60 Micro ELectron beam welder.* [Online]
Available at: http://www.focus-e-welding.de/resources/MEBWBroschure2017.pdf
[Accessed 14 April 2018].

Fuentes, G. F., 2010. Chapter 14 - Surface Engineering and Micro-Manufacturing. In: Y. Qin, ed. *Micro-Manufacturing Engineering and Technology.* Oxford, England: Elsevier, pp. 221-240.

Furlong, R. & Osborn, J., 1991. Fixation of hip prostheses by hydroxyapatite ceramic coatings. *Bone & Joint Journal,* 73-B(5), pp. 741-745.

Galvani, A., 1791 [translated 1953]. *De Viribus Electricitatas in Motu Musculari Commentarius (Translated: The effects of artificial electricity on muscular motion).* Bologna, De Bononiensi scientiarum et artium instituto atque academia.

Gebauer, H., Fleisch, E. & Friedli, T., 2005. Overcoming the Service Paradox in Manufacturing Companies. *European Management Journal,* 23(1), pp. 14-26.

Hailer, N. P., Garellick, G. & Kärrholm, J., 2010. Uncemented and cemented primary total hip arthroplasty in the Swedish Hip Arthroplasty Register. *Acta Orthopaedica,* 81(1), pp. 34-41.

Hamilius, A. & de Soete, D., 1997. *Electron beam technology for the controlled roughing of cold mill rolls for steel-making companies,* Luxembourg: Office for Official Publications of the European Communities.

Haug, E. & Nakel, W., 2004. *The Elementary Process of Bremsstrahlung.* New Jersey, USA: World Scientific Publishing Co Pte Ltd.

Hawley, T., 2012. *Making Knowledge Management Work for Your Organisation.* London: Ark Group.

HeatSculptor - Novel Electron Beam Surface Sculpting for Efficient Heat Exchange. 2015. [Film] Directed by T. M. Pinto. UK: TWI Ltd.
Available at: https://www.youtube.com/watch?v=LoGwhucUO28
[Accessed 26 March 2017].

Heiple, C. R. & Roper, J. R., 1982. Mechanism for minor element effect on GTA fusion zone geometry. *Welding Journal,* 61(4), pp. 97-102.

Heiple, C. R., Roper, J. R., Stagner, R. T. & Aden, R. J., 1983. Surface active element effects on the shape of GTA, laser, and electron beam welds. *Welding Journal,* 62(3), pp. 72-77.

Hilton, P. & Nguyen, L., 2008. *A new method of laser beam induced surface modification using the Surfi-Sculpt process.* Beijing, Laser Institute of America.

Honda, H. & Wei, J. J., 2004. Enhanced boiling heat transfer from electronic components by use of surface microstructures. *The International Symposium on Compact Heat Exchangers, Experimental Thermal and Fluid Science,* 28(2), pp. 159-169.

Horowitz, S. M., Doty, S. B., Lane, J. M. & Burstein, A. H., 1993. Studies of the mechanism by which the mechanical failure of polymethylmethacrylate leads to bone resorption. *Journal of Bone & Joint Surgery (American),* 75(6), pp. 802-813.

Huang, J., 2011. *The Characterisation and Modelling of Porosity Formation in Electron Beam Welded Titanium Alloys,* Birmingham, UK: School Metallurgy and Materials, University of Birmingham.

Hug, V., 2009. *European Commission Directorate General Environment - Bridging the Valley of Death: public support for commercialisation of eco-innovation,* Copenhagen, Denmark: COWI A/S.

The Ionising Radiations Regulations, 1999, London, UK: The Stationery Office Limited; Statutory Instruments. Health and Safety.
Available at: http://www.legislation.gov.uk/uksi/1999/3232/contents/made
[Accessed 26 May 2018].

The Ionising Radiations Regulations, 2017, London, UK: The Stationery Office Limited; Statutory Instruments. Health and Safety.
Available at: http://www.legislation.gov.uk/uksi/2017/1075/pdfs/uksi_20171075_en.pdf
[Accessed 26 May 2018].

Jamshidinia, M., Kong, F. & Kovacevic, R., 2013. Numerical Modeling of Heat Distribution in the Electron Beam Melting of Ti-6Al-4V. *Journal of Manufacturing Science and Engineering,* 135(6).

Jones, L. C., Tsao, A. K. & Topoleski, L. D. T., 2012. Factors contributing to orthopaedic implant wear. In: S. Affatato, ed. *Wear of orthopaedic implants and artificial joints.* Cambridge, UK: Woodhead Publishing Ltd, pp. 310-350.

Karachalios, T., Komnos, G. & Kolonia, K., 2014. Current Evidence in Designs and Fixation Surfaces in Total Hip Arthroplasty. In: T. Karachalios, ed. *Bone-Implant Interface in Orthopedic Surgery: Basic Science to Clinical Applications.* London: Springer, pp. 1-12.

Kaur, A. P., 2016. PhD Thesis: Electron Beam Diagnosis for Weld Quality Assurance, London: Brunel University London.

Khorasani, A. M., Gibson, I. & Ghaderi, A. R., 2018. Rheological characterization of process parameters influence on surface quality of Ti-6Al-4V parts manufactured by selective laser melting. *International Journal of Advanced Manufacturing Technology*, 97 (9-12), pp. 3761-3775.

Kohn, D. H., 2011. 6.605. Porous Coatings in Orthopedics. In: P. Ducheynen, ed. *Comprehensive Biomaterials.* s.l.:Elsevier Ltd, pp. 65-76.

Koleva, E. G. & Mladenov, G. M., 2011. 4. Experience on electron beam welding. In: M. R. Nemtanu & M. Brasoveanu, eds. *Practical Aspects and Applications of Electron Beam Irradiation.* Kerala, India: Transworld Research Network, pp. 95-133.

Kou, S., 2002. *Welding metallurgy*. 2nd ed. Publ: New York NY 10158-0012, USA; John Wiley & Sons Inc.

Kristianto, J., Ajmal, M., Tenkorang, R. A. & Hussain, M., 2012. A study of technology adoption in manufacturing firms. *Journal of Manufacturing Technology Management*, 23(2), pp.198-211.

Lee, P., Quested, P. N. & Mclean, M., 1998. Modelling of Marangoni effects in electron beam. *Phil. Trans. R. Soc. Lond. A.,* Volume 356, pp. 1027-1043.

Lee, S., Yoo, S. & Kim, D., 2016. When is servitization a profitable competitive strategy?. *Int. J. Production Economics,* Volume 173, pp. 43-53.

Leskov, G. I. & Živaga, L. I., 1978. Plavlenie metalla bol'šoj tolščiny pri svarke koničeskim èlektronnym pučkom. *Avtomaticheskaya Svarka,* 31(4), pp. 11-14.

Li, K., Fu, P., Tang, D., Wu, B. & Liu, X., 2018. Electron beam processed surface textures on titanium alloys for fluid-drag reduction. *The International Journal of Advanced Manufacturing Technology,* 96(5-8), pp. 1553–1563.

Lima Corporate, 2017. *Lima Corporate Celebrates 10 years of 3D printing: Trabecular Titianium.* [Online]
Available at:
https://www.limacorporate.com/repo/transfers/13/Lima_Corporate_Press_Release_TT_FINAL_EN_ITA.pdf
[Accessed 24 March 2018].

Livio, M., 2003. *The Golden Ratio: The Story of Phi, the World's Most Astonishing Number.* 1st ed. New York, USA: Broadway Books.

Lord Carter of Coles, 2016. *Operational productivity and performance in English NHS acute hospitals:Unwarranted variations.* [Online]
Available at:
https://www.gov.uk/government/uploads/system/uploads/attachment_data/file/499229/Operational_productivity_A.pdf
[Accessed 18 November 2017].

Lütjering, G. & Williams, J. C., 2007. *Titanium*. 2nd ed. Berlin, Germany: Springer.

Macheras, G. A., Koutsostathis, S. D. & Galanakos, S. P., 2014. Cementless Fully Porous-Coated Implant-Bone Interface in Revision Total Hip Arthroplasty. In: T. Karachalios, ed. *Bone-Implant Interface in Orthopedic Surgery: Basic Science to Clinical Applications.* London: Springer-Verlag, pp. 169-182.

Man, H. C.; Zhao, N. Q. & Cui, Z. D., 2003. Surface and adhesion characteristics of laser surface textured Ti-6Al-4V. *In: Applications of Lasers and Electro-Optics. Proceedings, 22nd International Congress, ICALEO 2003,* Jacksonville, FL, 13-16 Oct.2003. Vol.95. Laser Materials Processing Conference, Section E - Forming, Cutting, Drilling and Other Applications. Paper no.508. pp. 255-264.

Markel, D. C., Hora, N. & Grimm, M., 2002. Press-fit stability of uncemented hemispheric acetabular components: a comparison of three porous coating systems. *International Orthopaedics (SICOT),* Volume 26, pp. 72–75.

Matsushita, T., 2010. Orthopaedic applications of metallic biomaterials. In: M. Niinomi, ed. *Metals for biomedical devices.* Cambridge, UK: Woodhead Publishing Ltd, pp. 329-354.

Matthyssens, P. & Vandenbempt, K., 2008. Moving from basic offerings to value-added solutions: Strategies, barriers and alignment. *Industrial Marketing Management,* 37(3), pp. 316-328.

Meleka, A. H., 1971. *Electron-beam Welding: Principles and Practice.* London: The Welding Institute by McGRAW-HILL.

Meyer, W. E., Scheffels, W. & Steigerwald, K. H., 1965. *A study of the formation and the energy balance of the capillary in electron beam deep penetration welding.* Pennsylvania State University, Proceedings of the Electron and Laser Beam Symposium, pp. 531-540.

Mills, K. C., 2002. Recommended Values of Thermophysical Properties for selected Commercial Alloys. Cambridge: Woodhead Publishing.

Mills, K. C., Keene, B. J., Brooks, R. F. & Shirali, A., 1998. Marangoni effects in welding. *Phil. Trans. R. Soc. Lond. A.,* Volume 356, pp. 911-925.

Moore, P. & Booth, G., 2015. Welding problems and defects. In: *The Welding Engineer's Guide to Fracture and Fatigue.* Cambridge: Woodhead Publishing, pp. 23-36.

Morshed, S., Bozic, K. J., Ries, M. D., Malchau, H. & Colford Jr., J. M., 2007. Comparison of cemented and uncemented fixation in total hip replacement. *Acta Orthopaedica,* 78(3), pp. 315-326.

Norwegian Arthroplasty Register, 2016. *Norwegian National Advisory Unit on Arthoplasty and Hip Fractures: Annual Report 2016,* Haukeland, Bergen, Hordaland, Norway: Helse Bergen HF, Department of Orthopaedic Surgery, Haukeland University Hospital.

Ohmura, E., Murayama, R. & Miyamoto, I., 2000. Thermohydrodynamics analysis on the mechanism of bump formation in laser texturing. *Proceedings of SPIE,* n. 1, pp. 244-247.

Oluleke, R., 2014. PhD Thesis: Metallurgical performance of hyper-joints in composite to metal joining, Manchester, UK: University of Manchester.

OSD Manufacturing Technology Program in collaboration with The Joint Service/Industry MRL Working Group, 2017. *Manufacturing Readiness Level (MRL) Deskbook Version 2017.* [Online]
Available at: http://www.dodmrl.com/MRL_Deskbook_2017.pdf
[Accessed 5 May 2018].

Otten, C., Reisgen, U., Olschok, S., Fischer, H. & Panfil, C., 2012. *Electron beam structurisation of titanium materials for medical applications: potential for improved bone ingrowth behaviour.* In: 2nd International Electron Beam Welding Conference (IEBW2012) Aachen, Germany, 26-30 March 2012. Miami, FL, USA:
American Welding Society.

Painter, J. D., Fitzmaurice, B. C., Goff, M., Appleby-Thomas, G. J., Wood, D. C. & Pinto, T., 2017. *On a novel graded areal density solution to facilitate ramp wave generation in plate impact studies*. AIP Conference Proceedings, Volume 1793,
pp. 060017-1 - 060017-5.

Pakos, E. E. & Xenakis, T., 2014. Titanium Porous-Coated Implant-Bone Interface in Total Joint Arthroplasty. In: T. Karachalios, ed. *Bone-Implant Interface in Orthopedic Surgery.* London: Springer-Verlag, pp. 67-82.

Pang, S. Y., Chen, L. L., Yin, Y. J., Zhou, J. X., Hu, L. J. & Liu, J. H., 2009. Three dimensional simulation of the transient process of fibre laser keyhole welding of aluminium alloys. *Proc. SPIE 7515, Photonics and Optoelectronics Meetings (POEM) 2009: Industry Lasers and Applications, 75150T* (21 October 2009).

Panin, A., Kazachenok, M., Martynov, S. & Builuk, A., 2018. *Surface modification of 3D-printed Ti-6Al-4V parts by continuous electron beam*. AIP Conference Proceedings, 2051, art. no. 020225.

Park, H. S., Llinas, A., Goel, K. V. & Keller, J. C., 2000. Hard Tissue Replacements. In: J. D. Bronzino, ed. *The Biomedical Engineering Handbook Second Edition Volume 1.* CRC Press LLC, pp. 44-1 - 44-21.

Pegg, E. C., Mellon, S. J. & Gill, H. S., 2014. Early and Late Mechanical Stability of the Cementless Bone-Implant Interface in Total Joint Arthroplasty. In: T. Karachalios, ed. *Bone-Implant Interface in Orthopedic Surgery: Basic Science to Clinical Applications.* London: Springer, pp. 13-26.

Pinto, T. M., 2013. *Applied Statistical Methods Post Module Assignment (PMA) Questions 1, 3 and 5. ASM, ES949-10 02MC 12/13 Reference EngD/3/2013.*

Pinto, T. M., Buxton, A. L., Neailey, K. & Barnes, S., 2014. Surface Engineering Improvements and Opportunities with Electron Beams. *Elektrotechnica & Elektronica*, 49(5-6), pp. 221-225.

Pinto, T. M., 2017. *Doctor of Engineering Submission 4: Improved knowledge management of the electron beam texturing and Surfi-Sculpt processes Reference EngD/4/2017.,* Great Abington: TWI Ltd.

Popiolkowski, A. R., Hart, S. M., Schweitzer, M. O., Liu, A. B., Watia, J. L., West, B. & Menzie, M., 2003. *Method of surface texturizing.* US, Patent No. US6812471B2.

Posew, K., Laohalertdecha, S. & Wongwises, S., 2009. Evaporation heat transfer enhancement of R-134a flowing inside smooth and micro-fin tubes using the electrohydrodynamic. *Energy Conversion and Management, ,* 50(7), pp. 1851-1861.

Prakash, S. & Kumar, S., 2014. Fabrication of microchannels: A review. *Proc IMechE Part B: J Engineering Manufacture,* 229(8), pp. 1273-1288.

Prüss, J., Shimizu, S., Simonett, G. & Wilke, M., 2016. On incompressible two-phase flows with phase transitions and variable surface tension. *Advances in Mathematical Fluid Mechanics*, pp. 411-442.

Rabetino, R., Kohtamäki, M. & Gebauer, H., 2017. Strategy map of servitization. *International Journal of Production Economics,* Volume 192, pp. 144-156.

Rai, R., Burgardt, P., Milewski, J. O., Lienert, T. J. & DebRo, T., 2009. Heat transfer and fluid flow during electron beam welding of 21Cr–6Ni–9Mn steel and Ti–6Al–4V alloy. *Journal of Physics D: Applied Physics,* 42(2).

Ramskogler, C., Warchomicka, F., Mostofi, S., Weinberg, A. & Sommitsch, C., 2017. Innovative surface modification of Ti6Al4V alloy by electron beam techni que for biomedical application. *Materials Science and Engineering C,* Volume 78, pp. 105-113.

Reay, D. A., 1991. Heat Transfer Enhancement - a Review of Technoiques and thier Possible Impact on Energy Efficiency in the UK. *Heat Recovery Systems and CHP,* 11(1), pp. 1-40.

Reay, D., Ramshaw, C. & Harvey, A., 2013. Chapter 3 - The Mechanisms Involved in Process Intensification. In: D. Reay, C. Ramshaw & A. Harvey, eds. *Isotopes in Organic Chemistry.* Oxford: Butterworth-Heinemann, pp. 57-90.

Revell, P. A., 2008. The healing response to implants used in joint replacement. In: P. A. Revell, ed. *Joint replacement technology.* Cambridge, UK: Woodhead Publishing Ltd, pp. 315-348.

Ribton, C. N. & Atkinson, T., 2007. *High-Brightness Electron Beams For Micro Processing [15057.02/2006/1266.3],* Great Abington, Cambridge: TWI Ltd.

Rogers, G., Walsh, D. & Lo, G., 1993. Minor effects on superalloy weld pools. *Proc. Conf. '3rd International Conference on Trends in Welding Research',* pp. 709-712.

Rotshtein, V. P. & Shulov, V. A., 2011. Surface modification and alloying of aluminium and titanium alloys with low-energy, high-current electron beams. *Journal of Metallurgy*, Vol. 2011. pp. 1-15.

Sawhney, R., 2006. Interplay between uncertainty and flexibility across the value-chain: Towards a transformation model of manufacturing flexibility. *Journal of Operations Management,* 24(5), pp. 476-493.

Saxberg, B. O., 2005. Taking Technical Risks: How Innovators, Executives, and Investors Manage High-Tech Risk. *Personnel Psychology,* 58(1), pp. 242-244.

Schiller, S., Heisig, U. & Panzer, S., 1982. *Electron Beam Technology.* New York: John Wiley and Sons.

Schultz, H., 1993. *Electron Beam Welding.* Great Abington, Cambridge: Woodhead Publishing.

Short , A. B., 2009. Literature Review Gas tungsten arc welding of α + β titanium alloys: a review. *Materials Science and Technology*, 25(3), pp. 309-324.

Smith, F., 2004. *COMELD - An innovation in composite to metal joining.* Bromsgrove, UK, Composites Processing 2004, CPA.

Steigerwald Strahltechnik GmbH, 2013. *Description of SST-sub-routines for programming: SIEMENS 840D machine control,* Maisach, Germany: Steigerwald Strahltechnik GmbH.

Swift, K. G. & Booker, J. D., 2003. *Process selection: from design to manufacture.* 2nd ed. Oxford: Boston: Butterworth-Heinemann.

Taendl, J. & Enzinger, N., 2014. Electron beam surface structuring of AA6016 aluminum alloy. *Welding in the World,* 58(6), pp. 795-803.

Temmler, A., Küpper, M., Walochnik, M. A., Lanfermann, A., Schmickler, T., Bach, A., Greifenberg, T., Oreshkin, O., Willenborg, E., Wissenbach, K. & Poprawe, R., 2017. Surface Structuring by Laser Remelting of Metals. *Journal of Laser Applications,* 29(1), pp. 012015.

Temmler, A., Walochnik, M. A., Willenborg, E. & Wissenbach, K., 2015. Surface Structuring by Remelting of Titanium Alloy Ti6Al4V. *Journal of Laser Applications,* 27(S2), pp. S29103:1-8.

Terentyev Y. V., Dragunov V. K., Silva, A. P. & Scherbakov, A. V., 2015. Effect of welding speed on weld formation in electron beam welding with continuous penetration. *Welding International*, Vol.29, no.2. pp. 150-154.

Tseng, C.-C. & Li, C.-J., 2019. Numerical investigation of interfacial dynamics for the melt pool of Ti-6Al-4V powders under a selective laser. *International Journal of Heat and Mass Transfer*, pp. 906-919.

TWI Ltd, 2019. *TWI pairs with Daicel Polymer Ltd. for DLAMP project.* [Online] Available at: https://www.twi-global.com/media-and-events/press-releases/2019/twi-pairs-with-daicel-polymer-ltd-for-dlamp-project
[Accessed 7 December 2019].

Uno, T., Itakura, M., Okuyana, N. & Kutsuna, M., 2018. *Laser Surface Pre-treatment of Metal for Joints of Metal and Dissimilar Materials.* Bali, Indonesia, International Institute of Welding.

Vaittinen, E., Martinsuo, M. & Ortt, R., 2018. Business customers' readiness to adopt manufacturer's new services. *Journal of Service Theory and Practice,* 28(1), pp. 52-78.

Vandermerwe, S. & Rada, J., 1988. Servitization of business: Adding value by adding services. *European Management Journal,* 6(4), pp. 314-324.

Vogel, H., 1979. A better way to construct the sunflower head. *Mathematical Biosciences,* 44(3), pp. 179-189.

Wakefield-Vette Inc, 2017. *Liquid Cold Plates.* [Online]
Available at: http://www.wakefield-vette.com/products/liquid-cooling/liquid-cold-plates.aspx
[Accessed 13 March 2018].

Wang, Q., Chen, Q., Wang, L., Zeng, M., Huang, Y. & Xiao, Z., 2007. Experimental study of heat transfer enhancement in narrow rectangular channel with longitudinal vortex generators. *Nuclear Engineering and Design,* 237(7), pp. 686-693.

Wang, X., Ahn, J., Bai, Q., Lu, W. & Lin, J., 2015. Effect of forming parameters on electron beam Surfi-Sculpt protrusion. *Materials and Design,* Volume 76, pp. 202-206.

Webb, R. L. & Kim, N. H., 2005. *Principles of enhanced heat transfer.* 2nd ed. New York, USA: Taylor and Francis.

Weglowski, M. S., Błacha, S. & Phillips, A., 2016. Electron beam welding – Techniques and trends – Review. *Vacuum,* 130, pp. 72-92.

West, B. T., Boyd Jr, W. & Tan, S., 2009. *Lavacoat pre-clean and pre-heat.* US, Patent No. US 2010/0108641 A1.

Wong, M., Owen, I., Sutcliffe, C. J. & Puri, A., 2009. Convective heat transfer and pressure losses across novel heat sinks fabricated by Laser Selective Melting. *International Journal of Heat and Mass Transfer,* 52(1), pp. 281-288.

Yang, Y., Oh, N., Liu, Y., Chen, W., Oh, S., Appleford, M., Kim, S., Kim, K., Park, S., Bumgardner, J., Haggard, W. & Ong, J., 2006. Enhancing osseointegration using surface-modified titanium implants. *JOM*, 58(7), pp. 71-76.

Zeren, Z., Hillewaert, K., Pinto, T., Ferhati, A., Serri, M. & Malagutti, M., 2017. Optimization of electron beam generated inclined conical pin fins for efficient heat sinks. *International Journal of Computational Methods and Experimental Measurements,* 5(1), pp. 66-75.

Zou, X., Grosdidier, T., Zhang, M., Dong, C. & Weber, S., 2008. Mechanism of surface modifications on a NiTi alloy treated with low energy high current pulsed electron beam. *EPJ Applied Physics*, 43 (3), pp. 327-331.

Appendix A

List of Published Papers

The following is a list of papers that have been published to date by the author related to either the EBT or Surfi-Sculpt processes:

Painter, J. D., Fitzmaurice, B. C., Goff, M., Appleby-Thomas, G. J., Wood, D. C. & Pinto, T., 2017. *On a novel graded areal density solution to facilitate ramp wave generation in plate impact studies*. AIP Conference Proceedings, Volume 1793, pp. 060017-1 - 060017-5.

Pinto, T. M., Buxton, A. L., Neailey, K. & Barnes, S., 2014. Surface Engineering Improvements and Opportunities with Electron Beams *Elektrotechnica & Elektronica*, 49(5-6), pp. 221-225.

Pinto, T, M., Buxton, A. L., Nunn, M. E., Neailey, K. & Barnes, S., 2016. *Novel Surface Modification Improvements and Opportunities Utilising Electron Beams.* XXXI International Conference on Surface Modification Technologies (SMT31) July 5-7, 2016, Mons, Belgium.

Zeren, Z., Hillewaert, K., Pinto, T., Dallari, D. & Serri, M., 2015. *Numerical analysis of the heat transfer performance of two novel types of pin-fin and plate-fin heat sinks*. Napoli, Italy, ASME-ATI-UIT 2015 Conference on Thermal Energy Systems: Production, Storage, Utilization and the Environment.

Zeren, Z., Hillewaert, K., Pinto, T., Ferhati, A., Serri, M. & Malagutti, M., 2017. Optimization of electron beam generated inclined conical pin fins for efficient heat sinks. *International Journal of Computational Methods and Experimental Measurements*, 5(1), pp. 66-75.

Appendix B

Calibration Sheet for Mitutoyo Shadowgraph

CERTIFICATE OF CALIBRATION

Issued By: Mitutoyo (UK) Ltd Calibration Laboratory

Date of Issue: 26-JUN-2013 Certificate No.: 251522

UKAS CALIBRATION
0332

Mitutoyo

Calibration Laboratory:
Mitutoyo (UK) Ltd
6 Banner Park, Wickmans Drive
Coventry, West Midlands
CV4 9XA, United Kingdom
T +44 (0)2476 426300
F +44 (0)2476 426339
calibration@mitutoyo.co.uk

Head Office:
Mitutoyo (UK) Ltd
West Point Business Park, Joule Road
Andover, Hampshire
SP10 3UX, United Kingdom
T +44 (0)1264 353123
F +44 (0)1264 354883
enquiries@mitutoyo.co.uk

Approved Signatories:
> G. P. WYKES
D. GREER
A. T. BROWN

CUSTOMER	TWI Ltd Catcliffe - Rotherham
MANUFACTURER	Mitutoyo
DESCRIPTION	PJ300 Projector
IDENTIFICATION	N/A SERIAL No. 395
CALIBRATION CONDITIONS	Temperature Range during calibration 24.2 - 24.5 deg C.
BASIS OF CALIBRATION	To calibrate using traceable media to the accuracy requirements of the Manufacturers Specification to procedure CP 064: issue 8 2008 agreed with UKAS.
DATE OF CALIBRATION	17-JUN-2013

The Projector was calibrated in comparison with Glass Scales on site at the customers premises and checked for the following characteristics.

Magnification in X & Y Axis, Requirement :+/- 0.1%
Displacement in X & Y Axis, Requirement :+/- 0.003mm
Angular Scale, Requirement :+/- 6'

Lens used during calibration: 10x Magnification Serial number 111222

NOTE: Items identified thus * exceed the requirements.

The errors found are recorded on pages 2 and 3.

Certified By

CERTIFICATE OF CALIBRATION

Mitutoyo

UKAS Accredited Calibration Laboratory No. 0332
Mitutoyo (UK) Ltd, 6 Banner Park, Wickmans Drive
Coventry, West Midlands CV4 9XA, United Kingdom

Certificate No.: 251522

MAGNIFICATION

The accuracy of magnification of this machine was checked and found to be within the Manufacturers Specification.

Magnification 10x standard lens
measured points circumference
and 2/3 screen radius from centre
of plane and all values recorded conform

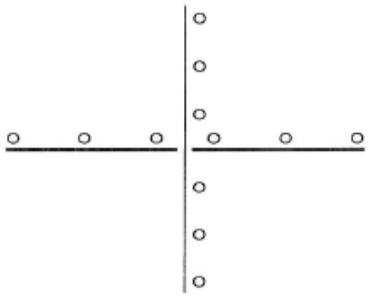

MEASURING STAGE

The accuracy of the micrometer heads of this machine have been checked and found to be within Manufacturers Specification as stated below except where identified thus *.

Axis	Model Number	Serial Number	Accuracy
X	350-351	55032576	+/-0.003mm
Y	350-351	75033808	+/-0.003mm

CERTIFICATE OF CALIBRATION

Mitutoyo

UKAS Accredited Calibration Laboratory No. 0332
Mitutoyo (UK) Ltd, 6 Banner Park, Wickmans Drive
Coventry, West Midlands CV4 9XA, United Kingdom

Certificate No.: 251522

X AXIS NOMINAL (mm)	X AXIS ACTUAL (mm)
0	0
4.2	4.200
8.4	8.400
12.6	12.601
16.8	16.804*
21.0	21.004*
25.2	25.204*

Y AXIS NOMINAL (mm)	Y AXIS ACTUAL (mm)
0	0
4.2	4.201
8.4	8.400
12.6	12.600
16.8	16.799
21.0	21.000
25.2	25.201

ANGULAR SCALE NOMINAL (Degrees & Minutes)	ANGULAR SCALE ACTUAL (Degrees & Minutes)
0	0
26°34'	26°30'
45°00'	44°55'
63°26'	63°30'
90°00'	90°00'
120°58'	121°00'
135°00'	135°00'
180°00'	180°00'
225°00'	225°00'
270°00'	270°05'
329°02'	329°05'
360°00'	360°00'

Estimated uncertainty of measurement:

Magnification	+/- 0.012mm
Linear Measurement	+/- 1.8 + (10 x length in metres)um
Angle measurement	+/- 2.1'

The reported expanded uncertainty is based on a standard uncertainty multiplied by a coverage factor k=2, providing a level of confidence of approximately 95%. The uncertainty evaluation has been carried out in accordance with UKAS requirements.

Appendix C

Data from Deflection Offset Study

Table C1 Summary of data collected from beam offset study conducted in Section 2.3.8.

Sample	Column	Mean feature height (mm)	Variance (mm)	Mean feature height (mm)	Variance (mm)
0	a	0.528	0.005	0.810	0.057
	b	0.613	0.009		
	d	0.810	0.026		
	e	0.730	0.015		
	g	0.910	0.067		
	h	0.931	0.049		
	j	0.960	0.048		
	k	0.999	0.057		
1	a	0.550	0.006	0.618	0.023
	b	0.557	0.008		
	d	0.486	0.019		
	e	0.641	0.037		
	g	0.575	0.010		
	h	0.570	0.006		
	j	0.772	0.016		
	k	0.795	0.003		
2	a	0.454	0.002	0.524	0.010
	b	0.541	0.010		
	d	0.426	0.001		
	e	0.505	0.006		
	g	0.578	0.016		
	h	0.509	0.009		
	j	0.593	0.013		
	k	0.589	0.005		
3	a	0.743	0.010	0.645	0.009
	b	0.660	0.019		
	d	0.654	0.010		
	e	0.658	0.003		
	g	0.592	0.006		
	h	0.611	0.006		
	j	0.622	0.008		
	k	0.616	0.002		
4	a	0.625	0.003	0.545	0.007
	b	0.664	0.010		
	d	0.561	0.005		
	e	0.514	0.003		
	g	0.491	0.003		
	h	0.511	0.002		
	j	0.487	0.002		
	k	0.510	0.001		
5	a	0.599	0.002	0.651	0.008
	b	0.689	0.010		
	d	0.633	0.012		
	e	0.628	0.007		
	g	0.695	0.006		
	h	0.669	0.020		
	j	0.629	0.002		
	k	0.665	0.002		
6	a	0.579	0.014	0.540	0.009
	b	0.622	0.013		
	d	0.552	0.006		
	e	0.580	0.003		
	g	0.509	0.006		
	h	0.518	0.006		
	j	0.477	0.007		
	k	0.486	0.003		

Appendix D

Normalised S-SPS Record Data from EngD

Table D1 Normalised S-SPS record data from EngD.

Specimen Name	Voltage (kV)	Current (mA)	Power (W)	Processing Time (s) [W = Wait 60s, beam off]	Gun Type	Machine	Focus (mA)	Working Distance (mm)	X / U		Y / V		EB Deflection (Surfi-Sculpt®) Pattern File Name	Thickness (mm)	Approximate Surfi-Sculpt area (mm)	Resultant Surfi-Sculpt feature height (mm)	Number of swipes in the motif	Swipe length (mm)	Beam swipe speed in the motif (m/s)	Processing Time (s)	Beam on Time (s)	Heat Input (W)	Beam energy input (J/m)	Beam energy input per mm feature height (J/m/mm)	Material
									Amplitude (mA)	Freq. (Hz)	Amplitude (mA)	Freq. (Hz)													
HeatSculptor Design 1 - Pin-like features	130	6.8	884	20	R43	3EB	2.48	220	1.3 (X) 0.8 (U)	1.2 10.55	1.3 (Y) 0.8 (V)	1.2 10.55	Pin/fin motif Pin like motif	6	41mm x 56mm	3.00	70	3.03	67.0	20	20	170	13.2	4.4	Al6082
HeatSculptor Design 2 - Staggered ridge features	130	11.0	1430	20	R43	3EB	2.50	220	1.0 (X) 0.7 (U)	24 12.25	1.0 (Y) 0.7 (V)	24 12.25	Staggered ridge array Ridge motif	6	30mm x 40mm	2.46	96	3.03	177.9	20	20	275	8.0	3.3	Al6082
HeatSculptor Design 3 - Long ridge features	130	11.0	1430	25	R43	3EB	2.49	220	1.035 (X) 1.0 (U)	24 12.5	1.035 (Y) 1.0 (V)	24 12.5	Long ridge array Long ridge motif	6	33mm x 33mm	3.00	96	3.03	181.5	25	25	275	7.9	2.6	Al6082
HeatSculptor Design 4 - Fin-like features	130	6.0	780	20	R43	3EB	2.51	220	0.8 (X) 0.75 (U)	2.4 63.3	0.8 (Y) 0.75 (V)	2.4 63.3	Pin/fin motif Fin motif	6	25mm x 35mm	2.69	24	3.03	137.9	20	20	150	5.7	2.1	Al6082
HeatSculptor Design 5 - Inclined cones	130	8.5	1105	20	R43	3EB	2.50	215	1.04 (X) 0.8 (U)	6.4 10.55	1.0 (Y) 0.8 (V)	6.4 10.55	Cone array Cone motif	6	33mm x 33mm	3.10	70	2.96	65.5	20	20	212	16.9	5.4	Al6082
HeatSculptor Design 6 - Curved Ridges	130	7.5	975	20	R43	3EB	2.47	210	0.9 (X) 2.4 (U)	3.6 16.2	0.9 (Y) 2.4 (V)	3.6 16.2	Curved ridge array Curved ridge motif	6	40mm x 40mm	2.26	70	2.89	98.2	20	20	187	9.9	4.4	Al6082
HeatSculptor Design 7 - Pins in a curved array	130	7.0	910	20	R43	3EB	2.48	220	0.8 (X) 1.1 (U)	19.2 8	0.8 (Y) 1.1 (V)	19.2 8	Curved pin array Curved pin motif	6	27mm x 36mm	2.78	96	1.67	64.3	20	20	175	14.2	5.1	Al6082
HeatSculptor Design 8 - Square based pin features	130	5.0	650	30	R43	3EB	2.46	220	0.7 (X) 0.8 (U)	13.2 27	0.7 (Y) 0.8 (V)	13.2 27	Squared based array Square based pin motif	6	25mm x 25mm	3.34	22	2.25	40.1	30	30	125	16.2	4.9	Al6082
HeatSculptor Design 5 - Inclined cones	130	7.5	975	60s 100% UV ampl., W, 15s 75%, 15s 65%, W, 15s 55%, 15s 45%	R43	3EB	(2.525 ± 0.025)*	225	1.05 (X) 1.1 (U)	4.8 10.55	1.0 (Y) 1.1 (V)	4.8 10.55	Cone array Cone motif	20	35mm x 35mm	6.10	70	3.09	68.5	225	105	187	14.2	2.3	Al6xxx**
HeatSculptor Design 6 - Curved Ridges	130	8.5	1105	60s, W, 60s	R43	3EB	1st 60s: 2.45; 2nd 60s: 2.44	245	1.0 (X) 2.4 (U)	4.8 16.2	0.9 (Y) 2.4 (V)	4.8 16.2	Curved ridge array Curved ridge motif	20	35mm x 35mm	2.50	160	1.86	241.6	180	120	212	4.6	1.8	Al6xxx**
HeatSculptor Design 6 - Curved Ridges Prototype	130	8.5	1105	60s, W, W, 60s	R43	3EB	2.51	230	1.0 (X) 2.4 (U)	4.8 16.2	0.88 (Y) 2.4 (V)	4.8 16.2	Curved ridge array Curved ridge motif	20	31mm x 32mm	3.50	160	1.75	226.8	240	120	212	4.9	1.4	Al6xxx**
HeatSculptor Design 5 - Inclined cones Prototype	130	8.5	1105	40	R43	3EB	2.50 ± 0.1	240	0.77 (X) 0.88 (U)	4.8 10.55	0.77 (Y) 0.88 (V)	4.8 10.55	Cone array Cone motif	6	31mm x 32mm	2.60	70	3.30	73.1	40	40	212	15.1	5.8	Al6xxx**
HeatSculptor Design 5 - Inclined cones Prototype - final version	130	7.5	975	40	R43	3EB	2.50 ± 0.1	240	0.77 (X) 0.88 (U)	4.8 10.55	0.77 (Y) 0.88 (V)	4.8 10.55	Cone array Cone motif	16	31mm x 32mm	2.60	70	3.30	73.1	40	40	187	13.3	5.1	Al6xxx**
EngD Al6xxx** Dataset 1	60	8.0	480	5 W/6 10	Surfi-Sculpt gun	2EB	335.0	261	0.3 (X) 0.3 (U)	4.8 10.55	0.3 (Y) 0.3 (V)	4.8 10.55	Cone array Cone motif	20	23mm x 23mm	1.11	70	1.97	19.8	25	15	92	24.2	21.8	Al6xxx**
EngD Al6xxx** Dataset 2	60	8.0	480	10 W/6 10	Surfi-Sculpt gun	2EB	333.5	261	0.3 (X) 0.3 (U)	4.8 10.55	0.3 (Y) 0.3 (V)	4.8 10.55	Cone array Cone motif	20	23mm x 23mm	0.60	70	1.97	19.8	30	20	92	24.2	40.2	Al6xxx**
EngD Al6xxx** Dataset 3	60	10.0	600	10	Surfi-Sculpt gun	2EB	332.0	261	0.3 (X) 0.3 (U)	4.8 10.55	0.3 (Y) 0.3 (V)	4.8 10.55	Cone array Cone motif	20	23mm x 23mm	0.36	70	1.97	19.8	10	10	115	30.3	84.1	Al6xxx**
EngD Al6xxx** Dataset 4	60	10.0	600	10 W/6 10	Surfi-Sculpt gun	2EB	335.0	261	0.3 (X) 0.3 (U)	4.8 10.55	0.3 (Y) 0.3 (V)	4.8 10.55	Cone array Cone motif	20	23mm x 23mm	1.87	70	1.97	19.8	30	20	115	30.3	16.2	Al6xxx**
EngD Al6xxx** Dataset 5	60	12.0	720	10 W/6 10	Surfi-Sculpt gun	2EB	335.0	261	0.3 (X) 0.3 (U)	4.8 10.55	0.3 (Y) 0.3 (V)	4.8 10.55	Cone array Cone motif	20	23mm x 23mm	2.34	70	1.97	19.8	30	20	138	36.4	15.5	Al6xxx**
EngD Al6xxx** Dataset 6	60	18.0	1080	10 W/6 10	Surfi-Sculpt gun	2EB	335.0	261	0.3 (X) 0.3 (U)	4.8 10.55	0.3 (Y) 0.3 (V)	4.8 10.55	Cone array Cone motif	20	23mm x 23mm	2.11	70	1.97	19.8	30	20	207	54.5	25.9	Al6xxx**
EngD Al6xxx** Dataset 7	60	18.0	1080	20	Surfi-Sculpt gun	2EB	337.5	261	0.3 (X) 0.3 (U)	4.8 10.55	0.3 (Y) 0.3 (V)	4.8 10.55	Cone array Cone motif	20	23mm x 23mm	2.48	70	1.97	19.8	20	20	207	54.5	22.0	Al6xxx**
EngD Al6xxx** Dataset 8	60	18.0	1080	20 W/6 20	Surfi-Sculpt gun	2EB	337.5	261	0.3 (X) 0.3 (U)	4.8 10.55	0.3 (Y) 0.3 (V)	4.8 10.55	Cone array Cone motif	20	23mm x 23mm	2.41	70	1.97	19.8	50	40	207	54.5	22.6	Al6xxx**
EngD Al6xxx** Dataset 9	60	25.0	1500	15	Surfi-Sculpt gun	2EB	337.5	261	0.3 (X) 0.3 (U)	4.8 10.55	0.3 (Y) 0.3 (V)	4.8 10.55	Cone array Cone motif	20	23mm x 23mm	1.48	70	1.97	19.8	15	15	288	75.7	51.2	Al6xxx**
Beam Deflection Offset Study	100	14.0	1400	4	R43	3EB	3.00	405	15 (X)	7	3.5(Y)	7	Beam Deflection Offset Study	15	40mm x 40mm	0.78	60	1.28	80.6	4	4	269	17.4	22.3	Ti-6Al-4V
High-speed video	130	2.9	377	5	R40	3EB	3.46	245	0.7 (X)	10	0.7 (Y)	10	High speed video	15	18mm x 18mm	2.30	22	4.44	29.3	5	5	72	12.9	5.6	Ti-6Al-4V
Orthopaedic implant Case Study Design 2	60	4.5	270	C.S.***	Surfi-Sculpt gun	2EB	363.5	128	C.S.*** C.S.***	C.S.*** 10.55	C.S.*** C.S.***	C.S.*** 10.55	OrthoSculpt Design 2 array OrthoSculpt Design 2 motif	7	Hemisphere	0.50	50	2.33	1.2	C.S.***	C.S.***	52	219.7	439.4	Ti-6Al-4V
Orthopaedic implant Case Study Design 4	60	20.0	1200	18.2	Surfi-Sculpt gun	2EB	363.5	128	1.4 (X) 0.05 (U)	7.8 3,000	0.7 (Y) 0.05 (V)	7.8 3,000	OrthoSculpt Design 4 array OrthoSculpt Design 4 motif	7	Hemisphere	0.30	1	1.26	378.0	18	18	230	3.2	10.6	Ti-6Al-4V
Orthopaedic implant Case Study friction test Samples	60	4.5	270	4.35 W/15 4.35 W/15 4.35 W/15 4.35 W/15 4.35	Surfi-Sculpt gun	2EB	351.0	183	0.94	1.45	0.94	1.45	Friction case study	5	20mm x 20mm	0.70	504	1.65	1.2	38	22	52	223.9	319.9	Ti-6Al-4V
Ramskogler et al. (2017) Dataset 1	150	0.8	120	0.047	Unknown	Pro-beam EBG 45-150 K14	-	-	Unknown	3.54	Unknown	3.54	hexagon - 96 arms (swipes)	2	8mm x 6mm	0.09	96	1.00	0.34	0.047	0.047	23	355.0	3817.2	Ti-6Al-4V
Ramskogler et al. (2017) Dataset 2	150	2.5	375	0.023	Unknown	Pro-beam EBG 45-150 K14	-	-	Unknown	7.08	Unknown	7.08	hexagon - 96 arms (swipes)	2	8mm x 6mm	0.45	96	1.00	0.68	0.023	0.023	72	555.0	1227.9	Ti-6Al-4V
Ramskogler et al. (2017) Dataset 3	150	2.5	375	0.023	Unknown	Pro-beam EBG 45-150 K14	-	-	Unknown	7.08	Unknown	7.08	hexagon - 96 arms (swipes)	2	8mm x 6mm	0.31	96	1.00	0.68	0.023	0.023	72	555.0	1819.7	Ti-6Al-4V
EngD Ti-6Al-4V Dataset 1	60	9.0	540	10	Surfi-Sculpt gun	2EB	334.0	276	0.3 (X) 0.3 (U)	4.8 10.55	0.3 (Y) 0.3 (V)	4.8 10.55	Cone array Cone motif	5	24mm x 24mm	1.74	70	1.92	19.3	10	10	104	28.0	16.0	Ti-6Al-4V
EngD Ti-6Al-4V Dataset 2	60	12.0	720	10	Surfi-Sculpt gun	2EB	334.0	276	0.3 (X) 0.3 (U)	4.8 10.55	0.3 (Y) 0.3 (V)	4.8 10.55	Cone array Cone motif	5	24mm x 24mm	1.98	70	1.92	19.3	10	10	138	37.3	18.8	Ti-6Al-4V
EngD Ti-6Al-4V Dataset 3	60	7.0	420	10	Surfi-Sculpt gun	2EB	334.0	276	0.3 (X) 0.3 (U)	4.8 10.55	0.3 (Y) 0.3 (V)	4.8 10.55	Cone array Cone motif	5	24mm x 24mm	1.28	70	1.92	19.3	10	10	81	21.8	17.0	Ti-6Al-4V
EngD Ti-6Al-4V Dataset 4	60	7.0	420	10 W/6 10	Surfi-Sculpt gun	2EB	334.0	276	0.3 (X) 0.3 (U)	4.8 10.55	0.3 (Y) 0.3 (V)	4.8 10.55	Cone array Cone motif	5	24mm x 24mm	1.62	70	1.92	19.3	30	20	81	21.8	13.4	Ti-6Al-4V
EngD Ti-6Al-4V Dataset 5	60	12.0	720	10	Surfi-Sculpt gun	2EB	336.0	276	0.3 (X) 0.3 (U)	4.8 10.55	0.3 (Y) 0.3 (V)	4.8 10.55	Cone array Cone motif	5	24mm x 24mm	1.86	70	1.92	19.3	10	10	138	37.3	20.0	Ti-6Al-4V
EngD Ti-6Al-4V Dataset 6	60	12.0	720	10 W/6 10	Surfi-Sculpt gun	2EB	336.0	276	0.3 (X) 0.3 (U)	4.8 10.55	0.3 (Y) 0.3 (V)	4.8 10.55	Cone array Cone motif	5	24mm x 24mm	1.93	70	1.92	19.3	30	20	138	37.3	19.3	Ti-6Al-4V
EngD Ti-6Al-4V Dataset 7	60	12.0	720	10	Surfi-Sculpt gun	2EB	332.0	276	0.3 (X) 0.3 (U)	4.8 10.55	0.3 (Y) 0.3 (V)	4.8 10.55	Cone array Cone motif	5	24mm x 24mm	1.68	70	1.92	19.3	10	10	138	37.3	22.2	Ti-6Al-4V
EngD Ti-6Al-4V Dataset 8	60	12.0	720	5 W/6 5	Surfi-Sculpt gun	2EB	332.0	276	0.3 (X) 0.3 (U)	4.8 10.55	0.3 (Y) 0.3 (V)	4.8 10.55	Cone array Cone motif	5	24mm x 24mm	1.77	70	1.92	19.3	20	10	138	37.3	21.1	Ti-6Al-4V

Working distance measured from bottom of coils to work piece on TWI's EB machine with TWI deflection coils
Different machines and EB gun create different beams with varying properties
The normalised values in the above table will not be directly representatitve of values for other EB machines
* Due to the varying working distance of the part, the focus was varied. The specific details of which are commercially sensitive and are in Submission 3 only
** Due to commercial confidentiality, the specific grade of material is detailed in Submission 3 only
*** C.S. - Commercially sensitive and therefore not reported

Table D2 Regression analysis of normalised S-SPS record data from EngD.

SUMMARY	Al6082
Regression Statistics	
Multiple R	0.963
R Square	0.928
Adjusted R Square	0.494
Standard Error	0.251
Observations	8

ANOVA	Al6082				
	df	*SS*	*MS*	*F*	*Significance F*
Regression	6	0.81149842	0.1352497	2.1403972	0.480214423
Residual	1	0.06318908	0.0631891		
Total	7	0.8746875			

	Coefficients	*Standard Error*	*t Stat*	*P-value*	*Lower 95%*	*Upper 95%*
Intercept	-4.422	3.131	-1.413	0.392	-44.200	35.356
Number of swipes in the motif	0.024	0.016	1.445	0.385	-0.186	0.233
Swipe length (mm)	0.775	0.492	1.576	0.360	-5.476	7.027
Beam swipe speed in the motif (m/s)	0.048	0.026	1.889	0.310	-0.276	0.373
Beam on Time (s)	0.028	0.040	0.713	0.606	-0.474	0.530
Heat Input (W)	-0.038	0.021	-1.801	0.323	-0.307	0.230
Beam energy input (J/m)	0.464	0.221	2.097	0.283	-2.348	3.277

RESIDUAL	Al6082		
Observation	*Obs #*	*Predicted Resultant Surfi-Sculpt feature height (mm)*	*Residuals*
HeatSculptor Design 1 - Pin-like features	1	3.05	-0.050
HeatSculptor Design 2 - Staggered ridge features	2	2.63	-0.174
HeatSculptor Design 3 - Long ridge features	3	2.88	0.124
HeatSculptor Design 4 - Fin-like features	4	2.64	0.055
HeatSculptor Design 5 - Inclined cones	5	3.02	0.083
HeatSculptor Design 6 - Curved Ridges	6	2.27	-0.008
HeatSculptor Design 7 - Pins in a curved array	7	2.75	0.032
HeatSculptor Design 8 - Square based pin features	8	3.40	-0.062

SUMMARY	Al6xxx*
Regression Statistics	
Multiple R	0.944
R Square	0.891
Adjusted R Square	0.781
Standard Error	0.634
Observations	15

ANOVA	Al6xxx*				
	df	*SS*	*MS*	*F*	*Significance F*
Regression	7	22.903	3.272	8.147	0.006
Residual	6	2.811	0.402		
Total	14	25.715			

	Coefficients	*Standard Error*	*t Stat*	*P-value*	*Lower 95%*	*Upper 95%*
Intercept	5.529	27.595	0.200	0.847	-59.722	70.780
Number of swipes in the motif	-0.075	0.240	-0.312	0.764	-0.642	0.493
Swipe length (mm)	-0.289	6.544	-0.044	0.966	-15.763	15.185
Beam swipe speed in the motif (m/s)	0.022	0.085	0.257	0.804	-0.179	0.223
Processing Time (s)	0.022	0.012	1.871	0.104	-0.006	0.050
Beam on Time (s)	-0.005	0.026	-0.195	0.851	-0.067	0.056
Heat Input (W)	0.004	0.048	0.078	0.940	-0.110	0.118
Beam energy input (J/m)	0.009	0.186	0.049	0.962	-0.431	0.450

RESIDUAL	Al6xxx*		
Observation	*Obs #*	*Predicted Resultant Surfi-Sculpt feature height (mm)*	*Residuals*
HeatSculptor Design 5 - Inclined cones	1	6.15	-0.05
HeatSculptor Design 6 - Curved Ridges	2	2.48	0.02
HeatSculptor Design 6 - Curved Ridges Prototype	3	3.52	-0.02
HeatSculptor Design 5 - Inclined cones Prototype	4	2.54	0.06
HeatSculptor Design 5 - Inclined cones Prototype - 1st attempt	5	3.28	-0.18
HeatSculptor Design 5 - Inclined cones Prototype - final version	6	2.43	0.17
EngD Al6xxx Dataset 1	7	1.20	-0.09
EngD Al6xxx Dataset 2	8	1.28	-0.68
EngD Al6xxx Dataset 3	9	1.03	-0.67
EngD Al6xxx Dataset 4	10	1.42	0.44
EngD Al6xxx Dataset 5	11	1.56	0.78
EngD Al6xxx Dataset 6	12	1.99	0.12
EngD Al6xxx Dataset 7	13	1.77	0.71
EngD Al6xxx Dataset 8	14	2.33	0.09
EngD Al6xxx Dataset 9	15	2.18	-0.70

SUMMARY	Ti-6Al-4V
Regression Statistics	
Multiple R	0.992
R Square	0.985
Adjusted R Square	0.969
Standard Error	0.129
Observations	15

ANOVA	Ti-6Al-4V				
	df	*SS*	*MS*	*F*	*Significance F*
Regression	7	7.496	1.071	64.366	8.00557E-06
Residual	7	0.116	0.017		
Total	14	7.613			

	Coefficients	*Standard Error*	*t Stat*	*P-value*	*Lower 95%*	*Upper 95%*
Intercept	-0.358	0.286	-1.253	0.250	-1.034	0.317
Number of swipes in the motif	-0.001	0.001	-1.651	0.143	-0.002	0.000
Swipe length (mm)	0.878	0.099	8.855	0.000	0.644	1.113
Beam swipe speed in the motif (m/s)	-0.005	0.001	-8.605	0.000	-0.006	-0.003
Beam on Time (s)	0.017	0.010	1.762	0.122	-0.006	0.041
Heat Input (W)	0.008	0.001	6.047	0.001	0.005	0.011
Beam energy input (J/m)	-0.001	0.000	-1.810	0.113	-0.002	0.000

RESIDUAL	Ti-6Al-4V		
Observation	*Obs #*	*Predicted Resultant Surfi-Sculpt feature height (mm)*	*Residuals*
Beam Deflection Offset Study	1	0.78	0.001
High-speed video	2	2.30	-0.005
Orthopaedic implant Case Study Design 4	3	0.30	-0.001
Orthopaedic implant Case Study friction test Samples	4	0.70	0.000
Ramskogler et al. (2017) Data 1	5	0.13	-0.036
Ramskogler et al. (2017) Data 2	6	0.37	0.085
Ramskogler et al. (2017) Data 3	7	0.37	-0.062
EngD Ti-6Al-4V Dataset 1	8	1.57	0.177
EngD Ti-6Al-4V Dataset 2	9	1.83	0.152
EngD Ti-6Al-4V Dataset 3	10	1.39	-0.113
EngD Ti-6Al-4V Dataset 4	11	1.56	0.059
EngD Ti-6Al-4V Dataset 5	12	1.83	0.032
EngD Ti-6Al-4V Dataset 6	13	2.01	-0.073
EngD Ti-6Al-4V Dataset 7	14	1.83	-0.151
EngD Ti-6Al-4V Dataset 8	15	1.83	-0.065

* Due to commercial confidentiality, the specific grade of material is detailed in Submission 3 only